Study of ZnCdSe/ZnSe quantum wells grown by molecular-beam epitaxy on ZnSe substrates

V. I. Kozlovskiĭ, A. S. Artemov, Yu. V. Korostelin, A. B. Krysa, and P. V. Shapkin

P. N. Lebedev Physics Institute, Russian Academy of Sciences, 117924 Moscow, Russia

P. A. Trubenko, E. M. Dianov, and E. A. Shcherbakov

Fiber-Optics Scientific Center, Institute of General Physics, Russian Academy of Sciences, 117942 Moscow, Russia

(Submitted July 18, 1996; accepted for publication September 10, 1996)
Fiz. Tekh. Poluprovodn. **31**, 641–647 (June 1997)

ZnCdSe/ZnSe quantum wells of different thicknesses are grown by molecular-beam epitaxy on ZnSe(001) substrates. The latter are cut from ZnSe ingots obtained by gas transport in hydrogen. The substrate surface is prepared by colloid-chemical polishing followed by annealing in atomic hydrogen and deposition of a protective selenium film. The surface topography is monitored during epitaxial growth by reflection high-energy electron diffraction (RHEED). The surface microrelief of the samples is examined by atomic force microscopy, and the cathodoluminescence of the quantum-well structures is studied at 40 and 300 K. The relatively low microroughness of the surface, the high-contrast elongated reflections in the diffraction pattern, and the dependence of the spectral position of the quantum-well luminescence line on the well width attest to the high structural quality of the structures grown. © *1997 American Institute of Physics.* [S1063-7826(97)00106-3]

1. INTRODUCTION

A laser electron-beam tube (LEBT), which can be used to create high-clarity televisions and large displays for mass viewing, offers some unique possibilities.[1] However, one of the disadvantages of an LEBT is the relatively high lasing threshold (of the laser screen) at room temperature. The lasing threshold can be lowered significantly if a structure with many quantum wells serves as the active layer of the screen.[2] The first positive effect was achieved using a periodic ZnCdSe/ZnSe quantum-well structure grown by molecular-beam epitaxy (MBE) on GaAs substrates.[3] In that work the GaAs substrate was removed after the laser screen was formed, and the structure was cemented to a heat-conducting sapphire substrate. However, the adhesive layer degrades under the action of the electron beam and thus restricts the service life of the LEBT. The problem can be solved by employing ZnSe as the substrate for carrying out the growth.[2]

The interest in ZnSe homoepitaxy has increased considerably in the last few years,[4–8] primarily because of the possibility of lowering the growth-defect density and increasing the service life of blue laser diodes. Despite the first positive results in fabricating light-emitting diodes and laser diodes on ZnSe substrates,[6–8] many unelucidated points associated with optimization of the technology for preparing the substrate, with the requirements imposed on the structural quality of the bulk ZnSe, and with optimization of the regimes of epitaxial growth remain. In this paper we present the first results from an examination of these features in the case of ZnCdSe/ZnSe epitaxial quantum-well structures with several ZnCdSe quantum wells (QW's) of different width.

2. EXPERIMENT

The ZnSe substrates were cut in the form of rectangular plates with the (001) orientation and a thickness of 1–2 mm from an ingot grown from the vapor phase in sealed quartz cells by chemical transport in hydrogen.[9] The crystals were distinguished by the absence of intervening twin planes, and the dislocation density evaluated from etch pits on a (111) Se surface was $0.8-1.0\times10^5$ cm^{-2}. The maximum area of the plates was 50×20 mm^2. After being cut, the plates were ground and polished mechanically with step-by-step reduction of the grain size of the polishing powder to 1 μm. The final treatment was carried out by colloid-chemical polishing using a polish of the polivel type and a stabilized mixture of modified colloidal silica containing a 20% CrO_3 solution.[10] After the colloid-chemical polishing was completed (a 10 to 20-μm layer was removed), the substrate surface was washed with deionized water and subjected to a special chemical treatment by surfactant solutions to remove any traces of SiO_2 and ionic impurities. The surface microrelief determined on an atomic force microscope (AFM) was characterized by a root-mean-square deviation equal to 20–25 Å. However, a high-quality reflection high-energy electron diffraction (RHEED) pattern could not be obtained due to the presence of an oxide layer, which could not be evaporated in a vacuum even when it was heated to $T=600$ °C.

A preliminary anneal in atomic hydrogen at $T=400-450$ °C and a pressure equal to 0.1 Torr for 30 min was employed to remove the oxide layer. The atomic hydrogen was generated by a microwave discharge in a stream of purified H_2, which was passed through a quartz reactor. A diagram of the setup is shown in Fig. 1. To prevent intense etching the ZnSe sample was placed outside of

 1063-7826/97/060545-06$10.00

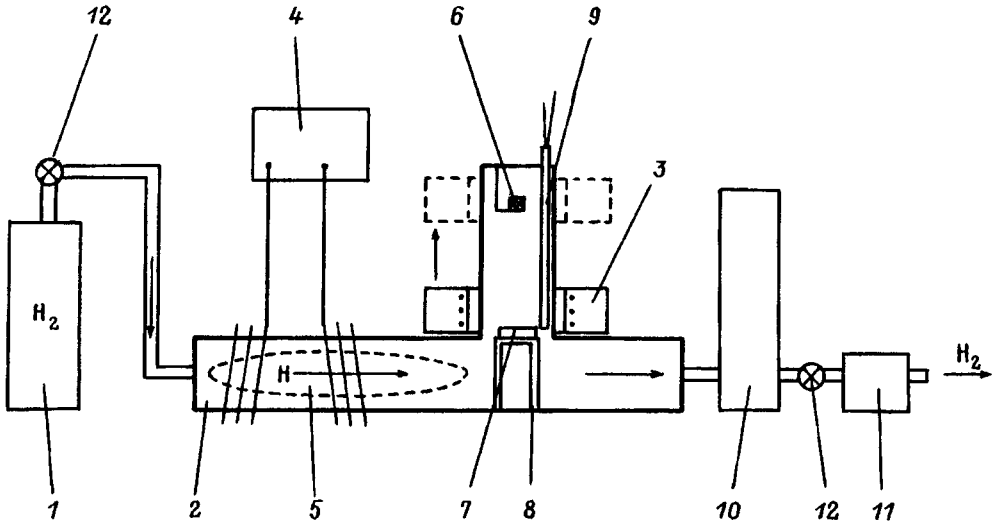

FIG. 1. Schematic representation of the setup for removing oxides from the surface of a ZnSe substrate: *1* — gas cylinder with H_2, *2* — quartz cell, *3* — electric resistance furnace, *4* — microwave generator, *5* — H plasma, *6* — container with Se, *7* — ZnSe substrate, *8* — quartz support, *9* — inlet with a thermocouple, *10* — liquid-nitrogen vacuum trap, *11* — forepump, *12* — vacuum valves.

the hydrogen plasma along the path of the hydrogen flow from the gas cylinder to the pumping system. To avoid oxidation of the surface when the substrate is transferred from the annealing chamber to the MBE system, a protective selenium film was applied to the surface after the anneal directly in the annealing chamber. For this purpose, after the ZnSe sample was cooled, the flow of hydrogen was stopped, the microwave discharge was switched off, and the furnace was moved to the upper position to evaporate Se. The selenium film could be removed by heating to $T=250$ °C.

The epitaxial growth was carried out in a TsNA-18 system (Russia) using separate sources with the pure Zn, Se, and Cd as starting materials and a substrate temperature equal to 270−300 °C.[11] The ratio between the fluxes of the elemental metals and selenium was approximately 1:1 with a small excess of selenium. The growth rate was about 1 Å/s. The surface quality was monitored during growth by reflection high-energy electron diffraction. Several ZnCdSe/ZnSe structures consisting of a ZnSe buffer layer of thickness 0.2 μm, several $Zn_{0.8}Cd_{0.2}Se$ quantum wells with thicknesses equal to about 10, 20, 40, and 80 Å separated by ZnSe layers of thickness 300 Å, and a ZnSe overlayer also of thickness 300 Å were grown.

The cathodoluminescence at $T=40$ and 300 K and the surface topography of the structures obtained were investigated. The cathodoluminescence spectra were recorded from an irradiated surface with electron energies $E_e=3$, 10, and 30 keV, a current $I_e=1-10$ μA, and an electron beam diameter $d_e=0.1-3$ mm. A PGS-2 spectrograph with a dispersion equal to 7 Å/mm and a photometric attachment containing an FÉU-100 photomultiplier was used. Topograms were obtained on an AFM in the contact mode with a resolution along the Z axis equal to 5 Å. Soft cantilevers with a force constant equal to 0.5 H/m and a radius of curvature on the tip equal to 500 Å were used in the AFM.

3. EXPERIMENTAL RESULTS AND DISCUSSION

Figure 2 presents topograms of the surface of a ZnSe substrate after colloid-chemical polishing (Fig. 2a) and after an anneal in atomic hydrogen (Fig. 2b) and of the surface of the epitaxial structure grown on that substrate (Fig. 2c). As can be seen from the figure, the maximum difference in elevation on the relief after polishing does not exceed 70 Å. Annealing in hydrogen lowers this difference to ~40 Å. During the growth of the epitaxial films, the roughness of the surface layer increases into the range 70−80 Å. If the substrate is prepared by mechanical polishing followed by treatment in a polishing etchant based on a solution of CrO_3 in concentrated HCl (such preparation is often used in the fabrication of laser screens from bulk ZnSe), the surface (see Fig. 2d) has a highly developed relief in the XY plane with a characteristic deviation along the Z axis of about 120 Å. In the case of epitaxial growth on substrates, whose surface is prepared by this method, the characteristic height of the bumps reaches 200 Å.

Figures 3a and 3b present the RHEED patterns in the [110] direction before and after growing an epitaxial structure on a substrate treated in atomic hydrogen. The fairly narrow, high-contrast, elongated reflections attest to the good quality of the surfaces of the substrate and the structure grown. If the anneal in atomic hydrogen is not carried out, the oxide cannot be removed from the substrate even when it is heated to 600 °C in an ultrahigh vacuum. In this case a diffraction pattern consisting of a highly diffuse background from the oxide film and weak elongated reflections from the surface layer of the substrate is generally observed (Fig. 3c). During growth on such substrates, the contrast of the diffraction pattern increases; however, instead of line-like reflections, point reflections, which are characteristic of bulk growth, and (or) concentric arcs, which are characteristics of polycrystalline growth, are observed (Fig. 3d). In this case

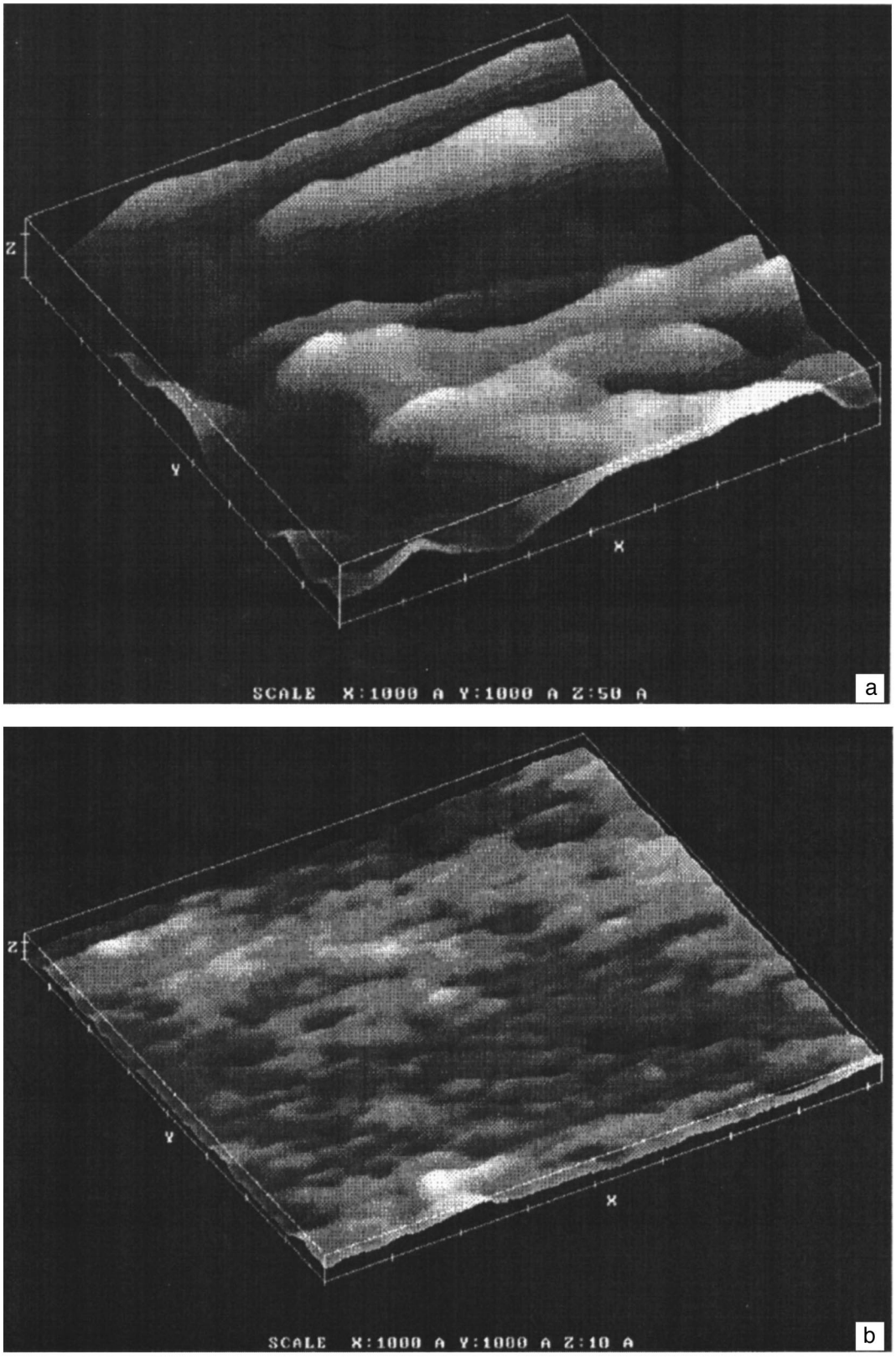

FIG. 2. Topograms of the surface of a ZnSe substrate after colloid-chemical polishing and before (a) and after (b) annealing in atomic hydrogen and of the surface of the epitaxial ZnCdSe/ZnSe structure grown on that substrate (c). d — topogram of the surface of a chemically polished substrate.

quantum wells do not form, as is evidenced by the data from the cathodoluminescence analysis of the samples.

The cathodoluminescence spectra of four different structures at $T=40$ K for $E_e=3$ keV and approximately the same current density $j_e=10^{-3}$ A/cm^2 are presented in Fig. 4. The spectrum of structure 100 (three QW's of widths 10, 20, and

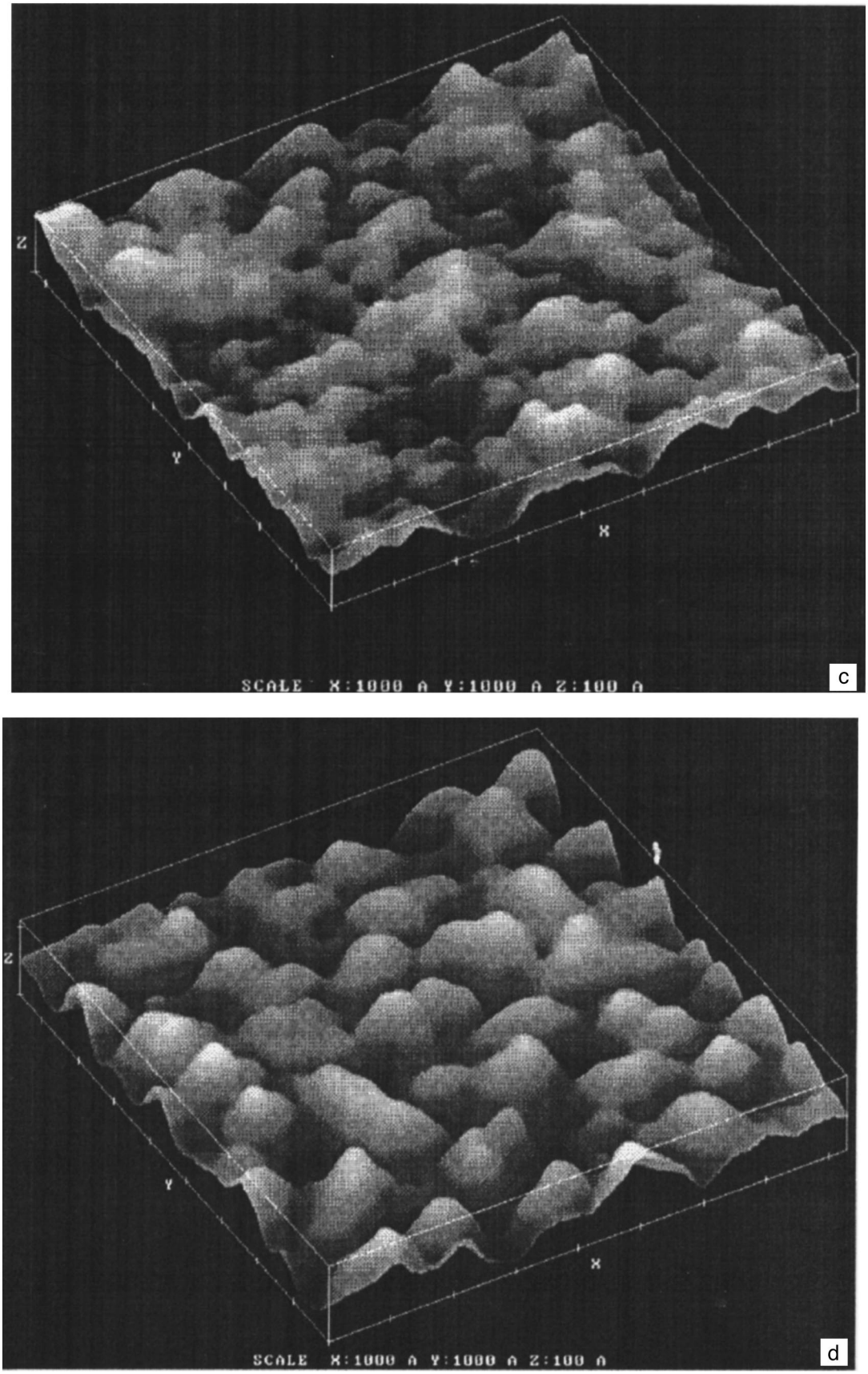

FIG. 2. (continued).

40 Å) consists of weak emission at 443−448 nm and a broad band with a maximum at 485−490 nm, which is characteristic of exciton (FX) emission and emission associated with a complex consisting of an intrinsic defect and an impurity

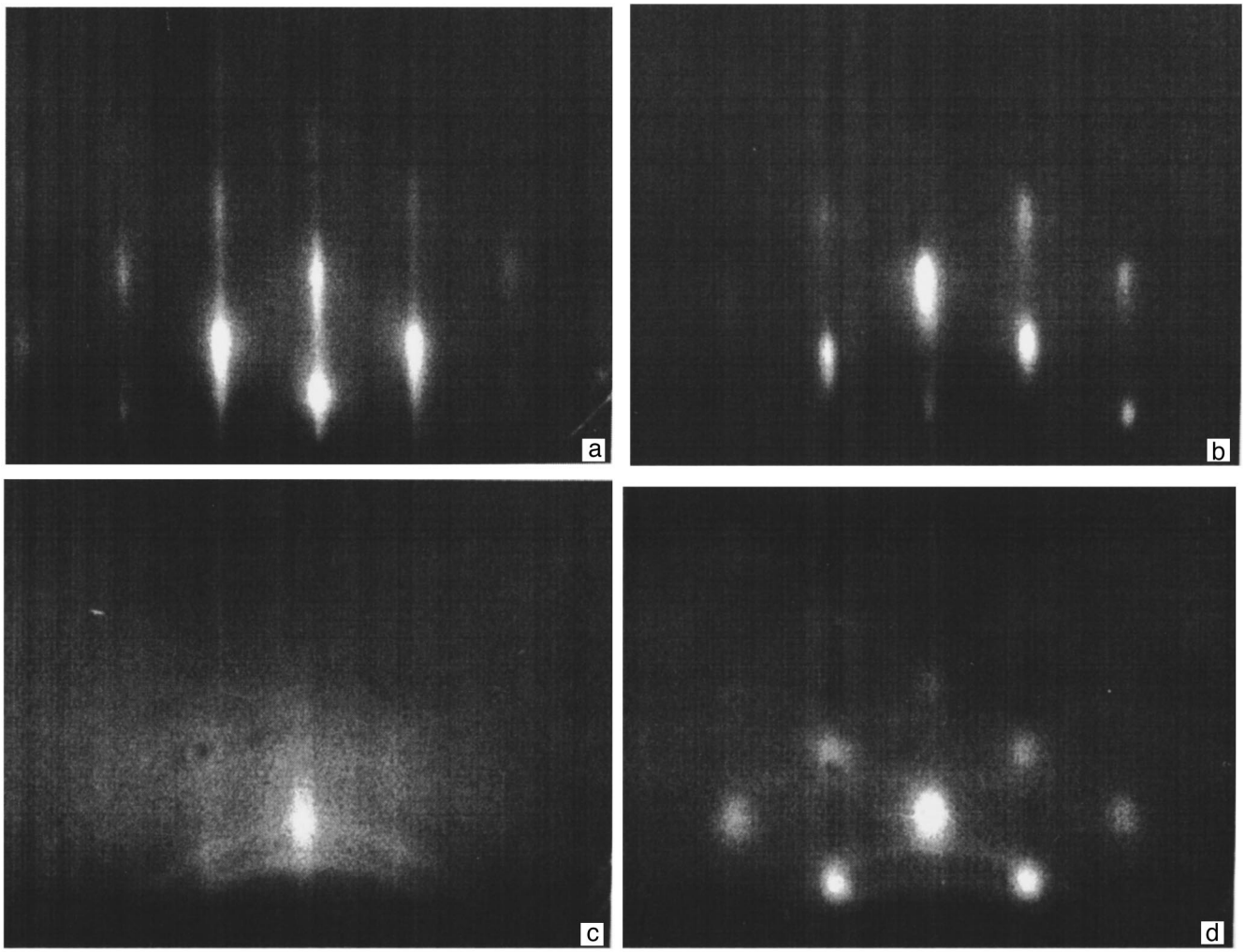

FIG. 3. Reflection high-energy electron diffraction pattern before (a, c) and after (b, d) the growth of an epitaxial structure on ZnSe substrates annealed (a, b) and not annealed (c, d) in atomic hydrogen.

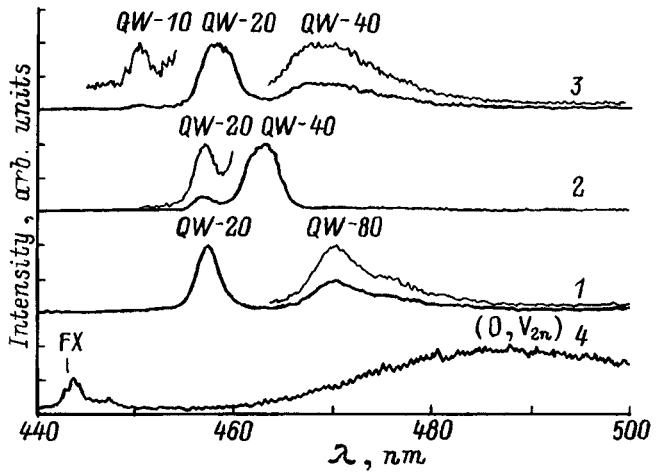

FIG. 4. Cathodoluminescence spectra. Structures: *1* — 92 (two QW's of widths 20 and 80 Å), *2* — 94 (two QW's of widths 20 and 40 Å), *3* — 98 (three QW of widths 10, 20, and 40 Å), and *4* — 100 (three QW's of widths 10, 20, and 40 Å). $T=40$ K and $E_e=3$ keV.

atom, presumably of oxygen (O, V_{Zn}), in ZnSe.[9] Therefore, we assigned the observed emission to the buffer and intermediate ZnSe layers. When $E_e=3$ keV, the penetration depth z_0 of the electrons into the structure amounts to less than 0.1 μm, and the probability of excitation of the ZnSe substrate is small. Thus, the spectrum of this structure does not contain any sign of the formation of a QW. The reason for this was the bulk growth, which was indicated by the electron diffraction pattern.

The spectra of three other structures, viz., 92 (two QW's of widths 20 and 80 Å), 94 (two QW's of widths 20 and 40 Å), and 98 (three QW'S of widths 10, 20, and 40 Å) consist of several lines, which we assign to QW luminescence. The full-width at half-maximum (FWHM) of the line with a maximum at $\lambda_m=450$ nm (spectrum *3*, QW-10 — a QW of width 10 Å in sample 98) and of the line with a maximum at $\lambda_m=457$ nm (spectra *1* and *2*, QW-20 — a QW of width 20 Å in samples 92 and 94) was approximately 1.5 meV. These widths are comparable to the widths of the luminescence lines of similar QW's grown on GaAs substrates.[12] The spectral positions of these lines also coincide with those in the case of growth on GaAs. We assign this luminescence to the

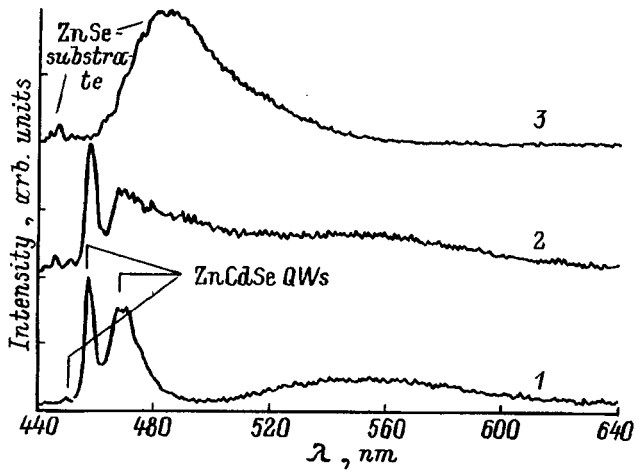

FIG. 5. Cathodoluminescence spectra of structure 98 (three QW's of widths 10, 20, and 40 Å). $T=40$ K. E_e, keV: *1* — 3, *2* — 10, *3* — 30. The emission lines of the QW's are marked by arrows.

emission of free excitons or excitons localized on fluctuations of the QW width. The line with $\lambda_m=458$ nm for sample 98 (spectrum *3*, QW-20) and the line with $\lambda_m=463$ nm for sample 94 (spectrum *2*, QW-40) can also be interpreted as the emission of localized QW's with widths equal to 20 and 40 Å, respectively. Their FWHM's are somewhat greater than those of the lines discussed above. An even larger FWHM (approximately 60 meV) is exhibited by the line with $\lambda_m=468$ nm in sample 98 (spectrum *3*, QW-40) and the line with $\lambda_m=470$ nm in sample 92 (spectrum *1*, QW-90), which are apparently associated with QW's of widths 40 and 80 Å, respectively; however, we believe that they are produced by the recombination of an electron and a hole that are localized separately (like a donor-acceptor transition). It is noteworthy that the width of the emission line in each of the structures presented increases as the width of the QW increases. The reason for this law is not yet clear.

Figure 5 compares the cathodoluminescence spectra of sample 98 for three different values of E_e: 3, 10, and 30 keV. The values of z_0 for 10 and 30 keV are estimated as 0.25 and 2.5 μm, respectively.[13] In the case of surface excitation (3 eV), the spectrum contains a broad long-wavelength band with $\lambda_m=555$ nm along with the QW luminescence. This band is not observed in the case of deep excitation (30 keV), in which the spectrum actually corresponds to the emission spectrum of the ZnSe substrate. It should be assigned to emission via deep centers caused by defects in the epitaxial layers.

Quantum-well luminescence is also observed in the emission spectrum at room temperature. However, the emission lines for different QW's are poorly resolved, and their intensity is still significantly smaller than the intensity of the emission lines of similar QW's grown on a GaAs substrate, which have approximately the same dislocation density (0.8×10^5 cm^{-2}). Therefore, it can be assumed that the main cause of the low intensity of the QW luminescence is a higher degree of contamination by an uncontrollable impurity (for example, oxygen) and the presence of a high concentration of intrinsic point defects (especially zinc vacancies V_{Zn}), rather than the structural imperfection of the ZnSe substrate. Following Ref. 5, we assume that vacancies of the V_{Zn} type bound in complexes in the substrate are released from those complexes during epitaxial growth and diffuse into the epitaxial layer, forming nonradiative recombination centers in it. Nevertheless, this question requires the performance of additional investigations.

4. CONCLUSIONS

Quantum-size $Zn_{0.8}Cd_{0.2}Se/ZnSe$ structures with solitary quantum wells grown by molecular-beam epitaxy on twin-free ZnSe(001) substrates have been obtained and investigated in this work.

A technology for preparing the surface for epitaxial growth, including colloid-chemical polishing followed by annealing in a stream of atomic hydrogen at 400−450 °C with protection of the surface by a layer of selenium, has been found.

In the cathodoluminescence spectrum of the structures the emission of the quantum wells greatly predominates over the emission of the background and the intermediate ZnSe layers, and the spectral position varies with the well width in accordance with a quantum-size effect similar to what occurs in QW's grown on GaAs substrates. However, the intensity of the QW luminescence on the ZnSe substrates, especially at room temperature, remains insufficiently high because of the large number of point defects.

This work was performed with the financial support of the Russian Foundation for Fundamental Research (Grants Nos. 95-02-05646 and 96-02-17688).

[1] A. S. Nasibov, V. I. Kozlovsky, P. V. Reznikov, Ya. K. Skasyrsky, and Yu. M. Popov, J. Cryst. Growth **117**, 1040 (1992).
[2] V. I. Kozlovsky, A. S. Nasibov, Yu. M. Popov, P. V. Reznikov, and Ya. K. Skasyrsky, in *IS&T/SPIE Symposium on Electronic Imaging: Science and Technology (Topic 2407: Projection Display)*, San Jose, California, 1995.
[3] N. G. Basov, E. M. Dianov, V. I. Kozlovskiĭ, A. B. Krysa, A. S. Nasibov, Yu. M. Popov, A. M. Prokhorov, P. A. Trubenko, and E. A. Shcherbakov, Kvantovaya Elektron. **22**, 756 (1995).
[4] M. Ohishi, K. Ohmory, Y. Fujii, and H. Saito, J. Cryst. Growth **86**, 324 (1988).
[5] T. Yodo, T. Koyama, and K. Yamashita, J. Appl. Phys. **64**, 2403 (1988).
[6] M. H. Jeon, L. C. Calhoun, and R. M. Park, J. Electron Mater. **24**, 177 (1995).
[7] D. B. Eason, Z. Yu, W. C. Hughes, C. Boney, J. W. Cook Jr., J. F. Schetzina, D. R. Black, G. Cantwell, and W. C. Harsch, J. Vac. Sci. Technol. B, **13**, 1566 (1995).
[8] Z. Yu, C. Boney, W. C. Hughes, W. H. Rowland Jr., J. W. Cook Jr., J. F. Schetzina, G. Cantwell, and W. C. Harsch, Electron. Lett. **31**, 1341 (1995).
[9] Yu. V. Korostelin, V. I. Kozlovsky, A. S. Nasibov, and P. V. Shapkin, J. Cryst. Growth **161**, 51 (1996).
[10] A. S. Artemov, V. P. Alekhin, N. A. Antokhin, V. I. Kravchenko, and V. I. Laptev, in *Abstracts of Reports to the 2nd All-Union Conference ''Materials of Chalcogenides and Oxygen-Containing Semiconductors* [in Russian], 1986, Vol. 1, p. 84.
[11] E. M. Dianov, A. M. Prokhorov, P. A. Trubenko, and E. A. Shcherbakov, Fiz. Tekh. Poluprovodn. **28**, 1278 (1994) [Semiconductors **28**, 725 (1994)].
[12] V. I. Kozlovsky, E. A. Shcherbakov, E. M. Dianov, A. B. Krysa, A. S. Nasibov, and P. A. Trubenko, J. Cryst. Growth **159**, 609 (1996).
[13] C. Trager-Cowan, F. Yang, and K. P. O'Donnell, Adv. Mater. Opt. Electron. **3**, 295 (1994).

Translated by P. Shelnitz

Mesoscopic effects in the hopping conductivity region of macroscopic quasi-two-dimensional systems

B. A. Aronzon

Kurchatov Institute Russian Scientific Center, 123182, Moscow, Russia
Scientific-Research Center for Applied Problems in Electrodynamics, 103498 Moscow, Russia

A. S. Vedeneev

Institute of Radio Engineering and Electronics, Russian Academy of Sciences, 141120 Fryazino, Russia

V. V. Ryl'kov

Scientific-Research Center for Applied Problems in Electrodynamics, 103498 Moscow, Russia
Institute of Radio Engineering and Electronics, Russian Academy of Sciences, 141120 Fryazino, Russia
(Submitted July 31, 1996; accepted for publication September 10, 1996)
Fiz. Tekh. Poluprovodn. **31**, 648–652 (June 1997)

Mesoscopic effects are discovered in the conductivity of macroscopic (50×150 μm) metal-oxide-semiconductor (MOS) structures based on Si layers with a high boron content (10^{18} cm^{-3}) in the classical field-effect configuration. These effects are manifested as the gate voltage is varied in the form of stationary quasiperiodic fluctuations of the transverse voltage between potential probes located on opposite lateral faces of the sample. The fluctuations are observed at relatively high temperatures ($\leqslant$30 K) and are associated with restructuring of the percolation cluster, which determines the quasi-two-dimensional hopping conductivity at the intersection of the bulk impurity band with the Fermi level. © *1997 American Institute of Physics.* [S1063-7826(97)00206-8]

Mesoscopic effects are inherent to systems whose dimensions are commensurate with the characteristic scales of their electric inhomogeneity. In the case of hopping conductivity, these dimensions are limited by the correlation radius L_c of the percolation cluster.[1,2] The principal experiments that have been devised to study the incoherent mesoscopic phenomena in hopping conductivity were carried out on short-channel ($L\ll L_c$, where L is the channel length) structures.[3,4] In this case the conductivity is determined by isolated one-dimensional chains of impurity atoms with an exponentially small resistance. These atoms, however, do not form an infinite cluster and, therefore, do not make a significant contribution to the conductivity when $L\gg L_c$.[5] Such effects are usually observed in the region of conduction with a variable hopping distance and are manifested as regular fluctuations of the conductivity, which intensify as the dimensions of the sample are diminished and the temperature is lowered.[3,4]

In the present work mesoscopic fluctuations of the transverse voltage between Hall probes were discovered in macroscopic (with dimensions much greater than L_c) quasi-two-dimensional systems based on layers of doped Si when the gate voltage V_g was varied. These fluctuations are observed at relatively high temperatures in the region for conduction with a constant hopping distance even when the contribution of the free charge carriers to the conductivity of the system is significant.

The p-Channel metal-oxide-semiconductor (MOS) structures based on ion-implanted Si:B layers of thickness 0.5 μm with a boron density $N_a=10^{18}$ cm^{-3} were investigated; the density of the compensating donors was 10^{15} cm^{-3} (Ref. 6). The samples (Fig. 1), which were equipped witha pair of current-carrying p^+ electrodes and two pairs of potential (Hall) probes, were fashioned in the form of a double cross. The channel length and width were 150 and 50 μm, respectively, the dimensions of the tips on the potential probes were 15×5 μm, and the thickness of the subgate oxide was 620 Å. The conductivity $G=I_x/V_x$ (V_x is the longitudinal voltage, and I_x is the current) of the p-layer and the voltage V_y between the potential probes on opposite faces of the sample (see Fig. 1) were measured in a longitudinal electric field $E_x\leqslant10$ V/cm as a function of the gate voltage V_g in the temperature range $T=10-30$ K in a magnetic field $\leqslant1$ T and in the absence of such a field. The experiments were performed using a low-current (>0.1 nA) electromechanical preamplifier and a voltage repeater with an input resistance greater than 10^{12} Ω.

One significant feature of the structures investigated is the presence of a layer of p-Si with a very high doping level. As a result, at positive values of V_g a quasi-two-dimensional hopping-conductivity channel forms in the region of intersection of the acceptor states with the Fermi level (Fig. 1).[7] The activation energy for quasi-two-dimensional hopping conductivity is determined by the electric field in the space-charge region, and the thickness of the channel is of the order of the mean interimpurity distance r_d.[7]

Under conditions conducive for the formation of such a quasi-two-dimensional channel, the $V_y(V_g)$ curve exhibits highly reproducible fluctuations, which intensify as the temperature is lowered, but the positions of the maxima and minima of V_y on the V_g axis scarcely vary with the temperature (see Fig. 2). Conversely, in a regime with strong enrichment of the Si surface with holes ($V_g<-2$ V) no fluctuations are observed. In this case V_y has a value of the order of 5×10^{-4} V_x, which attests to an insignificant original asym-

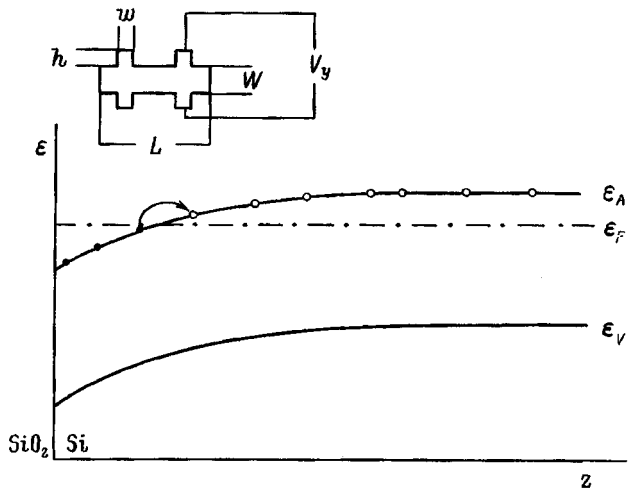

FIG. 1. Band diagram of the space-charge region of Si:B under conditions conducive to the formation of a quasi-two-dimensional hopping-conductivity channel. The arrow schematically depicts a hop of an electron from an ionized boron atom to a neutral atom: ε_V, ε_F, and ε_A are the energy positions of the top of the valence band, the Fermi level, and the acceptor level, respectively. The configuration of the sample is shown in the inset.

metry of the geometric configuration of the potential probes of the order of 5×10^{-4} relative to the sample length.

At relatively high temperatures (20–30 K) application of a magnetic field perpendicular to the plane of the channel leads to displacement of the $V_y(V_g)$ curve along the vertical axis by the value of the Hall voltage V_H (Fig. 2a, curve *1′*). Figure 2b presents plots of the Hall voltage $V_H(V_g)=(V_y^{\uparrow}-V_y^{\downarrow})/2$ and the fluctuating component $V_f=(V_y^{\uparrow}+V_y^{\downarrow})/2$ of the signal V_y, where $V_y^{\uparrow}$ and $V_y^{\downarrow}$ are the values of V_y for different polarities of the magnetic field. The figure also presents the $V_y^0(V_g)$ curve obtained in the absence of a magnetic field. It becomes clear from Fig. 2b that the Hall voltage and the fluctuating component are additive and separable and that V_H does not undergo fluctuations, while V_f scarcely depends on the magnetic field B in the range of values investigated [compare the $V_y^0(Vg)$ and $V_f(V_g)$ curves in Fig. 2b]. The latter is not surprising, since at $B<1$ T the magnetic length $(hc/eB)^{1/2}>200$ Å significantly exceeds the localization radius of holes on the boron atoms $a_B\cong23$ Å and the mean interimpurity distance $r_d\cong60$ Å; therefore, the variation of L_c in a magnetic field is negligible ($\approx10^{-4}$).[1] At $T>20$ K the increase in V_H with increasing temperature in the depletion regime indicates that the Hall voltage is determined primarily by free holes. However, the value of V_H is underestimated because of the shunting effect of the hopping conductivity. When the Si surface is enriched with holes ($V_g<0$), the contribution of the hopping conductivity to $G(V_g)$ becomes increasingly less significant, and V_H increases sharply (Fig. 2b).

We note that the possibility for the formation of two types of surface channels, viz., a classical hole channel for metallic conduction in the enrichment regime ($V_g<0$) and a quasi-two-dimensional hopping-conductivity channel when $V_g>0$, leads to several special features in the behavior of $G(V_g)$. In particular, upon passage from the enrichment regime to the depletion regime, there is a drop in $G(V_g)$ followed by an increase and achievement of a plateau at a gate voltage $V_g\cong2$ V, which corresponds to the condition for the formation of the quasi-two-dimensional channel (Fig. 3). The value of $G(V_g)$ in the vicinity of the minimum is determined by the bulk flat-band conductivity G_{fb} of the structure, while in the region of the plateau ($V_g\geqslant2$ V) the difference $G_c=G(V_g)-G_{fb}$ gives the value of the quasi-two-dimensional hopping conductivity, which varies only slightly as the channel deepens with increasing V_g.[7] Finally, the passage to two-dimensional hole conduction in the enrichment regime, which is accompanied by filling of the states of the A^+ band of the boron atoms, occurs at relatively low values of the gate voltage $V_g\leqslant-2$ V.[8] The $G(V_g)$ curves at different T undergo a smooth discontinuity in this region and merge when degeneracy is achieved ($V_g\leqslant-3$ V) (Fig. 3).

Thus, comparing the results presented in Figs. 2 and 3, we conclude that the fluctuations of V_y appear upon passage from the transport of free holes in the valence and A^+ impurity bands in the enrichment regime ($V_g<0$) to the quasi-two-dimensional hopping conductivity of electrons via ground acceptor states at $V_g>0$. The characteristic amplitude of the fluctuations is maximal in the region of the minimum on the $G(V_g)$ curves, i.e., under flat-band conditions. Then, as V_g increases, it decreases sharply, and, finally, it practically ceases to vary with V_g in the region of the $G(V_g)$ plateau.

We associate the detected fluctuations of V_y with the mesoscopic effects, i.e., with manifestations of the electric inhomogeneity of the microscopic scales under the conditions of electron transport via localized impurity states. In our opinion, the basis for this is the reproducibility of the V_y fluctuations, the constancy of their positions on the V_g axis in a broad temperature range, and the qualitative correlation of the dependence of the fluctuation amplitude on V_g as the characteristic spatial scale of the electric inhomogeneity varies. In the hopping-conductivity regime the latter is determined by the density of states at the Fermi level:[1] the density of states is smallest under flat-band conditions, where the Fermi level is located in the Mott-Hubbard gap,[9] and is constant in the strong-depletion regime, where the Fermi level intersects the acceptor levels near the Si surface.[8]

The physical picture of the phenomenon observed is as follows. At positive values of V_g (Fig. 1) the low-temperature conduction of the macroscopic system investigated is mediated predominantly along a quasi-two-dimensional channel by hops of the charge carriers between nearby acceptors,[7,8] which form an infinite percolation cluster, i.e., a quasi-two-dimensional random net.[1,2] The mean dimension of the cells in such a net, which characterizes the spatial scale of the electric inhomogeneity of the system, is determined by the correlation length $L_c=R_c(2R_c/3a_B)^{\nu}$, where $R_c=0.865/N_a^{1/3}$ is the percolation radius, and ν is the critical index from percolation theory; in the 2D case we have[1,2] $\nu=1.33$. Under experimental conditions ($N_a=10^{18}$ cm^{-3}) $L_c\cong300$ Å. In the presence of a weak longitudinal electric field E_x the mean voltage drop across on a cell is E_xL_c. Therefore, the potential of an arbitrarily selected point in a quasi-two-dimensional channel differs from

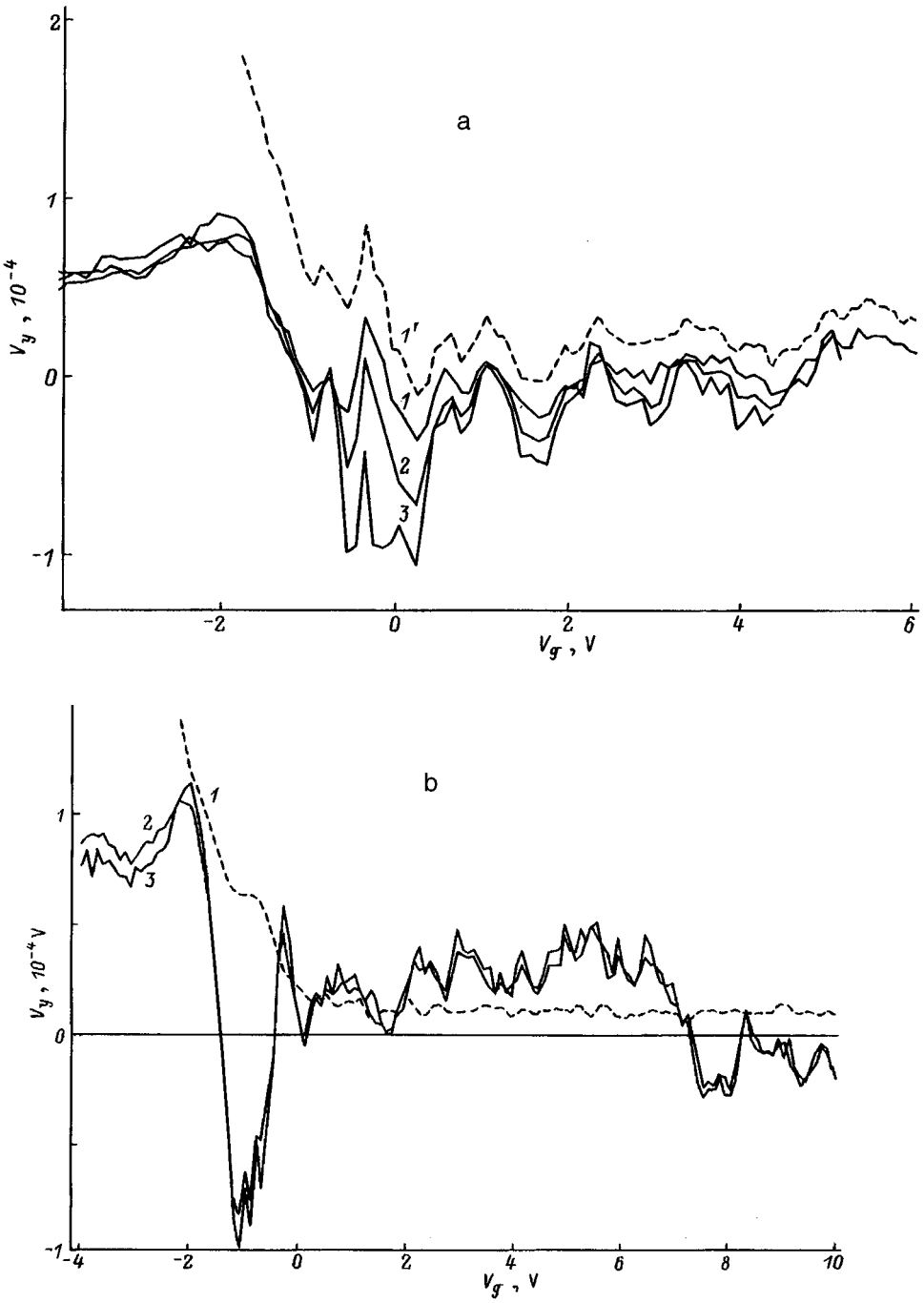

FIG. 2. Dependence of the interprobe potential difference V_y on the gate voltage V_g for $V_x=0.125$ V. a) At various temperatures, K: *1*, *1′* — 23.6; *2* — 20.5; *3* — 18.1. Curve *1′* was obtained in a 0.7-T magnetic field perpendicular to the plane of the structure, and the remaining curves were obtained in the absence of a magnetic field. b) At $T=22.6$ K with $B=0.9$ T: *1* — $V_H=(V_y^{\uparrow}-V_y^{\downarrow})/2$, *2* — $V_f=(V_y^{\uparrow}+V_y^{\downarrow})/2$, 3 — V_y^0. Here $V_y^{\uparrow}$ and $V_y^{\downarrow}$ are the values of V_y for different polarities of the magnetic field.

its potential in the homogeneous case by an amount on the order of E_xL_c because of the chaotic structure of the percolation cluster. As V_g is increased, the quasi-two-dimensional hopping-conductivity channel moves into the p-Si layer along a normal to the surface. This process, in turn, is accompanied by alteration of the configuration of the percolation net, because different groups of impurity atoms form it at different values of V_g. Accordingly, as V_g varies, the concrete distribution of the potential will vary, and its local value at a fixed point will vary within $\sim 2E_xL_c$, reflecting the restructuring of the percolation cluster. It would appear that the dimensions of the potential probes must be smaller than L_c to observe such effects.

Turning now to the real configuration of the objects of investigation (see the inset in Fig. 1), we note that the metallized contact areas of the potential probes are separated from the lateral boundary of the electron-transport channel by the tips on them and, therefore, weakly disturb the distribution of the longitudinal electric field in the channel plane. In fact, even in the absence of metallization the contact surface (the end surface of the tip) is nearly equipotential. In an electrically homogeneous sample the longitudinal potential difference between the extreme points of this surface is approximately equal to $E_x\times w\times\exp(-\pi h/w)$,[10] where h and w are, respectively, the length and width of the tip. In the samples investigated ($h/w=3$; see Fig. 1) the dimension of

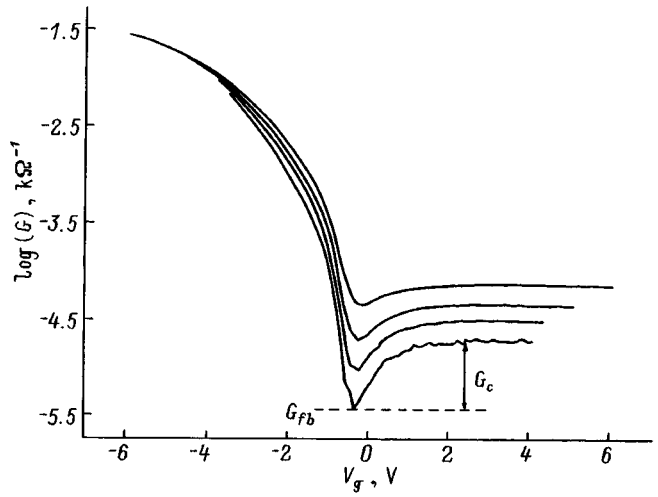

FIG. 3. Conductivity of the p-type Si layer as a function of V_g at various temperatures, K: *1* — 23.6, *2* — 20.5, *3* — 18.1, *4* — 15.7.

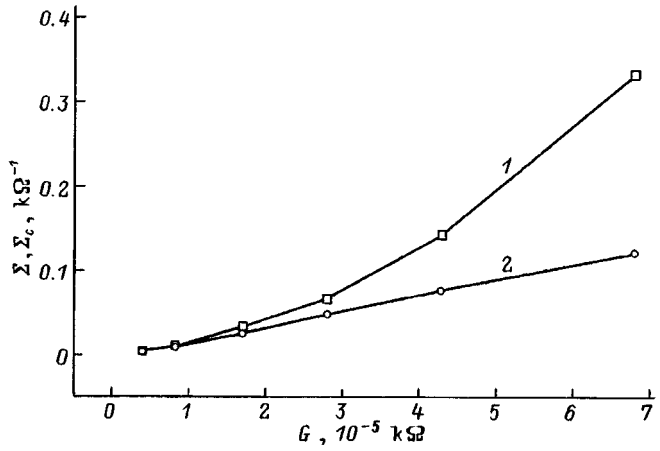

FIG. 4. Dependence of the ratio $\Sigma = I/dV_y$ (*1*) and the normalized value $\Sigma_c = (I/dV_y) \times G_c/(G_e + C_{\text{fb}})$ (*2*) on G for $V_g \geqslant 2$ V.

the region on the lateral faces of the channel corresponding to this potential difference is, in order of magnitude, $w' \sim w \times \exp(-\pi h/w) \cong 5$ Å. In other words, the potential of the contact surface of a tip is equivalent to the potential of an ''effective probe'' measuring ~ 5 Å that is located on the lateral boundary of the channel near the tip axis. In the inset in Fig. 1 the positions of the ''effective probe'' are marked by points. Since the inhomogeneity scale L_c is significantly smaller than the dimensions of the tips, the picture just considered remains valid as a whole in the hopping-conductivity regime, i.e., as in a homogeneous sample, the dimension of the effective probe should be assumed to be of the order of $w' < L_c$. However, in the hopping-transport regime, as soon as the potential of an arbitrarily selected point in the channel differs from its value in the homogeneous case by $\sim E_x L_c$, the effective probe is displaced over a distance of order L_c relative to the tip axis. As V_g varies, the position of the effective probe fluctuates within $\pm L_c$, causing fluctuations of V_y with an amplitude $\sim 2E_x L_c$.

Let us examine the experimental data presented in Fig. 2 on the basis of these arguments. As indicated, as V_g varies, the local value of the potential of each probe varies within $2L_c E_x = 2I_x(L_c/L)G^{-1}$; therefore, the characteristic amplitude of the fluctuations of the interprobe voltage dV_y should be of the same order of magnitude. Within percolation theory[1,2] L_c has virtually no temperature dependence under the conditions of hopping conductivity via nearest neighbors. For this reason, it should be expected that the ratio of the current I_x to the mean amplitude dV_y of the fluctuations of the interprobe voltage, $\Sigma = I_x/dV_y = G \times L/2L_c$, will vary with the temperature in proportion to $G(T)$ with the proportionality factor $L/2L_c$. In practice (Fig. 4, curve *1*) the dependence of Σ on G constructed from the data in Figs. 2a and 3 is not linear, in apparent contradiction to the arguments presented above. However, we should take into account the finite conductivity of the p-type Si layer G_{fb} (see Fig. 3), which is caused by the hopping of electrons between impurity atoms in the bulk, as well as the presence of free holes at $T > 20$ K, as is evidenced by the appreciable value of the Hall component V_y in a magnetic field (Fig. 2b). In the bulk of the p-Si layer the configuration of the percolation paths scarcely varies with V_g; therefore, the existence of bulk conduction does not lead to additional fluctuations of V_y. Nevertheless, in cases in which G_{fb} is commensurate with the conductivity of the quasi-two-dimensional channel G_c, it has a shunting effect on the fluctuations of V_y. When this circumstance is taken into account, the normalized value of Σ corresponding to the absence of bulk conduction, $\Sigma_c = \Sigma \times G_c/(G_c + C_{\text{fb}})$, is a linear function of G (Fig. 4, curve *2*), in accordance with the proposed picture of the phenomenon. The scale of the electric inhomogeneity determined from the slope of the $\Sigma_c(G)$ curve, 390 Å, is consistent with the theoretical estimate $L_c \cong 300$ Å determined above.

It is also noteworthy that the experimental curves in Fig. 2 exhibit a clearly expressed ''period'' $\delta V_g \cong 1$ V for the fluctuating component $V_y(V_g)$, if it is construed as the mean distance between the maxima of this function. Calculations show that an increase in V_g by δV_g leads to displacement of the position of the quasi-two-dimensional hopping-conductivity channel into the p-type Si layer over a distance $l = \varepsilon_d \delta V_g/(4\pi e d N_A) \cong 40$ Å, i.e., by an amount of the order of the mean interimpurity distance $r_d \cong 60$ Å (ε is the dielectric constant of the insulator, and d is its thickness). This displacement corresponds to significant alteration of the spatial configuration of the percolation paths forming the quasi-two-dimensional percolation cluster (with a thickness $\sim r_d$), since the positions of the acceptors in planes separated by more than r_d are uncorrelated. Therefore, the variation of the position of the quasi-two-dimensional channel relative to the Si surface, which can be monitored under the conditions of the experiment and is unavoidably accompanied by restructuring of the percolation cluster, leads to the appearance of quasiperiodic fluctuations of the transverse interprobe voltage.

Thus, the data presented comprise a direct experimental observation of the characteristic scale of the electric inhomogeneity of macroscopic systems, which is determined in the case of hopping conductivity by the correlation radius of the

percolation cluster. This essentially opens up a new possibility for studying mesoscopic effects in disordered systems having a percolation type of conduction.

We thank V. A. Volkov and M. S. Kagan for some discussions. This work was performed with the support of the Russian Fund for Fundamental Research (Grant No. 96-02-18429-a) and the ''Physics of Solid State Nanostructures'' Interdisciplinary Scientific-Technical Program (Grant No. 1-052).

[1] B. I. Shklovskii and A. L. Efros, *Electronic Properties of Doped Semiconductors*, Springer-Verlag, Berlin (1984).
[2] I. P. Zvyagin, *Kinetic Phenomena in Unordered Semiconductors* [in Russian], Izd. MGU, Moscow (1984).
[3] A. O. Orlov, M. É. Raĭkh, I. M. Ruzin, and A. K. Savchenko, Zh. Éksp. Teor. Fiz. **96**, 2172 (1989) [Sov. Phys. JETP **69**, 1229 (1989)].
[4] A. I. Yakimov, N. P. Stepina, and A. V. Dvurechenskiĭ, Zh. Éksp. Teor. Fiz. **102**, 1882 (1992) [Sov. Phys. JETP **75**, 1013 (1992)].
[5] M. É. Raĭkh and I. M. Ruzin, JETP Lett. **43**, 562 (1986).
[6] S. Manzini and A. Modelli, J. Appl. Phys. **65**, 2361 (1989).
[7] A. S. Vedeneev, A. G. Gaivoronskii, A. G. Zhdan, V. V. Rylkov, Yu. Ya. Tkach, and A. Modelly, Appl. Phys. Lett. **64**, 2566 (1994).
[8] A. S. Vedeneev, A. G. Gaĭvoronskiĭ, A. G. Zhdan, A. Modelli, V. V. Ryl'kov, and Yu. Ya. Tkach, JETP Lett. **60**, 475 (1994).
[9] N. F. Mott and E. A. Davis, *Electronic Processes in Non-Crystalline Materials*, 2nd ed., Clarendon Press, Oxford (1979) [Russ. transl., Mir, Moscow (1982)].
[10] W. Versnel, J. Appl. Phys. **52**, 4659 (1981).

Translated by P. Shelnitz

Sulfide passivation of GaSb/GaInAsSb/GaAlAsSb photodiode heterostructures

I. A. Andreev, E. V. Kunitsyna, V. M. Lantratov, T. V. L'vova, M. P. Mikhaĭlova, and Yu. P. Yakovlev

A. F. Ioffe Physicotechnical Institute, Russian Academy of Sciences, 194021 St. Petersburg, Russia
(Submitted August 5, 1996; accepted for publication September 10, 1996)
Fiz. Tekh. Poluprovodn. **31**, 653–657 (June 1997)

Gallium antimonide and its solid solutions are widely used to create optoelectronic devices for the spectral range 2–5 μm. However, the high chemical activity of their surfaces leads to a high growth rate of the native oxide and to degradation of the characteristics of devices based on these materials. The passivation of GaSb and the quaternary compounds GaInAsSb and GaAlAsSb based on it in aqueous solutions of Na_2S and $(NH_4)_2S$ is investigated. It was found that an etching phase is present when such semiconductor materials are treated in aqueous sulfide solutions. The effect of the treatment process (the type and molarity of the solution and the treatment time) on the etch rate of the test materials was investigated. The optimum technological conditions for passivating GaSb/GaInAsSb/GaAlAsSb mesa photodiode structures are determined on the basis of the results obtained, and a significant decrease (5–10 fold) in the value of the reverse dark current is obtained.
[S1063-7826(97)00306-2]

The passivation of a surface is an important problem in the technology of structures based on semiconducting III–V compounds, since this group of semiconductors is characterized by a high density of states, rigid pinning of the Fermi level, high chemical activity, and, consequently, rapid oxide growth. Passivation is one of the ways to control the electronic properties of a surface by altering its chemical structure.

Various treatment techniques and different chemical compounds, particularly H_2S and sulfide solutions of $Na_2S \times 9H_2O$ and $(NH_4)_2S$, have been proposed to solve this problem. Already the first investigations showed that the treatment of III–V semiconductors in sulfide solutions removes the oxides and forms an adsorbed coating on the semiconductor surface consisting of sulfur atoms covalently bonded to the semiconductor.[1] The changes in the chemical structure of the surface cause changes in its electronic characteristics, viz., displacement of the surface Fermi level[2] and a decrease in the rate of surface recombination,[3] which, in turn, lead to improvement of the electric[4] and photoelectric characteristics of the semiconductor devices.[5]

Until now, the phenomena caused by sulfide treatment have been investigated most thoroughly for binary semiconductors, such as InP, GaP, InAs, and especially GaAs.[6–9] At the same time, the passivation of GaSb and its solid solutions has not been thoroughly investigated.[5,10] Nevertheless, the interest in these materials is attributable to their promising nature from the standpoint of creating optoelectronic devices (light sources and high-speed photodetectors) for the spectral range $2-5$ μm.[11–14] Unfortunately, the high chemical activity of the surfaces of these semiconductors leads to degradation of the characteristics of devices based on them.

It was recently shown in Refs. 5 and 10 that the treatment of a GaSb surface in sulfide solutions during the fabrication of Schottky diodes made it possible to reduce the reverse dark current by an order of magnitude. In addition, the density of surface states reached the lowest known value for GaSb: $2-8\times10^{12}$ $cm^{-2}\cdot eV^{-1}$. However, the results of investigations on the influence of sulfide treatment for ternary and quaternary compounds based on GaSb are inconclusive.[10]

In the present paper we report the results of an experimental study of the influence of the treatment of sulfide solutions of Na_2S and $(NH_4)_2S$ on the electrical properties of the semiconductor compounds GaSb, GaInAsSb, and GaAlAsSb and structures based on them, which are used to fabricate photodiode heterostructures for the spectral range $1.5-2.5$ μm.

OBJECT OF INVESTIGATION

The photodiode structures investigated were created by liquid-phase epitaxy. Isoperiodic layers of the solid solutions n-type $Ga_{0.78}In_{0.22}As_{0.18}Sb_{0.82}$ and p-type $Ga_{0.66}Al_{0.34}As_{0.025}Sb_{0.975}$ were grown successively on (100) n-type GaSb substrates, which were doped with Te to a concentration equal to 1.8×10^{17} cm^{-3}. The mismatch between the lattice periods of the layers and the substrates $\Delta a/a$ determined by x-ray diffractometry did not exceed 6×10^{-4}. The chemical composition of each solid solution was determined on a JXA-5 Comebax x-ray microanalyzer. The composition indicated for the narrow-gap GaInAsSb solid solution (its gap width is $E_g=0.52$ eV) determines the long-wavelength sensitivity boundary of the photodiode at the 10% level: $\lambda=2.4$ μm. The GaAlAsSb layer ($E_g=1.2$ eV) serves as a broad-band ''window'' and is used to allow the effective entry of radiation into the structure. Mesa photodiodes with a diameter of the sensitive area equal to 300 μm were created by conventional plate photolithography.

EXPERIMENT

It was shown in Refs. 15 and 16 that not only removal of the oxides from the surface, but also etching of the crystal take place during the sulfide treatment of the surfaces of

 1063-7826/97/060556-04$10.00

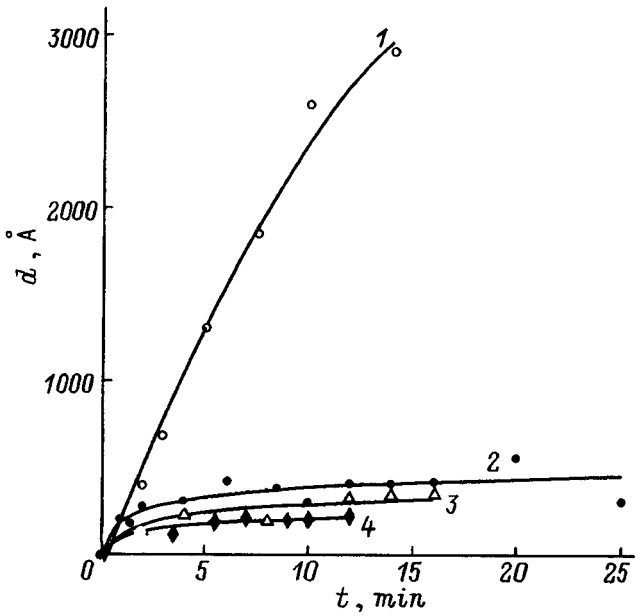

FIG. 1. Dependence of the etch depth d of GaSb on the treatment time t in 0.6-M (*1*, *3*) and 2.4-M (*2*, *4*) Na_2S solutions: *1*, *3* — *n*-GaSb; *2*, *4* — *p*-type GaSb.

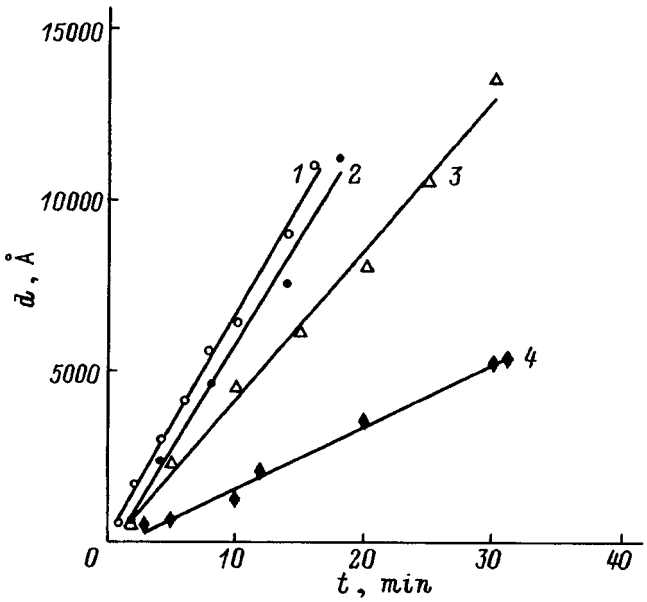

FIG. 2. Dependence of the etch depth d of GaSb on the treatment time t in$(NH_4)_2S$ solutions: *1* — *p*-type GaAlAsSb, *2* — *n*-type GaSb, *3* — *p*-type GaSb, *4* — *p*-type GaInAsSb.

semiconductors like GaAs. These data indicate that an etching phase (with different dynamics for each of the layers) can exist during the sulfide passivation of the multilayer structures investigated and that the etching can result in distortion of the profile of the mesa structure and, as a consequence, in degradation of the electrical characteristics of the devices. Therefore, in the initial stage of this research we had to determine the nature of the physicochemical processes taking place on the (100) GaSb surface and each epitaxial layer individually. For this purpose, experiments were performed on *n*-type GaSb(100) substrates doped with Te to a density $n=1.8\times10^{17}$ cm^{-3} and on *p*-type GaSb(100) substrates, which were not intentionally doped, with a density $p=1.0-1.4\times10^{17}$ cm^{-3}, as well as on solitary layers of GaInAsSb solid solutions with the densities $n,p=5-10\times10^{16}$ cm^{-3} or GaAlAsSb solid solutions with $p=5\times10^{18}$ cm^{-3} specially grown on GaSb(100) substrates.

To detect etching phenomena in the materials investigated and to determine the etch rate during the sulfide treatment, part of the original surface was covered by a SiO_2 layer, which protected it from contact with the solution. The etch rate of the materials was determined from the dependence of the etch depth on the holding time of the crystals in the solution. After the samples were held in the solution, the crystals were washed with deionized water and dried in a stream of nitrogen. Then the SiO_2 film was dissolved, and the etch depth was measured by a profilometer relative to the original surface. The treatment was performed using 0.6-M and 2.4-M solutions of Na_2S and 3.0-M solutions of $(NH_4)_2S$. The measured pH values were 13.6 and 13.9, respectively, for the sodium solutions and 9.2 for the ammonium solutions.

Figure 1 presents the results obtained when *n*- and *p*-type GaSb were treated in the 0.6-M and 2.4-M Na_2S solutions. It was found that the etching process is nonuniform in both solutions. The etch rate decreases with time. The etch rates for *n*-GaSb in both solutions are approximately the same in the initial stage of the treatment. However, the etching process ends very quickly in the saturated (2.4 M) solution. It should be noted that an etching effect is observed for *p*-type GaSb only under illumination by an incandescent lamp. At the same time, the dynamics of the etching of *p*-type GaSb are highly nonuniform in the 0.6-M solution and the 2.4-M solution.

The character of the etching of the surfaces of *n*- and *p*-type GaSb and the multicomponent compounds based on them in $(NH_4)_2S$ differs significantly from that observed in the Na_2S solutions (see Fig. 2). The dependence of the etch depth on the time for all the crystals is linear. However, the etch rates for each of the compounds investigated are different, the slowest etch rate being observed for the sample of *p*-type GaInAsSb. The etching of the *p*-type GaInAsSb and *p*-type GaAlAsSb samples in the ammonium solutions also depends on illumination. As the temperature rises, the etch rates increase severalfold.

The results obtained on the etching dynamics during the sulfide treatment served as a starting point for selecting the regimes for passivating the lateral surfaces of the *n*-GaSb/*n*-GaInAsSb/*p*-GaAlAsSb photodiode heterostructures.

One of the problems arising in working with photodiodes based on narrow-gap materials is associated with the high level of the reverse dark current. The sensitivity and the transmission band of photodiodes are known to increase considerably when they operate under a reverse bias. The limiting sensitivity of a photodiode is determined by its noise, whose level depends on the magnitude of the reverse dark current. Lowering the reverse current by an order of magnitude can be regarded as a significant achievement.

Our preliminary investigations on decreasing the dark

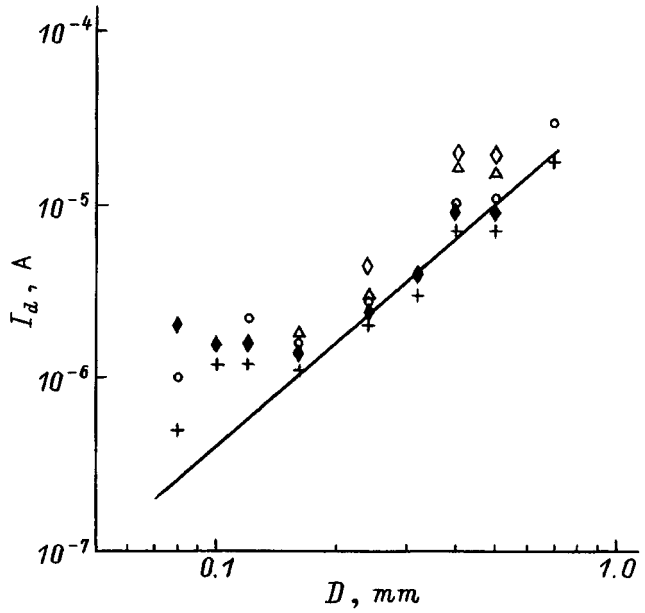

FIG. 3. Dependence of the reverse dark current I_d on the mesa diameter D of n-type GaSb/n-type GaInAsSb/p-type GaAlAsSb photodiode structures for a reverse bias $U=0.5$ V.

current by lowering the concentration in the active region and growing more perfect layers in GaSb/GaInAsSb/GaAlAsSb photodiode structures made it possible to attain values of the reverse dark current equal to $1-10\times10^{-6}$ A.[12,14] We previously employed protection of the lateral surfaces by the anodic oxide. Such protection made it possible to avoid the influence of the external medium on the surfaces of the photodiodes, but did not lead to significant improvement in their parameters.

Further progress in this direction can be achieved by diminishing the component of the dark current caused by the presence of surface leaks when the lateral surfaces of the mesa are passivated. The surface component of the dark current makes an appreciable contribution to the total leakage current of a photodiode structure. For example, a study of the dependence of the dark current on the diameter (D) of the mesa diode showed (see Fig. 3) that as D decreases from 1 to $0.2-0.3$ mm, the value of the dark current decreases in proportion to D^2 (in proportion to the area of the mesa), and then the dark current decreases in proportion to the diameter (the perimeter of the mesa); i.e., the contribution of the surface component of the current becomes significant.

An array of a hundred photodiodes of diameter 300 μm was arranged on semiconductor plates that had undergone photolithography. We investigated each of these photodiodes using a point-probe apparatus. The current-voltage characteristics of the diodes were measured. Figures 4a and 4b (curves *1*) present the results of the measurements of typical current-voltage characteristics of the photodiodes for two different plates which had undergone photolithography (K399 and K405). After the measurements were performed, each plate was split into parts, each of which contained at least $20-30$ devices. Then each of these parts of a plate was subjected to a separate treatment in sulfide solutions under different conditions. The current-voltage characteristics of

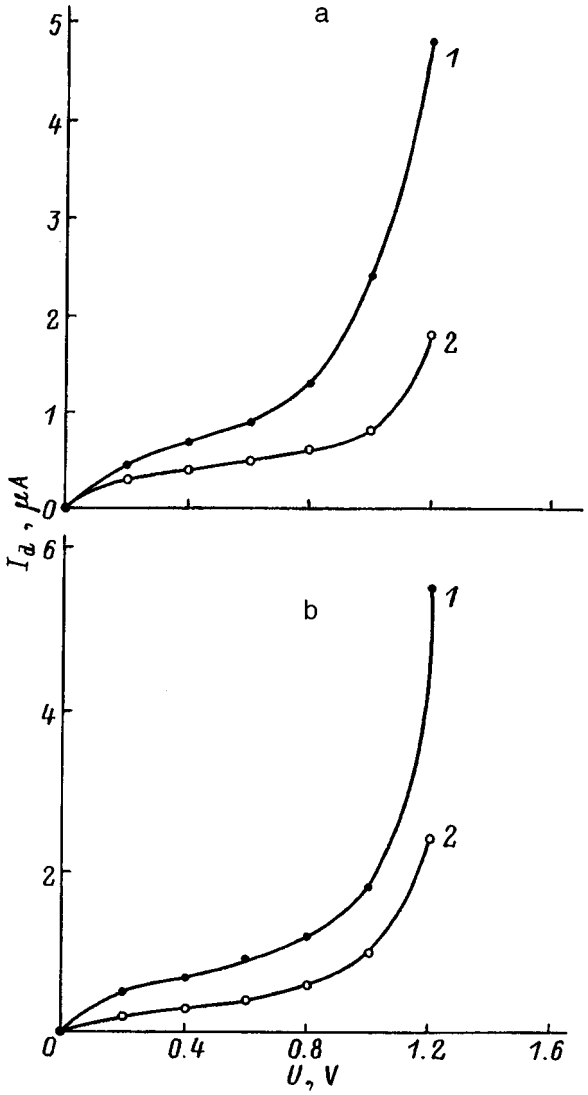

FIG. 4. Dark current-voltage characteristics of n-GaSb/n-GaInAsSb/p-GaAlAsSb mesa photodiodes before (*1*) and after (*2*) treatment in an aqueous sulfide solution of $(NH_4)_2S$: a — epitaxial plate K399, b — epitaxial plate K405.

the already passivated devices were measured again on the probe apparatus. Figure 4 (curves *2*) shows typical current-voltage characteristics for devices subjected to treatment in an aqueous solution of $(NH_4)_2S$. We note that these figures present the data from the investigation of the plates which provided the best results with respect to the dark current.

As can be seen from the plots, after treatment in a sulfide solution of $(NH_4)_2S$, the dark current decreases $2-5$ fold (up to 10 fold in individual samples). When the diameter of the mesa is 300 μm, the dark current is less than 1 μA in the range of reverse biases $0-1$ V. It can be concluded, therefore, that our proposed treatment in ammonium sulfide solutions altered the state of the surface in such a way that it caused a decrease in the surface component of the current.

DISCUSSION OF THE RESULTS AND CONCLUSIONS

The experimental data obtained indicate that an etching phase is observed during the treatment of gallium antimonide and its multicomponent compounds in sulfide solutions.

1. When they are treated in either the unsaturated (0.6 M) and or the saturated (2.4 M) Na_2S solution, the etch rate of the crystals is nonuniform and decreases with time until the etching process stops. This points out the occurrence of a competing process, viz., adsorption, i.e, the formation of a passivating coating on the surface that protects the latter from further etching.

In the saturated (2.4 M) solution the etching stops in the first minutes of contact of the crystal surface with the solution; the difference between the etch depths of the *n*- and *p*-type semiconductors is significantly smaller than in the case of dilute Na_2S solutions.

2. In the $(NH_4)_2S$ solutions the character of the etching of surfaces of gallium antimonide and its solid solutions differs significantly from that observed in the Na_2S solutions. The etching of *n*- and *p*-type crystals is uniform, without slowing, and the values of the etch rates are approximately identical.

The treatment of materials based on GaSb in sodium and ammonium sulfide solutions is characterized not only by different etching dynamics, but also, as was shown in Ref. 17 in the case of GaAs, by different surface compositions and structures.

In $(NH_4)_2S$ solutions the (100) surface of the crystal is formed in a stationary etching regime by Ga atoms with SH groups adsorbed on them, while in the case of treatment in Na_2S solutions the (100) surface is occupied predominantly by As atoms, which initially adsorb SH groups. Subsequently, the SH groups are replaced by sulfur atoms as a result of the adsorption of a S^{-2} anion with the formation of a S–As–S bridging bond. We suggest that qualitatively identical processes take place in the case of GaSb. However, because of the smaller energy of the S–Sb–S bond compared with the S–As–S bond, the rate of the replacement of SH groups by sulfur adatoms is appreciably higher, as is confirmed by the etching dynamics in the saturated solutions (Fig. 1). It should be noted that the etch depth of the GaSb crystals is smaller than that of GaAs. This is evidence that the etching process takes place only in the first moment of contact between the surface of a GaSb crystal and a Na_2S solution and is then suppressed very rapidly due to the formation of a passivating coating.

At the same time, the attempts to treat multilayer GaInAsSb/GaAlAsSb mesa structures in Na_2S solutions did not lead to a decrease in the reverse currents, possibly because of the appearance of an energy level in the band gap of GaSb due to an Sb–S bond, which can serve as a channel for surface currents.

We note that the treatment of multilayer mesa structures in ammonium is also associated with certain difficulties, since the rate-limiting step in the etching of GaSb is the dissolution of gallium hydroxide, which passes into solution only by interacting with $(NH_4)OH$ to form the $[Ga(NH_3)_6]^{-3}$ cationic complex. In the case of GaInAsSb solid solutions the dissolution rate decreases significantly because of the low solubility of indium hydroxide $In(OH)_3$ in alkaline ammonium solutions.

Ignoring the difference between the etch rates of the different solid solutions can lead to the appearance of microsteps on the lateral surfaces of the mesa photodiodes during passivation, which can have an unfavorable effect on the current-voltage characteristics of the devices.

In conclusion, we wish to note that the first results that we obtained on the passivation of the surfaces of multilayer *n*-type GaSb/*n*-GaInAsSb/*p*-type GaAlAsSb mesa photodiode structures attest to the prospects of using this method. The first experiments demonstrated a nearly 10-fold decrease in the reverse dark current. However, the problem of the stability of such coatings, their durability, and degradation of the characteristics of the passivated devices calls for a separate investigation.

We thank Dr. T. Piotrowski from the Institute of Electronic Engineering (Warsaw, Poland) for taking an interest in this work and for several useful discussions.

[1] A. M. Green and W. F. Spicer, Vac. Sci. Technol. A **11**, 1061 (1993).
[2] V. L. Berkovits, V. N. Bessolov, T. V. L'vova, E. B. Novikov, V. I. Safarov, R. V. Khasieva, and B. V. Tsarenkov, J. Appl. Phys. **70**, 3707 (1991).
[3] T. Ohno and K. Shiraishi, Phys. Rev. B **42**, 11 194 (1990).
[4] C. J. Sandroff, R. N. Nottenburg, J.-C. Bischoff, and R. Bhat, Appl. Phys. Lett. **51**, 33 (1987).
[5] A. G. Milnes and A. Y. Polyakov, Solid–State Electron. **36**, 803 (1993).
[6] T. K. Paul and D. M. Bose, J. Appl. Phys. **70**, 7387 (1991).
[7] H. Oigawa, J. F. Fan, Y. Nannichi, H. Sugahara, and M. Oshima, Jpn. Appl. Phys., **30**, L322 (1991).
[8] Yu. A. Kudryavtsev, E. B. Novikov, N. M. Stus, and E. A. Chaikina, Sov. Phys. Semicond. **26**, 975 (1992).
[9] Z. H. Lu, X. H. Feng, and B. X. Yang, Appl. Phys. Lett. **62**, 2932 (1993).
[10] A. Y. Polyakov, M. Stam, A. G. Milnes, A. E. Bochkarev, and S. J. Peatron, J. Appl. Phys. **71**, 4411 (1992).
[11] M. P. Mikhailova and A. N. Titkov, Semicond. Sci. Technol. **9**, 1279 (1994).
[12] I. A. Andreev, M. A. Afrailov, A. N. Baranov, V. G. Danil'chenko, M. A. Mirsagatov, M. P. Mikhailova, and Yu. P. Yakovlev, Sov. Tech. Phys. Lett. **12**, 542 (1986).
[13] I. A. Andreev, M. A. Afrailov, A. N. Baranov, M. A. Mirsagatov, M. P. Mikhailova, and Yu. P. Yakovlev, Sov. Tech. Phys. Lett. **14**, 435 (1988).
[14] I. A. Andreev, M. A. Afrailov, A. N. Baranov, S. G. Konnikov, M. A. Mirsagatov, M. P. Mikhailova, O. V. Salata, V. E. Umansky, G. M. Filaretova, and Yu. P. Yakovlev, Sov. Tech. Phys. Lett. **15**, 71 (1989).
[15] V. L. Berkovits, V. M. Lantratov, T. V. L'vova, G. A. Shakiashvili, V. P. Ulin, and D. Paget, Semiconductors **28**, 260 (1994).
[16] J.-W. Seo, T. Koker, S. Agarwala, and I. Adesida, Appl. Phys. Lett. **60**, 1114 (1992).
[17] V. L. Berkovits, A. O. Gusev, V. M. Lantratov, T. V. L'vova, D. Paget, A. B. Pushnyi, and V. P. Ulin, Phys. Low-Dimens. Struct. **12**, 293 (1995).

Translated by P. Shelnitz

Radiative recombination on the interface in a *p*-GaInAsSb/*p*-InAs type-II (broken-gap) heterostructure upon pulsed excitation

N. L. Bazhenov, G. G. Zegrya, M. P. Mikhaĭlova, K. D. Moiseev, V. A. Smirnov, O. Yu. Solov'eva, and Yu. P. Yakovlev

A. F. Ioffe Physicotechnical Institute, Russian Academy of Sciences, 194021 St. Petersburg, Russia
(Submitted March 13, 1996; accepted for publication September 10, 1996)
Fiz. Tekh. Poluprovodn. **31**, 658–661 (June 1997)

The electroluminescence appearing upon pulsed excitation in a solitary *p*-GaInAsSb/*p*-InAs type-II (broken-gap) heterostructure is investigated at $T=77$ K. It is shown that just as in the case of excitation by a constant current, two emission bands with maxima corresponding to 384 and 311 meV, respectively, are observed in the spectra. The half-widths of the emission bands equal 18–19 meV. Time-resolved spectroscopy is used to evaluate the relaxation time of the nonequilibrium carriers, which amounts to 6–7 μs. The emission spectrum is calculated on the basis of the Kane model, and the radiative recombination time is estimated. The theoretical estimates are in reasonable agreement with experiment. © *1997 American Institute of Physics.* [S1063-7826(97)00406-7]

1. INTRODUCTION

Electroluminescence (EL) was recently discovered and investigated in a solitary *p*-GaInAsSb/*p*-InAs type-II (broken-gap) heterojunction upon excitation by a constant current.[1,2] As was shown, the electroluminescence mechanism in this $p-p$ heterostructure is based on the recombination of electrons and holes located in self-consistent quantum wells on opposite sides of the interface.[1]

In the present work the electroluminescence appearing upon pulsed excitation in a *p*-GaInAsSb/*p*-InAs heterostructure was investigated further to refine the shape and position of the spectral lines, as well as to evaluate the characteristic relaxation times and to refine the mechanism of recombination on a type-II interface. A theoretical analysis of the rate of radiative and Auger recombination was performed, and the emission line shape was investigated.

2. EXPERIMENTAL METHOD AND SAMPLES

Solitary GaInAsSb/InAs heterostructures were obtained by using liquid-phase epitaxy (LPE) to grow layers of the solid solution on a *p*-InAs(100) substrate doped with zinc (5×10^{16} cm^{-3}). The epitaxial wide-gap layer of the solid solution $Ga_{1-x}In_xAs_ySb_{1-y}$ ($x=0.17$, $y=0.22$) of thickness 2 μm was isoperiodic to the substrate to within $\Delta a/a=2\times10^{-4}$. The solid-solution layer was also doped with Zn to a concentration $p=10^{18}$ cm^3. According to the photoluminescence data, the gap width of the solid solution at $T=77$ was $E_g=0.630$ eV.[1]

The measurements were performed in a pulsed regime at $T=77$ K. The current pulses had a rectangular form, their duration was between 0.1 and 100 μs, and the repetition rate was 10^2-10^3 Hz. A negative potential was applied to the narrow-gap semiconductor *p*-type InAs, which is positive toward wide-gap *p*-GaInAsSb. The current pulses passing through the sample and the voltage applied to the structure were recorded separately. The radiation was directed by a special optical system into an MDR-23 monochromator with a 150 line/mm grating and recorded by an InSb photoresistor using a BCI-280 pulsed synchronous detector, in which the gate length could be varied from 10 ns to 10 μs.

3. EXPERIMENTAL RESULTS AND DISCUSSION

Figure 1 presents the EL spectra for a solitary *p*-type GaInAsSb/*p*-type InAs heterostructure recorded at 77 and 100 K with a pulse duration of 10 μs and a repetition rate of 1 kHz. The current through the sample during a pulse was equal to 0.25 A. As is seen from Fig. 1, the EL spectrum contains two well separated emission bands, the energy distance between the maxima amounting to $\sim$70 meV. At 77 K the energy positions of the band maxima are $h\nu_1=311$ meV and $h\nu_2=384$ meV, and the full width at half-maximum (FWHM) equals 18–19 meV. The intensity of the short-wavelength emission band is approximately four times greater than the intensity of the long-wavelength band. When the temperature is increased from 77 to 100 K, both maxima are shifted 2–3 meV toward longer wavelengths, and slight broadening of the spectral lines occurs. In addition, when the temperature is increased, a relative increase in the intensity of the long-wavelength emission band is observed.

When the duration of the current pulses is decreased from 10 to 0.1 μs, no significant change in the shape or position of the lines is observed in the electroluminescence spectrum. Therefore, the filling time of the quantum levels cannot exceed 0.1 μs.

Figure 2 presents plots of the dependence of the energy position of the maxima of the two emission bands on the duration of the current pulse passing through the heterostructure. The measurements were performed in the following manner: as the pulse duration was varied, the emission was recorded using a gating pulse with a duration of 1 μs, which was positioned at the end of the current pulse. The shift of both maxima of the emission bands toward longer wavelengths attests to heating of the sample during passage of the current. The luminescence line shape was subsequently ana-

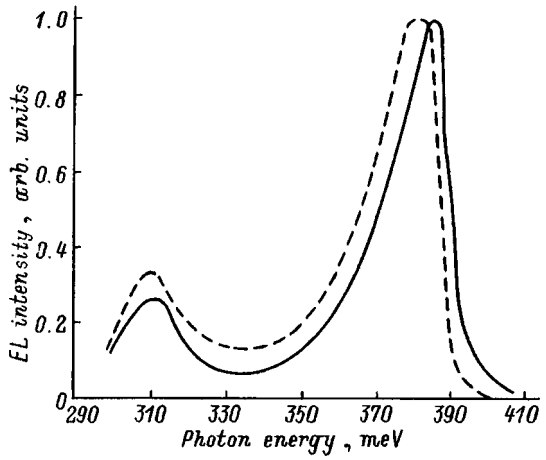

FIG. 1. Electroluminescence spectra at $T=77$ K (solid line) and $T=100$ K (dashed line).

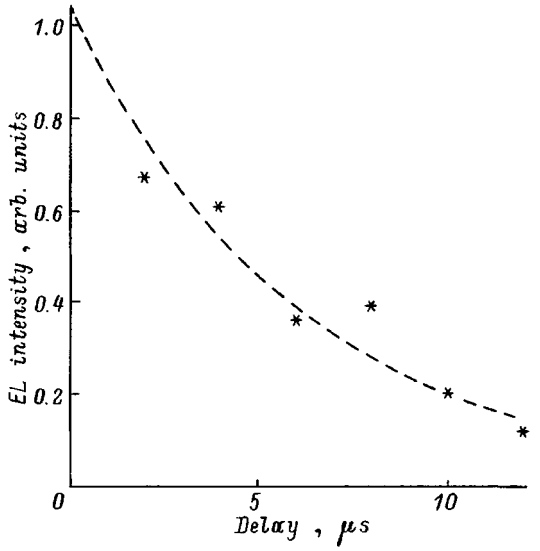

FIG. 3. Dependence of the intensity of the short-wavelength emission band on the time elapsed after the current through the heterojunction was switched off.

lyzed with pulse durations that ruled out heating of the sample.

Time-resolved spectroscopy was used to experimentally evaluate the recombination time of the nonequilibrium charge carriers. Figure 3 presents the dependence of the intensity of the short-wavelength emission band on the time that has elapsed since the current through the heterojunction was switched off. As is seen from Fig. 3, the intensity is reduced by a factor of e approximately 6 μs after the current is interrupted. This value corresponds to the recombination time.

Our interpretation of the experimental data was based on the mechanism for electroluminescence in a type-II (broken-gap) $p-p$ heterostructure proposed in Ref. 1. Figure 4 presents an energy diagram of a heterojunction for the case in which a negative potential is applied to the narrow-gap semiconductor p-InAs and a positive potential is applied to the wide-gap component p-GaInAsSb (a reverse-biased structure). Under the action of the applied electric bias, electrons can tunnel from the narrow-gap semiconductor to levels localized in the quantum well and then effectively recombine with holes from the wide-gap semiconductor.

We calculated the energy spectrum for the p-GaInAsSb/p-InAs heterostructure in a quasiclassical approximation. The quantum well for the electrons on the p-InAs side of the interface was deep and narrow, and its shape is described by the potential $u(x)=(\beta x)^{1/4}$, where $\beta=8.3\times10^{-3}$ eV^4/cm. An estimate of the position of the electron levels in the quantum well gave $E_1\approx247$ meV and $E_2\approx315$ meV. The quantum well for the holes is wider, and the energy of the corresponding local level is $E_h\approx50$ meV.

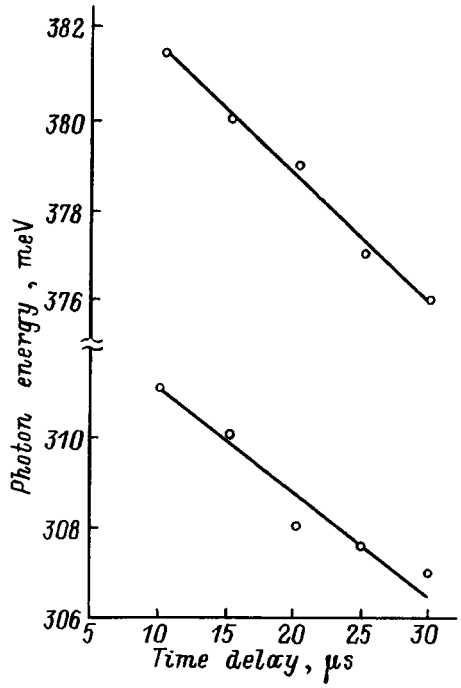

FIG. 2. Dependence of the energy position of the emission band maxima on the duration of the current pulse passing through the heterostructure.

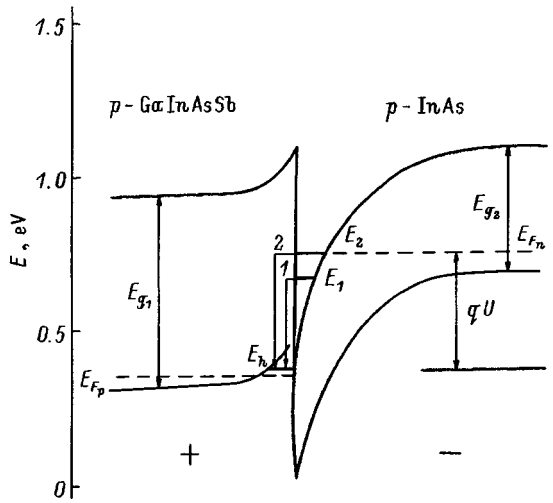

FIG. 4. Energy diagram of a reverse-biased heterojunction.

As the analysis showed, the main contribution to the optical matrix element is made by a narrow region near the interface. The matrix element is therefore virtually independent of the shape of the potential wells for the electrons and holes and depends only on the heights of the potential barriers ΔE_c and ΔE_ν. Therefore, to estimate the rate of radiative recombination we adopted a model of rectangular wells for the electrons and holes. The wave functions of the carriers were calculated in a simple multiple-band approximation, viz., the Kane model with a vanishingly small spin-orbit interaction. In this case for the rate of radiative recombination we have[3]

$$R=\frac{\pi\varepsilon_\infty}{\sqrt{\chi_0}}\frac{e^2}{c}E_g^*\frac{E_g^*}{m_c c^2}\frac{np}{m_c\Delta E_c}\frac{T}{\Delta E_c}\frac{m_h}{m_c}, \tag{1}$$

where E_g^* is the effective gap width (the distance between the quantum levels of the electrons and holes), ΔE_c is the height of the interface barrier for electrons, and n and p are the two-dimensional densities of the electrons and holes in the quantum wells. The remaining notation is conventional.

The following parameters of the structure were used to estimate the rate of radiative recombination at $T=77$: $n=p=3\times10^{11}$ cm^{-2}, $m_c=0.023m_0$, $m_h=0.41m_0$, $\varepsilon_\infty=11.6$, and $\chi_0=14.5$. The height of the interface barrier for electrons is $\Delta E_c=0.38eV$, and the effective gap width for the second electron level is $E_g^*=380$ meV. Then, according to (1), for the radiative recombination rate we obtain the value $R=2\times10^{18}$ cm$^2\cdot$s^{-1}.

We also theoretically estimated the radiative recombination time for electrons at the interface. According to (1), the reciprocal radiative recombination time for electrons has the form

$$\frac{1}{\tau_R}=\frac{R}{n}. \tag{2}$$

Therefore, the radiative recombination time for electrons from the second level E_2 is $\tau_{R2}=1.8\times10^{-7}$ s. For the first level $E_g^*=310$ meV, and $\tau_{R1}=2.0\times10^{-7}$ s. Thus, the radiative recombination time increases as the effective gap width E_g^* decreases.

The Auger recombination rate behaves in a totally different way. According to Ref. 3, the Auger recombination rate in type-II heterostructures can be represented in the form

$$G=32\sqrt{2}\pi^2\frac{E_B}{h}\frac{T^2}{E_cE_g^*}\frac{m_h^2}{m_c^2}n^2p\frac{\chi\lambda_g^9}{a^2b}\cos^4\frac{ka}{2}\left(\frac{3E_c-E_\nu}{4E_c}\right)^2, \tag{3}$$

where a and b are the quantum-well widths for electrons and holes, respectively, $E_B=m_ce^4/(2h^2\chi_0^2)$ is the Bohr electron energy, $k^2=2m_cE_{\rm gr}/h^2$, $\chi^2=\{2m_c(E_c-E_{\rm gr})/h^2\}$, $E_{\rm gr}$ is the energy of the electron size-quantized ground-state level, and $\lambda_g=h/(2m_cE_g^*)^{1/2}$. Thus, the Auger recombination rate is a function of the gap width E_g^*, i.e., $G\sim E_g^{*-11/2}$, and the radiative recombination rate is an increasing function of E_g^*, i.e., $R\sim E_g^{*2}$. The Auger recombination rate from the second level is smaller than the rate from the first. In fact, a calculation according to (3) gives $\tau_{A2}=1.4\times10^{-7}$ s and $\tau_{A1}=4.5\times10^{-8}$ s. Therefore, the carrier lifetime is controlled by two recombination processes, viz., radiative and Auger recombination: $1/\tau_\Sigma=1/\tau_R+1/\tau_A$.

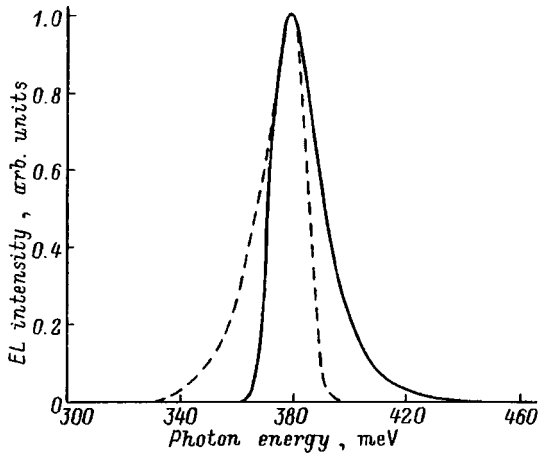

FIG. 5. Short-wavelength luminescence line: solid line – calculation; dashed line – experiment.

We theoretically analyzed the EL line shape. It was found that the shape of the short-wavelength luminescence line closely conforms to the Gaussian line shape (Fig. 5). However, it is noteworthy that, while the short-wavelength edge of the EL line is steeper in the experiment, the long-wavelength edge on the calculated curve obtained within the model described is steeper. Therefore, elucidation of the EL line broadening mechanism is a separate problem. Additional investigations, both theoretical and experimental, are needed to resolve it.

4. CONCLUSIONS

In this study we have investigated the EL spectra of a solitary p-GaInAsSb/p-InAs heterostructure in pulsed electric fields. The experimental data obtained can be explained using a model of the radiative recombination of electrons localized in a self-consistent quantum well on the p-InAs side of the interface. The experimentally obtained EL relaxation times ($\tau\sim6\times10^{-6}-7\times10^{-6}$ s) do not contradict the tunneling mechanism for filling the quantum-well levels with electrons. The theoretical evaluations of the radiative and Auger recombination times performed are in reasonable agreement with the experimental data.

We wish to thank Prof. V. I. Ivanov-Omskiĭ for participating in the discussion of the results and for offering some valuable comments.

This work was supported in part by the Russian Foundation for Fundamental Research (Grant No. 96-02-17841-a) and by the international association INTAS (Grant No. 94-0789).

[1] M. P. Mikhaĭlova, G. G. Zegrya, K. D. Moiseev, I. N. Timchenko, and Yu. P. Yakovlev, Fiz. Tekh. Poluprovodn. **29**, 686 (1995) [Semiconductors **29**, 357 (1995)].
[2] M. P. Mikhaĭlova, G. G. Zegrya, K. D. Moiseev, and Yu. P. Yakovlev, Solid–State Electron. **40**, 673 (1996).
[3] G. G. Zegrya and A. D. Andreev, Appl. Phys. Lett. **67**, 2681 (1995).

Translated by P. Shelnitz

Influence of charge carriers on tuning in InAsSb lasers

T. N. Danilova, O. I. Evseenko, A. N. Imenkov, N. M. Kolchanova, M. V. Stepanov, V. V. Sherstnev, and Yu. P. Yakovlev

A. F. Ioffe Physicotechnical Institute, Russian Academy of Sciences, 194021 St. Petersburg, Russia
(Submitted August 13, 1996; accepted for publication September 10, 1996)
Fiz. Tekh. Poluprovodn. **31**, 662–665 (June 1997)

Tuning of the output wavelength of 3.2 to 3.4-μm lasers with an InAsSb active layer and separate electron and optical InAsSbP confining layers is investigated. Displacement of the dominant mode toward shorter wavelengths by 3–5 Å during a current pulse is achieved at 78–100 K. This blue shift is attributed to a decrease in the refractive index due to an increase in the carrier concentration and lowering of the radiated intensity during the pulse. © *1997 American Institute of Physics.* [S1063-7826(97)00506-1]

1. Semiconductor lasers operating at 3.2–3.4 μm are of interest for diode laser spectroscopy, since they should make it possible to distinguish the fundamental absorption lines of many hydrocarbons, viz., methane, propane, acetone, ethylene, ether, benzene, methanol, etc. The required smooth tuning of the output wavelength has been discovered in double heterostructure lasers with a narrow-gap InAsSb layer and InAsSbP confining layers.[1–4] The observed increase in the wavelength during a current pulse was attributed in Refs. 1 and 2 to heating of the active region. When the current was increased continuously at a rate greater than the thermal relaxation rate,[4] the wavelength decreased at first. This behavior was attributed to an increase in the concentration of nonequilibrium charge carriers. Then the wavelength began to increase. In Ref. 4 the increase in the wavelength was attributed to self-focusing of the radiation due to an increase in the refractive index as the amplitude of the electromagnetic radiation increases.

In lasers with separate electron and optical confinement (separate-confinement lasers) the concentration of nonequilibrium carriers in the narrow-gap layer is greater than in double heterostructure lasers.[1] Therefore, a stronger influence of the concentration of nonequilibrium charge carriers on the tuning of the output wavelength would be expected in separate-confinement lasers.

In the present work we studied the tuning of the output wavelength of separate-confinement lasers during a current pulse.

2. Five-layer structures n-$InAs_{1-x-y}Sb_xP_y$ / n-$InAs_{1-x-y}Sb_xP_y$ /n-$InAs_{1-x}Sb_x$/ p-$InAs_{1-x-y}Sb_xP_y$ / p-$InAs_{1-x-y}Sb_xP_y$, with separate optical and electron confinement, were investigated (Fig. 1). In the narrow-gap layer x was between 0.035 and 0.06. In the electron confining layers $x=0.06$, and $y=0.1$. All the heterojunctions were of type I and had a valance-band offset $\sim$1.5 times larger than the conduction-band offset (Fig. 1c). The structures were grown by liquid-phase epitaxy on InAs substrates oriented in the (100) crystallographic plane. The narrow-band layer was not doped and had a thickness of about 1 μm. The density of the equilibrium electrons in it was 10^{16} cm^{-3}. The electron confining layers also had a thickness of about 1 μm. The n-type layers were doped with Sn to an electron density of 2×10^{17} cm^{-3}, and the p-type layers were doped with Zn to a hole density of 1×10^{18} cm^{-3}. The optical confining layers of thickness 2–3 μ were doped 4–5 times more strongly than were the electron confining layers. The lasers had a mesa-stripe design with a stripe width equal to 20 μm. The cavity length was 270–350 μm.

3. Let us examine the measurement results. When a rectangular current pulse above the threshold value is supplied to the laser (Fig. 2a), the output intensity decreases during the pulse (Fig. 2b, dashed curves). When an external cavity is introduced, the output intensity is modulated sinusoidally (Fig. 2b, solid curves). The sinusoids appear because of the variation of the output wavelength, under which its value runs through the resonance values of a Fabry–Perot interferometer. During a time corresponding to one sinusoidal period, the wavelength λ varies by $\Delta\lambda$, which is specified by the expression

$$\Delta\lambda=\frac{\lambda^2}{2ln}, \tag{1}$$

where l is the length of the external cavity, and n is its refractive index. If the optical length of the interferometer is increased, the sinusoidal waves shift to the right on the screen (toward longer times) when λ increases and to the left when λ decreases. Increasing the optical length of the external cavity by turning it displaces the sinusoidal waves for the lasers investigated to shorter times. Therefore, the output wavelength decreases during the pulse. The sinusoidal period increases during the pulse and decreases with increasing current at a fixed time (Fig. 2b). Accordingly, the decrease in the output wavelength slows during the pulse (Fig. 3a).

The investigations at 80–100 K showed that the threshold current I_{th} increases rapidly with increasing temperature T according to a power law, $I_{th}\sim T^{\gamma}$, where $\gamma=3.5-4$. At 77–90 K single-mode lasing is usually observed in the range of currents from I_{th} to $2I_{th}$. When the temperature rises above 90 K, the range for single-mode lasing narrows sharply, its width tending to zero at 100 K. The predominance of a single mode is maintained in the temperature range 4–5 K. As the temperature rises, a longer-wavelength mode at a distance of one, two, or three intermodal distances

 1063-7826/97/060563-04$10.00

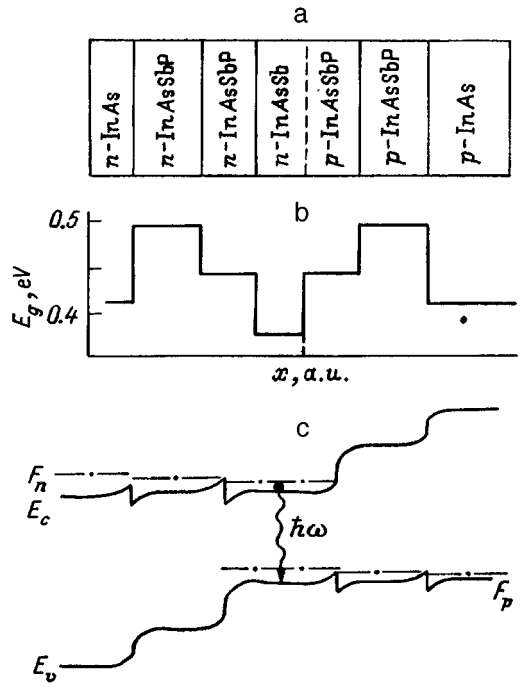

FIG. 1. Schematic representation of the layers in the laser structure (a), layer-by-layer distribution of the band-gap width (b), and energy diagram of the laser in the working regime.

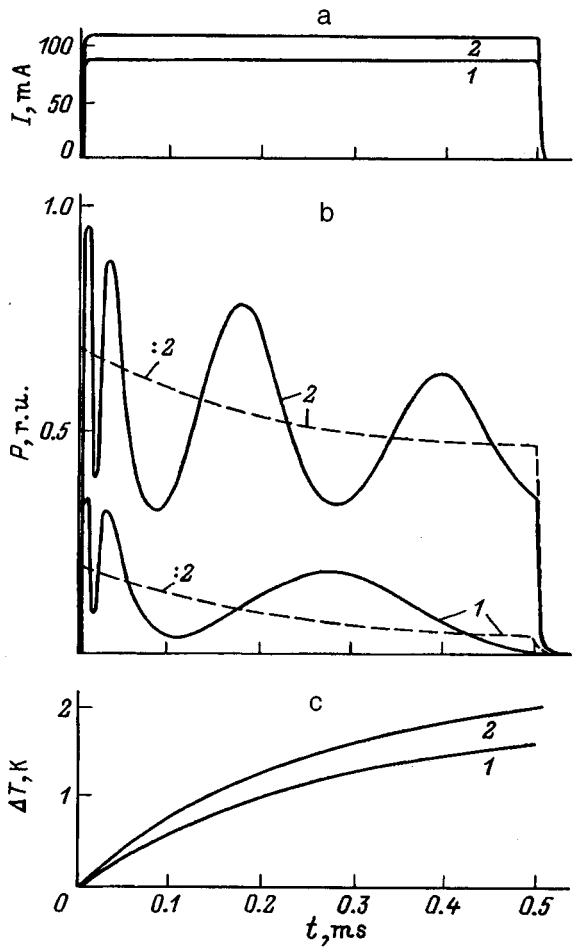

FIG. 2. Oscillograms of current pulses (a) and the radiated intensity P (b) with (solid curves) and without (dashed curves) an external cavity at various currents, mA: *1* — 90, *2* — 110. The temperature is 79 K. The threshold current is 82 mA. The length of the external Si cavity is 11 mm. Calculated variation of the laser temperature during the current pulses (c).

becomes dominant. The mean rate of displacement is ~20 Å/K. When the temperature increases, the working current increases in the single-mode regime due to the increase in the threshold current I_{th}. The variation of the wavelength during the pulse accelerates accordingly (Fig. 3b). The total change in the wavelength during the pulse amounts to 3–5 Å (0.3–0.5 cm^{-1}).

The half-width of the radiation pattern in the plane of the $p-n$ junction decreases slightly from 13 to 10 deg as I/I_{th} increases from 1 to 2 (Fig. 4). The half-width of the radiation pattern in the plane perpendicular to the plane of the $p-n$ junction and to the plane of the mirror in the range of values of I/I_{th} from 1 to 1.4 equals 40 deg and then decreases to 35 deg as I/I_{th} increases to 2.

4. Let us analyze the experimental results. The drop in the radiated intensity P during the current pulse (Fig. 2) attests to heating of the active region of the laser. If the dependence of the threshold current I_{th} on the temperature T is represented by the power law $I_{\text{th}} \sim T^{\gamma}$ and the differential quantum efficiency is assumed to be independent of the temperature, the increment of the laser temperature ΔT can be expressed in terms of the change in the radiated intensity P by the formula

$$\Delta T = -\frac{\Delta P}{P\gamma}\left(\frac{I}{I_{\text{th}}}-1\right)T. \tag{2}$$

As a calculation for $\gamma=4$ using Eq. (2) shows (Fig. 2c), the active region of the laser is heated during the pulse by ~2 K. The heating rate decreases during the pulse. Therefore, the rate of variation of the wavelength also decreases (Fig. 3).

Since the coefficient of linear thermal expansion of III–V compounds and their solid solutions is extremely small at temperatures near 78 K, the change in wavelength $\Delta\lambda$ is naturally related to the change in the refractive index Δn upon heating:

$$\Delta\lambda = \frac{\lambda}{n}\Delta n. \tag{3}$$

The susceptibility of the lattice and the valence electron produces an increase in the refractive index n_r with increasing temperature,

$$\frac{dn_r}{dT} \cong -\frac{n}{4E_g}\frac{dE_g}{dT}. \tag{4}$$

Therefore, it cannot express the decrease in the wavelength during a current pulse.

However, the threshold carrier density N_{th} and the depth of the Fermi level in the conduction band F_{th} increase with increasing temperature. The decrease in the interband absorption due to the increase in F_{th} lowers the refractive index in accordance with the Kramers–Kronig relation and makes a contribution to the decrease in the output wavelength. A somewhat smaller contribution of the same sign, which is governed by the increase in N_{th}, is made by the susceptibil-

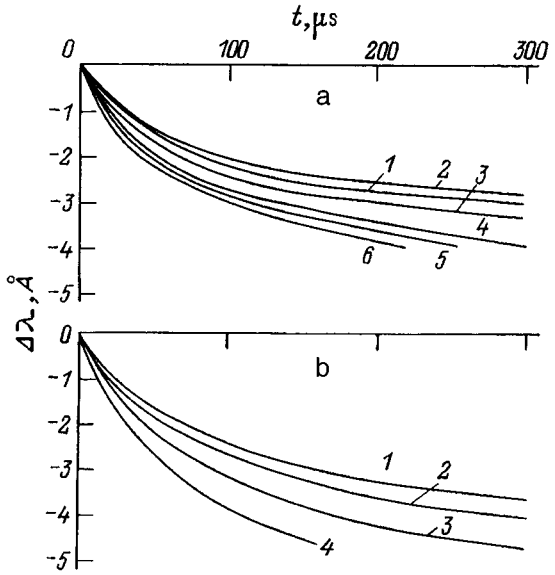

FIG. 3. Variation of the wavelength of the dominant laser mode during a current pulse. a – At a fixed temperature ($T=79$ K, $I_{th}=82$ mA) and various currents, mA: *1* — 90, *2* — 110, *3* — 130, *4* — 140, *5* — 150, *6* — 160. b — At a fixed ratio of I to I_{th} ($I/I_{th}=1.3$) and various temperatures, K: *1* — 78, *2* — 88, *3* — 92, *4* — 100.

ity of the electron-hole plasma. The contributions of the other phenomena are estimated to be considerably smaller. An increase in the radiated intensity, as well as an increase in the carrier concentration, should lower the refractive index.

For systematic quantitative evaluations we integrate the Kramers–Kronig relation without allowance for the erosion of the Fermi function after expressing the dependence of the absorption coefficient of the unexcited semiconductor on the difference between the photon energy $\hbar\omega$ and the band-gap width E_g by the formula $\alpha=A(\hbar\omega-E_g)^{1/2}$. When the coefficient A is independent of $\hbar\omega$, we obtain the change in the refractive index n_α:

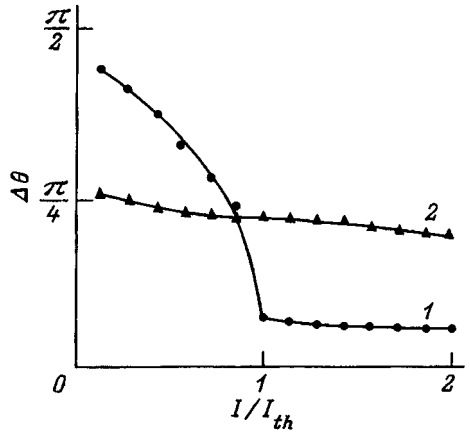

FIG. 4. Dependence of the half-width of the radiation pattern in the plane of the $p-n$ junction (*1*) and in the plane perpendicular to it and to the plane of the mirror (*2*) on the current. $T=79$ K.

$$n_\alpha=-\frac{cA\sqrt{F_{th}^*+\Delta E_g}}{\pi\omega_L}\times\left(1-\sqrt{\frac{-\Delta E_g-E_L}{F_{th}^*+\Delta E_g}}\ \arctan\ \sqrt{\frac{F_{th}^*+\Delta E_g}{-\Delta E_g-E_L}}\right), \tag{5}$$

where c is the velocity of light, $F_{th}^*=F_{th}(1+m_e/m_p)$, m_e and m_p are the effective electron and hole masses, respectively, ΔE_g is the change in the band-gap width due to excitation, $E_L=\hbar\omega\lesssim -E_g$, ω_L is the frequency of the laser emission, and $E_L<|\Delta E_g|<F_{th}$. In accordance with Ref. 5, we have

$$\Delta E_g=-\frac{2\sqrt{\pi}e^3\sqrt{2N_{th}}}{n^3(F_{th}+kT)^{1/2}}, \tag{6}$$

where e is the electron charge, and k is the Boltzmann constant. Differentiating (6) with respect to the temperature T and disregarding the weak dependence of ΔE_g on T, we obtain

$$\frac{dn_\alpha}{dT}=-\frac{cA\sqrt{F_{th}^*+\Delta E_g}}{2\pi\omega_L T}\left(1-\frac{E_L}{F_{th}^*}\right)^{-1}. \tag{7}$$

We express the contribution of the susceptibility of the plasma in accordance with Ref. 6 by the formula

$$\frac{dn_p}{cT}=-\frac{2\pi e^2}{n\omega_L^2}\left(\frac{1}{m_e}+\frac{1}{m_p}\right)\frac{dN_{th}}{dT}. \tag{8}$$

Within the ideas in Ref. 6 we can obtain an expression for the change in the refractive index Δn during a current pulse

$$\Delta n=\Delta T\left\{\frac{dn_r}{dT}+\left(\frac{dn_\alpha}{dT}+\frac{dn_p}{dT}\right)\times\left[1+\frac{\gamma}{r}\left(\frac{N_{th}}{N_0}-1\right)\left(\frac{I}{I_{th}}-\frac{N_0}{N_{th}}\right)^{-1}\right]\right\}, \tag{9}$$

where N_0 is the carrier density at the population-inversion threshold, and r is the exponent in the expression describing the temperature dependence of the threshold density ($N_{th}\sim T^r$). The second term in the square brackets in expression (9) is related to the decrease in the radiated intensity during the pulse. When radiative recombination dominates, it equals unity, if the current I is close to I_{th}, and decreases rapidly with increasing current. In the case of predominant impact recombination $\gamma>r$; this term attains the value $\gamma/r=3$ when the current slightly exceeds the threshold, but it decreases with increasing current, becoming equal to unity, when the current exceeds the threshold by 5–10%. It should be noted that in a real laser the dependence of the magnitude of this term on the current is smooth, since the photon density in it varies across the width of the stripe.

Experimentally, when the current exceeds the threshold by a small amount (Fig. 3a, curves *1* and *2*), the slowing of the decrease in the wavelength during the pulse as the current is increased is appreciable. When the amount by which the threshold is exceeded is increased, the slowing gives way to acceleration due to the increase in the scattering power. Ap-

parently, in the lasers investigated the current dependence of the influence of the radiated intensity on the refractive index is not as strong as would be expected according to Eq. (9). In addition, masking of this dependence as a result of the defocusing of the radiation in the plane of the $p-n$ junction (Fig. 4) and the focusing in the perpendicular planes is possible.

The quantitative evaluations show that without the influence of the radiated intensity on the refractive index, the output wavelength should have only increased during the pulse. A decrease in the carrier concentration in the narrow-gap layer, for example, in the case of deepening of the interface potential wells, would have produced the same effect.

Thus, the blue shift of the laser modes during a current pulse in lasers with separate optical and electron confinement is caused by the high concentration of nonequilibrium charge carriers in the narrow-gap layer and the influence of the charge carriers and the radiated intensity on the refractive index of the active medium.

This work was supported by Copernicus contract No. CIPA-CT 94-158, as well as by a grant from the Ministry of Science of the Russian Federation as part of the Optics and Laser Physics Program.

[1] A. N. Baranov, T. N. Danilova, O. G. Ershov, A. N. Imenkov, V. V. Sherstnev, and Yu. P. Yakovlev, Pis'ma Zh. Tekh. Fiz. **18**, 6 (1992) [Sov. Tech. Phys. Lett. **18** (11), 725 (1992)].
[2] Yu. P. Yakovlev, A. N. Baranov, A. N. Imenkov, V. V. Sherstnev, E. V. Stepanov, and A. Ya. Ponurovskiĭ, Kvantovaya Elektron. **20**, 839 (1993) [Quantum Electron. **23**, 726 (1993)].
[3] A. N. Baranov, A. N. Imenkov, V. V. Sherstnev, and Yu. P. Yakovlev, Appl. Phys. Lett. **64**, 2480 (1994).
[4] T. N. Danilova, O. I. Evseenko, A. N. Imenkov, N. M. Kolchanova, M. V. Stepanov, V. V. Sherstnev, and Yu. P. Yakovlev, Pis'ma Zh. Tekh. Fiz. **16**, 7 (1996) [Tech. Phys. Lett. **22**, 645 (1996)].
[5] V. M. Asnin and A. A. Rogachev, Fiz. Tverd. Tela (Leningrad) **5**, 1730 (1963) [Sov. Phys. Solid State **5**, 1257 (1963)].
[6] P. G. Eliseev and A. P. Bogatov, in *The Nonlinear Optics of Semiconductor Lasers (Proceedings of the Lebedev Physics Institute, Academy of Sciences of the USSR, Vol. 166)*, N. G. Basov (ed.), Nova Science, Commack, N.Y. (1987) [Russ. original, Tr. Inst. Fiz. Inst. Akad. Nauk SSSR **166**, 15 (1986)].

Translated by P. Shelnitz

Depolarization and photoionization effects in quantum wells

A. G. Petrov and A. Ya. Shik

A. F. Ioffe Physicotechnical Institute, Russian Academy of Sciences, 194021 St. Petersburg, Russia
(Submitted August 15, 1996; accepted for publication September 16, 1996)
Fiz. Tekh. Poluprovodn. **31**, 666–669 (June 1997)

The influence of depolarization effects on the intersubband optical absorption spectra of quantum wells is investigated theoretically. In general, the matrix elements of the corresponding transitions are determined from the solution of a system of integral equations. For wells containing a bound or quasibound state with a small energy, the problem is simplified significantly and reduces to a system of algebraic equations that permit finding the matrix elements in an explicit form. It is shown that the absorption spectrum coincides with the spectrum obtained without consideration of the depolarization for a quantum well of small depth or width. In particular, for wells with a shallow bound state the absorption peak caused by transitions to that state reaches the photoionization threshold as the doping level is increased. It then vanishes.
 [S1063-7826(97)00606-6]

1. INTRODUCTION

The effects of intraband optical absorption in quantum wells (QW's) due to transitions of carriers from localized levels to continuum states above the QW's have been the object of fairly vigorous experimental research in recent years, mainly because of the utilization of these effects to create a new type of detector of infrared radiation.[1] Numerous studies have been devoted to the theoretical investigation of the photoionization of QW's (see, for example, Refs. 2–6). At the same time, the important question of the influence of the depolarization effects at significant carrier concentrations in QW's on the photoionization kinetics and spectra has scarcely been studied. The situation here is considerably more complicated than in the case of a transition between two discrete levels, which was discussed, in particular, in Ref. 7. The character of the dependence of the absorption spectra on the carrier concentration in QW's was discussed in Refs. 8–10, but the approach employed there is highly approximate and the results obtained differ from the real picture not only quantitatively, but sometimes even qualitatively. In particular, one of the most serious omissions in the papers just cited is the disregard of the nonlocal character of the relation between the electric field and the polarization.

In the present study we attempt to more rigorously treat the photoionization spectra of QW's and some other closely related effects, which are associated with the depolarization phenomena in structures with a two-dimensional electron gas. The preliminary results of this study were published in Ref. 11.

2. BASIC EQUATIONS

Let us consider a quantum well of an arbitrary shape $U(z)$, assuming, in order to be specific, that $U(-\infty)=U(\infty)=0$ and that the approach of $U(z)$ to zero as $z\to\pm\infty$ is fairly rapid, i.e., at least exponential.[1)] Let there be N bound states with the energies $E_n<0$ and the wave functions $\psi_n(z)$ $(n=0,1,\ldots,N-1)$ in the QW. The continuum states above the QW are characterized by a continuous spectrum of energies $E>0$ and are described by the delocalized wave functions $\psi_E(z)$ with the normalization condition $\int\psi_E^*(z)\psi_{E'}(z)dz=\delta(E-E')$.

We shall restrict the discussion to the case of a not excessively high carrier density n_s, at which the carriers fill only the ground subband of the QW. We shall examine the intraband optical properties of the system that are caused by electronic transitions from the $n=0$ level to higher-lying states under the influence of light with a frequency ω, which is polarized along the z axis (a TM mode). The main characteristic which determines these properties and is subject to calculation is the optical matrix element $P_{\nu 0}=(ie/\omega)\int j_{\nu 0}^*(z)F(z)dz$, where ν is the quantum number of the final state (n or E, respectively, for localized and delocalized states), F is the intensity of the high-frequency electric field, and $j_{\nu 0}=(i\hbar/2m)[\psi_0(d\psi_\nu^*/dz)-(d\psi_0/dz)\psi_\nu^*]$ is the current of the respective transition.

The calculation of $P_{\nu 0}$ in the presence of depolarization is complex, because the true distribution of the electric field of light $F(z)$ is unknown and must be found self-consistently. Only F_0, i.e., the field strength at a sufficient distance from the layer of electrons, where they have no screening influence, can be considered assigned. At the same time, for z-polarized light the electric induction D is not dependent on z and equals $\varepsilon_\infty F_0$, where ε_∞ is the lattice dielectric constant. As for the field strength $F(z)$, in the quantum layers that we considered it is related to D in a nonlocal manner: $D(z)=\int_{-\infty}^{\infty}\varepsilon_{zz}(z,z')F(z')dz'$.

According to the expressions obtained in Ref. 12, for a two-dimensional quantum system the component of the nonlocal dielectric constant of interest to us can be written in the random-phase approximation in the form

$$\varepsilon_{zz}(z,z')=\varepsilon_\infty(z-z')-8\pi n_s e^2\hbar^3\times\left\{\sum_{n=1}^{N-1}\frac{j_{n0}(z)j_{n0}^*(z')}{(E_n-E_0)[\hbar^2\omega^2-(E_n-E_0)^2]}+\int_0^\infty\frac{j_{E0}(z)j_{E0}^*(z')dE}{(E-E_0)[\hbar^2\omega^2-(E-E_0)^2]}\right\}. \quad (1)$$

 1063-7826/97/060567-04$10.00

We multiply Eq. (1) by $F(z')j_{E0}^*(z)$ and integrate over z and z' in infinite limits. The result has the form

$$P_{E0}^0 = P_{E0} - \frac{8\pi n_s e^2 \hbar^3}{\varepsilon_\infty} \times \left\{ \sum_{n=1}^{N-1} \frac{P_{n0} \int_{-\infty}^{\infty} j_{n0}(z) j_{E0}^*(z')dz}{(E_n - E_0)[\hbar^2\omega^2 - (E_n - E_0)^2]} + \int_0^\infty \frac{P_{E'0} \int_{-\infty}^{\infty} j_{E'0}(z) j_{E0}^*(z')dz}{(E' - E_0)[\hbar^2\omega^2 - (E' - E_0)^2]} dE' \right\}. \quad (2)$$

Here $P_{E0}^0 = (ie/\omega)\int j_{E0}(z)F_0 dz$ is a standard matrix element in a uniform field, which is proportional to the momentum matrix element. Similarly, multiplication by $F(z')j_{n0}^*(z)$ followed by integration gives

$$P_{n0}^0 = P_{n0} - \frac{8\pi n_s e^2 \hbar^3}{\varepsilon_\infty} \times \left\{ \sum_{m=1}^{N-1} \frac{P_{m0} \int_{-\infty}^{\infty} j_{m0}(z) j_{n0}^*(z')dz}{(E_m - E_0)[\hbar^2\omega^2 - (E_m - E_0)^2]} + \int_0^\infty \frac{P_{E0} \int_{-\infty}^{\infty} j_{E0}(z) j_{n0}^*(z)dz dE}{(E - E_0)[\hbar^2\omega^2 - (E - E_0)^2]} \right\}. \quad (3)$$

Eliminating P_{n0} from the system consisting of (2) and (3), we obtain an integral equation for the matrix element P_{E0} describing the photoionization of the QW. When the equation is solved and P_{E0} is found, the matrix elements of the transitions between the discrete levels P_{n0} are already easily found from the system of linear equations (3). The problem just described is very complicated, but it can be handled for one particular, but important case, which is described below in Sec. 3.

As will be shown below, the depolarization effects play the most important role in a QW with near-resonant parameters, i.e., when there is a bound or virtual state with a near-zero energy in the QW. Therefore, we shall focus our attention on this case, especially since just such QW's are used to create photodetectors.

3. NEAR-RESONANT QUANTUM WELLS

The expression ''the near-resonant potential well $U(z)$'' means that it can be made resonant by slightly varying its depth and (or) width. In other words, the numbers β and γ, which differ slightly from unity and are such that the well $U_{\text{res}}(z) = \beta U(\gamma z)$ will be resonant, can be found. We introduce the auxiliary function $\chi(z)$, the zero-energy wave function for the resonant well $U_{\text{res}}(z)$, which obeys the condition $|\chi| = 1$ as $z \to \pm\infty$. We use it to define the parameter ρ, which is a numerical measure of the proximity of a QW to the resonant well,

$$\rho = (2\gamma - \beta - 1)m/\hbar^2 \int_{-\infty}^{\infty} dz |\chi(z)|^2 U_{\text{res}}(z) \quad (4)$$

(the multiplier following $2\gamma - \beta - 1$ is of the order of the reciprocal characteristic width of the QW). It can be shown that the choice of β and γ is not unique (resonance can be achieved by varying only the width or only the depth of the QW or by varying both in different proportions), but the value of ρ does not depend on this choice. It is a unique characteristic of the particular potential well, which has the meaning of the wave vector of a shallow bound state (when $\rho < 0$, it is a virtual state).

For near-resonant QW's, i.e., for small $|\rho|$, the basic equations of the problem consisting of (2) and (3) can be simplified appreciably by utilizing the fact that in a finite region of space of dimension $L \ll |\rho^{-1}|$ the wave function of a state with a near-zero energy is proportional to $\chi(z)$: $\psi_E(z) = C_E(\rho)\chi(z)$ if $E > 0$, and $\psi_N(z) = \sqrt{\rho}\chi(z)$ if $E < 0$, where

$$C_E(\rho) = \frac{\sqrt[4]{mE/2}}{\sqrt{\pi\hbar(E + \hbar^2\rho^2/2m)}}. \quad (5)$$

Now, in the wave functions which determine the transition matrix elements the dependence on the coordinate z and the energy E is separated. Hence it follows that

$$\int_{-\infty}^{\infty} j_{E'0}(z) j_{E0}^*(z)dz = \hbar^2/m^2 C_E(\rho) C_{E'}(\rho) J, \quad (6)$$

$$J = \int_{-\infty}^{\infty} \left| \psi_0 \frac{d\chi^*}{dz} - \frac{d\psi_0}{dz}\chi^* \right| dz.$$

As a result, the integral equation (2) is factored, and the system consisting of (2) and (3) reduces to a system of algebraic equations. Of course, approximate Eq. (6) is valid only for small values of $|E|$. However, for optical frequencies close to the photoionization threshold of the QW just these values make the decisive contribution to the integral, justifying our approximate approach.

4. ABSORPTION SPECTRUM

To be specific in the further calculations we assume that in the QW there is only one deep bound state, i.e., that the energy of the first excited level is close to zero. When $\rho < 0$, this means that the system contains only the ground-state level ψ_0 and continuum states. There are no interlevel transitions with the matrix elements P_{n0} in the system, and we have a single integral equation (2) with a degenerate kernel for determining P_{E0}. This easily solvable equation gives

$$P_{E0} = P_{E0}^0 \frac{\rho - i\sqrt{2mE}/\hbar}{\rho - \tilde{n} - i\sqrt{2mE}/\hbar}, \quad (7)$$

where the parameter $\tilde{n}$ is proportional to the two-dimensional carrier density n_s:

$$\tilde{n} = \frac{n_s \pi e^2 \hbar^2}{E_0^2 \varepsilon_\infty m} J. \quad (8)$$

When $\rho > 0$, there is another shallow level in the QW with the wave function $\psi_1 = \sqrt{\rho}\chi$, and there is a second equation (3) associated with it for determining P_{10}. However, the calculations show that Eq. (7) maintains its validity at not excessively large values of ρ.

As an example, let us consider two concrete types of QW's: a modified Poschl–Teller potential well $U(z)=-\hbar^2\alpha^2\lambda(\lambda+1)/[2m\cosh^2(\alpha z)]$ and a rectangular QW of width b and depth U_0. In the former case the integer values $\lambda=N$ and $\chi(z)=P_N[\tanh(\alpha z)]$, where P_N is a Legendre polynomial, correspond to resonant QW's. Let us consider the situation for $\lambda\simeq 1$. As can easily be shown, in this case

$$\rho=(3/2)\alpha(\lambda-1), \tag{9}$$

$$\tilde{n}=\frac{4n_s}{\alpha^2 a_B}. \tag{10}$$

Here $a_B=\varepsilon_\infty\hbar^2/me^2$. For a rectangular QW with $\sqrt{2mU_0}b\simeq\pi\hbar$

$$\rho=\frac{\pi^2}{4b}\left(1-\frac{\pi^2\hbar^2}{2mU_0b^2}\right), \tag{11}$$

$$\tilde{n}=\frac{\pi n_s b^2}{a_B\xi^4}\left[\frac{2\pi^2-6\xi^2+(\pi^2/2-2\xi^2)\xi}{1+\xi/2}\right], \tag{12}$$

$$\xi=\sqrt{2m|E_0|}b/\hbar.$$

As follows from Eq. (5), the one-electron matrix element P^0_{E0} has a pole at $E=-\hbar^2\rho^2/2m$, which determines its amplitude at small positive values of E. However, it cancels out in Eq. (7), and we find that the expressions for P^0_{E0} and P_{E0} differ only by the replacement $\rho\to\rho-\tilde{n}$.

We proceed directly to an analysis of the dependence of the absorption coefficient α on the frequency of the light ω. We, first of all, recall that in the absence of depolarization effects there is an absorption edge with a red boundary $\omega_0=|E_0|/\hbar$, which corresponds to transitions to continuum states above the QW, and when $\rho>0$ and there are two bound states in the QW, there is also a discrete peak at $\hbar\omega=|E_0|-\hbar^2\rho^2/2m$, which corresponds to transitions between these states.

As has already been noted, consideration of the depolarization effects reduces essentially to the replacement $\rho\to\rho-\tilde{n}$ in the matrix elements and the absorption spectra. This is a key factor for understanding the role of depolarization. As was already noted in Ref. 8, the position of the absorption edge ω_0 does not depend on the doping level. In all other respects, an increase in the carrier concentration in a QW has the same influence on the absorption spectra as a decrease in its depth or width. If $\rho>0$, as the concentration increases, the position of the discrete peak shifts according to the law $\hbar\omega=|E_0|-\hbar^2(\rho-\tilde{n})^2/2m$ and vanishes at $\tilde{n}=\rho$ after reaching the absorption edge (see Fig. 1). Formally, this is because the pole of the matrix element moves over to the nonphysical surface of the complex plane. Thus, for wells with a power $0<\rho<\tilde{n}$ the shallow electron bound state is not manifested in the intersubband optical absorption spectra.

The absorption edge, which corresponds to transitions to the continuum, is given by the formula

$$\alpha(\omega)\propto\frac{\sqrt{\hbar\omega+E_0}}{\hbar^2(\rho-\tilde{n})^2/2m+\hbar\omega+E_0}. \tag{13}$$

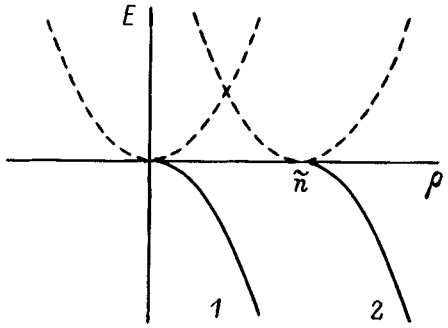

FIG. 1. Schematic representation of the dependence of the position of the discrete line of the $0\to1$ transition (solid curve) and the maximum in the photoionization spectrum of a QW (dashed line) on the parameters of the QW without regard for the depolarization (*1*) and with allowance for the depolarization (*2*).

With the exception of the case of an exact equality between ρ and $\tilde{n}$, this expression has a maximum at a quantum energy $\hbar\omega_{\max}=|E_0|+\hbar^2(\rho-\tilde{n})^2/2m$ that exceeds $|E_0|$. Figure 1 shows the position of the maximum as a function of the parameters of the QW. We note that the expression just presented is an even function of $\rho-\tilde{n}$. Therefore, either an increase or a decrease in the width or depth of the QW in comparison with the critical value transforms the shape of the absorption curve in an identical manner (to within the shift of its edge). The cases of positive and negative values of $\rho-\tilde{n}$ are distinguished only by the presence of an additional discrete absorption line in the former case (see Fig. 2).

It can easily be seen that at large values of $|\rho|$, i.e., far from resonance, the depolarization effects influence the absorption spectra only at very high values of n_s. This justifies our focusing on a ''near-resonant'' QW, in which, as was previously noted (then, without substantiation), the depolarization effects are most significant.

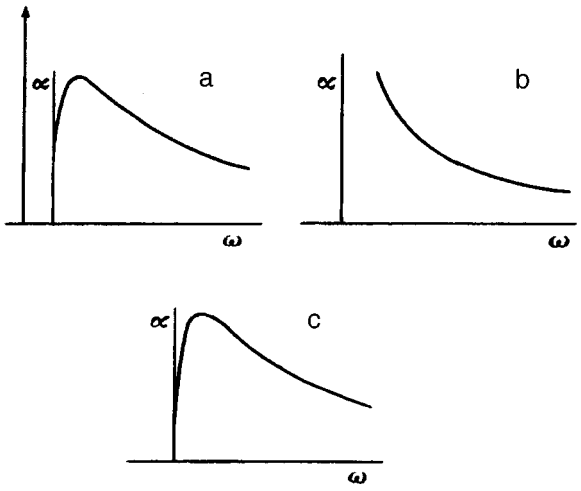

FIG. 2. Evolution of the absorption spectrum in a QW with $\rho>0$ as the doping level is increased: a — $\tilde{n}<\rho$; b — $n=\rho$; c — $n>\rho$. a — The arrow marks the position of the absorption line for transitions between bound states.

A resonant QW, in which the energy of one of the excited levels after the first one is close to zero, can be treated in a similar manner. The actual calculation is complicated, since the system consisting of (2) and (3) reduces to an algebraic equation of an order higher than second.

5. CONCLUSIONS

The influence of depolarization effects on the intersubband absorption in QW's has been considered in this work. A system of equations for determining the corresponding matrix elements has been obtained. An analytic expression for the absorption spectrum has been obtained for the case of a near-resonant QW, which is of greatest interest and practical importance. When there is a shallow bound state in the QW, the absorption line caused by the transition to that state shifts toward higher frequencies as the carrier concentration increases and ultimately vanishes after reaching the optical ionization threshold of the QW. The threshold value does not depend on the carrier concentration. As for the shape of the photoionization spectrum, the delocalization effects have the same influence on the spectrum as a decrease in its depth or width. From the practical standpoint, this means that, if we wish to create a photodetector with the highest possible absorption coefficient based on a QW, the latter should be deeper or wider (by an amount determined by the doping level) than indicated by a calculation in the one-electron model.

It should be stressed once again that intraband optical transitions to the shallow excited state are not observed for $0<\rho<\tilde{n}$. Nevertheless, the state actually exists and can be detected in other experiments, for example, by measuring the Raman scattering or the interband optical absorption.

This work was performed with support from the Russian Fund for Fundamental Research (Project 96-02-17961) and the Ministry of Science of the Russian Federation as part of the Physics of Solid-State Nanostructures Program (Project 1-081/4).

[1)]When necessary, it is not difficult to generalize the results to the asymmetric case $U(-\infty) \neq U(\infty)$.

[1] B. F. Levine, J. Appl. Phys. **74**, R1 (1993).
[2] A. Ya. Shik, Fiz. Tekh. Poluprovodn. **20**, 1598 (1986) [Sov. Phys. Semicond. **20**, 1002 (1986)].
[3] K. W. Goosen and S. A. Lyon, J. Appl. Phys. **63**, 5149 (1988).
[4] V. D. Shadrin and F. L. Serzhenko, Confr. Phys., **32**, 345 (1992).
[5] H. C. Liu, J. Appl. Phys. **73**, 3062 (1993).
[6] P. Man and D. S. Pan, Appl. Phys. Lett. **64**, 321 (1994).
[7] T. Ando, A. B. Fowler, and F. Stern, ''Electronic properties of two-dimensional systems,'' Rev. Mod. Phys. **54**, 437–672 (1982) [Russ. transl., Mir, Moscow (1985)].
[8] A. Ya. Shik, Pis'ma Zh. Tekh. Fiz. **15**, 40 (1989) [Sov. Tech. Phys. Lett. **15**, 430 (1989)].
[9] M. Zaluzny, Solid State Commun. **79**, 1013 (1991).
[10] F. L. Serzhenko and N. F. Johnson, Appl. Phys. Lett. **63**, 3467 (1993).
[11] A. G. Petrov and A. Ya. Shik, in *Abstracts of Reports to the 2nd Russian Conference on the Physics of Semiconductors* [in Russian], Zelenogorsk, 1996, Vol. 2, p. 185.
[12] D. A. Dahl and L. J. Sham, Phys. Rev. B **16**, 651 (1977).

Translated by P. Shelnitz

Optical properties of vertically coupled InGaAs quantum dots in a GaAs matrix

M. V. Maksimov, Yu. M. Shernyakov, S. V. Zaĭtsev, N. Yu. Gordeev, A. Yu. Egorov, A. E. Zhukov, P. S. Kop'ev, A. O. Kosogov, A. V. Sakharov, N. N. Ledentsov, V. M. Ustinov, A. F. Tsatsul'nikov, and Zh. I. Alferov

A. F. Ioffe Physicotechnical Institute, Russian Academy of Sciences, 194021 St. Petersburg, Russia

J. Böhrer and D. Bimberg

Technische Universität Berlin, D-10623 Berlin, Germany
(Submitted August 22, 1996; accepted for publication September 10, 1996)
Fiz. Tekh. Poluprovodn. **31**, 670–673 (June 1996)

It is shown that the self-organization effects appearing during the N-cycle deposition of $In_{0.5}Ga_{0.5}As$(12 Å)/GaAs(50 Å) lead to the formation of ordered arrays of vertically coupled quantum dots (VCQD's). The optical properties are investigated as a function of the number of deposition cycles ($N=1-10$). In cases of injection heterostructure lasers with an active region based on VCQD's it is shown that increasing the number N of deposition cycles from 1 to 10 makes it possible to lower the threshold current density at 300 K from 950 to 97 A/cm^2 and to achieve a continuous lasing regime at room temperature with an output power of 160 mW per mirror. © *1997 American Institute of Physics.* [S1063-7826(97)00706-0]

A dramatic increase in the interest in the investigation of heterostructures with spatial confinement of the carriers in two or three dimensions, i.e., in quantum wires and quantum dots, has recently been observed around the world.[1] Such structures are of considerable interest from the standpoint of their fundamental properties and are very promising for employment in micro- and optoelectronic devices. Injection heterostructure lasers with an active region based on (In, Ga)As/GaAs quantum dots exhibit ultrahigh temperature stability of the threshold current density J_{th} with a characteristic temperature T_0 of order 350–400 K over a broad temperature range (80–150 K).[2] As a result of the thermal ejection of carriers from quantum dots at higher temperatures, J_{th} increases, T_0 decreases ($T_0=60$ K), and the wavelength of the laser output undergoes a blue shift (i.e., a shift toward energies close to the energy of the optical transition in the two-dimensional wetting layer).[2] The use of arrays of vertically coupled InAs quantum dots in a GaAs matrix has made it possible to significantly improve the working characteristics of such lasers and to achieve laser emission via the ground state at 300 K (at a wavelength of 1.03 μm).[3–5] At the same time, the threshold current density remained fairly high (700 A/cm^2 at 300 K).

In the present work we used photoluminescence, calorimetric absorption, and electroluminescence to investigate the optical and laser properties of vertically coupled quantum dots (VCQD's) with different numbers (N) of InGaAs layers. Information on the structural perfection and geometry of the VCQD's was obtained using transmission electron microscopy (TEM).

The structures were grown on GaAs(100) substrates. The active region, which has the form of an array of VCQD's, was located in the middle GaAs layer with a thickness of 0.2 μm, which was bound on both sides by short-period AlAs(20 Å)/GaAs(20 Å)$\times$10 superlattices. The array of VCQD's was formed as a result of the N-cycle deposition of InGaAs with a thickness of 12 Å separated by intervening GaAs layers with a thickness of 50 Å. Each of the N InGaAs layers was grown in a submonolayer regime: (1 ÅGaAs+1Å InAs+10s interruption)$\times$6.[6] When the active layer and the GaAs cladding layer with a thickness of 100 Å were deposited, the substrate temperature was equal to 485 °C, while it was equal to 600 °C during growth of the remainder of the structure. The laser structures were grown in the standard geometry for a separate-confinement double heterostructure (an SC DHS laser) with a graded-index waveguide. The geometry of the laser structure was similar to that described in Ref. 3. The active region was an array of VCQD's. The substrate temperature was 485 °C during growth of the active region and the 100 Å GaAs cladding layer, 630 °C for the waveguides, and 600 °C for the remainder of the structure.

For the photoluminescence investigations of the sample, an upper contact layer was removed on the laser structures by chemical etching. The photoluminescence was excited by an Ar^+ laser, and a cooled germanium photodetector was employed to detect it. The calorimetric absorption spectra (CAS) were recorded at 500 mK. The minimum detectable value of αd was 10^{-5}.[7] To minimize the output losses and attain the minimum threshold current density, lasers with four cleaved faces were selected for the electroluminescence investigations. The working characteristics were measured under pulsed pumping (the pulse duration was 100 ns, and the repetition rate was 5 kHz) in the temperature range 80–300 K. Stripe laser diodes were used to measure the power-current characteristics in a continuous regime. The lasers were soldered by an indium strip on the inner wall of a copper heat dissipator. No reflecting or transmitting coatings were deposited on the cavity faces.

Figure 1 presents photomicrographs of a sample with six layers of InGaAs VCQD's, which were obtained by transmission electron microscopy.

We investigated elsewhere[8] the formation of the InAs–GaAs VCQD's. We showed that the VCQD's form because

 1063-7826/97/060571-04$10.00

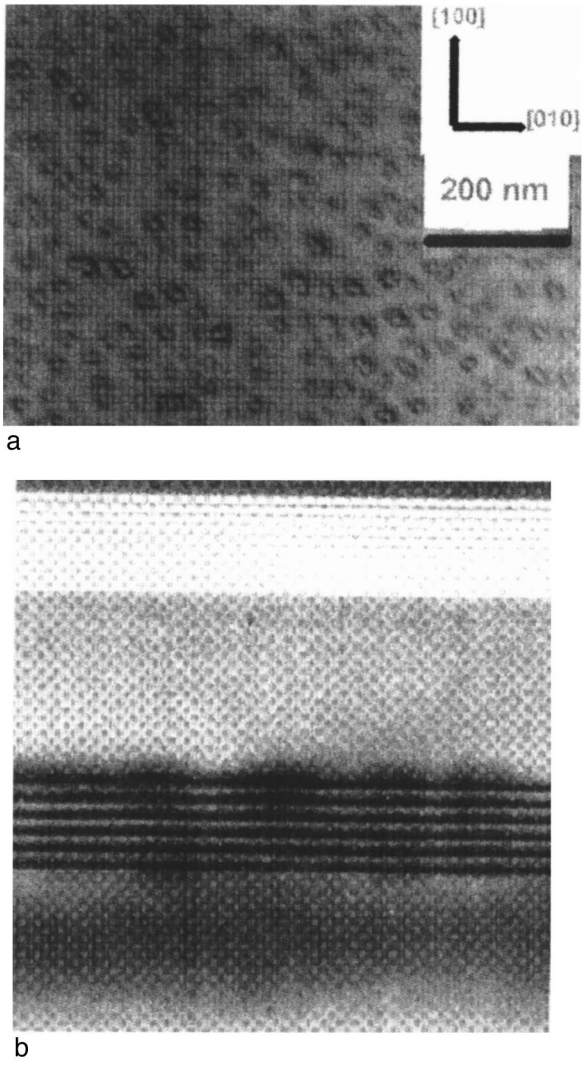

FIG. 1. Photomicrographs of a sample with six layers of InGaAs quantum dots obtained by transmission electron microscopy: a — view from above, b — cross section.

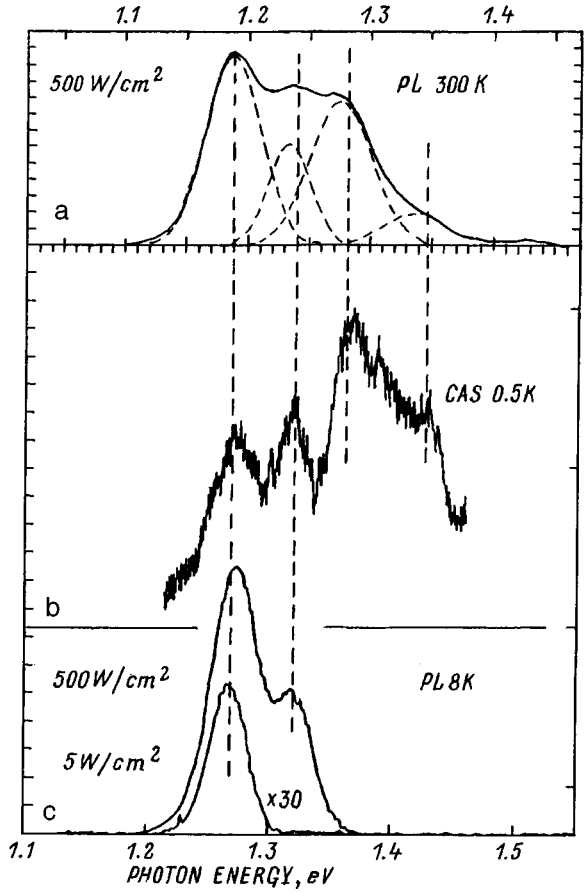

FIG. 2. PL spectra of structures with InGaAs VCQD's ($N=3$) at 300 (a) and 8 K (c) (in Fig. 2a the energy axis has been displaced by the magnitude of the temperature shift of the GaAs gap width for the sake of clarity) and calorimetric absorption spectrum of the same structure at 500 mK (b).

of self-organization involving the transfer of In(Ga, As) from lower dots to upper dots and its replacement by GaAs.[8] As can be seen from Fig. 1, the lateral dimension of the lower island in an InGaAs VCQD is about 140 Å. The lateral dimensions of the islands in each successive row gradually increase, reaching 260 Å for the upper island. The density of the dots is about $5-6\times10^{10}$ cm^{-2}. The dots are locally ordered in the lateral plane along the [001] and [011] directions (Fig. 1a). As can be seen from Fig. 1b, each vertically coupled quantum dot consists of six InGaAs islands separated by narrow intervening GaAs layers. Thus, the wave functions of the upper and lower islands overlap significantly, i.e., from the standpoint of their electronic properties, the VCQD's comprise a single system.[8]

Figure 2 shows the photoluminescence (PL) and calorimetric absorption spectra of a structure with $N=3$. At low excitation densities the spectrum exhibits an intense line, which is caused by the ground exciton state of the VCQD's. At higher excitation densities the spectrum displays an additional peak caused by the excited exciton state in a quantum dot.[9] At high observation temperatures it is also possible to identify a PL line from the wetting layer. As the temperature rises, these lines shift to longer wavelengths in accordance with the temperature shift of the GaAs gap width. The peaks from the ground state and the excited state in the PL spectrum coincide with the analogous peaks in the calorimetric absorption spectrum, attesting to the presence of a high density of well- formed quantum dots of uniform size, in agreement with the data from electron microscopy.

Figure 3 presents the PL spectra of structures with different values of N at a high excitation density. It is seen from the figure that for the sample with $N=1$ considerable saturation of the luminescence associated with the principal transition in the VCQD's occurs at such excitation densities and that the spectrum contains an intense line associated with transitions involving ground-state holes in a dot and electrons localized in the wetting layer. The emission of the wetting layer is observed on the short-wavelength edge of the PL line of the quantum dots. For the sample with $N=3$ the saturation of the luminescence via the ground state is less pronounced, and, finally, in the case of $N=6$ virtually no saturation is observed. This finding is consistent with the decrease in the radiative lifetime for InAs/GaAs VCQD's as N increases.[8]

Increasing the number of layers in growing the VCQD's

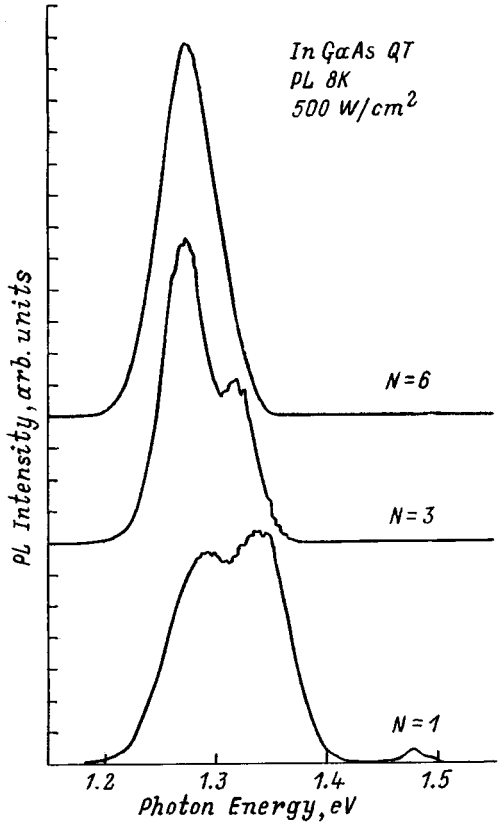

FIG. 3. PL spectra of structures with InGaAs VCQD for various values of the number of deposition cycles N (high pump density).

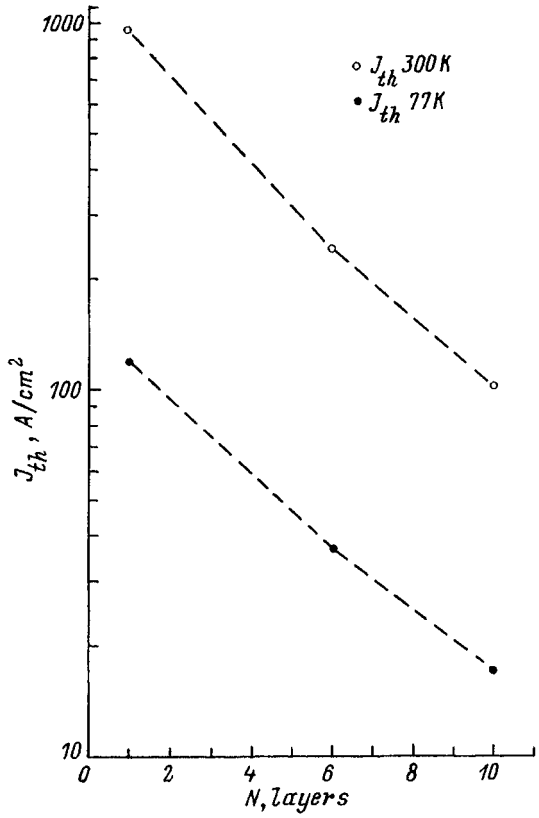

FIG. 4. Dependence of the threshold current density on the number of deposition cycles N in VCQD laser diodes with four cleaved faces.

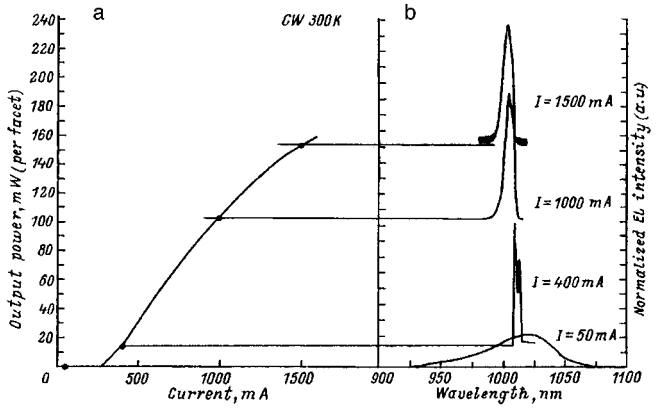

FIG. 5. Power-current characteristic of an InGaAs VCQD laser with $N=10$ (the stripe width was 60 μm, and the cavity length was 1200 μm) at 300 K in the continuous regime (a) and electroluminescence spectra at various pump currents (b).

to $N=10$ permits a sharp decrease in the threshold current density J_{th} at 300 K (from 950 A/cm^2 for $N=1$ to 97 A/cm^2 for $N=10$) as a result of the increase in the overlap factor of the light wave with the active region of the laser (Fig. 4). The sharp decrease in the threshold current density permitted the achievement of a continuous operating regime for a VCQD stripe laser ($N=10$) at room temperature. Figure 5a presents the power-current characteristic of a laser with a stripe width equal to 60 μm and a cavity length equal to 1200 μm at 300 K. The differential efficiency was 23%. The maximum power level obtained per laser mirror was equal to 160 mW. The emission spectra in the spontaneous and stimulated emission regimes are shown in Fig. 5b. As can be seen from Fig. 5b, an increase in the pump current from 400 mA to a maximum value of 1500 mA leads only to weak broadening of the laser output spectrum and a slight shift of its maximum toward shorter wavelengths. The spectrum does not contain additional lines associated with lasing involving states of the wetting layer. Thus, up to the maximum pump current corresponding to an output power of 160 mW per mirror, the generation of the laser emission involves the ground state of the quantum dots, and gain saturation is not observed.

Thus, the optical properties of VCQD's have been investigated in the present work, and it has been shown that the use of VCQD's in laser structures permits the achievement of laser emission via the ground state of the quantum dots at room temperature in a continuous regime with an output power of 160 mW per mirror.

This work was supported by the Russian Fund for Fundamental Research, the Volkswagen Foundation, the Soros Foundation, and INTAS Grant No. 94-1028.

[1] Y. Arakawa and H. Sakaki, Appl. Phys. Lett. **40**, 939 (1982).
[2] N. Kirstaedter, N. N. Ledentsov, M. Grundmann, D. Bimberg, U. Richter, S. S. Ruvimiv, P. Werner, J. Heydenreich, V. M. Ustinov, M. V. Maximov, P. S. Kop'ev, and Zh. I. Alferov, Electron. Lett. **30**, 1416 (1994).
[3] F. I. Alfërov, N. A. Berg, A.Yu. Egorov, A. E. Zhukov, P. S. Kop'ev, A. O. Kosogov, I. L. Krestnikov, N. N. Ledentsov, A. V. Lunev, M. V. Maksimov, A. V. Sakharov, V. M. Ustinov, A. F. Tsapul'nikov, Yu. M.

Shernyakov, and D. Bimberg, Fiz. Tekh. Poluprovodn. **30**, 351 (1996) [Semiconductors **30**, 194 (1996)].
[4] V. M. Ustinov, A. Yu. Egorov, A. E. Zhukov, N. N. Ledentsov, A. V. Lunev, M. V. Maximov, A. F. Tsatsulnikov, N. A. Bert, A. O. Kosogov, P. S. Kop'ev, D. Bimberg, and Zh. I. Alferov, in *Proceedings of the Material Research Society Full Meeting, Nov. 27–Dec. 1, 1995*, Boston, USA.
[5] P. S. Kop'ev, N. N. Ledentsov, V. M. Ustinov, I. V. Kochnev, N. A. Bert, A. Yu. Egorov, A. E. Zhukov, V. V. Komin, A. O. Kosogov, I. L. Krestnikov, MN. V. Maximov, S. S. Ruvimov, A. V. Sakharov, Yu. M. Shernіakov, A. F. Tsatsul'nikov, S. V. Zaitsev, Zh. I. Alferov, and D. Bimberg, in *Proceedings of CLEO*, Anaheim, CA, 1996.
[6] A.Yu. Egorov, A. E. Zhukov, P. S. Kop'ev, N. N. Ledentsov, M. V. Maksimov, and V. M. Ustinov, Fiz. Tekh. Poluprovodn. **28**, 604 (1994) [Semiconductors **28**, 809 (1994)].
[7] D. Bimberg, T. Wolf, and J. Böhrer, in *Advances in Nonradiative Processes in Solids*, B. di Bartolo (ed.), Plenum, New York (1991), p. 577.
[8] M. Grundmann, N. N. Ledentsov, R. Heitz, D. Bimberg, V. M. Ustinov, A. Yu. Egorov, M. V. Maximov, P. S. Kop'ev, Zh. I. Alferov, A. O. Kosogov, P. Werner, J. Heydenreich, and U. Gösele, in *Proceedings of the 8th International Conference on Indium Phosphide and Related Materials*, Schwäbish Gmünd, Germany, 1996.
[9] M. Grundmann, N. N. Ledentsov, O. Stier, D. Bimberg, V. M. Ustinov, P. S. Kop'ev, and Zh. I. Alferov, Appl. Phys. Lett. **68**, 979 (1996).

Translated by P. Shelnitz

Formation of carrier generation centers in pure Si upon interaction with fast ions

A. M. Ivanov and N. B. Strokan

A. F. Ioffe Physicotechnical Institute, Russian Academy of Sciences, 194021 St. Petersburg, Russia
(Submitted September 2, 1996; accepted for publicationSeptember 10, 1996)
Fiz. Tekh. Poluprovodn. **31**, 674–679 (June 1997)

The radiation defects in p^+-n-n^+ structures based on pure n-type Si irradiated by α particles and fission fragments from natural-decay sources are studied by deep-level transient spectroscopy (DLTS). The nature of the components of the reverse current in the structures caused by carrier generation via deep levels is investigated. The systems of deep centers for light and heavy ions are found to be identical. A correlation between the generation component of the current and the concentration of the $E_v+0.33$ eV centers bound to interstitial carbon is observed after a low-temperature anneal. In the case of heavy ions the DLTS spectra do not have the expected peak positions and shapes associated with the pileup of local defects. An estimate of the generation rate in a model of local $p-n$ junctions shows that clusters of defects create a significantly smaller current than does an equivalent number of defects with deep levels located in the n-type host of the structure. © *1997 American Institute of Physics.* [S1063-7826(97)00806-5]

Considerable attention has been focused in recent years on the behavior of pure Si exposed to hard nuclear radiation. The appearance of electrically active centers in neutron fields has aroused special interest. This process is associated with the possible utilization of silicon p^+-n-n^+ detectors in supercollider systems. One of the problematic points is the increase in the reverse current of p^+-n-n^+ structures with the neutron dose, i.e., the appearance of generation centers.

The formation of defects under neutron bombardment occurs as a result of the formation of Si recoil atoms; therefore, the process is essentially determined by the interaction of the Si lattice with ions of ''medium'' mass. We previously observed a number of special features in the behavior of the generation current when diode structures were ion-irradiated.[1,2] In the present work a comparative analysis of the Si radiation defects from light and heavy ions is performed, and conclusions regarding their nature and the generation activity are drawn.

EXPERIMENTAL SAMPLES AND METHOD

The investigation was performed on p^+-n-n^+ structures prepared according to a planar technology from pure Si with a resistivity (ρ) greater than 500 $\Omega\cdot$cm. In addition, Si with $\rho=60\Omega\cdot$cm, on which a rectifying barrier was created by sputtering gold, was used for a precision determination of the concentration of the centers upon irradiation by ions with a short mean free path.

Radioactive ^{238}Pu and ^{244}Cm were employed as sources of light ions (α particles). The heavy ions were ^{252}Cf fission fragments. Data on deuteron irradiation in an electrostatic accelerator were also used. Ion irradiation was generally carried out in small doses, at which the ion tracks in Si did not overlap one another.

The principal investigations were performed using deep-level transient spectroscopy (DLTS). The spectrum of the levels of the radiation centers and their concentrations were determined by this method. The increment of the reverse current for each structure served as the reading of the integral radiation-center generation activity. Simulation of the appearance of vacancies when ions are stopped using the TRIM program[3] was also employed.

The methods indicated are well known and do not need further explanations, with the exception of the observation of the current in a reverse-biased p^+-n-n^+ structure, which is a form of an ''ionization chamber.'' The value of the reverse current clearly corresponds to the rate of the generation of carriers in the region of the field, including their thermal generation, via centers introduced by the hard radiation. However, not all the types of radiation defects are manifested in the current. As will be shown below, extended defects, which create a potential well, can make a vanishingly small contribution to the current.

GENERATION BY POINT CENTERS

We previously observed[4] that the increment of the generation component of the current of a p^+-n structure per ion for α particles and fission fragments does not correspond to the number of primary Frenkel pairs formed. For example, when the ratio between the numbers of pairs was 300:1 in favor of the fission fragments, the currents per ion were equal to 4.5×10^{-5} nA and 5×10^{-8} nA, i.e., they differed by a factor of 900. It is significant that the DLTS spectra had a similar structure. The difference between the currents was attributed to the less favorable conditions for charge exchange involving the primary Frenkel pairs in the fragment tracks, since the regions of intense carrier generation and the formation of atomic displacements (in contrast to the track of an α particle) are spatially separated. Accordingly, a small fraction of the defects that were created recombine. As a result, the emission of vacancies and interstitials from the track of an ion (followed by the formation of complexes in the Si bulk) is more effective for fission fragments.

Let us see whether it is possible to relate the current

 1063-7826/97/060575-05$10.00

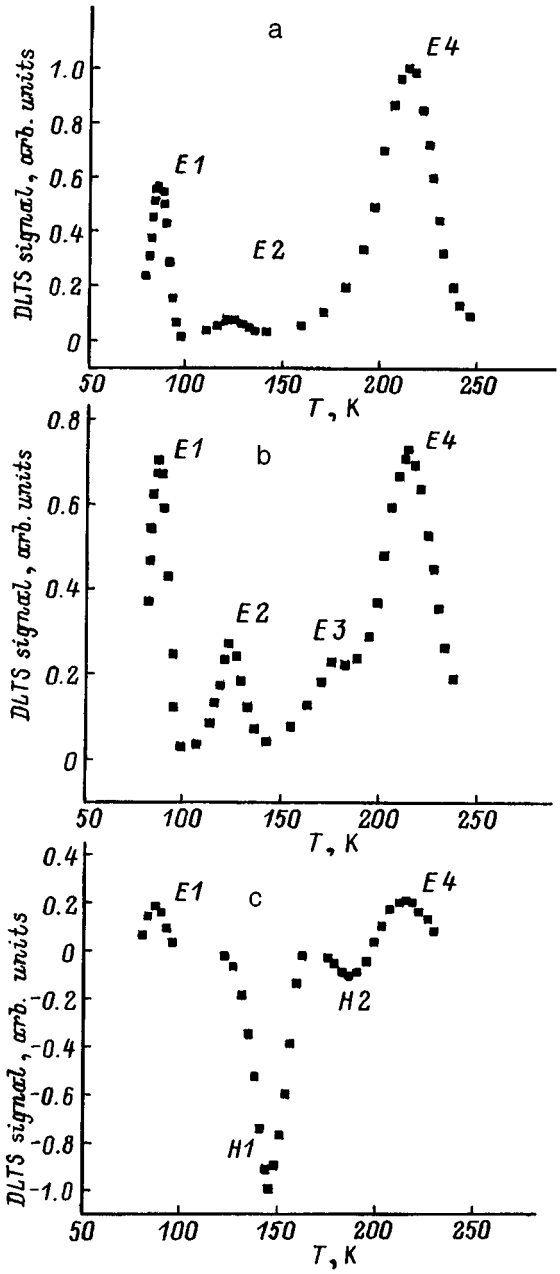

FIG. 1. DLTS spectra for bombardment by fission fragments (a) and α particles (b, c). Measurement regimes: a, b — without injection, c — with injection of minority carriers for determining the levels in the lower half of the band gap. Similarity between the positions and shape of the peaks in the spectra is observed.

increment to the content of a specific level in the DLTS spectrum. Figure 1a presents the spectrum of a sample irradiated by ^{252}Cf fragments. The structure of the spectrum mimics the system of levels for α particle (Fig. 1b). The $E1$ peak ($E_c-0.18$ eV; $\sigma_n=2\times10^{-14}$cm^{-2}) [$\sigma_{n,p}$ is the electron (hole) capture cross section] characterizes the vacancy-oxygen complexes (A centers), as well as the complexes formed by an interstitial carbon atom and a carbon atom at a lattice site (a C_i–C_s center). The $E2$ peak ($E_c-0.22$ eV; $\sigma_n=2\times10^{-16}$ cm^2) is assigned to a doubly charged negative divacancy state, and the $E4$ peak

TABLE I. Values of K for ions of different mass.

Treatment regime	K, nA		
	^{252}Cf fragments	α-particles	deuterons
After irradiation	20.1×10^{-8}	7.9×10^{-8}	6.4×10^{-8}
Annealing for 1 h, 180 °C	6.7×10^{-8}		
Annealing for 2 h, 77 °C +1 h, 150 °C		3.3×10^{-8}	

($E_c-0.4$ eV; $\sigma_n=2\times10^{-16}$ cm^2) is produced by at least two centers: a divacancy (a singly charged negative state) and a vacancy-donor complex (an E center). After exposure to α particles, the $E3$ peak ($E_c-0.29$ eV; $\sigma_n=2\times10^{-17}$ cm^2), which is assigned to a phosphorus-interstitial carbon complex, was also observed.

The lower half of the band gap was investigated in the hole injection regime. Here the following carbon centers were observed both in the case of α particles and in the case of fission fragments (Fig. 1c): C_i ($H1=E_v+0.33$ eV; $\sigma_p=9\times10^{-14}$ cm^2) and C_i-C_s ($H2=E_v+0.4$ eV; $\sigma_p=3\times10^{-14}$ cm^2) (see also Ref. 4).

In the system of levels just described the E center is most active in generation. This center, which is located near the middle of the band gap, has large carrier capture cross sections[5] ($\sigma_n=5\times10^{-15}$ cm^2, $\sigma_p=2.7\times10^{-13}$ cm^2). Let us see how the current and the number of centers forming the $E4$ peak are related in our case. To compare ions of different mass we introduce the quantity $K=\Delta I/VN(E4)$, i.e., we normalize the current increment to the concentration $N(E4)$ of these centers and the volume V in the region of radiation damage.

The values of K for Si samples irradiated by ^{252}Cf fragments, α particles, and deuterons from the data in Ref. 2 are presented in Table I. Instead of the expected constancy of K, we observe an increase in it with increasing mass of the ion, which makes it difficult to unequivocally relate the nature of the current to the levels of the $E4$ peak. It is also indicative that low-temperature treatments, during which the E centers (and possibly the divacancies[1)]) usually anneal out, do not eliminate the difference between the values of K for bombardment by fission fragments and α particles.

To visualize the significance of the data in Table I with respect to the variation of the amplitude of the $E4$ peak upon annealing in the case of α particles, the concentration of the centers was compared with the value of the current (Fig. 2). According to Ref. 8, the annealing time constant τ_a of the E centers in seconds at the temperature T_a is described as

$$\tau_a=1.4\times10^{-9}\exp(E_a/kT_a). \quad (1)$$

The value of the activation energy $E_a=0.95$ eV was obtained for a neutral E center. This value corresponds to large irradiation doses, at which the Fermi level is displaced toward the middle of the band gap. If the E center is located below the Fermi level (is negatively charged), E_a increases, and it is annealed out at higher temperatures. According to Eq. (1), only a very small percentage of the centers are annealed out during 1 h at $T_a=50$ and 75 °C (1.0 and 3.5%, respectively), and the bulk of the centers are annealed out at

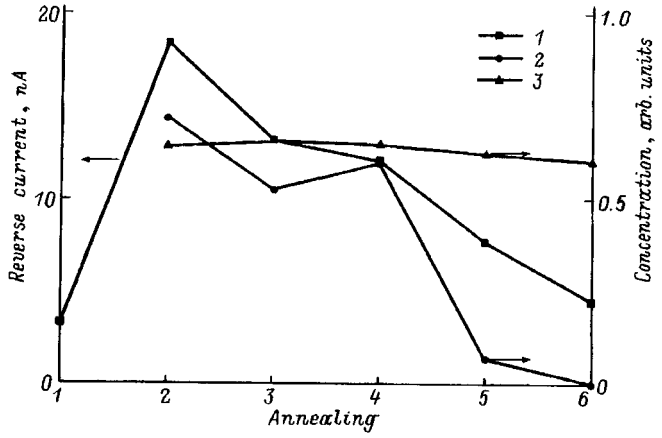

FIG. 2. Variation of the reverse current (*1*) and the concentration of the $H1$ (*2*) and $E4$ (*3*) centers after bombardment by α particles. The numbers along the horizontal axis correspond to the situations: *1* — before irradiation; *2* — after irradiation by a dose $\Phi \simeq 2\times 10^9$ cm^{-2}; *3–6* — after irradiation followed by annealing over the course of 1 h at $T_a = 50$ °C (*3*), 50 °C (*4*), 75 °C (*5*), and 150 °C (6). A correlation between the behavior of the current and the concentration of the carbon-containing $H1$ centers is observed.

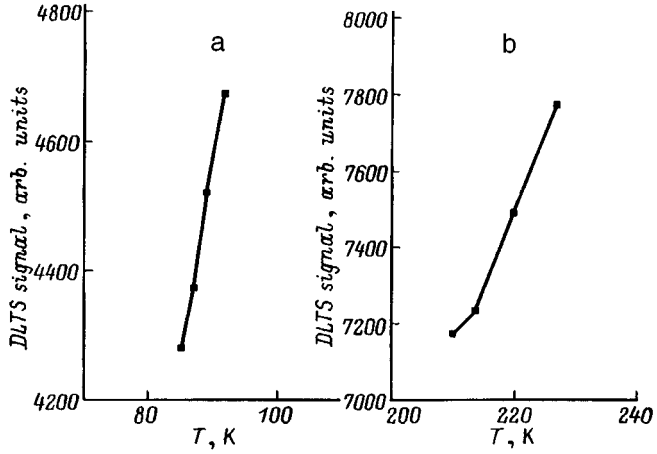

FIG. 3. Dependence of the amplitude of the peaks in the DLTS spectra for the $E1$ (a) and $E4$ (b) centers on the temperature. The characteristic drop in the amplitude of the DLTS peaks with the temperature for defect clusters is not displayed.

$T_a = 150$ °C.[9] However, in the experiment (Fig. 2) the amplitude of the $E4$ peak scarcely decreased during annealing in the temperature range 50–150 °C (1 h). The remaining parameters determined from this peak, viz., the ionization energy of the center and the carrier capture cross section, also remained essentially the same. Conversely, the current decreased significantly after annealing at $T_a = 50$, 75, and 150 °C.

The results with respect to the $E4$ peak can be explained by taking into account the small concentration of donors, $\sim 3\times 10^{12}$ cm^{-3}. The irradiation dose of α particles in the experiment, $\sim 2\times 19^9$ cm^{-2}, corresponds to a concentration of primarily created vacancies of $\sim 6\times 10^{13}$ cm^{-3}. Under these conditions the role of the E centers in the $E4$ peak is insignificant, and the divacancies, which anneal out mainly at ~300°, predominate.

However (even without allowance for the absence of a correlation with the current upon annealing), for the concrete values of the parameters of the level it is difficult to attribute the increase in the generation current following irradiation to the appearance of divacancies, as in Refs. 10 and 11. For example, substituting the value $\sigma_p = 4\times 10^{-16}$ cm^2 and the divacancy concentration $N_t = 1\times 10^{12}$ cm^{-3} into the formula of the generation rate according to Shockley–Read statistics (see, for example, Ref. 12)

$$\frac{n_i}{\tau_{\text{eff}}} = n_i \frac{\sigma_n \sigma_p \nu_{\text{th}} N_t}{\sigma_n \exp[(E_t - E_i)/kT] + \sigma_p \exp[(E_i - E_t)/kT]} \tag{2}$$

(n_i is the intrinsic carrier concentration, E_i and E_t are the energies corresponding to the middle of the band gap and the position of the generation center), for the lifetime we obtain $\tau_{\text{eff}} = 40$ ms. Such a value cannot account for the observed current densities of $\sim 2\times 10^{-7}$ A/cm^2, which correspond to $\tau_{\text{eff}} = 20$ μs. Therefore, it should be concluded that the current drop in the temperature range in Fig. 2 is not caused by the centers responsible for the $E4$ peak.

The $H1$ center, which is bound to an interstitial carbon atom (C_i), can be responsible for the generation current to a large degree. An estimate (with consideration of the methodical details of the measurement of C_i according to Ref. 13) gives $\tau_{\text{eff}} = 90$ μs, which is significantly closer to experiment than is the value for the case of divacancies considered. Additional confirmation is provided by the low-temperature annealing data (Fig. 2), where a clear correspondence between the decreases in the concentration of the $H1$ centers and the current is observed. These results allow us to conclude that the nature of the generation current is largely traceable to the interstitial carbon.

GENERATION OF EXTENDED DEFECTS

Above we considered the manifestations of simple (single) centers. However, it is generally known that regions of lattice defects with dimensions greater than the interatomic distances form when the energy of the recoil atoms is large. The type of conduction in regions with dimensions <200 Å is generally altered. Let us see how such formations can be manifested in our case for irradiation by heavy ions (fission fragments).

First, the presence of defect clusters has an influence on the position of the peaks in DLTS spectra, because the parameters of the point defects in a cluster and at its periphery differ from those in the matrix of a crystal.[14] In our experiments we did not observe any differences between the positions of the peaks after bombardment by α particles and ^{252}Cf fragments (Fig. 1).

In addition, an important role is played by the field created by the contact potential difference between each cluster and the host. In the region of the field, the position of the point defect centers relative to the Fermi level varies over the radius of the cluster. This gives rise to a characteristic dependence of the amplitude of the peak on the temperature,

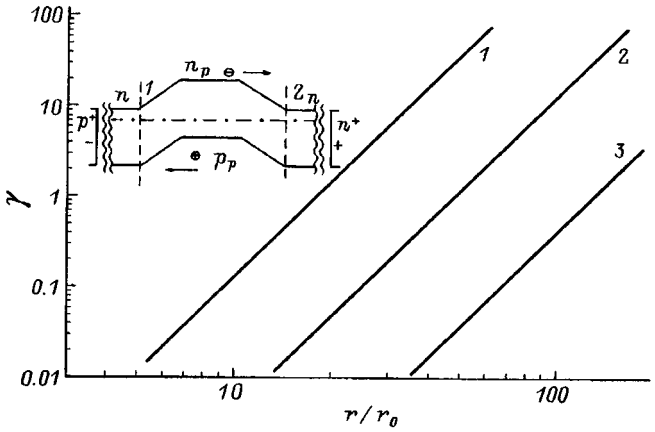

FIG. 4. Ratio between the generation currents ($\gamma = I_{p-n}/I_c$) for the formation of a local p-region by defects and for dispersal of the same number of defects in the n-type host as a function of the radius of the neutral core of the p-region r. $r_0 = 100$ Å. Number of defects: *1* — 10; *2* — 10^2; *3* — 10^3. Inset – variation of the potential near a p-type inclusion for a linear geometry. The values $\gamma > 1$ are realized for ''loose'' formations.

which can be revealed by varying the velocity window when the spectra are recorded.[15] Under these conditions the amplitude of the peaks at high temperatures drops.[16] Figure 3 shows the dependence of the amplitude of the DLTS peaks on the temperature for bombardment by fission fragments. The reverse effect, i.e., an increase in amplitude with the temperature, is observed. Thus, changes in the DLTS spectra that are characteristic of defect clusters were not observed.

This raises the question of how clusters can influence the value of the generation current. In this context, we note that when point centers are introduced into a certain volume V, only the mean concentration in the volume is important for generation. The actual distribution of M centers (for example, in the form of clusters) has no effect on the resultant value of the lifetime. In fact, the total number of centers actually appears in the expression for the current:

$$I_c = \frac{en_i}{2}\sigma \nu_{\text{th}} M.$$

Here, for clarity, we have presented a simplified version of Eq. (2). This situation is maintained as long as the presence of the clusters does not produce a potential well. Let us examine the case in which alteration of the type of conduction occurs and, of course, a local p-type region forms. This corresponds to the model in Ref. 7 (see also the monograph by Konopleva and Ostroumov[18]), where the presence of local $p^+ - n$ junctions was postulated in the case of Ge. For Si the situation regarding the conductivity of a region of defect clusters is less clear. However, the accumulation of a considerable charge of acceptors in the base region was established when $p^+ - n - n^+$ structures were irradiated by large doses of neutrons ($\leqslant 10^{15}$ cm^{-2}).[19] Therefore, our estimate of the generation activity of the defects is based on the model in Ref. 17.[2)] The potential well appearing for the minority carriers, i.e., the holes, is surrounded by a host with n-type conduction, and it has a floating potential (see the inset in Fig. 4).

The voltage applied to the elements of the structure displaces the regions of section *1* (see the inset in Fig. 4) forward and thereby creates the conditions for the injection of holes from the p-region. However, because of the neutrality condition, the currents through sections *1* and *2* should be equal. The escape of holes from the well can be compensated for by an outflow of electrons through section *2*. As a result, the stationary current through the structure initiated by the presence of the local p-region is determined by its minority carriers, i.e., the electrons. The electron current from a hemisphere of radius r (provided $r \geqslant L$) is written as

$$I_{p-n} = 2\pi r^2 \frac{enL}{\tau} = 2\pi e n_i^2 \sqrt{D/\tau}\ \frac{r^2}{p}.$$

Here the diffusivity D, the lifetime τ, and the diffusion length $L = (D\tau)^{1/2}$ refer to electrons. The hole (p) and electron (n) concentrations are related to one another through the value of n_i as $pn = n_i^2$.

For simplicity, we assume that τ is determined by the deep centers of the p-region with a concentration $M = p$. This means that defects in the p-region make an equal contribution to the formation of the deep and shallow centers which are responsible for recombination and conduction, respectively. Since $\tau = (M\sigma_n \nu_{\text{th}})^{-1}$, we have

$$I_{p-n} = 2\pi e n_i^2 \sqrt{D\sigma_n \nu_{\text{th}}}\ \frac{r^2}{\sqrt{p}} = 4\pi e n_i^2 \sqrt{\frac{2\pi}{3}\frac{D\sigma_n \nu_{\text{th}}}{N_d}} r^{7/2}.$$

Here N_d is the number of defects (single defects) that participate in the formation of the p-region. On the other hand, if the same number of defects, which act as point centers, generate carriers in the host, the current, according to Eq. (2), is $I_c = en_i/\tau_{\text{eff}}$.

The ratio between the currents for the two possibilities for the manifestation of defects in carrier generation described above is

$$\gamma = \frac{I_{p-n}}{I_c} = 4\pi \sqrt{\frac{2\pi}{3}} n_i \sqrt{\frac{D}{\sigma_n \nu_{\text{th}}}} r^{7/2} N_d^{-3/2} \times \left[\frac{\sigma_n}{\sigma_p}\exp\left(\frac{E_t - E_i}{kT}\right) + \exp\left(\frac{E_i - E_t}{kT}\right)\right].$$

The dependence of γ on the cluster dimensions for different values of the number of defects in a cluster N_d is presented in Fig. 4. It follows from the figure that the values $\gamma > 1$ are realized when the geometric dimensions of the defect clusters exceed the normalized value $r_0 = 100$ Å. This means that regions of p-type conduction with a high concentration of defects [for example, classical ''disordered regions'' with $p \simeq 10^{19}$ cm^{-3} and $r \simeq 200$ Å (see Refs. 17 and 18) are virtually not seen in the generation current.

It should also be stressed that $\gamma \geqslant 1$ simultaneously corresponds to a hole concentration $\leqslant 10^{14}$ cm^{-3}. The assumption that there is a neutral core in the p-region can be violated at these values. If there is no screening of the electric field by the shell of ionized acceptors, the deep levels of the p-region perform generation like centers in the n-type host.

In general, from the standpoint of lowering the generation current it is advantageous that the defects appear in

dense clusters of small radius, $\leqslant 10^3$ Å. Such ''conglomerations'' generate to a significantly weaker extent than does the same number of centers dispersed in the matrix of a p^+-n-n^+ structure.

CONCLUSIONS

The application of penetrating radiation unquestionably increases the reverse currents of silicon p^+-n structures. However, the traditional ideas that the deepest radiation defect (the E center in our case) determines the thermal generation of carriers have not been confirmed experimentally. We stress that high-resistivity pure n-Si was used in the experiments with light ions and that the irradiation was carried out in doses at which phosphorus depletion could occur. Under these conditions the E center is weakly manifested, and annealing of the excess current occurs on a background of restructuring of the carbon defects.

The larger current increments in the case of heavy ions, i.e., fission fragments, suggest that the decisive contribution to the generation current is made by spatial defects, which create a potential well in the silicon band gap. However, manifestations of such formations could not be detected by capacitance spectroscopy. The evaluation of the generation rate by clusters of primary defects has established their insignificant role in the appearance of the generation current. This property is most clearly manifested in the case of classical ''disordered regions'' with a high density of structural defects.

The experimentally observed decrease in the reverse current of the irradiated structures at room temperature is attributed to the establishment of equilibrium in the system of radiation defects. The restructuring of the radiation defects associated with carbon can be regarded as a characteristic manifestation of the latter. The deep $H1$ level (interstitial carbon) is one of the levels responsible for the generation of carriers in a system of deep centers of radiation origin.

We express our sincerest thanks to V. V. Emtsev for discussing some aspects of the dynamics of Frenkel pairs in a Si lattice, and to E. M. Verbitskaya for a useful discussion.

[1)] In the literature there are indications (see Refs. 6 and 7) that divacancies also have an annealing step at temperatures <200 °C.

[2)] In a recent paper[20] Bruzzi *et al.*, proposed considering a more complicated barrier structure, in which the p^+ region does not have an electrically neutral part.

[1] E. M. Verbitskaya, V. K. Eremin, A. M. Ivanov, and N. B. Strokan, Fiz. Tekh. Poluprovodn. **27**, 205 (1993) [Semiconductors **27**, 115 (1993)].
[2] E. M. Verbitskaya, V. K. Eremin, A. M. Ivanov, and N. B. Strokan, Fiz. Tekh. Poluprovodn. **27**, 1113 (1993) [Semiconductors **27**, 612 (1993)].
[3] *Ion Implantation Science and Technology*, J. F. Ziegler (Ed.), Academic Press (1984).
[4] A. M. Ivanov, I. N. Il'yashenko, N. B. Strokan, and B. Shmidt, Fiz. Tekh. Poluprovodn. **29**, 543 (1995) [Semiconductors **29**, 281 (1995)].
[5] P. V. Kuchinskii and V. M. Lomako, Solid-State Electron. **29**, 1041 (1986).
[6] I. V. Antonova, A. V. Vasil'ev, V. I. Panov, and S. S. Shaĭmeev, Fiz. Tekh. Poluprovodn. **23**, 1076 (1989) [Sov. Phys. Semicond. **23**, 671 (1989)].
[7] L. S. Berman, V. B. Voronkov, V. A. Kozlov, and A. D. Remenyuk, Fiz. Tekh. Poluprovodn. **26**, 1507 (1992) [Sov. Phys. Semicond. **26**, 847 (1992)].
[8] L. S. Kimerling, H. M. De Angelis, and J. W. Diebold, Solid State Commun. **16**, 171 (1975).
[9] S. D. Brotherton and P. Bradley, J. Appl. Phys. **53**, 5720 (1982).
[10] O. V. Aleksandrov, B. N. Shevchenko, I. P. Matkhanova, and A. V. Kamenets, Fiz. Tekh. Poluprovodn. **26**, 868 (1992) [Sov. Phys. Semicond. **26**, 488 (1992)].
[11] E. Borchi, M. Bruzzi, and M. S. Mazzoni, Nucl. Instrum. Methods Phys. Res., Sect. A **310**, 273 (1991).
[12] S. M. Sze, *Physics of Semiconductor Devices*, 2nd ed. Wiley-Interscience, New York (1969) [Russ. transl., Mir, Moscow (1984), Vol. 1].
[13] L. S. Berman, V. A. Zhepko, V. N. Lomasov, and V. N. Tkachenko, Fiz. Tekh. Poluprovodn. **23**, 2129 (1989) [Sov. Phys. Semicond. **23**, 1318 (1989)].
[14] A. I. Baranov, A. V. Vasil'ev, A. S. Gusev, S. A. Smagulova, and N. A. Ukhin, Fiz. Tekh. Poluprovodn. **15**, 2296 (1981) [Sov. Phys. Semicond. **15**, 1336 (1981)].
[15] I. V. Antonova and S. S. Shaĭmeev, Fiz. Tekh. Poluprovodn. **25**, 847 (1991) [Sov. Phys. Semicond. **25**, 513 (1991)].
[16] I. A. Baranov, P. V. Kuchinskiĭ, V. M. Lomako, A. P. Petrunin, S. O. Tsepelevich, and L. N. Shakhlevich, Fiz. Tekh. Poluprovodn. **24**, 731 (1990) [Sov. Phys. Semicond. **24**, 460 (1990)].
[17] B. R. Gossick, J. Appl. Phys. **30**, 1214 (1959).
[18] R. F. Konopleva and V. N. Ostroumov, *Interaction of High-Energy Charged Particles with Germanium and Silicon* [in Russian], Atomizdat, Moscow (1975).
[19] E. Fretwurst, N. Claussen, N. Croitoru, G. Lindström, B. Papendick, U. Pein, H. Schatz, T. Schulz, and R. Wunstorf, Nucl. Instrum. Methods Phys. Res. A **326**, 357 (1993).
[20] M. Bruzzi, A. Baldini, E. Borchi, and I. Lukianov, Nucl. Instrum. Methods Phys. Res., Sect. A **326**, 344 (1993).

Translated by P. Shelnitz

Influence of hydrostatic pressure on the electron mobility and the correlation properties of a mixed-valence system of iron impurity ions in HgSe:Fe crystals

I. G. Kuleev and G. L. Shtrapenin

Institute of the Physics of Metals, Russian Academy of Sciences, Ural Branch, 620219 Ekaterinburg, Russia
(Submitted April 3, 1996; accepted for publication September 16, 1996)
Fiz. Tekh. Poluprovodn. **31**, 680–685 (June 1997)

The influence of hydrostatic pressure on the mobility of the electrons in HgSe:Fe crystals in the low-temperature region is investigated theoretically. The pressure dependences of the contributions of the scattering on the correlated system of Fe^{3+} ions, the alloy potential, and the randomly distributed ions to the electron mobility are analyzed. The variation of the degree of spatial ordering of the Fe^{3+} ions as the pressure increases is considered. © *1997 American Institute of Physics.* [S1063-7826(97)00906-X]

1. INTRODUCTION

The unusual character of the physical properties of HgSe:Fe crystals is attributed to the formation of a Fe^{2+}–Fe^{3+} mixed-valence state at the Fermi level when the concentration of iron impurity ions[1] $N_{Fe} > N_{Fe}^{*} \simeq 4.5\times10^{18}$ cm^{-3}. The presence of mixed-valence iron ions at the Fermi level, which have the same energy, allows the d holes (positive charges in the iron ions) to redistribute themselves among the crystal-lattice sites occupied by Fe^{2+} ions. Therefore, the Coulomb repulsion between the d holes under mixed-valence conditions leads to their spatial ordering. As the concentration of iron impurity ions increases at $N_{Fe} > N_{Fe}^{*}$, the concentration of lattice-neutral Fe^{2+} centers ($N_0 \approx N_{Fe} - N_{Fe}^{*}$), which are available sites for the redistribution of d holes, increases. The degree of spatial ordering of the Fe^{3+} ions increases, and the scattering of electrons on them weakens. This leads to an anomalous increase in the electron mobility μ in HgSe:Fe crystals at low temperatures as the content of iron impurity ions increases.[2,3]

Hydrostatic pressure applied to HgSe crystals leads to a decrease in the effective mass and the density of states in the conduction band.[4] When these crystals are doped by donor impurities, for example, Ga, or when $N_{Fe} < N_{Fe}^{*}$, the concentration of the conduction electrons n_e remains constant, and the Fermi level rises as the pressure increases. We shall call this the donor-impurity regime. For the mixed-valence state the Fermi level is fixed at the iron d level ($\varepsilon_F = \varepsilon_a = 0.21$ eV), and an increase in hydrostatic pressure leads to a decrease in the electron number density n_e. Therefore, measurements of the Hall effect and the Schubnikov-de Haas oscillations under the conditions of hydrostatic pressure permit fairly reliable identification of the presence of the mixed-valence state in HgSe:Fe crystals when they are doped with donor impurities. It is noteworthy that pressure allows us to vary the ratio between the concentrations of charged ions $N_{Fe^{3+}} = N_+$ and lattice-neutral iron ions $N_{Fe^{2+}} = N_0$ and thereby to alter the degree of spatial ordering of the correlated system of Fe^{3+} ions. Therefore, investigations of the dependence of the electron mobility on the pressure can provide new information on the ordering of Fe^{3+} ions in HgSe:Fe crystals.

The influence of pressure on the Hall effect and the electron mobility was investigated experimentally in HgSe:Fe crystals in Ref. 5 and in HgSe:Fe,Ga crystals in Ref. 6. It was established that under the mixed-valence conditions the electron concentration decreases with increasing pressure and that in the HgSe:Fe samples the electron mobility is an increasing function of the pressure,[5] while in HgSe:Fe, Ga samples with $N_{Fe} = 2\times10^{19}$ cm^{-3} and $N_{Ga} \geqslant 2\times10^{18}$ cm^{-3} the electron mobility decreases with increasing pressure.[6] The interpretation of the experimental data in those studies was based on a modified version of the model of short-range correlations proposed in Refs. 7 and 8. As was shown in 3, such a version of the model of short-range correlations is valid only in the case of Coulomb correlations and can be used to qualitatively account for the behavior of the mobility in HgSe:Fe crystals with a small content of iron impurity ions $N_0/N_+ \ll 1$. Therefore, the conclusions in Refs. 5 and 6 regarding the influence of pressure on the electron mobility cannot be considered fully substantiated. Moreover, the contribution of the scattering of electrons on the correlated system of Fe^{3+} ions was separated in Refs. 5 and 6, and thus it became possible to extract information on the influence of pressure on the degree ordering of the iron ions.

Here we shall base our discussion on the version of the model of short-range correlations proposed in Ref. 3. This version is valid for weak and strong Coulomb correlations in the correlated system of Fe^{3+} ions. In Ref. 3 this made it possible to quantitatively account for the dependence of the electron mobility μ on N_{Fe} over a broad range of concentrations of iron impurity ions. In the present work, in contrast to Refs. 5 and 6, we shall analyze the influence of pressure on the scattering mechanisms that determine the electron mobility in HgSe:Fe crystals at low temperatures, as well as on the degree of spatial ordering of the correlated system of Fe^{3+} ions.

2. INFLUENCE OF PRESSURE ON THE SCATTERING OF ELECTRONS IN HgSe:Fe CRYSTALS AT LOW TEMPERATURES

It was established in Ref. 3 that the main mechanisms for the scattering of electrons in HgSe:Fe crystals under mixed-valence conditions at low temperatures ($T \approx 4$ K) are scattering by the correlated system of Fe^{3+} ions and alloy

 1063-7826/97/060580-05$10.00

scattering. According to the model proposed in Ref. 3, the system of Fe^{2+} and Fe^{3+} ions in these compounds can be regarded as a binary alloy consisting of charged (Fe^{3+}) and lattice-neutral (Fe^{2+}) ions. Relaxation of the electron momentum occurs as a result of interactions with these centers. The expression for the electron mobility can be written in the form[3]

$$\mu(N_{\mathrm{Fe}})=\mu_{\mathrm{BH}}\Phi_{\mathrm{BH}}\left\{\Phi_c(k_F)+\Lambda(k_F)\times\left[2\left(\frac{N_0}{N_+}\right)^{1/2}\Phi_{+0}(k_F)+\frac{1}{2}\Lambda(k_F)\frac{N_0}{N_+}\right]\right\}^{-1}, \quad (1)$$

$$\mu_{\mathrm{BH}}=3\pi he/(m(\varepsilon_F)E_B(\varepsilon_F)\Phi_{\mathrm{BH}}(k_F)),$$

$$\Phi_{\mathrm{BH}}=\ln(1+b_s^{-1})-(1+b_s^{-1}). \quad (2)$$

Here μ_{BH} is the Brooks–Herring electron mobility caused by scattering by randomly distributed ions with a concentration $N_i=n_e$; $m(\varepsilon_F)$ is the electron effective mass at the Fermi level; $E_B(\varepsilon_F)$ is the Bohr energy; $b_s=(2k_Fr_s)^2$; r_s is the screening radius; $\Lambda(k_F)=(k_F^2\varkappa V_0)/(\pi e^2)$ is the ratio between the interaction constants of electrons with the neutral (V_0) and charged iron ions; $\varkappa$ is the dielectric constant; according to the estimate in Ref. 3, $\Lambda(k_F)\approx 0.1$, and $V_0\approx 9\times 10^{-23}$ cm, which is consistent with the data in Ref. 9 regarding the scattering of electrons by neutral centers in gapless semiconductors; N_+ and N_0 are the concentrations of the charged and lattice-neutral iron ions;

$$\Phi_c(k_F)=2\int_0^1 x^3S(2xk_F)\frac{dx}{(x^2+b_s^{-1})},$$

$$\Phi_{+0}(k_F)=1-b_s\ln(1+b_s). \quad (3)$$

The structure factor S_q, which characterizes the degree of spatial ordering of the correlated system of Fe^{3+} ions, was defined in Ref. 3, and for randomly distributed ions $S_q=1$ and $\Phi_c=\Phi_{\mathrm{BH}}$. In the case of interimpurity Coulomb correlations of arbitrary strength, the structure factor is calculated in the Percus–Yevich approximation[10] for a model system of solid phases. The use of this approximation is justified by the fact that, as was shown by one of us, the most closely arranged d holes in a correlated system of Fe^{3+} ions move away from one another first due to Coulomb repulsion when such a system is ordered. This guarantees a maximum free-energy gain and leads to the formation of correlation spheres of radius r_c around each Fe^{3+} ion, where there are no d holes. As the concentration of iron impurity ions increases, the number of empty sites N_0 for redistributing the d holes increases. The degree of spatial ordering of the correlated system of Fe^{3+} ions and r_c increase. This allows us to approximate a correlated system of Fe^{3+} ions by a system of solid spheres with a diameter $d=r_c$.[3] The degree of ordering in such a system is characterized by the packing parameter $\eta=\pi d^3N_+/6$, which is equal to the ratio of the volume occupied by the solid spheres to the total volume of the system. For a system of solid spheres the integral equation for the direct correlation function of the distribution can be solved exactly,[10] and the structure factor appearing in (3) is determined according to Refs. 10 and 11 without the use of perturbation theory with respect to a small parameter. The following equation, which specifies the dependence of the packing parameter η on N_{Fe}, was derived in Ref. 3:

$$\eta(N_{\mathrm{Fe}})=\eta_L[1-\exp(-\eta N_{\mathrm{Fe}}/\eta_LN_+)]. \quad (4)$$

This equation makes it possible to calculate the contribution of the scattering on the correlated system of Fe^{3+} ions to the electron mobility μ_c.

Let us now consider the influence of pressure individually on each of the electron scattering mechanisms in HgSe:Fe crystals at low temperatures in the donor-impurity regime and in the mixed-valence state. The main effect of hydrostatic pressure is a decrease in the energy gap ε_g between the Γ_6 and Γ_8 bands. Its influence on the other band-structure parameters is significantly smaller and can therefore be ignored.[4] The influence of pressure on the electron density and the kinetic characteristics of HgSe:Fe crystals can be analyzed using the two-band Kane model:[4]

$$\varepsilon(k)=\frac{\varepsilon_g}{2}\left[\left(1+\frac{2}{\varepsilon_g}\frac{\hbar^2k^2}{m_0^*}-1\right)\right],$$

$$m_0^*=\frac{4}{3}\frac{p^2}{\hbar^2\varepsilon_g}\left(\frac{\Delta+3/2\cdot\varepsilon_g}{\Delta+\varepsilon_g}\right). \quad (5)$$

For HgSe crystals $\Delta=0.45$ eV, $\varepsilon_g=0.22$ eV, and $m_0^*\approx 0.024m_e$, where m_e is the free electron mass. The magnitude of the energy gap between the p and s bands, $\varepsilon_g=|\varepsilon(p)-\varepsilon(s)|$, decreases linearly with increasing pressure:

$$\varepsilon_g(P)=\varepsilon_g-\beta P=\varepsilon_g-\Delta\varepsilon_g(P), \quad (6)$$

where β is the pressure coefficient, and, according to Refs. 5–7, $\beta\approx 6\pm 1$ meV/kbar.

For the mixed-valence state the Fermi level is fixed at the iron donor level, i.e., $\varepsilon_F\approx\varepsilon_d=\mathrm{const}$; therefore, as the pressure increases, the effective mass at the Fermi level m_F, the electron density n_e, and the Fermi momentum k_F will vary:

$$m_F(P)\simeq m_F(0)\left\{1-\frac{\Delta\varepsilon_g(P)}{\varepsilon_g+2\varepsilon_F}\right\},$$

$$m_F(0)=m_0^*[1+2\varepsilon_F/\varepsilon_g],$$

$$n_e(P)\simeq n_e(0)\left\{1-\frac{\Delta\varepsilon_g(P)}{\varepsilon_g+2\varepsilon_F}\right\}^{3/2},$$

$$k_F(P)\simeq k_F[n_e(P)/n_e(0)]^{1/3}. \quad (7)$$

In the donor-impurity regime in HgSe:Fe crystals ($N_{\mathrm{Fe}}<N_{\mathrm{Fe}}^*$) the concentration of conduction electrons and the Fermi momentum do not vary, but the Fermi energy increases and the electron effective mass decreases with increasing pressure:

$$\varepsilon_F(P)=\varepsilon_{F^+}\Delta\varepsilon_g(P)\frac{\varepsilon_g(P)}{\varepsilon_g+2\varepsilon_F},$$

$$m_F(P)=m_F(0)\left[1-\frac{\Delta\varepsilon_g(P)\varepsilon_g}{(\varepsilon_g+2\varepsilon_F)^2}\right]. \quad (8)$$

Equations (7) and (8) enable us to determine the dependence of the contributions and the mobility for the various electron scattering mechanisms in HgFe:Se crystals in the low-temperature region in the donor-impurity regime and for the mixed-valence state. In the donor-impurity regime in HgFe:Se (when $N_{\mathrm{Fe}}<N_{\mathrm{Fe}}^{*}$) or in HgSe:Ga when scattering takes place on randomly distributed ions with a concentration $N_i=n_e$ we have

$$\mu_{\mathrm{BH}}(P)=[m_F(0)/m_F(P)]^2\mu_{\mathrm{BH}}(0). \tag{9}$$

The electron mobility increases with increasing pressure as a result of the decrease in the electron effective mass at the Fermi level.

In the region of the mixed-valence state the concentration of Fe^{3+} ions $N_+(P)=N_+(0)-\Delta n$ decreases and the concentration of lattice-neutral centers $N_0(P)=N_0(0)+\Delta n$, where $\Delta n=n_e(P)-n_e(0)$, increases with increasing pressure. Therefore, for the mixed-valence state the electron mobility varies with increasing pressure not only because of the decrease in the effective mass, but also as a result of the variation of the spatial correlations of the correlated system of Fe^{3+} ions. For the contribution to the mobility due to scattering on the correlated system of Fe^{3+} ions we obtain

$$\mu_c(P)=\mu_{\mathrm{BH}}(0)[m_F(0)/m_F(P)]^2 \times\Phi_{\mathrm{BH}}(k_F)/\Phi_c(k_F(P),\eta(P)). \tag{10}$$

To calculate $\eta(P,N_{\mathrm{Fe}})$, from Eq. (4) we must take into account the dependence of $N_+(P)$ and $N_0(P)$ on the pressure. For the contribution of the alloy scattering we obtain

$$\mu_{\mathrm{al}}=\mu_{\mathrm{BH}}(0)[m_F(0)/m_F(P)]^2\Phi_{\mathrm{BH}}(k_F)[\Lambda(P)]^{-1} \times\left\{2[N_0(P)/N_+(P)]\Phi_{+0}(k_F(P)) +\frac{1}{2}\Lambda(P)N_0(P)/N_+(P)\right\}^{-1}. \tag{11}$$

Here $\Lambda(P)=[n_e(P)/n_e(0)]^{2/3}\Lambda(0)$, and $\Lambda(0)\approx 0.1$. Thus, the dependence of the total mobility on the pressure is specified by the expression

$$\mu(P)=[1/\mu_c(P)+1/\mu_{\mathrm{al}}(P)]^{-1}.$$

Figures 1 and 2, respectively, present the dependence of the total electron mobility and the partial contributions of the alloy scattering and the scattering on Fe^{3+} ions to the mobility on the concentration of impurity iron ions for three pressure values, $P=0$, 5, and 10 kbar. The $\mu(N_{\mathrm{Fe}})$ curve for zero pressure coincides with the dependence calculated in Ref. 3. It is seen from the figures that the total mobility and the partial contributions increase with increasing pressure. The maximum variation of the mobility with the pressure is observed at a relatively small concentration of iron impurity ions, where $N_0(0)/N_+(0)\ll 1$. An increase in the concentration of lattice-neutral Fe^{2+} ions leads to an increase in the degree of spatial correlations in the correlated system of Fe^{3+} ions and, accordingly, to a significant increase in the electron mobility.

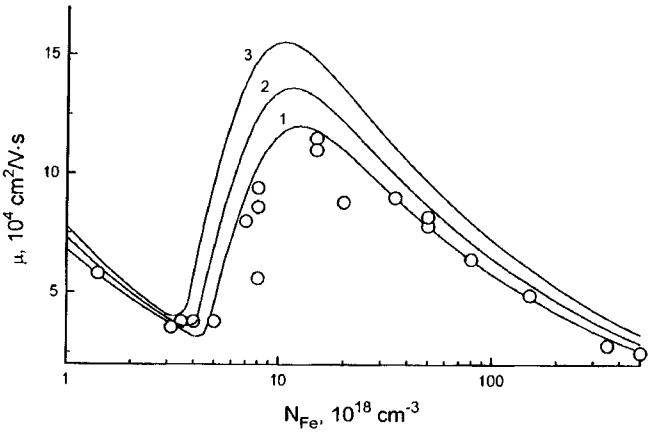

FIG. 1. Dependence of the electron mobility on the concentration of iron impurity ions at various pressures P, kbar: *1* — 0, *2* — 5, *3* — 10. The points denote experimental data taken from the review in Ref. 1 for $P=0$.

3. COMPARISON OF THE THEORY WITH EXPERIMENT

In comparing the results of the calculation of the $\mu(P)$ curves with the experimental data in Ref. 5 it must be taken into account that HgSe:Fe crystals, like HgSe crystals, always contain uncontrolled intrinsic defects (interstitial atoms, mercury vacancies, etc.) with a concentration N_d of the order of 1×10^{18} cm^{-3} or more.[1] These defects lead to an appreciable spread (up to 25%) of values for the electron mobility at liquid-helium temperatures in HgSe:Fe samples with the same content of iron impurity ions (Fig. 1). A comparison of the values of the electron mobility $\mu(0)$ calculated from Eqs. (10)–(12) with the experimental data in Ref. 5 also shows that the scattering of electrons on the randomly distributed intrinsic defects must be included in the treatment. Under the assumption that Matthiessen's rule holds for the relaxation mechanisms of the electron momentum considered, the expression for the total mobility with consideration of the scattering at the intrinsic defects can be presented in the form

$$\mu(P)=(1/\mu_e(P)+1/\mu_{\mathrm{al}}(P)+1/\mu_d(P))^{-1}, \tag{13}$$

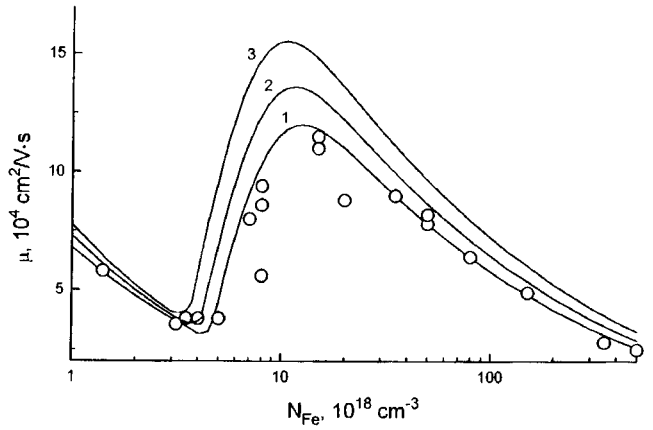

FIG. 2. Dependence of the contributions of the scattering on Fe^{3+} ions (*1*a, *2*a, and *3*a), and the scattering on the alloy potential (*1*, *2*, and *3*) to the electron mobility on the concentration of the iron impurity ions at various pressures P, kbar: *I*, *1*, *1*a — 0; *2*, *2*a — 5; *3*, *3*a — 10.

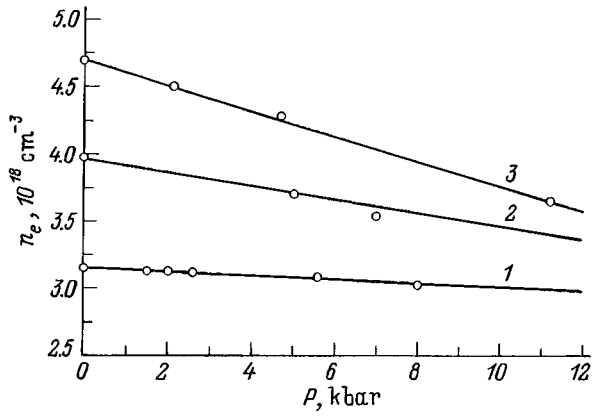

FIG. 3. Dependence of the electron density on the pressure for samples with various concentrations of iron impurity ions N_{Fe}, 10^{18} cm^{-3}: *1*, — 2, *2* — 4, *3* — 8. The points denote experimental data from Ref. 5.

where $\mu_d(P)=\mu_{\mathrm{BH}}(P)N_+/N_d$, N_d is the concentration of intrinsic defects, and $N_+=N_{\mathrm{Fe}}^{3+}+N_d$ is the total concentration of charged impurity atoms. In the region of the mixed-valence state $N_+\approx N_{\mathrm{Fe}}^*$. Thus, the concentration of intrinsic defects in the samples can be calculated from a comparison of the values of the mobility $\mu(0)$ calculated from Eqs. (10), (11), and (13) with the experimental values. We obtained values of N_d equal to 1.1×10^{18} and 0.35×10^{18} cm^{-3} for samples with concentrations of iron impurity ions equal to 8×10^{18} and 20×10^{18} cm^{-3}, respectively.

Figures 3 and 4 present calculated $n_e(P)$ and $\mu(P)$ curves for samples with different concentrations of iron impurity ions. The good agreement between the calculated and measured values of $n_e(P)$ is evidence that the two-band Kane model defined by (5) and (6) can be used to analyze the influence of pressure on the electron density and kinetic characteristics of HgSe:Fe crystals. As is seen from Fig. 4, disregarding the scattering at the intrinsic defects, the calculated values of the mobility are appreciably greater than the experimentally measured values. When the scattering at the intrinsic defects is taken into account, the theory that we

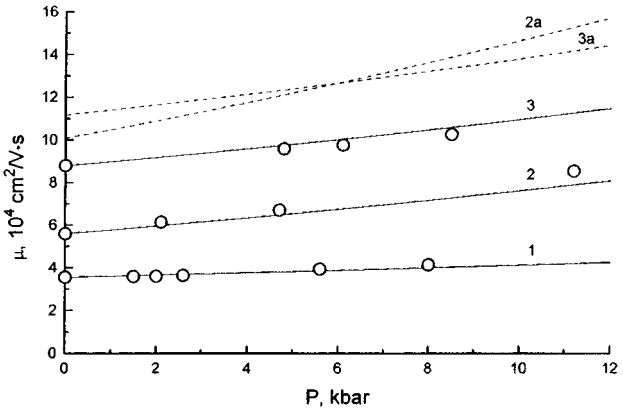

FIG. 4. Pressure dependence of the electron mobility for samples with various concentrations of impurity ions N_{Fe}, 10^{18} cm^{-3}: *1* — 2, *2* — 8, *3* — 20. Curves *2*a and *3*a were calculated for the respective concentrations of iron without allowance for the scattering by intrinsic defects. The points denote experimental data from Ref. 5.

developed provides fairly good quantitative agreement with the experimental data from Ref. 5. It is noteworthy that the method based on Matthiessen's rule for taking into account the contribution to the mobility $\mu(P)$ from the scattering of electrons on intrinsic defects (13) can provide only a rough estimate of N_d. Actually, when the scattering of electrons on the correlated system of Fe^{3+} ions and at the randomly distributed intrinsic defects is considered, the effects of the mutual influence of the electron momentum relaxation processes must be taken into account. In fact, under mixed-valence conditions the *d* holes, in contrast with the intrinsic defects, can be redistributed among the crystal lattice sites occupied by iron ions. Therefore, the *d* holes effectively ''screen'' the interaction of electrons with intrinsic defects, which leads to weakening of the scattering of electrons by the latter. The screening effect of the *d* holes depends not only on their concentration, but also on the number of free sites, to which the *d* holes can pass. As the pressure increases, the concentration of lattice-neutral Fe^{2+} centers and, thus, the degree of spatial ordering of the Fe^{3+} ions increase. The screening effect of the *d* holes also increases. As can be seen from Fig. 4, the experimental values of $\mu(P)$ for the sample with $N_{\mathrm{Fe}}=8\times10^{18}$ cm^{-3} increases more rapidly than would follow from the results of a calculation without allowance for the influence of the mixed-valence iron impurity ions on the scattering of electrons by the intrinsic defects. A more detailed discussion of the mutual influence of the electron relaxation processes on the correlated system of ions and the randomly distributed ions is beyond the scope of this study and calls for a separate treatment.

Equations (10)–(13) enable us to isolate the contribution to the mobility caused by scattering on the correlated system of Fe^{3+} ions from the experimentally obtained $\mu^{\mathrm{exp}}(P)$ curves:

$$\mu_c^{\mathrm{exp}}(P)=[1\mu^{\mathrm{exp}}(P)-1/\mu_{\mathrm{al}}(P)=1/\mu_d]^{-1}. \tag{14}$$

We note that the degree of spatial order of the correlated system of Fe^{3+} ions in our theory is described by the packing parameter η, which appears in the expression for the structure factor[3] and determines $\Phi_c(k_F,\eta)$. Therefore, we first find the values of N_{Fe}, $N_0(P_1)$, $N_+(P_1)$, $k_F(P_1)$, etc. appearing in (14) for assigned values of P_1 and N_{Fe}. Then we calculate $\mu_c^{\mathrm{theor}}(P_1,\eta)$ as a function of η, and from the expression

$$\mu_c^{\mathrm{exp}}(P_1)=\mu_c^{\mathrm{theor}}(P_1,\eta) \tag{15}$$

we find the $\eta(P)$ curves for different concentrations of iron impurity ions, which are presented in Fig. 5. It can be seen from the figure that the packing parameter is a function of the pressure in the range considered when $N_{\mathrm{Fe}}=8\times10^{18}$ cm^{-3}, while the degree of spatial ordering of the Fe^{3+} ions scarcely varies with increasing pressure when $N_{\mathrm{Fe}}=2\times10^{19}$ cm^{-3}. We note that the calculation of $\eta(P)$ was performed without regard for the influence of the mixed-valence iron impurity ions on the scattering of electrons by the intrinsic defects, which led to overestimated values of the packing parameter.

Thus, at a large concentration of iron impurity ions $(N_0/N_+\gg1)$ the increase in electron mobility with the pres-

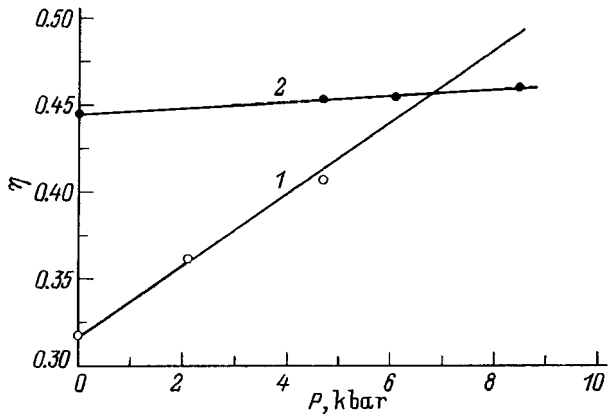

FIG. 5. Pressure dependence of the packing parameter η for samples with various concentrations of iron impurity ions N_{Fe}, cm10^{18} cm^{-3}: *1* — 8, *2* — 20. The points denote the values of η obtained from Eqs. (14) and (15).

sure is caused mainly by the decrease in the electron effective mass at the Fermi level and the constant $\Lambda(P)$, which determines the contribution of the alloy scattering. When the concentration of the impurity iron ions is small $(N_0/N_+ \leqslant 1)$, the main contribution to the mobility is made by the scattering of electrons on the correlated system of Fe^{3+} ions. An increase in the pressure in this case leads to an appreciable increase in the degree of ordering of the correlated system of Fe^{3+} ions (Fig. 5) and, accordingly, in the electron mobility.

4. CONCLUSIONS

We have investigated the influence of hydrostatic pressure on the parameters of the band structure and the electron mobility in HgFe:Se crystals in the low-temperature region. A donor-impurity regime and a mixed-valence state have been considered, and the pressure dependences of the contributions of the scattering on the correlated system of Fe^{3+} ions, the scattering by the randomly distributed ions, and the alloy scattering to the electron mobility have been isolated and analyzed. It is shown that at a relatively small concentration of iron impurity ions in the region of the mixed-valence state the increase in the electron mobility with the pressure is caused mainly by the increase in the degree of spatial ordering in the correlated system of Fe^{3+} ions. When $N_0 \gg N_+$, the increase in the mobility with the pressure is caused predominantly by the decrease in the electron effective mass and the contribution of the alloy scattering. The variation of the degree of spatial ordering of the Fe^{3+} ions as the pressure is increased has been analyzed.

Unfortunately, the experimental material at our disposal from investigations of the influence of hydrostatic pressure on the kinetic characteristics of gapless semiconductors is quite sparse. In our opinion, this is due not only to the complexity of such investigations, but also to the lack of a theory which would permit extracting information regarding the influence of pressure on the correlation properties of the system of iron ions. It would be desirable to perform more detailed experimental investigations of the influence of pressure on the properties of HgFe:Se crystals over a broad range of concentrations of the iron impurity ions. In particular, it would be of interest to investigate samples with $N_{\mathrm{Fe}} > 5 \times 10^{19}$ cm^{-3}, in which alloy scattering makes the dominant contribution to the electron momentum relaxation. This would permit experimental verification of the pressure dependence of the alloy scattering contribution. We would like to hope that our work will serve as an stimulus for such research.

This work was performed with the support of the Russian Fund for Fundamental Research (Project No. 95-02-03847) and INTAS (Grant No. 93-3657-EXT).

[1] I. M. Tsidil'kovskiĭ, Usp. Fiz. Nauk **162**, 63 (1992) [Sov. Phys. Usp. **35**, 85 (1992)].
[2] F. S. Pool, J. Kossut, U. Debska, and R. Reifenberger, Phys. Rev. B **35**, 3900 (1987).
[3] I. G. Kuleev, I. I. Lyapilin, and I. M. Tsidil'kovskiĭ, Zh. Éksp. Fiz. Fiz. **102**, 1652 (1992) [Sov. Phys. JETP **75**, 893 (1992)].
[4] I. M. Tsidilkovskĭ, *Electron Spectrum of Gapless Semiconductors*, Springer, New York (1996).
[5] C. Skierbiszewski, Z. Wilamowski, T. Suski, J. Kossut, and B. Witkowska, Semicond. Sci. Technol., **8**, 40 (1993).
[6] C. Skierbiszewski, T. Suski, E. Litwin-Staszewska, W. Dobrovolski, K. Dybko, and A. Mycielski, Semicond. Sci. Technol. **4**, 293 (1989).
[7] Z. Wilamowski, K. Świątek, D. Dietl, and J. Kossut, Solid State Commun. **74**, 833 (1990).
[8] Z. Wilamowski, Acta Phys. Pol. A **77**, 133 (1990).
[9] J. Kossut, Phys. Status Solidi B **86**, 593 (1978).
[10] J. M. Ziman, *Models of Disorder: the Theoretical Physics of Homogeneously Disordered Systems*, Cambridge University Press, Cambridge–New York (1979) [Russ. transl., Mir, Moscow (1982)].
[11] E. I. Khar'kov, V. I. Lysov, and V. E. Fedorov, *The Physics of Liquid Metals* [in Russian], Kiev (1979).

Translated by P. Shelnitz

Drift-induced production of concentration gratings in an electron-hole plasma in a high-frequency electric field

V. L. Borblik

Institute of Semiconductor Physics, Ukrainian National Academy of Sciences, 252650 Kiev, Ukraine
(Submitted April 12, 1996; accepted for publication September 16, 1996)
Fiz. Tekh. Poluprovodn. **31**, 686–691 (June 1997)

The role of the frequency of the alternating current used for the drift-induced production of dynamic plasma gratings from seed electron-hole mobility ratio gratings created by an optical interference pattern is investigated. It is shown that the phase mismatch appearing between it and the concentration grating supported by it when the frequency of the alternating current is increased leads to a significant increase in the proportion of the stationary component and the component varying with the fundamental frequency of the plasma gratings produced in comparison with the previously considered low-frequency case. © *1997 American Institute of Physics.* [S1063-7826(97)01006-5]

1. Transient holography[1] is faced with the problem of increasing the recording efficiency of holograms in a nonlinear recording medium. In photorefractive crystals, in particular, this problem is solved by going over to nonstationary recording regimes.[1,2]

Considerably less attention has been focused in this respect on dynamic free-carrier gratings. These gratings, which are recorded as a result of the one- or two-photon interband absorption of light at the maxima of an interference pattern, are destroyed fairly rapidly as a result of the diffusion and/or recombination of the nonequilibrium carriers, and their investigation has been directed for the most part at determining the kinetic parameters of the recording media and the characteristics of the laser radiation recording the grating from the rate of this destruction process.[3–6]

The ways in which the recording efficiency of plasma gratings could be increased were discussed in Refs. 7–9. In those studies[7–8] the utilization of the drift of a bipolar plasma in a longitudinal electric field was proposed for enhancing the contrast of gratings recorded in semiconductors. This effect is due to the nonuniformity of the ratio b between the mobilities of the electrons and holes, which are heated differently by the field of the interference pattern. It is observed even for intraband optical absorption and is essentially nonlocal. This is important for ensuring energy conversion when such gratings are used for a two-wave interaction. On the other hand, the experimental studies of the influence of the heating of free charge carriers by an electric field on the self-diffraction of light in Refs. 10–13 revealed enhancement of the diffraction efficiency of light-induced gratings when both constant and variable longitudinal electric fields were applied to the semiconductor.[1)] The theory of longitudinal bipolar drift under the conditions of weak nonuniformity of b was recently extended[14,15] to the case of an alternating current, and it was shown that the conversion of a weak seed b grating into a more highly contrasted concentration grating of the same spatial frequency also takes place in a variable electric field. Although drift occurs alternately in opposite directions under these conditions, there are always regions for both directions of the current. A stationary concentration grating is created in just these regions in a time-variable field. The greater is the amplitude of the current, the more appreciable is the constant component of the nonequilibrium concentration distribution. In the limit of asymptotically large current amplitudes, the nonequilibrium distribution becomes completely stationary.

Several limiting cases were considered in Refs. 14 and 15. They included, in particular, gratings of arbitrary contrast at quasistationary electric field frequencies and low-contrast gratings at arbitrary frequencies. In the former case the concentration distribution contained (for finite values of the current amplitude) a large set of transient harmonics of the fundamental frequency. In the latter case an increase in the frequency of the working current led to an increase in the phase shift between the concentration grating with the fundamental frequency and the current and, as a consequence, to frequency dispersion of the effect, but the higher harmonics were disregarded. In our study we evaluated the high-frequency case without imposing the specified restrictions. We showed that a time lag in establishing a concentration grating leads to a significant decrease in the proportion of higher transient harmonics in it.

2. The continuity equation which specifies the spatial distribution of the concentration of a quasineutral electron-hole plasma ($p \simeq n \gg N \equiv n-p$) has the form

$$\frac{\partial p}{\partial t} = D\frac{\partial^2 p}{\partial x^2} + \frac{bJ\cos\omega t}{(1+b)^2}\frac{\partial}{\partial x}\left(\gamma(x) + \frac{N}{p}\right) - \frac{p}{\tau_p} + G, \qquad (1)$$

where G is the rate of generation of the plasma, τ_p is its lifetime, J is the amplitude of the density of the variable current (in flux units), $D = 2D_pD_n/(D_p+D_n)$ is the ambipolar diffusivity, which is assumed to be constant here, $\gamma(x) = \gamma_m[1+\cos(2\pi x/\lambda)]$, and λ is the spatial period of the interference pattern.

We first show that outside the asymptotic limit Eq. (1) cannot be solved correctly without allowance for the transient harmonics in the distribution $p(x,t)$. In fact, let us assume that

$$p(x,t) = p_0(x) + p_{1c}(x)\cos\omega t + p_{1s}(x)\sin\omega t + \alpha(2\omega, 3\omega, \ldots), \qquad (2)$$

 1063-7826/97/060585-05$10.00

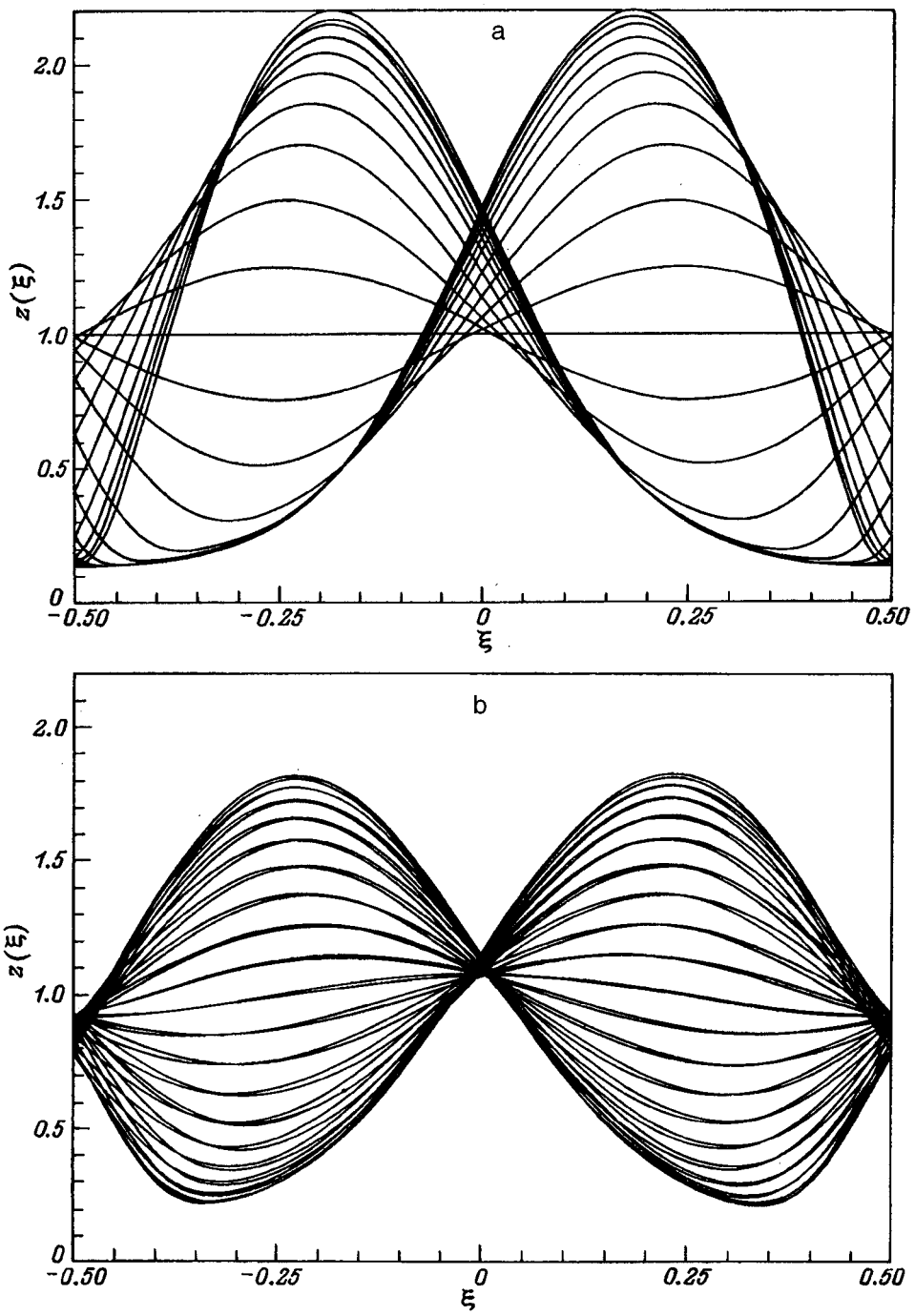

FIG. 1. Distribution of the concentration of electron-hole pairs in one cell of a plasma grating after equal time intervals during one time period of variation of the current for $\Lambda=20$ and $\tau_p/T=1$ (a) and 10^3 (b).

where all the higher harmonics of the fundamental frequency, which are described by the quantity $\alpha(2\omega,3\omega,\dots)$, are small. The function $1/p$ that appears in (1) can then be represented in the form

$$\frac{1}{p(x,t)}=\frac{1}{p_0+p_{1c}\cos\omega t+p_{1s}\sin\omega t}-\frac{\alpha(2\omega,3\omega,\dots)}{(p_0+p_{1c}\cos\omega t+p_{1s}\sin\omega t)^2}. \tag{3}$$

Calculating the coefficients in the Fourier expansion of this function, we obtain

$$\left(\frac{1}{p}\right)_0=\frac{2}{\sqrt{p_0^2-p_1^2}},$$

$$\left(\frac{1}{p}\right)_{1c}=\frac{2p_{1c}}{p_1^2}\left(1-\frac{p_0}{\sqrt{p_0^2-p_1^2}}\right),$$

$$\left(\frac{1}{p}\right)_{1s}=\frac{2p_{1s}}{p_1^2}\left(1-\frac{p_0}{\sqrt{p_0^2-p_1^2}}\right),$$

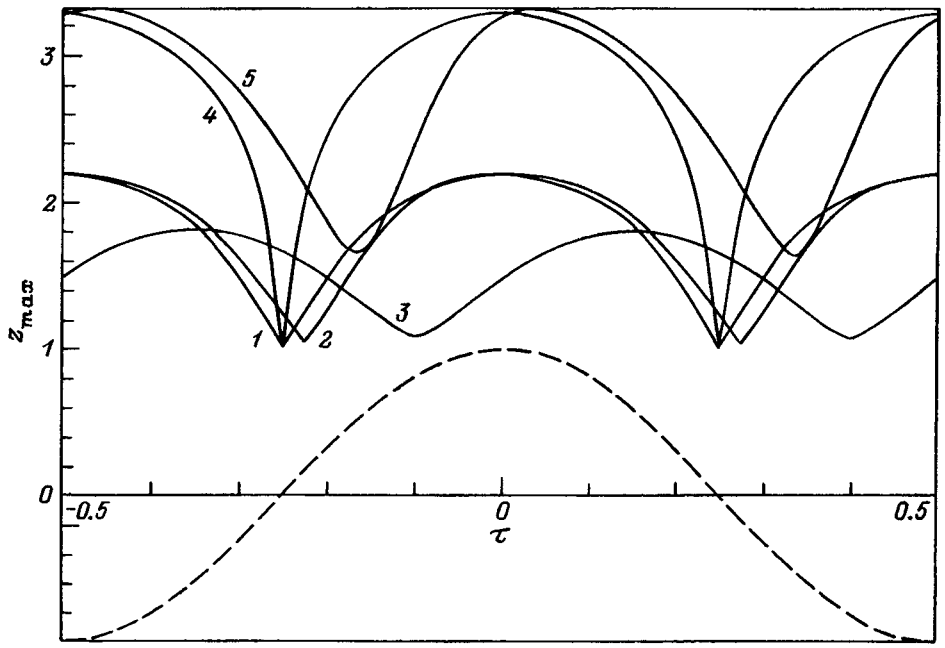

FIG. 2. Time dependence of the peak values of the plasma concentration in a grating for $\Lambda=20$ and $\tau_p/T=1$ (*1*), 10 (*2*), and 10^3 (*3*) and for $\Lambda=100$ and $\tau_p/T=1$ (*4*) and 10^3 (*5*); dashed curve – corresponding variation of the current.

$$\left(\frac{1}{p}\right)_{2c}=2\frac{p_{1c}^2-p_{1s}^2}{p_1^2}\frac{1}{\sqrt{p_0^2-p_1^2}},$$

$$\left(\frac{1}{p}\right)_{2s}=2\frac{p_{1c}p_{1s}}{p_1^2}\frac{1}{\sqrt{p_0^2-p_1^2}},$$

etc., where $p_1^2=p_{1c}^2+p_{1s}^2$. We see from these expressions that when the contribution of the higher harmonics to $p(x,t)$ is small (when p_1 is close to p_0), all the Fourier coefficients of the function $1/p(x,t)$ increase without bound, precluding confinement to a finite Fourier representation. Therefore, direct numerical integration of Eq. (1) was undertaken here to study high-contrast plasma gratings at arbitrary frequencies.

3. In dimensionless variables

$$\xi=\frac{x}{\lambda},\quad \tau=\frac{t}{T},\quad z=\frac{p}{G\tau_p},$$

where T is the period of variation of the current, Eq. (1) takes the form

$$\frac{\lambda^2}{L^2}\frac{\tau_p}{T}\frac{\partial^2 z}{\partial\xi^2}=\frac{\partial^2 z}{\partial\xi^2}\Lambda\cos(2\pi\tau)\times\left(\pi\sin(2\pi\xi)-\frac{\Gamma}{z^2}\frac{\partial z}{\partial\xi}\right)-\frac{\lambda^2}{L^2}(z-1),\quad (4)$$

where

$$\Lambda=\frac{J\lambda\gamma_m}{(D_n+D_p)G\tau_p},\quad \Gamma=\frac{N}{2\gamma_m G\tau_p},\quad L^2=D\tau_p.$$

In the ranges of values of τ and ξ from $-1/2$ to $1/2$ we found the solution of Eq. (4) which satisfies the spatial and temporal periodicity conditions

$$z(-1/2,\tau)=z(1/2,\tau),\quad z(\xi,-1/2)=z(\xi,1/2) \quad (5)$$

and which is normalized to the total plasma concentration

$$\int_{-\frac{1}{2}}^{\frac{1}{2}} z(\xi,\tau)d\xi=1. \quad (6)$$

Such temporal families of solutions for the dimensionless current amplitude $\Lambda=20$ are presented in Fig. 1 for two values of the frequency, which is measured here in terms of the ratio τ_p/T: 1 in Fig. 1a and 10^3 in Fig. 1b. The calculation was performed for the case of a high contrast ($\Gamma=0.1$) and a weak influence of recombination ($\lambda^2/L^2=10^{-2}$). A comparison of these two families reveals that there is no solution in the form of an unperturbed concentration distribution corresponding to passage of the working current through zero at the higher frequency, while such a solution exists at the lower frequency.

The influence of the frequency and the amplitude of the working current on the shaping of a plasma grating is conveniently traced by plotting the time dependence of the peak value of the plasma concentration. Such plots are presented in Fig. 2, together with the time dependence of the alternating current (the dashed curve). The figure reveals how the phase mismatch between the peak value of the concentration and the peak value of the current increases with increasing frequency at a fixed current amplitude (curves *1–3* or *4* and *5*). The contrast of the grating, which is characterized by the spread of the fluctuations of the peak value of the concentration, also drops. All of these phenomena are typical manifestations of the frequency dispersion of the effect.

As the current amplitude increases, the phase mismatch naturally decreases (curves *4* and *5*). However, even a small lag of the concentration distribution behind the current leads to a significant nonequilibrium concentration even at times close to the passage of the working current through zero. As

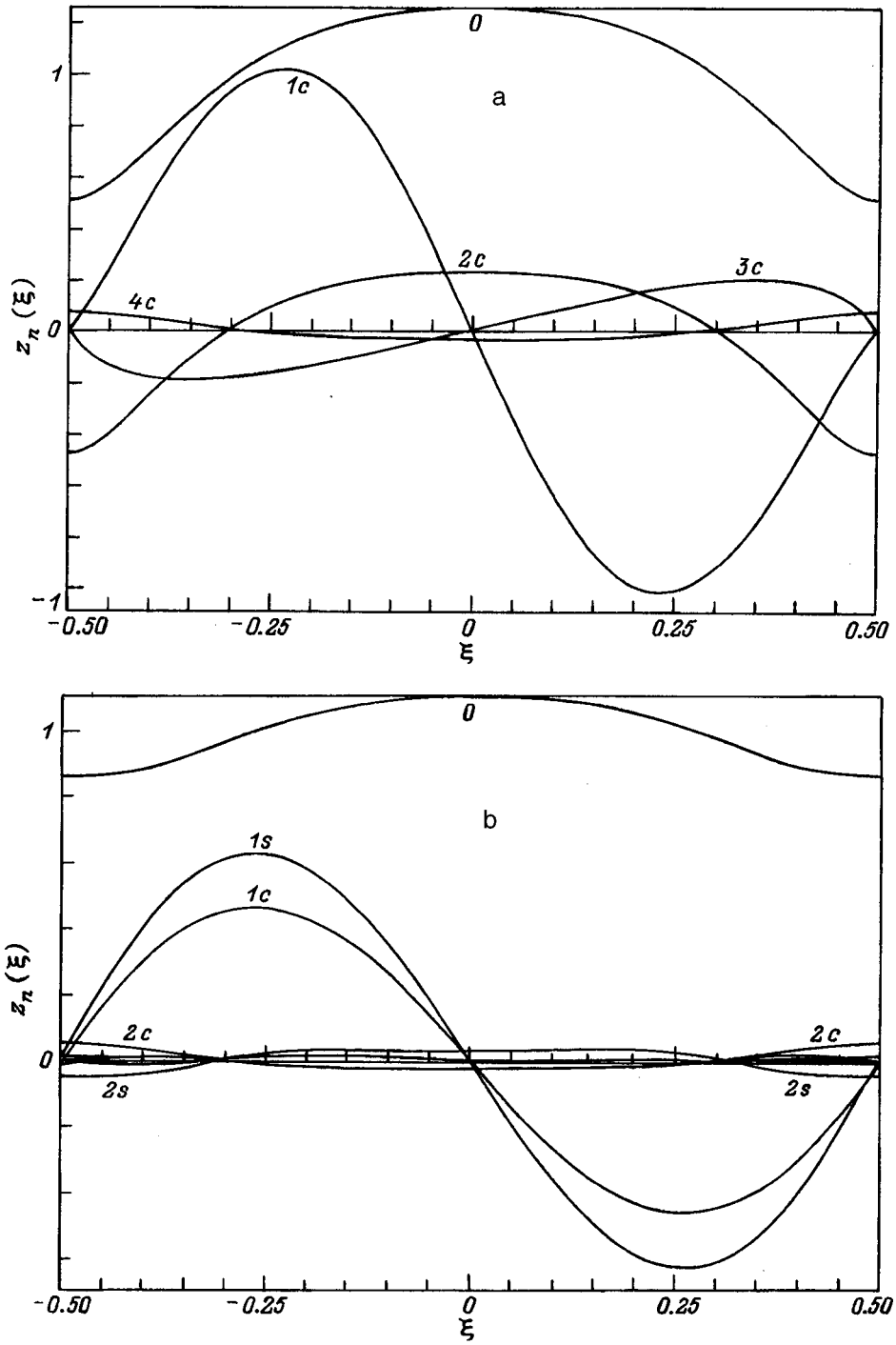

FIG. 3. Spatial profile of the first five coefficients in the Fourier expansion of $p(x,t)$ for $\Lambda=20$ and $\tau_p/T=1$ (a) and 10^3 (b). The curves are labeled by the numbers of the harmonics.

a result, the constant component of the plasma grating increases at high frequencies.

Fourier analysis of the exact solutions obtained completely confirms this conclusion and shows that the fraction of the component of the plasma grating which oscillates with the fundamental frequency also increases significantly at high frequencies (Fig. 3), since the amplitudes of the higher harmonics drop sharply [as was presumed in the expansion (2)]. For just this reason, the amplitudes of the first four Fourier components of the function $1/p(x,t)$ corresponding to the numerically determined solution are of the same order here, as is demonstrated by Fig. 4 (this is also consistent with the results of the preliminary analysis). We note that the amplitudes of the harmonics [both $p(x,t)$ and $1/p(x,t)$] exhibit a significant spatial dependence. In particular, the grating lines which oscillate with the fundamental frequency undergo shifts relative to the lines of the constant component, which can be of additional interest for applications.

4. Thus, an increase in the frequency of the alternating current used for the drift-induced production of plasma gratings leads (because of the time-lag effects) to significant depletion of their nonstationary components from the frequency spectrum. However, this cannot be utilized to obtain an approximate solution of the problem that would be a basis

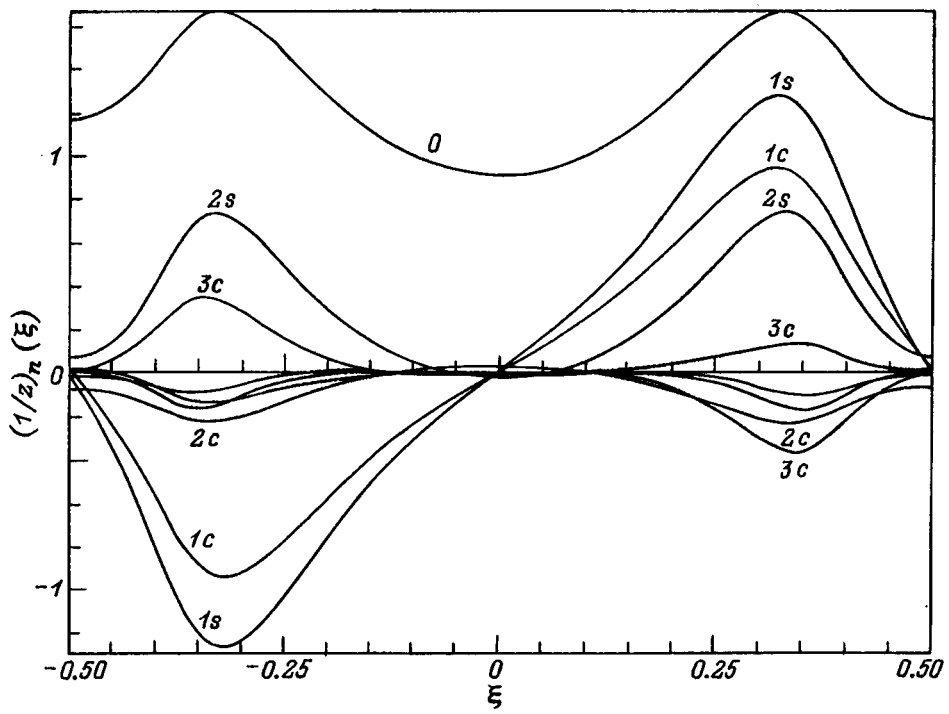

FIG. 4. Spatial profile of the first five coefficients in the Fourier expansion of $1/p(x,t)$ for $\Delta=20$ and $\tau_p/T=10^3$. The curves are labeled by the numbers of the harmonics.

for neglecting all the transient harmonics of the fundamental frequency.

We thank Z. S. Gribnikov for discussing this work.

This work was performed as part of Project No. 2.3/345, which is supported by the Foundation for Fundamental Research of the State Committee for Science and Technology of Ukraine.

[1)]Jarasiunas *et al.*[13] interpreted the effect that they discovered as being due to Gunn domain formation in the InP and GaAs samples; however, they also observed similar enhancement of the self-diffraction efficiency in a longitudinal electric field of the order of 1 kV/cm in Si.

[1] V. L. Vinetskiĭ, N. V. Kukhtarev, S. G. Odulov, and M. S. Soskin, Usp. Fiz. Nauk **129**, 113 (1979) [Sov. Phys. Usp. **22**, 742 (1979)].
[2] M. P. Petrov, S. I. Stepanov, and A. V. Khomenko, *Photorefractive Crystals in Coherent Optical Systems*, Springer-Verlag, Berlin–New York (1992).
[3] A. A. Borshch, M. S. Brodin, V. I. Volkov, V. V. Ovchar, and D. T. Tarashchenko, Kvantovaya Elektron. **4**, 646 (1977) [Sov. J. Quantum Electron. **7**, 358 (1977)].
[4] Yu. Vaıtkus and K. Yarashyunas, Litov. Fiz. Sb. **19**, 211 (1979).
[5] A. L. Smirl, S. C. Moss, and J. R. Lindle, Phys. Rev. B **25**, 2645 (1982).
[6] H. J. Eichler and F. Massmann, J. Appl. Phys. **53**, 3237 (1982).
[7] T. Z. Gribnikova and Z. S. Gribnikov, Ukr. Fiz. Zh. **27**, 1350 (1982).
[8] Z. S. Gribnikov, Fiz. Tekh. Poluprovodn. **16**, 1843 (1982) [Sov. Phys. Semicond. **16**, 1183 (1982)].
[9] Z. S. Gribnikov, R. N. Litovskiĭ, and E. V. Mozdor, Fiz. Tekh. Poluprovodn. **17**, 1438 (1983) [Sov. Phys. Semicond. **17**, 913 (1983)].
[10] Yu.Yu. Vaĭtkus, L. E. Subachyus, and K.Yu. Yarashyunas, Litov. Fiz. Sb. **25**, 107 (1985).
[11] J. Vaitkus, K. Jarasiunas, E. Gaubas, L. Jonikas, R. Pranaitis, and L. Subachius, IEEE J. Quantum Electron. **22**, 1298 (1986).
[12] Yu. Vaĭtkus, E. Starikov, L. Subachyus, and K. Yarashyunas, Litov Fiz. Sb. **30**, 336 (1990).
[13] J. K. Jarasiunas, V. Gruzinskis, P. Shiktorov, E. Starikav, L. Subachius, and G. Valusis, in *Proceedings of the 9th Symposium on Ultrafast Phenomena in Semiconductors*, Vilnius, Lithuania, published in Lith. J. Phys. **35**, 426 (1995).
[14] V. L. Borblik and Z. S. Gribnikov, Fiz. Tekh. Poluprovodn. **30**, 793 (1996) [Semiconductors **30**, 425 (1996)].
[15] V. L. Borblik and Z. S. Gribnikov, in *Proceedings of the 9th Symposium on Ultrafast Phenomena in Semiconductors*, Vilnius, Lithuania, published in Lith. J. Phys. **35**, 488 (1995).

Translated by P. Shelnitz

Thermal-gradient concentration in a bipolar semiconductor with phonon drag of charge carriers

A. M. Konin

Institute of Semiconductor Physics, 2600 Vilnius, Lithuania
(Submitted June 3, 1996; accepted for publicationSeptember 16, 1996)
Fiz. Tekh. Poluprovodn. **31**, 692–694 (June 1997)

The influence of the ''hot-phonon drag'' of electron-hole pairs on the concentration distribution of the charge carriers in a semiconductor sample with a transverse lattice-temperature gradient is investigated theoretically. The most interesting case of maximum asymmetry of the boundary conditions and a sample thickness that is close to the diffusion length is considered. It is shown that the occurrence of drag leads to alteration of the dependence of the total concentration on the coordinate from an increasing function to a decreasing function and, on the other hand, to a dependence on the direction of the temperature gradient, as well as to considerable quantitative redistribution of the concentration along a cross section of the sample. © *1997 American Institute of Physics.* [S1063-7826(97)01106-X]

The transverse thermal-gradient concentration effect in an intrinsic semiconductor was investigated theoretically and experimentally in Ref. 1. The distribution of the nonequilibrium concentration of electron-hole pairs was calculated with allowance for the thermopower fields formed according to the scheme in Ref. 2, and good agreement between the theoretical and experimental results was obtained, providing definite support for the theoretical model proposed in Ref. 2.

However, the case which ignores the influence of the anisotropic part of the phonon distribution function on the anisotropy of the electron and hole distribution functions, i.e., the ''hot-phonon drag'' of electron-hole pairs,[3] was considered in Refs. 1 and 2. This assumption is valid for wide-gap semiconductors at relatively high temperatures.[3] In narrow-gap semiconductors at relatively low temperatures with weak phonon scattering on the defects, considerable hot drag of electron-hole pairs is perfectly realistic.[3] This drag leads to a significant increase in the electron and hole thermopowers and can, therefore (see Ref. 2), significantly alter the spatial distribution of the electron-hole pairs in the crystal.

In this study we extended the model proposed in Ref. 1 to the case of the hot-phonon drag of electron-hole pairs and we calculated the carrier concentration distribution in a semiconductor with a transverse lattice-temperature gradient.

Below we shall consider the temperature range in which the condition $\nu_{\text{ph-ph}} \gg \nu_{\text{ph-e}}$ holds.[3] Here $\nu_{\text{ph-ph}}$ is the frequency of phonon-phonon collisions, and $\nu_{\text{ph-e}}$ is the frequency of collisions between phonons and charge carriers. On the one hand, this allows us to consider nondegenerate semiconductors with intrinsic conductivity, in which the concentration effects are strongest. On the other hand, in this case the phonons comprise a bulk energy reservoir, since their thermal conductivity is considerably greater than the electronic thermal conductivity, and their mean free path is considerably smaller than the thickness of the semiconductor.[3]

According to Ref. 3, hot drag occurs under the condition

$$K_{n(p)} = \frac{es^2}{\mu_{n(p)} T \nu_{\text{ph-d}}} \gg 1, \tag{1}$$

where $K_{n(p)}$ is the electron (hole) drag factor, $\mu_{n(p)}$ is the electron (hole) mobility, s is the velocity of sound in the semiconductor, e is the charge of a hole, T is the lattice temperature, and $\nu_{\text{ph-d}}$ is the frequency of collisions between phonons and defects.

After calculating the kinetic coefficients[3] in the general case and separating, according to Ref. 2, the thermopowers into two components, one of which is stipulated by the gradient of the chemical potential, while the other is the ''external'' thermodynamic force, we find

$$\underline{j}_n = en\mu_n \left(\mathrm{E} + \frac{T}{en} \nabla n - \alpha_n^0 \nabla T - \left(\alpha_n^1 - \frac{1}{e} K_n \right) \nabla T \right),$$

$$\underline{j}_p = ep\mu_p \left(\mathrm{E} - \frac{T}{ep} \nabla p - \alpha_p^0 \nabla T - \left(\alpha_p^1 + \frac{1}{e} K_p \right) \nabla T \right), \tag{2}$$

where $n(p)$ is the electron (hole) density, E is the total electric field,

$$\alpha_n^0 = -\frac{1}{e}\left(\frac{F_n}{T} - \frac{3}{2} \right), \quad \alpha_n^1 = -\frac{1}{e}\left(q_n + \frac{5}{2} - \frac{F_n}{T} \right),$$

$$\alpha_p^0 = \frac{1}{e}\left(\frac{F_p}{T} - \frac{3}{2} \right), \quad \alpha_p^1 = \frac{1}{e}\left(q_p + \frac{5}{2} - \frac{F_p}{T} \right), \tag{3}$$

F_n and F_p are the electron and hole quasi-Fermi levels, and q_n and q_p are parameters which characterize the electron and hole momentum relaxation mechanisms.[4]

As is seen from Eqs. (2), the occurrence of the hot-phonon drag of electron-hole pairs leads to a considerable increase in the external thermodynamic force, which creates nonequilibrium charge carriers. On the other hand, the nonuniform equilibrium distribution of the electron-hole pairs does not depend at all on the drag factors $K_{n,p}$, i.e., it remains unchanged.[1]

Let us consider a semiconductor slab, whose surface $x = a$ is in thermal contact with a thermostat at a temperature T_+ and whose surface $x = -a$ is in contact with a thermostat

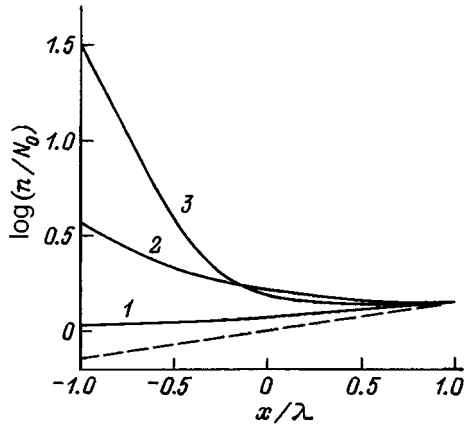

FIG. 1. Distribution of the concentration of electron-hole pairs across the thickness of an InSb sample for $\Delta T=10$ K, $T_0=100$ K, $S_-=0$, $S_+\to\infty$, and various values of K: *1* — 0, *2* — 100, *3* — 400.

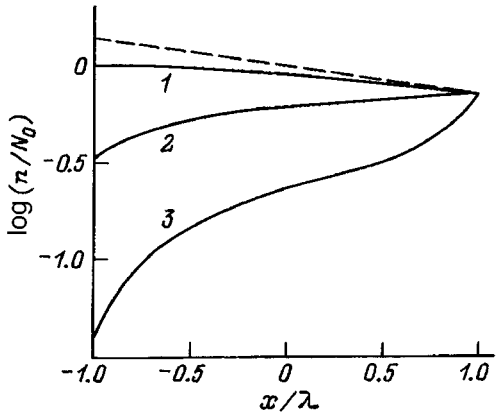

FIG. 2. Distribution of the concentration of electron-hole pairs across the thickness of an InSb sample for $\Delta T=-10$ K, $T_0=100$ K, $S_-=0$, $S_+\to\infty$, and various values of K: *1* — 0, *2* — 100, *3* — 400.

at a temperature T_-. We assume that the thickness of the sample is considerably greater than the electron (hole) cooling distance.[4] The temperatures of all the quasiparticles will then coincide[5], and

$$T(x)=T_0+\frac{\Delta T}{2}\frac{x}{a}, \tag{4}$$

where $T_0=\frac{1}{2}(T_++T_-)$, $\Delta T=T_+-T_-$, and $2a$ is the thickness of the sample.

Performing an iterative procedure for an intrinsic semiconductor according to the scheme proposed in Ref. 2 and taking into account the condition[6] $j_n^x+j_p^x=0$, we obtain

$$j_n^x=\frac{eDN_0}{\lambda}\left[\frac{d\tilde{\nu}}{d\xi}+2\varphi\tilde{\nu}+\beta\cdot e^{\alpha\xi}\right], \tag{5}$$

where

$$\xi=\frac{x}{\lambda},\quad u=\frac{a}{\lambda},\quad \alpha=\frac{E_g\Delta T}{4uT_0^2},$$

$$\varphi=(q_n+q_p+K+2)\frac{\Delta T}{8uT_0},$$

$$\tilde{\nu}=\frac{\Delta n}{N_0},\quad K=K_n+K_p,\quad \beta=2\varphi+\alpha+\frac{3}{4}\frac{\Delta T}{uT_0},$$

$D=2\mu_n\mu_p/\mu_n+\mu_p\ T_0/e$ is the ambipolar diffusivity, Δn is the concentration of nonequilibrium electron-hole pairs, λ is the diffusion length, τ is the lifetime of an electron-hole pair, and N_0 is the equilibrium carrier concentration at $x=0$. The dependence of the equilibrium concentration on the coordinate is described by the expression

$$n_0(\xi)=N_0e^{\alpha\xi}. \tag{6}$$

After solving the diffusion equation[6]

$$\frac{1}{e}\frac{dj_n^x}{dx}-\frac{\Delta n}{\tau}=0, \tag{7}$$

for the total concentration $\nu=\dfrac{n_0(\xi)+\Delta n}{N_0}$, we obtain

$$\nu=\frac{\beta}{1-\alpha(2\varphi+\alpha)}[A_1e^{r_1\xi}+A_2e^{r_2\xi}+\alpha e^{\alpha\xi}]+e^{\alpha\xi}, \tag{8}$$

where $r_1=-\varphi+\sqrt{\varphi^2+1}$, and $r_2=-\varphi-\sqrt{\varphi^2+1}$.

The constants A_1 and A_2 are found from the boundary conditions

$$\frac{1}{e}j_n^x|_{x=\pm a}=\mp S_\pm\Delta n|_{x=\pm a}, \tag{9}$$

where $S_\pm$ denotes the surface recombination rate on the surfaces $x=\pm a$ of the sample.

For the most interesting case of maximum asymmetry of the boundary conditions ($S_-=0$ and $S_+\to\infty$) A_1 and A_2 have the form

$$A_1=-\frac{\alpha r_1\exp(\alpha-r_2)u+\exp(r_2-\alpha)u}{r_1\exp(r_1-r_2)u-r_2\exp(r_2-r_1)u},$$

$$A_2=\frac{\alpha r_2\exp(\alpha-r_1)u+\exp(r_1-\alpha)u}{r_1\exp(r_1-r_2)u-r_2\exp(r_2-r_1)u}. \tag{10}$$

The results of a calculation of the distribution of the concentration of electron-hole pairs in InSb samples of thickness 2λ based on Eqs. (8) and (10) are presented in Figs. 1 and 2.

As can be seen from Fig. 1, in the absence of drag (curve *1*) carriers are not removed from the cold surface $x=-\lambda$ with a low surface recombination rate under the action of the phonon heat flux or, stated differently, the external thermodynamic force. In this case the total concentration on the cold surface increases, and its dependence on x remains, like that of the equilibrium concentration, a monotonically increasing function. We note that, as follows from (8) and (10), in sufficiently thin samples ($2a\ll\lambda$) the total concentration scarcely depends on the coordinate in the absence of drag and is equal to the equilibrium concentration of electron-hole pairs on the surface with a high surface recombination rate.

When drag occurs (Fig. 1, curves *2* and *3*), the transport of electron-hole pairs to the cold surface increases under the action of the considerable external thermodynamic force, and

the dependence of the total concentration on the coordinate x becomes a monotonically decreasing function. The electrical conductivity of the sample also increases significantly: by a factor of 1.9 in comparison to the equilibrium value when $K=100$ and by a factor of 4.55 when $K=400$.

For the same reasons, when the sign of the temperature gradient is reversed (Fig. 2), electron-hole pairs are transported to the surface with a high surface recombination rate, where they effectively recombine. Consequently, the concentration of electron-hole pairs decreases both in the bulk and on the ''hot'' surface $x=-\lambda$. An increase in drag leads to alteration of the functional dependence of $n(x)$ from a decreasing function (curve *1*) to an increasing function (curves *2* and *3*) and to a considerable decrease in the electrical conductivity of the sample, by a factor of 1.7, when $K=100$ and by a factor of 4, when $K=400$.

Thus, the phonon drag of electron-hole pairs leads to considerable alteration of the distribution of the carrier concentration under the action of the lattice-temperature gradient.

[1] A. M. Konin and A. P. Sashuk, Fiz. Tekh. Poluprovodn. (in press).
[2] Yu. G. Gurevich and O. L. Mashkevich., Fiz. Tekh. Poluprovodn. **24**, 1327 (1990) [Sov. Phys. Semicond. **24**, 835 (1990)].
[3] F. G. Bass, V. S. Bochkov, and Yu. G. Gurevich, *Electrons and Phonons in Organic Semiconductors* [in Russian], Nauka, Moscow (1984).
[4] F. G. Bass, V. S. Bochkov, and Yu. G. Gurevich, Fiz. Tekh. Poluprovodn. **7**, 3 (1973) [Sov. Phys. Semicond. **7**, 1 (1973)].
[5] V. S. Bochkov and Yu. G. Gurevich, Fiz. Tekh. Poluprovodn. **17**, 728 (1983) [Sov. Phys. Semicond. **17**, 456 (1983)].
[6] A. M. Konin, V. G. Rudaĭtis, and A. P. Sashuk, Litov Fiz. Sb. **30**, 285 (1990).

Translated by P. Shelnitz

Light-emitting diodes based on a metal-insulator-semiconductor structure

V. B. Katok, M. I. Panfilov, and G. E. Chaĭka

Ukrainian State Academy of Communications, 252110 Kiev, Ukraine
(Submitted March 20, 1996; accepted for publication October 14, 1996)
Fiz. Tekh. Poluprovodn. **31**, 695–696 (June 1997)

[S1063-7826(97)01206-4]

A situation in which the rate of information transmission is limited by the speed of the electron fluxes appearing in the elements of the information transmission system has now arisen. Information now must be transmitted in some other ways, primarily by means of light. The replacement of the electron fluxes by light fluxes raises the prospect of increasing the speed by many orders of magnitude, but it is accompanied by some fundamental difficulties. These difficulties stem from the fact that in electron fluxes the information carriers are charged particles, which can be regulated fairly simply by electric and magnetic fields. In light fluxes the information carriers are neutral particles, viz., photons, which are difficult to regulate. These fluxes can be regulated by varying the refractive index or, more precisely, either its real or imaginary component.

Variation of the imaginary component of the refractive index leads to damping of the light flux. Inhomogeneous semiconductor structures, most often $p-n$ structures, are used to regulate the damping. A light flux propagates parallel to the electrodes. The application of a voltage to such a structure alters the relationship between the i-region, where there are no carriers, and the doped n- and p-regions, where additional light scattering occurs on the free carriers. Thus, the light damping is regulated by applying a voltage (see Ref. 1).

Regulation of the real part of the refractive index is most often achieved by the electro-optic effect. However, the use of optoelectronic devices based on this effect has its own shortcomings. First, fairly strong electric fields are needed to vary the refractive index, and, second, the electro-optic effect is based on the influence of an electric field on a crystal lattice (a fairly sluggish process), which restricts the rate of modulation of a light beam.

The present report focuses attention on the possibility of using the free electrons present in a solid to vary the refractive index. A material based on GaAs, which is widely employed in micro- and optoelectronics, can serve as such a solid. For GaAs structures it is significant that GaAs can be doped by ions to a high concentration, which, in turn, produce a high concentration of free carriers. Therefore, the refractive index in such a medium depends not only on the refractive index of the crystal lattice proper, but also on the free carriers (the plasma effect) according to the relation

$$n=n_p^{1/2}\sqrt{1-(\omega/\omega_p)^2}, \tag{1}$$

where n_p is the refractive index of the crystal lattice, ω is the frequency of the light, $\omega_p=(Ne^2/\varepsilon_p m)^{1/2}$ is the plasma frequency, $\varepsilon_p=n_p\varepsilon_0$ is the dielectric constant of the crystal lattice, and m is the carrier effective mass.

Gallium arsenide was selected as the material for the proposed purposes, because the electrons in it have a very small effective mass. Therefore, the refractive index of n-type GaAs differs by $\Delta n=0.02$ from the refractive index of the lattice due to the free carriers when the electron density $N=10^{19}$ cm^{-3}. Such a difference in the refractive index is sufficient for forming light-guiding layers (waveguides) in semiconductor structures. InSb, which has an even smaller free-carrier effective mass, is an even more preferable material.

The time for variation of the refractive index under the action of an electric field that leads to variation of the concentration of free electrons is determined by the Maxwellian relaxation time ($10^{-14}-10^{-16}$ s), which is considerably smaller than the time for variation of the refractive index of the crystal lattice under the electro-optic effect.

The basis of the use of an MIS structure as a waveguide

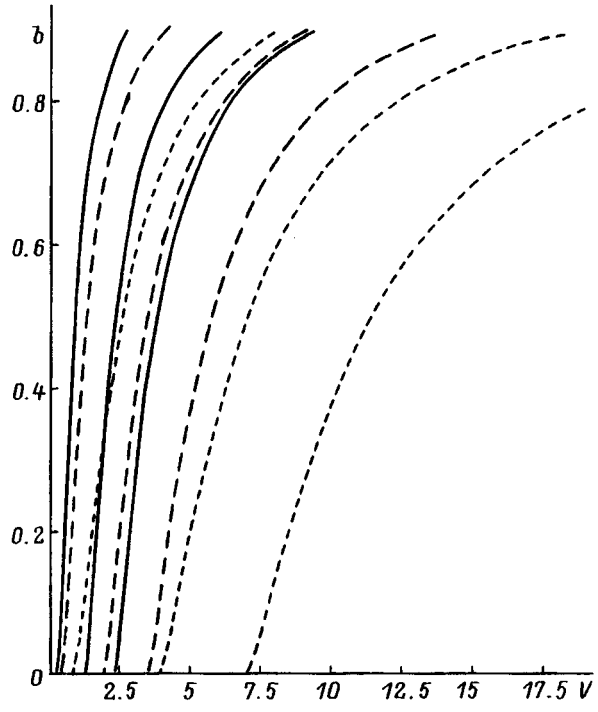

FIG. 1. Dependence of the normalized effective refractive index b of a planar homogeneous optical waveguide on the normalized thickness (or frequency) V for various mode indices m and various values of the dimensionless voltage x: solid curves — $x=8$, dashed curves — $x=3$, dotted curves — $x=0$. The mode index increases along the series $m=1$, 2, 3 for each family of curves with the same value of x as V increases and b remains constant.

 1063-7826/97/060593-02$10.00

is the possibility of creating a depleted layer in such a structure. Such a structure then consists of three layers (light propagates parallel to the junction) with the refractive indices n_1 (for the insulator), n_2 (for the depleted layer), and n_3 (for the highly doped n-region).

We note that a $p-i-n$ structure served as the guiding structure in Ref. 2. In our opinion, the use of such a structure is ineffective because of the appreciable value of the hole effective mass. For this reason, the value of Δn on the boundary with the p-region will be considerably smaller, and this will lead to considerable degradation of the guided propagation of light.

A calculation of the width L of the depleted (waveguide) layer as a function of the voltage applied to the MIS structure does not present any difficulty.[3] The relationship between the voltage u applied to the structure in units of kT/e and L is defined by the expression

$$u=\frac{Ld}{2L_D^2}+\frac{L^2}{L_D^2}, \tag{2}$$

where d is the width of the insulator layer, and $L_D=(n_p\varepsilon_0 kT/e^2N)^{1/2}$ is the Debye length. We note that light will propagate along a waveguide only if L exceeds the optical wavelength.

From the standpoint of integrated optics, an MIS structure is an ordinary planar three-layer waveguide. Therefore, standard expressions can be used to obtain the fundamental characteristic of such a waveguide, viz., the dependence of the wave propagation rate on the frequency, for $d<L$. This characteristic can be written in dimensionless variables in accordance with Ref. 4 for TE modes in the form

$$V\sqrt{1-b}\sqrt{1+x}=\pi(m-1)+\arctan[\sqrt{b/(1-b)}]+\arctan[\sqrt{(b+a)/(1-b)}]. \tag{3}$$

Here the frequency $V=K_\lambda L_D\sqrt{e\varphi/kT}$, where φ is the metal-semiconductor contact potential difference; the effective refractive index is $b=[(\beta/K_\lambda)^2-n_3^2]/(n_2^2-n_3^2)$, where β is the dimensional value of the propagation constant; K_λ is the absolute value of the wave vector; $a=(n_3^2-n_1^2)/(n_2^2-n_3^2)$; $x=U/\varphi$, where U is the applied voltage; $m=1,2,3,\ldots$. When $x=0$, relation (3), as it should, transforms into the standard expression presented in Ref. 4, but is distinguished from it by the factor $\sqrt{1+x}$ on the left-hand side. Setting $b=0$ and $m=1$ in the dispersion dependence, we determine the cutoff frequency for the fundamental mode

$$V=\frac{\arctan\sqrt{a}}{\sqrt{1+x}}. \tag{4}$$

Since, in accordance with the calculation presented in Ref. 4, b versus V characteristics depend weakly on a, we adopted the value $a=1$ in the numerical calculations. The results of the calculations for the first three modes at different values of x are presented in Fig. 1.

[1] I. M. Vikulin and V. I. Stafeev, *Physics of Semiconductor Devices* [in Russian], Radio i Svyaz', Moscow (1990).

[2] ''Optical coupler,'' European Patent Application No. 04 011 925, Cl. G02F1/015 (1990).

[3] E. V. Buzaneva, V. I. Strikha, and G. E. Chaĭka, Ukr. Fiz. Zh. **28**, 575 (1983).

[4] *Integrated Optics*, T. Tamir (ed.), Springer-Verlag, Berlin (1975) [Russ. transl., Moscow (1978)].

Translated by P. Shelnitz

Recombination model of the diffusion of zinc in GaAs

N. N. Grigor'ev and T. A. Kudykina

Institute of Semiconductor Physics, Ukrainian National Academy of Sciences, 252650 Kiev, Ukraine
(Submitted April 23, 1996; accepted for publication October 14, 1996)
Fiz. Tekh. Poluprovodn. **31**, 697–702 (June 1997)

The isothermal diffusion of Zn in GaAs is described within the Longini reaction and a proposed recombination model: during diffusion a highly mobile zinc interstitial recombines with a gallium vacancy and becomes a relatively immobile site defect. The concentration profile of the total zinc concentration is determined at large times mainly by the concentration profile of the vacancies. All the known diffusion profiles have been obtained for a constant diffusivity without fitting parameters. A new method for measuring the diffusivities of interstitial zinc, zinc in gallium lattice sites, and zinc in vacancies is proposed. The values of these coefficients are determined from existing experimental data. It is shown that the apparent dependence of the diffusivity of zinc on its background concentration previously calculated in several studies is due to its recombination with gallium vacancies. © *1997 American Institute of Physics.* [S1063-7826(97)01306-9]

1. INTRODUCTION

The investigation of the mechanisms of the diffusion of Zn in GaAs has been the subject of a large number of studies during the past three decades.[1–10] The problem is still of great interest because of the use of Zn in the production of $p-n$ junctions and the fabrication of high-quality, high-speed electrical and optical structures that have good noise characteristics. Anomalous concentration profiles were discovered back in the first studies of the diffusion of Zn in GaAs. The following forms of these profiles are observed, depending on the conditions under which diffusion takes place.

1. At Zn concentrations, N_{Zn}, less than a certain limiting value (for example, 10^{19} cm^{-3} at temperatures below 1000 °C) the concentration distribution closely conforms to the ordinary profile for diffusion from a constant source described by the complementary error function $\mathrm{erfc}(x)\equiv 1-\Phi(x/2\sqrt{Dt})$. Here $\Phi(x)$ is the probability integral, x is the coordinate, the X axis is perpendicular to the surface of the sample, t is the diffusion time, and D is the diffusivity. A profile described by a complementary error function is also obtained for the diffusion of the radioactive isotope ^{65}Zn in heavily zinc-doped GaAs ($N_{\mathrm{Zn}}>10^{20}$ cm^{-3}) (Fig. 1a),[7] as well as for short diffusion times.

2. A profile in the form of a step. A profile of this type is observed for the diffusion of Zn in both n-GaAs and p-GaAs (Fig. 1b) when the annealing time is sufficiently long and the Zn concentration is high.[5] Outwardly, these profiles appear as if there were an obstacle to diffusion.

3. A rapidly descending high-concentration portion, followed by a convex-upward front and a small step, is shown in Fig. 1c. A profile of this type was obtained in Ref. 8, where, before the diffusion of Zn in GaAs, the samples were preliminarily annealed at a temperature higher than the temperature for the subsequent diffusion of Zn and at an elevated AsH_3 pressure.

4. A profile consisting of two convex-upward portions with a kink between them is shown in Fig. 1d. This type of profile was obtained for the diffusion of Zn in both semi-insulating GaAs and n^+-GaAs after rapid thermal annealing at a temperature above 850 °C.[10]

The four types of diffusion profiles just described are characteristic of diffusion within a plate. The diffusion of Zn from a source located within GaAs is considerably slower. This suggests that different mass-transport processes characterized by different diffusivities take place in these two cases.

A surprising result was observed by researchers measuring the diffusivity of Zn: this coefficient increased sharply as the background Zn concentration increased,[6,7,11,12] the effect being stronger, if the diffusion of Zn takes place in an atmosphere without an excess of As, i.e., in the presence of a small concentration of gallium vacancies (Fig. 2, curves *c* and *d*). An excess of As (a large concentration of vacancies) leads to the absence of a dependence of the diffusivity of Zn on its concentration up to Zn concentrations $\sim 5\times 10^{18}$ cm^{-3}, above which a slower increase in D is observed (Fig. 2, curves *a* and *b*).

There are two basic models of the diffusion of Zn in GaAs. According to the first model, which was first proposed by Longini[4] in 1962 and further developed by numerous researchers,[5,6,9,13] some of the zinc atoms migrate among vacancies, while others migrate among interstitial sites. When zinc occupies a Ga vacancy, it exists in the Zn_s^- state, acts as an acceptor, and has a very small diffusivity. In interstitial sites it exists in the Zn_i^+ state, acts as a donor, and has a considerably higher diffusivity. These researchers postulated that there is a continuous exchange of particles between these flows and that flow via interstitial sites plays the main role in diffusion:

$$\mathrm{Zn}_i^+ + V_{\mathrm{Ga}} \leftrightarrow \mathrm{Zn}_s^- + 2h. \tag{1}$$

The Ga vacancies (V_{Ga}) are assumed to be either neutral or singly ionized, depending on the position of the Fermi level.[14]

In Ref. 4 Longini suggested that the stepped character of the concentration profile of Zn in GaAs is determined by the

 1063-7826/97/060595-05$10.00

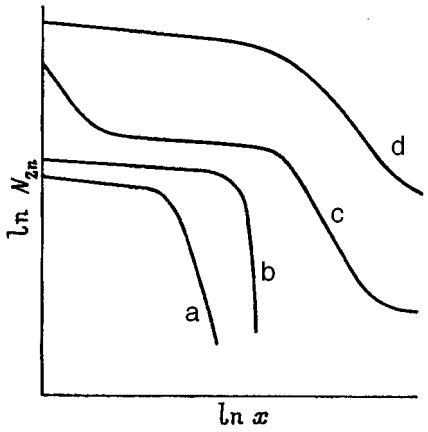

FIG. 1. Concentration profiles of Zn in GaAs: a — type 1 (Ref. 5), b — type 2 (Ref. 5), c — type 3 (Ref. 9), d — type 4 (Ref. 10).

presence of the field of a $p-n$ junction, which blocks the diffusion of Zn. However, the electromigration experiments in Ref. 5 showed that at high temperatures Zn migrates in the form of positively charged ions and that the field of a $p-n$ junction can only promote diffusion. In addition, it was also shown there that a stepped profile is characteristic of the diffusion of Zn not only in n-GaAs, but also in p-GaAs, where no $p-n$ junction appears.

The attempts to describe the diffusion profiles of Zn in GaAs performed in several studies required the introduction of additional conditions. For example, to describe a profile of type 4 it was theorized in Ref. 15 that the diffusivity increases according to a quadratic law as the concentration increases. The existence of different charge states of the vacancies and Zn atoms was proposed in Ref. 14.

The introduction of several fitting parameters allowed the authors of this model to satisfactorily describe the first three types of concentration profiles observed.

An alternative diffusion model (the kick-out model) presumes that interstitial Ga (I_{Ga}) has a significant influence on the transport of Zn in GaAs.[16,17] The basic reaction in this mechanism is

$$\mathrm{Zn}_i^+ \leftrightarrow \mathrm{Zn}_s^- + I_{\mathrm{Ga}} + 2h. \tag{2}$$

This model has been considered in many publications (see, for example, the review in Ref. 18). Profiles of types 2 and 3 are described on the basis of this model, and profiles of type 4 are attributed to the presence of voids, dislocations, and other extended defects.

An analysis of the experimental results, however, contradicts the kick-out model:

— an investigation of the defects by photoluminescence methods[9,13] showed that the decisive role in the diffusion of Zn in GaAs is played by gallium vacancies, but no interstitial Ga was discovered;

— the self-diffusion processes of lattice atoms are usually considerably slower than the diffusion of impurities, and the self-diffusivity of an atom is several orders of magnitude smaller than the diffusivity of an impurity atom, because an intrinsic atom is found in a deeper potential well;

— the main argument behind the kick-out model, i.e., the fact that Zn causes disordering in GaAs/AlGaAs superlattices, actually does not contradict the Longini model: when Zn diffuses in a GaAs/AlGaAs superlattice, Al, rather than Ga, is transported to the surface.

The displacement of Ga from a site requires an energy that is considerably greater than the energy needed to displace aluminum or zinc. This is also evidenced by the experiments in Ref. 8, where it was shown that the deposition of a GaAs layer on heavily zinc-doped p-GaAs$\langle$Zn$\rangle$ leads to the displacement of zinc onto the surface.

All of this supports the Longini model.

In this study we show that the diffusion of Zn in GaAs can be described on the basis of reaction (1) and our proposed recombination model: in the diffusion process a mobile zinc interstitial Zn_i recombines with a gallium vacancy, generating a relatively immobile site atom Zn_s. The lifetime of the zinc interstitial can be found experimentally and used to find the diffusivity of Zn_i: when the concentration of gallium vacancies is high ($N_{V_{\mathrm{Ga}}} \gg N_{\mathrm{Zn}}$), the zinc concentration profile is determined not by the diffusion rate of the zinc interstitial Zn_i, but by the probability of its recombination and the diffusion rate of Zn_s. In this case the profile of the diffusing zinc mimics the profile of the vacancies. The lifetime of Zn_i was estimated, and its diffusion parameters were determined. They are in good agreement with the results in Refs. 1 and 9. The diffusivity of Zn_s depends on the concentration of vacancies. The diffusivity of the vacancies in GaAs is much smaller than the diffusivity of the zinc atoms. The apparent dependence of the diffusivity of zinc on its background concentration is, in fact, related to the recombination process. All four types of diffusion profiles of the Zn concentration are obtained when a single constant diffusivity of Zn_i is introduced.

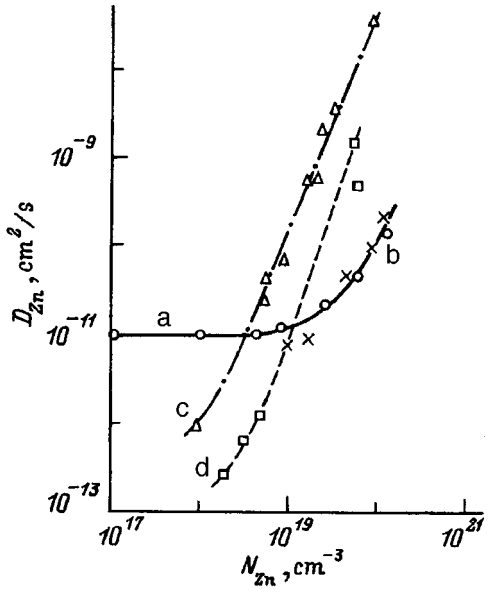

FIG. 2. Dependence of the ''effective diffusivity'' of zinc on its background concentration according to the data from different studies: a, b — Ref. 6, c — Ref. 22, d — Ref. 23.

2. SIMULATION OF THE DIFFUSION PROCESS

The available experimental data show that a zinc interstitial is highly mobile and has a considerable probability to recombine with Ga vacancies and to thereby form a relatively immobile Zn_s^- ion. In the absence of other impurities the concentration profile describing the distribution of Zn in GaAs is determined by a system of mass-transport equations: for interstitial zinc

$$\frac{\partial N_{\mathrm{Zn}_i}}{\partial t}=D_{\mathrm{Zn}_i}\frac{\partial^2 N_{\mathrm{Zn}_i}}{\partial x^2}-\beta N_{\mathrm{Zn}_i}N_{V_{\mathrm{Ga}}}; \tag{3}$$

with the boundary conditions

i) $N_{\mathrm{Zn}_i}(x,t=0)=0$,

ii) $N_{\mathrm{Zn}_i}(x=0,t)=N_0$;

for zinc in gallium sites

$$\frac{\partial N_{\mathrm{Zn}_s}}{\partial t}=D_{\mathrm{Zn}_s}\frac{\partial^2 N_{\mathrm{Zn}_s}}{\partial x^2}+\beta N_{\mathrm{Zn}_i}N_{V_{\mathrm{Ga}}}; \tag{4}$$

with the boundary conditions

i) $N_{\mathrm{Zn}_s}(x,t=0)=0$, ii) $N_{\mathrm{Zn}_s}(x=0,t)=N_{s0}$;

for gallium vacancies

$$\frac{\partial N_{V_{\mathrm{Ga}}}}{\partial t}=D_{V_{\mathrm{Ga}}}\frac{\partial^2 N_{V_{\mathrm{Ga}}}}{\partial x^2}-\beta N_{\mathrm{Zn}_i}N_{V_{\mathrm{Ga}}}; \tag{5}$$

with the boundary conditions

i) $N_{V_{\mathrm{Ga}}}(x,t=0)=V_1$, ii) $N_{V_{\mathrm{Ga}}}(x=0,t)=V_0$.

Here V_1 is the concentration of vacancies existing in the crystal before the diffusion of zinc, V_0 is the concentration of the vacancies, and N_0 and N_{s0} are the concentrations of Zn $_i$ and Zn_s introduced from the surface during diffusion. The coefficient β is proportional to the probability of the recombination of a zinc interstitial with a gallium vacancy.

Since $D_{\mathrm{Zn}_i}\gg D_{\mathrm{Zn}_s}$, an approximate solution of Eq. (4) can be written in the form

$$N_{\mathrm{Zn}_s}(x,t)\cong\beta\int_0^t N_{\mathrm{Zn}_i}(x,t_1)N_{V_{\mathrm{Ga}}}(x,t_1)dt_1, \tag{6}$$

which is determined completely by the solution of Eqs. (3) and (5). In general, such a problem can be solved numerically.

Let us analyze the analytic solution for several important particular cases.

3. DIFFUSION OF ZINC UNDER THE CONDITIONS OF A UNIFORM CONCENTRATION OF VACANCIES IN THE SAMPLE ($N_{\mathrm{Zn}}\ll N_{V_{\mathrm{Ga}}}$, $N_{V_{\mathrm{Ga}}}=\mathrm{CONST}$)

This case can be realized either by the technology for preparing the original GaAs crystal or by a preliminary treatment, during which a high concentration of V_{Ga} is created; the subsequent isothermal diffusion of Zn is carried out at lower temperatures. Under these conditions no significant variation of the concentration of the vacancies occurs during the diffusion process, $N_{V_{\mathrm{Ga}}}=V_1=\mathrm{const}(x,t)$. In this case the solution of Eq. (3) can be obtained analytically:

$$N_{\mathrm{Zn}_i}=N_0\ \exp(-\beta V_1 t)[1-\Phi(x/2\sqrt{D_{\mathrm{Zn}_i}t})]. \tag{7}$$

The concentration of site zinc will then be

$$N_{\mathrm{Zn}_s}(x,t)\cong N_0 J_s(x,t), \tag{8}$$

where

$$J_s=1-\exp(-t/\tau_i)\Phi(a/\sqrt{t})-0.5\{\exp(-2a/\sqrt{\tau_i})\times[1-\Phi(a/\sqrt{t}-\sqrt{t})]+\exp(+2a/\sqrt{\tau_i})\times[1-\Phi(a/\sqrt{t}+\sqrt{t})]\}. \tag{9}$$

Here $a=x/2\sqrt{D_{\mathrm{Zn}_i}}$, and $\tau_i=1/\beta V_1$. The total concentration of Zn atoms is

$$N_\Sigma(x,t)=N_0\ \exp(-\beta V_1 t)[1-\Phi(x/2\sqrt{D_{\mathrm{Zn}_i}})]+N_0 J_s(x,t). \tag{10}$$

Figure 3 presents concentration profiles described by the classical function $\mathrm{erfc}(x/2\sqrt{D_{\mathrm{Zn}_i}t})$ (curve *1*), the function (curve 7) for interstitial zinc (curve *2*), and the function (10)

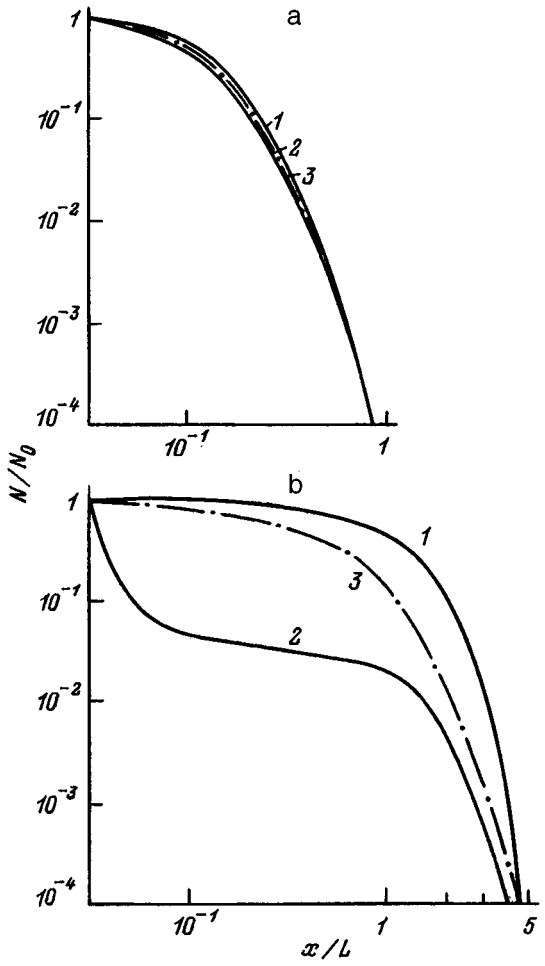

FIG. 3. Concentration profiles: *1* — the classical complementary error function $\mathrm{erfc}(x/2\sqrt{D_{\mathrm{Zn}_i}t})$; *2*, *3* — profiles described by Eq. (7) for N_{Zn_i} and (10) for N_Σ; the diffusion time t/τ equal 0.1 (a) and 3.0 (b), respectively.

for the total zinc concentration (curve *3*) for two values of the diffusion time t/τ_i: a — 0.1, b — 3. It is seen that at small values of the time the influence of recombination is small, and all three curves almost coincide. When $\beta V t \ll 1$, we can write in an approximation $J_s \sim t/\tau_i$, and the time factor for N_Σ is

$$\varphi(t) \cong 1-(\beta V_1 t)^2. \tag{11}$$

This time factor leads to a faster descent on the profile as the diffusion time increases. When $t/\tau_i > 1$, the most of the zinc atoms are in gallium sites, and the profile of N_Σ drops more rapidly than the classical profile. This is in good agreement with the experiment, for example, in Ref. 5: at small times the profile almost coincides with erfc(x) and then becomes highly precipitous and stepped. Such a description shows that the shape of the profile is determined by the recombination of zinc interstitials. In this case the diffusivity does not vary. Our treatment shows that finding the diffusivity from the depth L^* of the diffusing carriers is incorrect when a recombination process takes place: the value of L^* can be considerably smaller than the diffusion length $L_0 = \sqrt{D_{\mathrm{Zn}_i} t}$. This led to the erroneous conclusion that the diffusivity of zinc depends on the concentration of this element preliminarily introduced in the crystal. The higher is the concentration of the preliminarily introduced zinc, the smaller is the number of free vacancies, the weaker is the recombination of zinc interstitials, and the greater is the value of L^*. The classical complementary error function erfc(x) becomes the main function in the distribution of zinc. This explains the results in Ref. 6: in an atmosphere of excess As, in which a larger number of vacancies are introduced into the crystal, no increase in the ''diffusivity'' occurs up to a concentration of $\sim 5\times 10^{18}$ cm^{-3}, and then an increase which is slower than in the case of diffusion with a small concentration of vacancies is observed (Fig. 2).

If the zinc doping level of the crystal is high (usually greater than 10^{20} cm^{-3}), then there are very few free vacancies, and the profile of the distribution of the radioactive Zn introduced has the classical form of erfc(x), as was observed in the experiment in Ref. 7.

In the case considered the quantity

$$\tau_i = 1/\beta V_1 \tag{12}$$

plays the role of the lifetime of the zinc interstitials, Zn_i, before they recombine with a gallium vacancy and go over to the Zn_s state. A sharp drop occurs on the concentration profile at times of the order of τ_i. This parameter can be estimated approximately from the experimental data in Ref. 5, and the diffusion length of Zn_i, $L = \sqrt{D_{\mathrm{Zn}_i}\tau_i}$ can be estimated from the length of the concentration profile. For example, for a diffusion temperature of 950 °C the diffusion length is $L \sim 200$ μm, and $\tau_i \sim 12$ h; for $T_0 = 1150$ °C $L \sim 180$ μm, and $\tau_i = 1.5$ h. Estimation of the diffusivity D_{Zn_i} from these data leads to the following results: $D_{\mathrm{Zn}_i}(950\ ^\circ\mathrm{C}) \cong 9.25\times 10^{-9}$ cm^2/s, $D_{\mathrm{Zn}_i}(1150\ ^\circ\mathrm{C}) \cong 6.0\times 10^{-8}$ cm^2/s.

These values of the diffusivity lie within the spread of the diffusion parameters obtained in Refs. 1 and 9: $D_0 = 2.05 \pm 1.91$ cm^2/s, $E_A = 2.28 \pm 0.11$ eV [$D = D_0 \exp(-E_A/kT)$]. According to our data, $D_0 = 4.06\times 10^{-3}$ cm^2/s and $E_A = 1.37$ eV.

On the other hand, the results presented in Ref. 6 make it possible to estimate the diffusivity of zinc found in gallium sites. In fact, under the conditions of Ref. 6 the concentration of vacancies in the crystal was high (according to our estimates, $N_{V_{\mathrm{Ga}}} \sim 10^{19}$ cm^{-3}), and the authors noted constancy of the diffusivity up to background zinc concentrations below 5×10^{18} cm^{-3}. The diffusion was carried out at 850 °C, and $D = 10^{-11}$ cm^2/s. According to the estimates in our work and Ref. 9, $D_{\mathrm{Zn}_i}(850\ ^\circ\mathrm{C}) \cong 3.0\times 10^{-9}$ cm^2/s, i.e., it is more than two orders of magnitude greater. This result is attributed to the fact that under conditions for which $N_{\mathrm{Zn}} \ll N_{V_{\mathrm{Ga}}}$ the lifetime of the interstitial zinc is small, it recombines near the surface, and displacement of the concentration profile with time occurs as a result of the slow diffusion of site zinc. Therefore, it can be assumed that under the conditions of Ref. 6 $D_{\mathrm{Zn}_s}(850\ ^\circ\mathrm{C}) \cong 10^{-11}$ cm^2/s, and that it decreases with decreasing concentration of vacancies. This accounts for the $D_{\mathrm{Zn}}(N_{\mathrm{Zn}})$ curves obtained in Ref. 6.

4. STATIONARY DISTRIBUTION OF VACANCIES

This case was realized in the experiments in Ref. 8. Before the diffusion of Zn in GaAs at 500 °C, the samples were preliminarily annealed at a higher temperature equal to 800 °C for 10 min under the conditions of an elevated AsH_3 pressure. Since the diffusivity depends exponentially on the temperature, the diffusion of Zn was not accompanied by any significant change in the profile of the vacancies. From Eq. (5) we obtain the vacancy concentration profile which was created by a preliminary anneal for a time of $t = t_{\mathrm{an}}$

$$N_{V_{\mathrm{Ga}}}(x, t_{\mathrm{an}}) = V_1 + (V_0 - V_1)[1 - \Phi(x/2\sqrt{D_V t_{\mathrm{an}}})]. \tag{13}$$

The solution of the mass-transport equation (3) for Zn_i and of (6) for Zn_s and the determination of the total zinc concentration

$$N_\Sigma(x,t) = N_{\mathrm{Zn}_i}(x,t) + N_{\mathrm{Zn}_s}(x,t) \tag{14}$$

for the stationary distribution of the vacancies (13) shows that in this case the zinc concentration profile is determined by the recombination of zinc interstitials with gallium vacancies. The calculation shows that the profile of the diffusing zinc mimics the profile of N_Σ at sufficiently large diffusion times. Figure 4 presents the calculation of the vacancy concentration profile on the basis of the parameters estimated from the data in Ref. 8. The circles represent experimental points on the profile measured in Ref. 8. The calculation corresponds to the value of the diffusivity of the vacancies $D_V(800\ ^\circ\mathrm{C}) = 7.5\times 10^{-16}$ cm^2/s. We note that the diffusivity of the vacancies is six orders of magnitude smaller than D_{Zn_i}. The reverse relationship, i.e., $D_{\mathrm{Zn}_i} < D_V$, was presumed in many studies. Figure 4 also presents the plots of N_Σ that we calculated for several successive moments in time. It is seen that the zinc atoms gradually fill the vacancy profile.

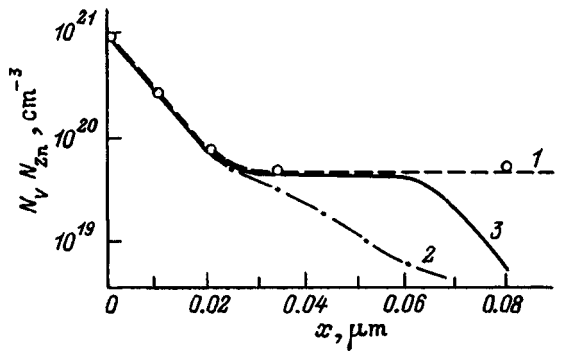

FIG. 4. Calculated profiles of N_V (*1*) and N_Σ (*2*, *3*) based on parameters calculated from the data in Ref. 8. Points — experimental data. Curves *2* and *3* correspond to different diffusion times: $t_3 = 10t_2$.

We note that the case just considered corresponds to a concentration profile of type 3. The first and second types were obtained in the preceding section. Type 4 can be described similarly to type 3 with the one difference that for type 3 $V_1/V_0 = 0.1$, while for type 4 $V_1/V_0 \ll 1$ (for example, 10^{-2} in Ref. 10).

Another reason for the fourth type of profile can be the presence of large temperature gradients, which lead to the appearance of thermal-diffusion fluxes.[20,21]

5. CONCLUSIONS

The analysis performed has shown that the diffusion of Zn in GaAs can be described within our proposed recombination model: the diffusion of zinc in gallium arsenide is controlled by vacancies; 2) a highly mobile zinc interstitial Zn_i can recombine during diffusion with a gallium vacancy and be converted into a relatively immobile site atom Zn_s; 3) the probability of this process is proportional to the concentration of vacancies and zinc interstitials; 4) the lifetime of a zinc interstitial is $\tau_i = 1/\beta V_1$ and can be used to find the diffusivity of Zn_i: $D_{Zn_i} = L^2/\tau_i$ (τ_i is the diffusion time at which a sharp drop is observed on the concentration profile, and L is the length of that profile); 5) when the concentration of gallium vacancies is large ($N_{V_{Ga}} \gg N_{Zn}$), the zinc concentration profile is determined not by the diffusion rate of the zinc interstitial Zn_i, but by the probability of its recombination and the diffusion rate of Zn_s; in this case the profile of the diffusing zinc mimics the profile of the vacancies.

The results in Ref. 5 were used to estimate the lifetime of Zn_i and to determine its diffusion parameters: $D_0 \cong 4.06 \times 10^{-3}$ cm^2/s, $E_A \cong 1.37$ eV. These parameters lie within the measurement errors in Refs. 1 and 9. The diffusivity of Zn_s depends on the concentration of vacancies and when $N_{V_{Ga}} \cong 10^{19}$ cm^{-3}, $D_{Zn_s}(850\ ^\circ\text{C}) \cong 10^{-11}$ cm^2/s. The diffusivity of the vacancies in GaAs is small: $D_V(800\ ^\circ\text{C}) \cong 10^{-16}$ cm^2/s. It was previously assumed that $D_V > D_{Zn_i}$.

It has been shown that the apparent dependence of the diffusivity of zinc on its background concentration is, in fact, related to the recombination process. The introduction of only one constant diffusivity is sufficient for describing all four types of diffusional concentration profiles of Zn.

[1] F. A. Cunnell and C. H. Gooch, J. Phys. Chem. Solids **15**, 127 (1960).
[2] B. Goldstein, Phys. Rev. **118**, 1024 (1960).
[3] I. W. Allen, J. Phys. Chem. Solids **15**, 134 (1960).
[4] R. L. Longini, Solid–State Electron. **5**, 127 (1962).
[5] B. I. Boltaks, T. D. Dzhafarov, V. I. Sokolov, and F. S. Shishiyanu, Fiz. Tverd. Tela **6**, 1511 (1964) [Sov. Phys. Solid State **6**, 1181 (1964)].
[6] H. Rupprecht and C. Z. LeMay, J. Appl. Phys. **35**, 1970 (1964).
[7] L. L. Chang and G. L. Pearson, J. Appl. Phys. **35**, 1960 (1964).
[8] Z. F. Paska, D. Haga, B. Willen, and M. K. Linnarsson, Appl. Phys. Lett. **60**, 1594 (1992).
[9] N. H. Ky, L. Pavesi, D. Araujo, J. D. Ganiere, and F. K. Reinhart, J. Appl. Phys. **69**, 7585 (1991).
[10] G. Rajeswaran, K. B. Kahen, and D. J. Lawrence, J. Appl. Phys. **69**, 1359 (1991).
[11] C. H. Ting and G. L. Pearson, J. Electrochem. Soc. **118**, 454 (1971).
[12] M. A. Kadhim and B. Tuck, J. Mater. Sci. **7**, 68 (1972).
[13] L. Pavesi, D. Araujo, N. H. Ky *et al.*, Opt. Quantum Electron. **23**, S789 (1991).
[14] K. B. Kahen, Appl. Phys. Lett. **55**, 2117 (1989).
[15] S. Reynolds, D. W. Vook, and J. F. Gibbons, J. Appl. Phys. **63**, 1052 (1988).
[16] H. R. Winteler, Helv. Chim. Acta **44**, 451 (1970).
[17] U. Gosele and F. Moreyead, J. Appl. Phys. **52**, 4617 (1981).
[18] S. Yu, T. Y. Tan, and U. Gosele, J. Appl. Phys. **69**, 3547 (1991).
[19] P. Enquist, J. A. Hutchby, and T. J. DeLyon, J. Appl. Phys. **63**, 4485 (1988).
[20] N. N. Grigor'ev and T. A. Kudykina, Ukr. Fiz. Zh. **33**, 574 (1988).
[21] N. N. Grigor'ev, T. A. Kudykina, and P. M. Tomchuk, J. Phys. D: Appl. Phys. **24**, 276 (1992).
[22] P. L. Kendall and M. E. Jones, *AIEEIRE Device Research Conference*, Stanford, 1961.
[23] C. L. Pearson, M. G. Buehler, and C. N. Berglund, Bull. M. Phys. Soc., St. Louis Meeting, 1963.

Translated by P. Shelnitz

Kinetics of the redistribution of an impurity in quasiperiodic structures appearing in heavily boron-doped silicon irradiated by boron ions

A. M. Myasnikov, V. I. Obodnikov, V. G. Seryapin, E. G. Tishkovskiĭ, B. I. Fomin, and E. I. Cherepov

Institute of Semiconductor Physics, Russian Academy of Sciences, Siberian Branch, 630090 Novosibirsk, Russia

(Submitted November 8, 1995; accepted for publication October 24, 1996)
Fiz. Tekh. Poluprovodn. **31**, 703–707 (June 1997)

The kinetics of the redistribution of an impurity between fragments of the quasiperiodic boron distribution appearing in heavily boron-doped silicon as a result of irradiation by boron ions followed by annealing are analyzed. It is established that the migration of boron accompanied by capture of the impurity in zones with fixed positions in space takes place with a conserved integral quantity of boron in the silicon regions containing quasiperiodic structures during anneals at 900–1075 °C. It is shown that the stage of the formation of the quasiperiodic distribution of the impurity in the range of times 10–240 min at 900 °C is similar to the stage of the coalescence of a supersaturated interstitial solid solution. © *1997 American Institute of Physics.* [S1063-7826(97)01406-3]

INTRODUCTION

It was established in Ref. 1 that the annealing of samples of heavily boron-doped silicon at 900 °C following irradiation by $^{10}B^+$ ions with an energy of 180 keV in a 10^{16} cm^{-2} dose results in the formation a quasiperiodic structure consisting of five maxima on the concentration profiles of both boron isotopes in the region subjected to ion implantation. The formation of the quasiperiodic structure can be divided hypothetically into two stages. In the rapid first stage zones for the accumulation of boron appear. These zones are apparently associated with the spontaneous formation of boron-containing clusters. In the second stage there is a comparatively slow process involving the accumulation of boron in spatially isolated zones as a result of the passage of the mobile component of the impurity into the clusters.

The purpose of the present work is to analyze the kinetics of the redistribution of the impurity between fragments of the structure in the slow second stage of final shaping of the profile of the nonuniform distribution of the impurity and to investigate the stability of the oscillating boron distributions with respect to heat treatment.

EXPERIMENT

The depth profile of the impurity in the samples was investigated by secondary-ion mass spectrometry using a Cameca-Riber MIQ-256 spectrometer. As part of the measurements, the yield of $^{30}Si^+$, which was used to monitor the constancy of the etch rate, was recorded along with the $^{10}B^+$ and $^{11}B^+$ secondary ions. The primary beam of O_2^+ ions had an energy of 13 keV. To eliminate the contribution of the secondary boron ions emerging from the crater walls, the signal being analyzed was recorded from a central region which amounts to 10% of the area scanned by the primary ion beam.

In the experiments devised to investigate the thermal stability of the quasiperiodic structures appearing on the boron concentration profiles, samples prepared according to a method which is completely analogous to the method employed in Ref. 1 served as the original specimens. Boron was introduced by diffusion into a plate of KÉF-7.5 silicon with the (100) orientation at 1150 °C so that a region of uniform doping with a boron concentration of the order of 2×10^{20} cm^{-3} would be created down to a depth of several microns. Then the implantation of $^{10}B^+$ ions with an energy of 180 keV in a 10^{16} cm^2 dose was carried out using an HVEE-400 system. The irradiated plates were annealed at 900 °C for 1 h to form an oscillating boron depth profile, and the original samples were cut from the plates thus prepared.

Control measurements of a set of original samples showed that in the ion-irradiated region the concentration profiles of the two boron isotopes are quasiperiodic structures consisting of five maxima (Fig. 1a), as was observed in Ref. 1. It was also established that the spatial distributions of the boron isotopes obtained on different samples scarcely differ, exhibiting disparities only in fine details, even for samples cut from different plates.

The original samples produced by the method described above were annealed at 950, 1000, 1075, 1150, and 1200 °C for 30 min.

EXPERIMENTAL RESULTS

The investigations of the thermal stability of the quasiperiodic structures shown in Fig. 1a revealed that the spatial positions of the maxima are conserved during heating in the temperature range 950–1075 °C. As the annealing temperature is raised (Fig. 1b), the concentration profiles of the ^{10}B and ^{11}B isotopes, which initially differed from one another, have a tendency to coincide. The conditions for irradiation by the ^{10}B isotope (the energy E and the dose D) were selected in such a way that the integral amounts of the two boron isotopes in the ion-irradiated region would be approximately the same ($1.86\times10^{16}cm^{-2}$ for ^{10}B and $1.85\times10^{16}cm^{-2}$ for ^{11}B). The thickness of this region, which is equal to about 900 nm, was determined in a control ex-

 1063-7826/97/060600-05$10.00

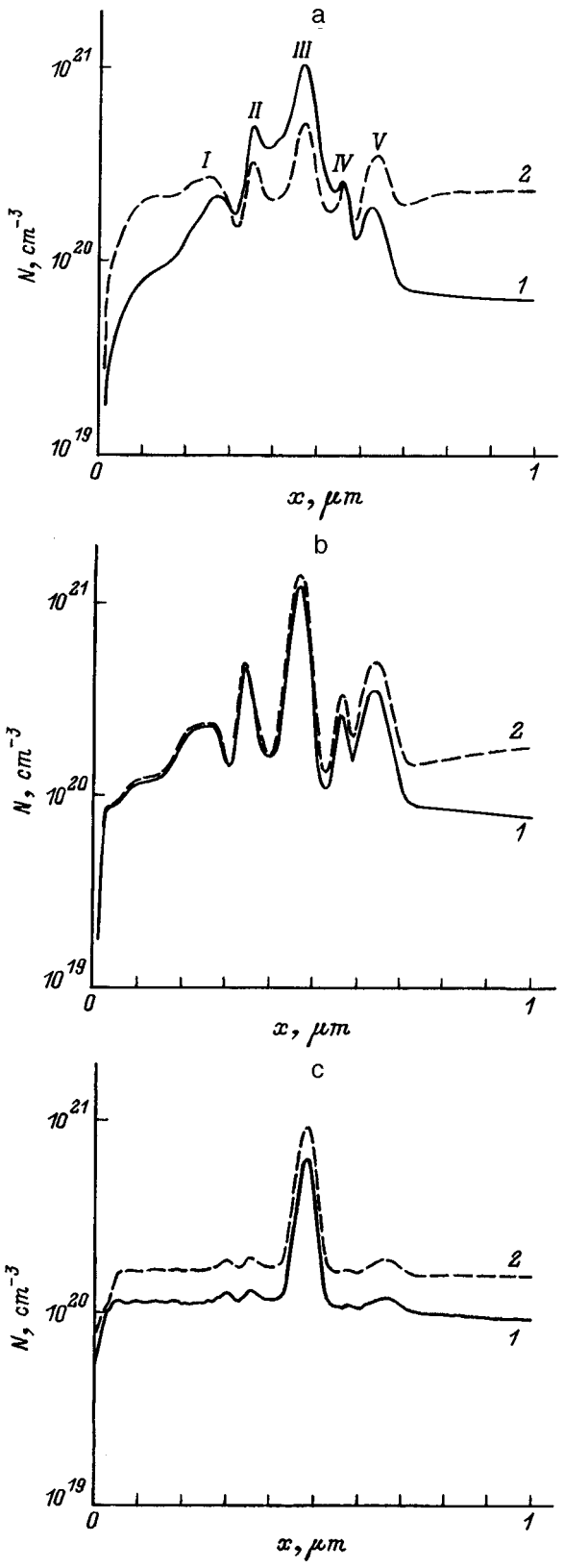

FIG. 1. Concentration profiles of boron isotopes (*1* — ^{10}B, *2* — ^{11}B) in silicon with an initial B concentration of 2×10^{20} cm^{-3} following the implantation of ^{10}B ions ($E=180$ keV, $D=10^{16}$ cm^{-2}) and annealing at various temperatures T (°C) for various times t (min): a — 900 and 60; b — 900 and 60 + 1075 and 30; c — 900 and 60 + 1150 and 30.

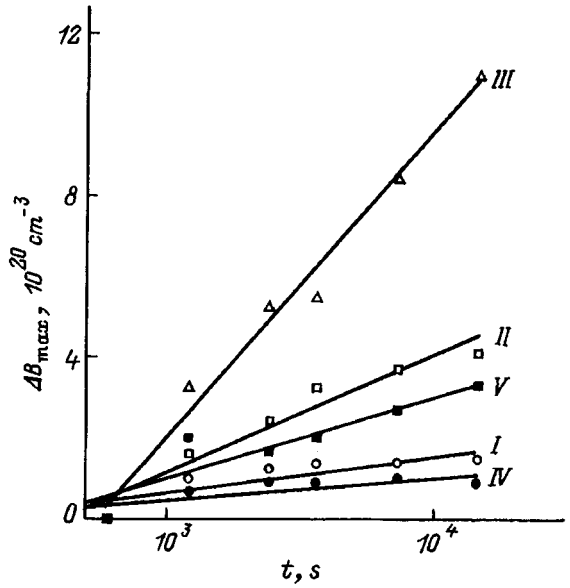

FIG. 2. Variation of the total concentration ΔB of the B isotopes at the maxima of the impurity distribution as a function of the annealing time at $E=900$ °C. The numbers of the curves correspond to the numbers of the maxima in Fig. 1a.

periment involving the irradiation of plates of KÉF-7.5 silicon. The concentration of the implanted impurity of approximately 10^{16} cm^{-3} at that depth corresponds to the sensitivity threshold of the method with respect to the ^{10}B isotope.

The tendency for the profiles to coincide is evidence that migration of the boron atoms takes place during the annealing, resulting in spatial mixing of the isotopes and their capture in the regions in which the maxima in the boron distribution are located. The impurity-capture centers remain effective at least up to 1075 °C. In the region to a depth of 900 nm the integral number of boron atoms is not altered to within 10% as a result of the annealing at temperatures up to 1075 °C.

When the annealing temperature is raised to 1150 °C (Fig. 1c), the amplitudes of the four outer maxima decrease sharply, while the amplitudes of the central maxima for the two isotopes decrease slightly. Annealing at 1200 °C results in complete disappearance of the quasiperiodic structure. These processes are accompanied by a decrease in the integral quantity of the impurity in the region where the bulk of the implanted impurity was previously concentrated.

Figures 2 and 3 present the results of the treatment of the experimental data obtained in Ref. 1, which characterize the spatial redistribution of the boron atoms as a function of the annealing time at 900 °C. Figure 2 shows the process of the accumulation of boron atoms at the maxima of the oscillating distribution. The increment of the total concentration of both isotopes ΔB in all five maxima as a function of time is satisfactorily described by the same dependence:

$$\Delta B_{\max}=A\,\ln(t/t_1)+N, \tag{1}$$

where t is the time, $t_1=600$ s, and A and N are time-independent parameters, which are characteristic of each maxima. Figure 3 shows plots of the variation of the total

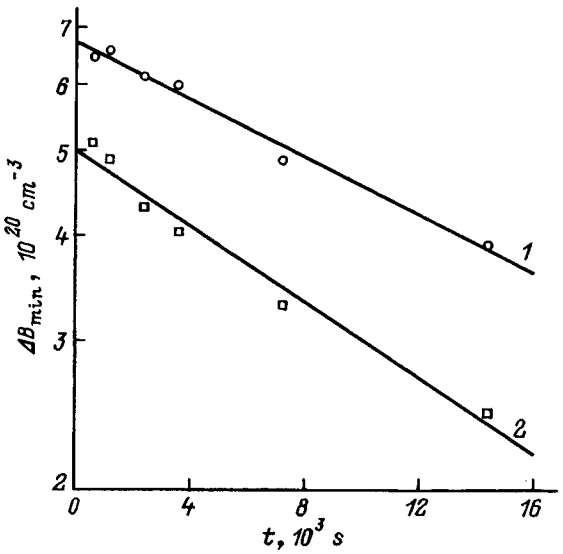

FIG. 3. Variation of the total concentration of the boron isotopes at the minima of the impurity distribution closest to the center as a function of the annealing time at $T=900$ °C. *1* — left-hand minimum, *2* — right-hand minimum (see Fig. 1).

concentration for both isotopes at the minima closest to the center of the structure, which satisfy the relation

$$\Delta B_{\min}=K\ \exp(-\lambda t), \tag{2}$$

where $K=5.0\times10^{20}$ cm^{-3} and $\lambda=5.2\times10^{-5}$ s^{-1} for the left-hand minimum, and $K=6.7\times10^{20}$ cm^{-3} and $\lambda=3.9\times10^{-5}$ s^{-1} for the right-hand peak.

It is significant that following the redistribution of the boron atoms observed in this experiment, their integral number in a region with a thickness up to approximately 900 nm remains constant to within 10%. It should be noted that no changes in the distribution of the impurity are observed in the bulk of the plate outside of this region, i.e., on the continuation of the flat part of the original diffusional profile and on its edges.

DISCUSSION

The experimental data obtained in Ref. 1 and in the present work show that the significant changes in the boron distribution profiles analyzed by us at temperatures below 1075° occur only in the ion-irradiated region itself and in the immediate vicinity of its nominal boundaries; i.e., they are spatially localized. These processes take place in a system with isolated zones containing impurity-capture centers, which are apparently boron-containing clusters. During the annealing, boron flows into the clusters and escapes from them.

As follows from Refs. 2–4, in the case of annealing at 900 °C the relaxation of the subsystem of the nonequilibrium elementary defects introduced when the ions are implanted is completed after a time far smaller than 10 min. It must be assumed that the impurity redistribution processes observed in the time interval 10–240 min are determined mainly by the behavior of the components of the nonequilibrium impurity subsystem: the boron atoms in lattice sites and in irregular positions (apparently in interstices), as well as the boron atoms in a bound state, apparently in precipitates.[5]

If this impurity subsystem is regarded as a supersaturated solid solution, it turns out that the above features of the redistribution of the impurity, taken together, fit well into the theory of the coalescence of supersaturated solid solutions developed in Ref. 6. We see a diffusional exchange of matter between grains characteristic of the coalescence stage, which alters the size distribution of the grains and thereby results in the gradual elimination of supersaturation. The presence of several sites of preferential clustering results only in the fact that the size of the grains increases at the maxima of the structure, where the supersaturation with respect to the interstitial component is accordingly eliminated. Conversely, dissolution of the grains, which results in the release of the impurity, occurs at the minima. The concentration gradient appearing is smoothed by the diffusional transport of the impurity in analogy to what occurs in a homogenous solution between individual grains.[6]

If the ensemble of precipitates existing at a given moment in time at a specific maximum of the structure is represented, as a consequence of the narrowness of their size distribution function,[6] by a set of identical grains with a radius equal to the mean radius of the precipitates r_p, then the process of the accumulation of the impurity at the maxima of the structure can be reduced in an approximation to a quasichemical reaction of the mobile component B_1 with capture centers of radius r_p. The concentration of the capture centers will then be determined by the mean number of precipitates N_p present in the region of a specific maximum at a given moment in time.

In the approximation of a diffusion-controlled reaction of a mobile component, the rate of variation of the concentration at the maximum is proportional to the size of the interaction region, the concentrations, and the relative mobilities of the reacting components:[7]

$$\frac{dB_p}{dt}=4\pi D r_p(t)B_1(t)N_p(t), \tag{3}$$

where B_p is the concentration of boron at the maximum of the structure, D is the diffusivity of the mobile component, $r_p(t)$ is the mean radius of a precipitate, $B_1(t)$ is the concentration of the mobile component, and $N_p(t)$ is the concentration of the precipitates. In accordance with Ref. 6, the variables $N_p(t)$, $r_p(t)$, and $B_1(t)$ appearing in Eq. (3) satisfy the relations

$$N_p(t)=\frac{Q_0}{2\sigma D}t^{-1}, \tag{4}$$

where Q_0 is the initial supersaturation with respect to the mobile boron component, and σ is a parameter, which characterizes the phase boundary between a crystal and a precipitate;

$$r_p(t)=r_{c0}\left(\frac{4}{9}\sigma D\right)^{1/3}t^{1/3}, \tag{5}$$

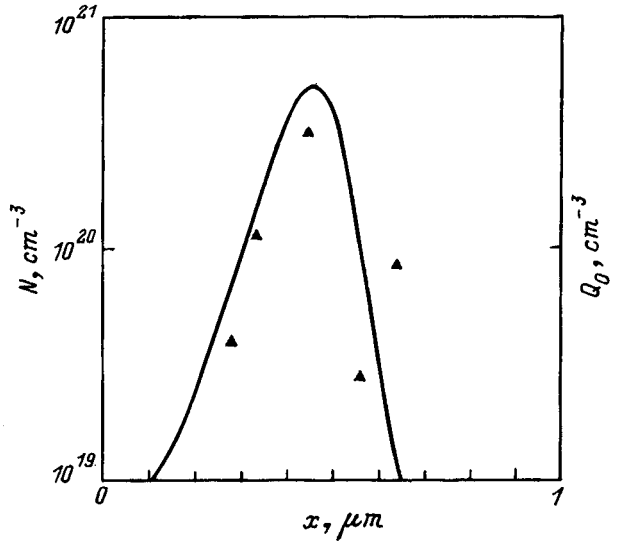

FIG. 4. Correlation of the concentration N of implanted B (solid line) and rate of increase in the impurity concentration Q_0 (points) at the maxima of the structure.

where r_{c0} is the critical radius corresponding to the initial degree of supersaturation. Since $Q(t)$ at a given moment in time is determined by the concentration of the mobile component, we also have

$$B_1 \equiv Q(t) = \left(\frac{9\sigma^2}{Dr_{c0}^3} \right)^{1/3} t^{-1/3}. \tag{6}$$

Substituting (4)–(6) into (3) and integrating from the beginning of the coalescence stage to the current moment in time, we obtain a logarithmic dependence similar to (1)

$$B_p(t) - B_{p0} = CQ_0 \ln(t/t_0), \tag{7}$$

where t_0 is the time of the onset of the coalescence stage, B_{p0} is the concentration of the impurity in the precipitates at that time, and C is a numerical coefficient. It follows from (7) that the slope of the plots presented in Fig. 2 is proportional to the initial supersaturation Q_0. The initial supersaturation in our case is assigned mainly by the profile of the implanted impurity. Therefore, a correlation should be observed between the initial degrees of supersaturation calculated in accordance with (7) from the data presented in Fig. 2 and the experimental profile of the distribution of the implanted impurity. As is seen from Fig. 4, in which such a comparison is made, this correlation is, in fact, observed, despite the highly approximate character of the treatment performed above.

Thus, an approximate analysis of the process of the accumulation of an impurity at the maxima of the structure considered shows that this stage in the formation of a quasiperiodic structure is similar, in general terms, to the phenomenon of coalescence in a supersaturated solid solution of boron atoms located at irregular positions in a silicon lattice.

It was noted above that the variation of the concentration at the minima of the structure is regulated mainly by the diffusional flow of the substance released from precipitates to nearby maxima, which act as absorbing walls for the mobile component. As we know,[8] the corresponding boundary-value problem for the diffusion equation in the restricted space between two adjacent maxima has a solution, which decays exponentially with time. Then the exponents in the experimental dependence (2) can be compared with the eigenvalues of that problem:

$$\lambda_m = m^2 \frac{\pi^2}{h^2} D \quad (m = 1,2,3, \ldots), \tag{8}$$

where h is the distance between the planes on which the boundary conditions are assigned. Taking a distance equal to the mean period of the structure, 95 nm, as h in an approximation, for $m=1$ we obtain an upper estimate for the diffusivity of the mobile boron component within the region perturbed by irradiation:

— $D \simeq 5\times10^{-16}$ cm^2/s at the minimum to the left of the central maximum,

— $D \simeq 4\times10^{-16}$ cm^2/s at the minimum to the right.

The estimates obtained are in satisfactory agreement with the available experimental data[9–13] on the diffusion of boron in silicon under conditions for which no dependence of the shape of the impurity distribution profile on the concentration of the latter is observed. The averaged temperature dependence of the diffusivity of boron for the data in Refs. 9–13 gives the value 9.9×10^{-16} cm^2/s for 900 °C.

It has generally been assumed that the diffusivity of boron atoms depends on their concentration in crystal-lattice sites. The agreement obtained above between the values of the diffusivities then indicates that in the regions of the samples where the formation of the oscillating structure occurs the concentration of boron in the substitutional sites is reduced in comparison with the original doping level.

CONCLUSIONS

1. It has been established that the migration of boron accompanied by capture of the impurity in zones with fixed positions in space takes place with a conserved integral quantity of boron in the silicon regions containing quasiperiodic structures during anneals at 900–1075 °C.

2. It has been shown that during an anneal at a fixed temperature of 900 °C the increment of the boron concentration at the maxima of the quasiperiodic structure is satisfactorily described by a logarithmic time dependence in the interval 10–240 min, while the decrease in the concentration at the minima is described by an exponential dependence. The main features of the redistribution of the impurity fit well into the theory of the coalescence of supersaturated solid solutions.

We wish to thank A. I. Baranov for a discussion of the results of this study.

[1] A. M. Myasnikov, V. I. Obodnikov, V. G. Seryapin, E. G. Tishkovskiĭ, B. I. Fomin, and E. I. Cherepov, Pis'ma Zh. Éksp. Teor. Fiz. **60**, 96 (1994) [JETP Lett. **60**, 102 (1994)].
[2] D. J. Eaglesham, P. A. Stolk. H.-J. Gossmann, and J. M. Poate, Appl. Phys. Lett. **65**, 2305 (1994).
[3] P. A. Stolk, H.-J. Gossmann, D. J. Eaglesham, D. C. Jacobson, J. M. Poate, and H. S. Luftman, Appl. Phys. Lett. **66**, 568 (1995).
[4] P. A. Stolk, D. J. Eaglesham, H.-J. Gossmann, and J. M. Poate, Appl. Phys. Lett. **66**, 1370 (1995).

[5] H. Ryssel, K. Muller, K. Haberger, R. Henkelmann, and F. Jahnel, Appl. Phys. **22**, 35 (1980).
[6] I. M. Lifshitz and V. V. Slyozov, J. Phys. Chem. Solids **19**, 35 (1961).
[7] T. R. Waite, Phys. Rev. **107**, 463 (1957).
[8] Ya. B. Zel'dovich, and A. D. Myshkis, *Elements of Mathematical Physics* [in Russian], Nauka, Moscow (1973).
[9] M. Miyake, J. Appl. Phys. **57**, 1861 (1985).
[10] R. N. Ghostagor, Phys. Rev. B **3**, 389 (1971).
[11] S. Wagner, J. Electrochem. Soc. **119**, 1570 (1972).
[12] D. A. Antoniadis, A. G. Gonzalez, and R. W. Dutton, J. Electrochem. Soc. **125**, 813 (1978).
[13] A. D. Kurtz and R. Yee, J. Appl. Phys. **31**, 303 (1960).

Translated by P. Shelnitz

Influence of impurity germanium on the properties of sulfur centers in silicon

M. S. Yunusov, M. Karimov, B. L. Oksengendler, and A. Yusupov

Institute of Nuclear Physics, Academy of Sciences of Uzbekistan, 702132 Ulugbek, Uzbekistan
(Submitted March 13, 1996; accepted for publication October 24, 1996)
Fiz. Tekh. Poluprovodn. **31**, 708–711 (June 1997)

The influence of the germanium atoms in n-Si⟨P, Ge, S⟩ on the parameters of the sulfur centers is investigated. An increase in the concentrations of some centers associated with S atoms and a small shift of their local levels is discovered. The detected effects are attributed to the influence of elastic strains that are caused by the presence of Ge in silicon crystal-lattice sites on the interstitial configuration of S. Elastic strain induces vibronic enhancement in such Jahn–Teller centers. © *1997 American Institute of Physics.* [S1063-7826(97)01506-8]

INTRODUCTION

The influence of impurity Ge and other isovalent impurities in silicon on a number of properties of transition-metal impurities (additionally introduced into Si by diffusion), viz., the diffusivity, the thermal decay of their electrically active centers, etc., was investigated in Refs. 1 and 2. As a result, these effects were attributed to the mechanical stresses caused by the straining of the crystal lattice due to the differences between the covalent and ionic radii of Si and the isovalent impurity. As the investigations of several researchers[3–7] have shown, such stresses cause the clustering of vacancies around each isovalent Ge_s impurity atom, the formation of Ge_s+V, and complexes in silicon. In the opinion of those researchers, these effects influence radiation-induced defect-formation processes. In our opinion, it is perfectly natural to expect such strain fields to influence both the details of defect formation and the energy spectrum of impurities with deep levels. We, therefore, investigated the influence of impurity Ge ($N_{Ge}=5\times10^{18}-5\times10^{19}$ cm^{-3}) on the parameters of S centers in silicon (n-Si⟨P, Ge, S⟩).

It should be noted that the question of the states of S in the Si crystal lattice and the relationship between the experimentally observed, diverse energy levels and just these states is extremely complicated. Therefore, despite the abundance of experimental results on this subject, even today it is very difficult to unequivocally say just which states of S are realized in Si and which energy levels they create. For example, the existing literature describes a large number of S impurity centers in silicon with their respective energy levels:[8–18]

$$E_1=E_c-0.13\ \text{eV},\quad E_2=E_c-0.27\ \text{eV},$$

$$E_3=E_c-0.36\ \text{eV},\quad E_4=E_c-0.5\ \text{eV},$$

$$E_5=E_c-0.18\ \text{eV},\quad E_6=E_c-0.31\ \text{eV},$$

$$E_7=E_c-0.62\ \text{eV}.$$

Some of the deep levels discovered, viz., E_3 and E_5 in Ref. 8, E_2 and E_4 in Ref. 12, E_1, E_3, E_5, and E_7 in Ref. 10, E_1, E_3, and E_5 in Ref. 11, E_1, E_2, E_3, and E_4 in Refs. 14 and 18, E_3, E_4, E_5, and E_6 in Ref. 15, E_6 and E_7 in Ref. 16, and E_1, E_2, E_4, and E_6 in Ref. 17, were assigned to site states of the S atoms; the E_4 and E_6 levels were assigned to complexes involving interstitial Si atoms in Ref. 15; and the E_3 level was assigned to a pair of S atoms or a pair consisting of an S atom and an Fe atom in Ref. 9. In addition, it was shown in Refs. 13, 14, 17, and 18 that, first, the concentration of the centers with the ionization energies E_3, E_4, and E_6 is of the order of 10% of the total concentration of electrically active S centers in Si and that, second, the formation of these centers is not regular, i.e., a dependence of their formation on the diffusion temperature and the postdiffusion quenching regime is observed.[14,18]

As we see, despite the numerous investigations of S impurity centers in Si, there is still no clear-cut unique model for them. Under these circumstances we started out from the following arguments. If the S centers are substitutional centers, the introduction of the internal elastic fields caused by the Ge atoms has a strong effect on the position of the local levels of such centers, although an increase in the solubility of S can be expected because of the appearance of vacancies induced by the elastic fields of the isovalent germanium atoms.[19] Additional complications arise, if a S center is a variant of an interstitial S state, since realization of the Jahn–Teller or pseudo-Jahn–Teller effect is then possible.[20] In this case, the elastic strain arising from the Ge atoms not only generates additional vacancies (V), but also causes so-called vibronic enhancement.[20] The latter results, first, in displacement of the local levels and, second, in alteration of the solubility of such S centers.

EXPERIMENTAL METHOD

The samples were doped with sulfur by thermal diffusion at a temperature of the order of 1000 °C for 20 h followed by rapid cooling (~250° C/min). The original sample used was of n-type Si⟨P, Ge, S⟩ with a resistivity equal to $10-50\ \Omega\cdot$cm. At the same time, control samples of n-type Si⟨P⟩, which did not contain isovalent Ge, but had similar electrical parameters, were also doped with sulfur. The parameters of the deep levels were measured by deep-level transient spectroscopy (DLTS).[21] The temperature dependence of the velocity of the charge carriers was determined by measuring gated windows with the measuring charge relaxation times $t_1=0.2-20$ ms and $t_2=2t_1$ after a pulse for filling the deep levels with majority carriers. Schottky barriers, which were obtained by sputtering Au after removing the surface layers of Si saturated with S, served as rectifying contacts on n-type Si.

TABLE I.

Type of sample	Parameters of centers	Centers investigated			
		E_1	E_2	E_3	E_4
Si⟨P, S⟩	E, eV	$E_c-0.13$	$E_c-0.257$	$E_c-0.36$	$E_c-0.50$
	N, cm^{-3}	3×10^{12}	2.8×10^{12}	$<10^{11}$	1.7×10^{12}
	σ_n, cm^2	–	5.4×10^{-14}	–	5×10^{-15}
Si⟨P, Ge, S⟩	E, eV	$E_c-0.13$	$E_c-0.265$	$E_c-0.37$	$E_c-0.519$
$N_{Ge}\simeq5\times10^{19}cm^{-3}$	N, cm^{-3}	3.5×10^{12}	3.8×10^{12}	3.8×10^{12}	4×10^{12}
	σ_n, cm^2	–	7.2×10^{-14}	4.1×10^{-14}	2.2×10^{-15}

3. EXPERIMENTAL RESULTS AND DISCUSSION

The results of the treatment of the DLTS spectra obtained are presented in Table I. These results show that the familiar spectrum of sulfur energy levels[18] is observed in the control samples of n-type Si⟨P, S⟩. The presence of the Ge and Si atoms leads, first, to an increase in the concentration of S centers (especially of the centers with the energies E_3 and E_4) and, second, to a small shift of the positions of their energy levels.[1)] We note that a similar phenomenon was observed in Si doped with Ge and Au,[22] as well as Ge and Mn.[23] The mechanism underlying this phenomenon was not disclosed in the references cited. Returning to our case, we note that while the S centers with an ionization energy $E_c-0.36$ eV in the samples without Ge have a very small concentration ($<10^{11}$ cm^{-3}) when the diffusion temperature is 1000°C, the concentration of these centers in the samples with Ge is significantly higher ($\sim4\times10^{12}$ cm^{-3}).

Let us analyze the results obtained from the standpoint of the influence of Ge atoms on the concentration of free vacancies and from the standpoint the strains appearing on the character of the Jahn–Teller distortions of the configuration of interstitial S, i.e., on the splitting of the p states in a field of T_d symmetry. We consider the system of kinetic equations

$$\frac{dN_V}{dt}=-k_1N_IN_V-k_2N_VN_{Ge}-N_V/\tau_V-k_4N_VN_S^i,$$

$$\frac{dN_I}{dt}=-k_1N_IN_V-N_I/\tau_I,$$

$$\frac{dN_S^i}{dt}=-k_4N_VN_S^i.$$

The initial conditions (at $t=0$) are: $N_V=N_V^0$; $N_I=N_I^0$; $N_S^i=(N_S^i)^0$. Here N_V, N_I, N_{Ge}, and N_S^i are the concentrations of vacancies, intrinsic interstitial Si atoms, Ge atoms in sites, and S atoms in interstices, respectively; N_V/τ_V and N_I/τ_I are the probabilities of the loss of the vacancies V and the intrinsic silicon interstitials I in sinks; and t the time for cooling and the occurrence of all the quasichemical reactions. Assuming that $1/\tau_V\ll k_2N_V$, we obtain

$$N_I=N_I^0\ \exp(-t/\tau_I).$$

Now, if $[k_1N_I,k_4N_S^i]<[k_2N_{Ge},1/\tau_V]$, we can write

$$N_V=N_V^0\ \exp[-(1/\tau_V+k_2N_{Ge})t].$$

Then, in turn, we can write

$$\frac{dN_S^i}{dt}=-k_4N_V^0(N_S^i)^0\ \exp[-(1/\tau_V+k_2N_{Ge})t],$$

which gives

$$N_S^i(t)=(N_S^i)^0-k_4N_V^0(N_S^i)^0\,\tilde{\tau}[-(1-\exp(-t/\tilde{\tau})],$$

where $1/\tilde{\tau}=1/\tau_V+k_2N_{Ge}$, and k_i denotes the constants of the respective quasichemical reactions. Thus, we have the kinetics for the concentration of interstitial sulfur atoms $N_S^i(t)$, which depend on the concentration of the Ge atoms. Here it is assumed that $dN_S/dN_{Ge}>0$.

Let us now consider the question of the possible influence of the isovalent impurity Ge_s on the electron spectrum of the other impurities that dope the Si. Here the case in which the Jahn–Teller effect is seen must be distinguished from the case in which it is not seen.

When the impurity atom does not exhibit the Jahn–Teller effect, the potential energy of the impurity atom with a captured electron in the elastic field $V=V_0(a/R)^3$ of the Ge atom has the form

$$V(q)=\varepsilon(q)+V_0\left(\frac{a}{R+q}\right)^3,$$

where $\varepsilon(q)=\varepsilon_0+(1/2)\kappa q^2$ is the energy of the local center as a function of the displacement of the impurity atom (q) from its localization center ($\varepsilon<0$), V_0 is the elastic interaction parameter, a is the interatomic distance, κ is the elastic constant of the center with the captured electron, and R is the distance between the impurity center and the Ge atom.

Since

$$\left(\frac{a}{R+q}\right)^3\approx\frac{a^3}{R^3}\left(1-3\frac{q}{R}\right),$$

$\overline{q}=6V_0a^3/R^4\kappa$; therefore, the local level rises, and its energy becomes

$$\varepsilon(\overline{q})=\varepsilon_0+\frac{\kappa^2}{2}\left[\frac{6V_0a^3}{R^4\kappa}\right]^2=\varepsilon_0+\frac{\text{const}}{R^8}.$$

The value of the constant in this equality is very small, so that the large exponent on R renders the effect of the shift appreciable only near the impurity atom. Thus, this effect is possible only at anomalously high concentrations of germanium. We note that such a level shift can be observed on a background of the temperature only if the following inequality is satisfied: $\text{const}/R^8>kT$ (Fig. 1a).

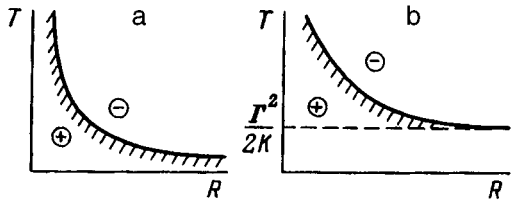

FIG. 1. $T-R$ phase diagrams, where T is the temperature, and R is the distance between an isovalent impurity atom and a nonisovalent defect for the cases in which the defect does not exhibit the Jahn–Teller effect (a) and the defect exhibits the Jahn–Teller effect (b). ⊕ — the lowering of the electron level of the defect is observable, ⊖— the lowering of the electron level of the defect is obscured by the temperature fluctuations.

When an impurity atom exhibits the Jahn–Teller effect and an electron is captured in the degenerate orbital, the potential energy of the impurity atom in the lattice has the form

$$V(q)=\frac{1}{2}\,Kq^2-\Gamma q,$$

so that the potential minimum is located at the point $q_0=\Gamma/k$ and the energy of the local level is lowered by $\Delta\varepsilon=\Gamma^2/2K$ (here Γ is the vibronic constant, and K is the elastic constant of the local center without the captured electron[20]). Allowance for the elastic interaction with Ge_s gives a barrier between the Jahn–Teller minima equal to

$$Q+\Delta Q=\frac{\Gamma^2}{2K}+3V_0\frac{\Gamma a^3}{KR^4}=Q+\frac{\text{const}}{R^4},$$

where Q is the barrier between equivalent minima in the adiabatic potential with allowance for the Jahn–Teller effect, and ΔQ is the additional barrier in the asymmetric adiabatic potential appearing under the action of fields due to the presence of Ge atoms in the silicon lattice. The condition for appreciable asymmetry in the positioning of the impurity is $Q+\Delta Q>kT$ (Fig. 1b).

The investigations in Refs. 24 and 25 show that for impurities like S the Jahn–Teller effects are fully realistic specifically for interstitial configurations. Therefore, the existence of a spread of energies for a local electron level[1)] is apparently attributable to the interstitial configuration of the sulfur impurity.

CONCLUSIONS

Thus, the experimental results obtained and the theoretical arguments presented allow us to consistently link, within the same quasichemical approximations, the physicochemical phenomena, which occur in a material when an isovalent impurity is introduced, and the electronic properties of a deep-level impurity, which is introduced into such a material.

This work was supported by the Foundation for the Development of Sciences of the State Committee for Science and Technology of the Republic of Uzbekistan.

[1)]In principle, this shift lies within kT, but it is always in the direction of deepening of the levels.

[1] M. K. Bakhadyrkhanov, F. M. Talipov, and U. S. Dzhurabekov, Pis'ma Zh. Tekh. Fiz. **16**, 77 (1990) [Sov. Tech. Phys. Lett. **16**, 633 (1990)].
[2] F. M. Talipov and R. Khamidov, Pis'ma Zh. Tekh. Fiz. **19** (1), 55 (1993) [Tech. Phys. Lett. **19**, 59 (1993)].
[3] V. G. Golubev, V. V. Emtsev, P. M. Klinger, G. I. Kropotov, and Yu. V. Shmartsev, Fiz. Tekh. Poluprovodn. **26**, 574 (1992) [Sov. Phys. Semicond. **26**, 328 (1992)].
[4] V. I. Kuznetsov, P. F. Lugakov, A. R. Salmanov, and A. V. Tsikunov, Fiz. Tekh. Poluprovodn. **23**, 1492 (1989) [Sov. Phys. Semicond. **23**, 925 (1989)].
[5] M. Ya. Dashevskiĭ, D. N. Korlyakov, E. A. Ladygin, A. M. Musalitin, and B. A. Shilin, Fiz. Tekh. Poluprovodn. **24**, 2073 (1990) [Sov. Phys. Semicond. **24**, 1289 (1990)].
[6] L. I. Khirunenko, V. I. Shakhovtsov, V. K. Shinkarenko, L. I. Shpinar, and I. I. Yaskovets, Fiz. Tekh. Poluprovodn. **21**, 562 (1987) [Sov. Phys. Semicond. **21**, 345 (1987)].
[7] G. D. Watkins, Trans. IEEE **NS-16**, 13 (1969).
[8] R. O. Carlson, R. N. Hall, and M. Pell, J. Phys. Chem. Solids **8**, 81 (1959).
[9] C. W. Ludwig, Phys. Rev. **137**, A1520 (1965).
[10] W. E. Krag, W. H. Kleiner, H. J. Zeiger, and S. Fischler, J. Phys. Soc. Jpn., Suppl. **21**, 230 (1966).
[11] D. L. Camphausen, H. M. James, and R. J. Sladek, Phys. Rev. B **2**, 1899 (1970).
[12] L. L. Rosier and C. T. Sah, Solid-State Electron. **14**, 41 (1941).
[13] M. S. Yunusov, Sh. Makhkamov, and M. Karimov, Fiz. Tekh. Poluprovodn. **10**, 1015 (1976) [Sov. Phys. Semicond. **10**, 601 (1976)].
[14] M. S. Yunusov, M. Karimov, and N. A. Tursunov, *Radiation-Activated Processes in Silicon* [in Russian], Fan, Tashkent (1977), p. 146.
[15] A. A. Lebedev and A. A. Lebedev, Fiz. Tekh. Poluprovodn. **17**, 2152 (1983) [Sov. Phys. Semicond. **17**, 1376 (1983)].
[16] H. G. Grimmeiss and M. Kleverman, J. Phys. Chem. Solids **49**, 615 (1988).
[17] G. Pensl, G. Roos, C. Holm, and P. Wagner, in *Defects in Semiconductors (Mater. Sci. Forum., Vols. 10–12*, H. J. van Bardeleben (ed.), (1986), p. 911.
[18] M. S. Yunusov, M. Karimov, R. Kh. Kochkarov, and A. A. Karimov, Dokl. Akad. Nauk UzR **6**, 22 (1991).
[19] E. V. Solov'eva and M. G. Mil'vidskiĭ, Fiz. Tekh. Poluprovodn. **17**, 2022 (1983) [Sov. Phys. Semicond. **17**, 1289 (1983)].
[20] I. B. Bersuker, *Electronic Structure and Properties of Transition Metal Compounds: An Introduction to the Theory*, Wiley, New York (1996).
[21] D. V. Lang, J. Appl. Phys. **45**, 3023 (1974).
[22] M. S. Saidov, A. Yusupov, and I. G. Atabaev, in *Abstracts of Reports to the 2nd All-Union Conference on Deep Levels in Semiconductors* [in Russian], Tashkent, 1980, p. 118.
[23] Sh. B. Utamuradova, T. A. Umarov, V. É. Rafikova, and R. M. Érgashev, in *Current Problems in the Physics of Semiconductors and Insulators* [in Russian], Fan, Tashkent (1995), p. 87.
[24] G. G. DeLeo, G. Watkins, and W. Fowler, Phys. Rev. B **37**, 1013 (1988).
[25] S. Pantelides, W. Harrison, and F. Yndurain, Phys. Rev. B **34**, 6038 (1986).

Translated by P. Shelnitz

Possibility of enhancing a photorefractive hologram using negative differential conductivity

Yu. V. Miklyaev

University Academic Department of Nonlinear Optics, Institute of Electrophysics, Russian Academy of Sciences, Ural Branch and Chelyabinsk Technical University, 454080 Chelyabinsk, Russia
(Submitted August 7, 1996; accepted for publication October 24, 1996)
Fiz. Tekh. Poluprovodn. **31**, 712–713 (June 1997)

The possibility of utilizing negative differential conductivity for photorefractive recording is considered. It is shown that the application of an external variable field of definite form to a crystal makes it possible to avoid the formation of macroscopic strong-field domains and, at the same time, to ensure enhancement of the hologram in the initial stage of reading. © *1997 American Institute of Physics.* [S1063-7826(97)01606-2]

High-resistivity crystals of such semiconductors as GaAs, CdTe, InP, etc. are employed, along with other materials, in photorefractive recording. These semiconductors can exhibit bulk negative differential conductivity (NDC) in a certain range of electric field strengths. For samples with a sufficiently high concentration of free charge carriers this phenomenon causes a Gunn effect and is widely used to generate microwave oscillations.[1] High-resistivity (with strongly compensated impurity conduction) semiconductors can also display NDC, but it can be caused not only by a decrease in the carrier drift velocity $\nu(E)$ with increasing field strength (Fig. 1), but also by the fact that the cross section for the capture of a carrier by an impurity center can increase with increasing field strength.[2] As was noted in Ref. 3, this phenomenon allows the appearance of growing spatial trap charge-exchange waves in addition to damped waves. As a result, slowly moving (recombination) domains form.

The recording of photorefractive gratings under the conditions of saturation of the carrier drift velocity at large values of the external constant electric field was investigated theoretically in Ref. 4. According to that work, zero differential carrier mobility permits an increase in the amplitude of a space-charge field grating.

In this paper we consider the possibility of enhancing a previously recorded photorefractive hologram as it is read by utilizing the phenomenon of NDC.

The treatment is based on a well-known model of photorefractive crystals,[5] but with consideration of the nonlinear character of the dependence of the electron drift velocity on the field strength $\nu(E)$ and the dependence of the mean lifetime of an electron in the conduction band on the field $\tau(E)$. We represent the field in a crystal in the form $E=E_0+E_{sc}\exp(iqx)+\text{c.c.}$, where E_0 is the external field, and q is the spatial frequency of the space-charge field (E_{sc}) grating. Assuming that $E_{sc}\ll E_0$ in the approximation of low contrast in the interference pattern ($m\ll 1$), by analogy with Ref. 5 we can easily obtain the equation describing the recording of a photorefractive grating

$$\frac{\varepsilon\varepsilon_0}{n_0|e|}\frac{\partial E_{sc}}{\partial t}-\Gamma E_{sc}=F, \tag{1}$$

where

$$\Gamma=\frac{\partial(\nu\tau)/\partial E-(i\nu-Dq)\tau/E_q+iDq(\partial\tau/\partial E)}{1-iq\nu\tau+Dq^2\tau}, \tag{2}$$

$$F=-\frac{m(\nu+iDq)}{1-iq\nu\tau+Dq^2\tau}. \tag{3}$$

Here D is the diffusion coefficient (we assume that D does not depend on E), ε and ε_0 are the dielectric constants of the crystal and the permittivity of a vacuum, respectively, e is the charge of the electron, $E_q=eN_a/(q\varepsilon_0\varepsilon)$ is the saturation field of the traps, N_a is the density of the deep traps, and n_0 is the density of the conduction electrons.

The reading process corresponds to zero on the right side of Eq. (3) (uniform illumination, $m=0$). The imaginary part of the coefficient Γ specifies the rate of motion of the space-charge grating along the x axis, and the real part gives the damping (or growth) rate of the grating.

If a variable field with a frequency Ω much greater than the hologram recording reciprocal time is applied to the crystal instead of a constant field, the space-charge grating is stationary. For the case of a variable field in the form of the meander $E(t)=E_0\,\text{sgn}(\cos(\Omega t))$, averaging Eq. (5) over the period of the external field and disregarding diffusion (when $Da\ll\nu$ and $Dq^2\tau\ll 1$), we can easily find the damping of the grating

$$\langle\Gamma\rangle=\frac{\partial(\nu\tau)/\partial E+q(\nu\tau)^2/E_q}{1+(q\nu\tau)^2}. \tag{4}$$

As can be seen, when $\partial(\nu\tau)/\partial E<-q(\nu\tau)^2/E_q$, enhancement of the grating should be observed during reading. However, when photorefractive holograms are recorded in semiconductors in an external field, the drift length of the free carriers $v\tau$ is comparable to or significantly greater than the period of the interference pattern, i.e., $q\nu\tau$ significantly exceeds unity. Thus, in the case of NDC the enhancement factor of the hologram will be considerably smaller than in noise gratings, in which $q\nu\tau\ll 1$. This will lead to the formation of macroscopic strong-field domains and distortion of the hologram. Curves a and b in Fig. 2 are plots of $\Gamma(q)$ in the case of positive and negative differential conductivity for the following values of the parameters (which correspond to

 1063-7826/97/060608-02$10.00

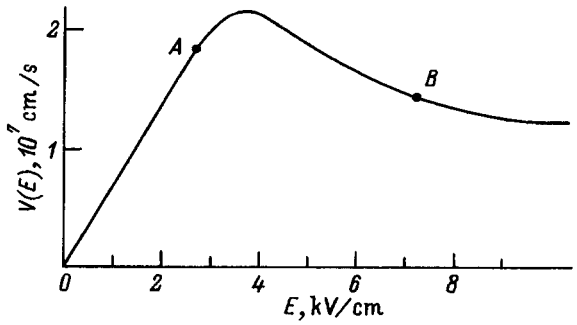

FIG. 1. Characteristic form of the dependence of the electron drift velocity on the electric field strength $v(E)$ for a gallium arsenide crystal.[1]

a GaAs crystal): $N_a=8\times10^{21}$ m^{-3}, $\varepsilon=13$, *a*) $\nu_a\tau=13$ μm (Ref. 6), $\tau'=0$, $\nu_a'/\nu_a=0.4\times10^{-5}$ cm/V (Ref. 1), *b*) $\nu_b=0.8\nu_a$, $\nu_b'=-0.3\nu_a'$.

The formation of macroscopic domains can be avoided by applying a variable field with a time dependence of a specific form. We assume that during its period the external field assumes values corresponding to enhancement and

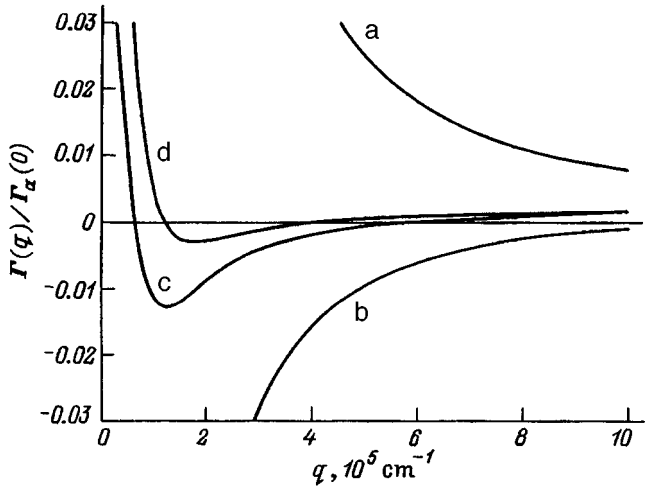

FIG. 2. Dependence of the damping $\Gamma(q)=(\Gamma_a(q)t_a+\Gamma_b(q)t_b)\times(t_a+t_b)^{-1}\Gamma_a^{-1}(0)$ of a grating on the spatial frequency q of the grating for various values of t_a/t_b: a — $t_b/t_a=0$; b — $t_a/t_b=0$; c — $t_b/t_a=2.8$; d — $t_b/t_a=2.4$.

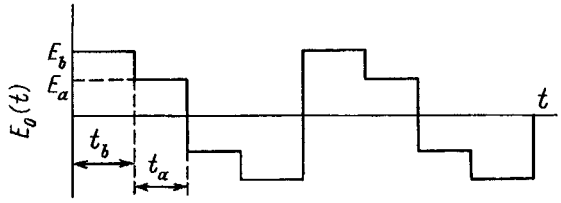

FIG. 3. Time dependence of the external field strength $E_0(t)$. The values of E_a and E_b correspond to positive and negative differential conductivity.

damping of the grating (Fig. 3). We assume that for macroscopic domains ($q\nu\tau\ll1$) erasing compensates for the growth: $\nu_a't_a=-\nu_b't_b$, where t_a and t_b are the lengths of the portions of the period of the external field corresponding to damping and enhancement of the grating, and ν_a' and ν_b' are the derivatives of the carrier velocity with respect to the field strength at these moments in time (Fig. 1). When $\nu_a>\nu_b$, erasing occurs more slowly for a grating with $q\nu\tau>1$, and the grating is enhanced as a result. Figure 2 presents plots of the dependence of the mean damping in a period of the external field $\Gamma(q)=(t_a+t_b)^{-1}(\Gamma_a(q)t_a+\Gamma_b(q)t_b)$ for various values of t_a/t_b. The values of Γ_a and Γ_b correspond to the dampings of the grating in an external field in the form of a meander with the amplitudes E_a and E_b (Fig. 3). As we can see, when the parameters have certain values (Fig. 2, curves c and d), enhancement of the gratings can be ensured in a certain range of spatial frequencies (in which $q\nu\tau<10$), and, at the same time, the appearance of macroscopic domains can be avoided.

[1] M. E. Levinshteĭn, Yu. K. Pozhela, and M. S. Shur, *The Gunn Effect* [in Russian], Sov. Radio, Moscow (1975).
[2] G. C. Valley, H. Rajbenbach, and H. J. von Bardebelen, in *Photorefractive Materials, Effects, and Devices, Technical Digest of Topical Meeting*, Aussois, France, 1990, p. 29.
[3] R. F. Kazarinov, R. A. Suris, and B. I. Fuks, Fiz. Tekh. Poluprovodn. **7**, 149 (1973) [Sov. Phys. Semicond. **7**, 102 (1973)].
[4] Q. N. Wang, R. M. Brubaker, and D. D. Nolte, Opt. Lett. **19**, 822 (1994).
[5] N. V. Kukhtarev, V. B. Markov, S. G. Odulov, M. S. Soskin, and V. L. Vinetskii, Ferroelectrics **22**, 949 (1979).
[6] A. M. Glass, A. M. Johnson, D. H. Olson, W. Simpson, and A. A. Ballman, Appl. Phys. Lett. **44**, 948 (1984).

Translated by P. Shelnitz

Dielectric constant and ac conductivity of semi-insulating $Cd_{1-x}Mn_xTe$ semiconductors

P. W. Zukowski

Lublin Technical University, Lublin, Poland

A. Rodzik

Jagiellonian University, Cracow, Poland

Yu. A. Shostak

Belarus State University, 220050 Minsk, Belarus

(Submitted July 11, 1995; accepted for publication October 25, 1996)
Fiz. Tekh. Poluprovodn. **31**, 714–718 (June 1997)

Plots of the temperature dependence of the dielectric constant and the ac resistance of the compounds $Cd_{1-x}Mn_xTe$ ($0 \leqslant x \leqslant 0.7$) are presented, and it is established from them that additional polarization of the compound is caused by hopping charge exchange among structural defects. The electron spin resonance and reflectance spectra of these materials are investigated. A model describing the thermally activated increase in the dielectric constant of the semiconductors is proposed. The main characteristics are determined, and a microscopic model of the structure of the defects whose hopping charge exchange leads to an increase in the dielectric constant of the compensated $Cd_{1-x}Mn_xTe$ semiconductors is proposed. © *1997 American Institute of Physics.* [S1063-7826(97)01706-7]

INTRODUCTION

Dynamic effects caused by hopping charge exchange among defects that create deep levels in the band gap can appear at high defect concentrations.[1] One such effect is the temperature-activated increase in the dielectric constant that we discovered in Si crystals irradiated with doses of neutrons greater than or of the order of 10^{18} cm^{-2} (Ref. 2). Hopping electron exchange among the defects present in a crystal leads to the appearance of dipoles and consequently to an increase in the dielectric constant.[3] In binary and ternary compounds defects appear not only as a result of irradiation, but also during growth.[4] Hopping charge exchange among them can also lead to an increase in the dielectric constant of the crystals.

In this paper we present a phenomenological model, which describes the increase in the dielectric constant of high-defect-density semiconductors due to hopping charge exchange among the defects, and report the results of measurements of the dielectric constant and the ac conductivity, as well as the electron spin resonance (ESR) spectra, of $Cd_{1-x}Mn_xTe$ semiconductors, which enable us to propose a microscopic structural model of the defects among which hopping charge exchange occurs.

1. HOPPING CHARGE EXCHANGE AND THE DIELECTRIC CONSTANT OF HIGH-DEFECT-DENSITY SEMICONDUCTORS

We start out the construction of the model from a crystal in which there are defects of one type that create deep levels in the band gap and whose charge states can take the values ''0,'' ''+,'' and ''−.'' Such defects are characteristic of II–VI semiconductors.[5]

At low temperatures the bulk of these defects will be in the neutral charge state. As the temperature rises, hopping charge exchange among the defects begins. Hops take place mainly between nearest neighbors.[6] The mean hopping distance $R \simeq N^{-1/3}$, where N is the defect density. A dipole appearing as a result of a hop has a dipole moment $p = eR$. The probability of hopping charge exchange is defined, according to Ref. 7, by the expression

$$P(T) = c(\alpha R)^2 \frac{\Delta E}{kT} \exp\left(-2\alpha R - \frac{\Delta E}{kT}\right), \tag{1}$$

where α is the rate of descent of the electron wave function in the potential well created by a defect, ΔE is the activation energy for hopping charge exchange, which is related to the energy positions of the defect levels in the band gap and the Fermi level, and c is a coefficient, which is determined by the phonon spectrum.

We assume that a defect can be in a nonzero charge state for a certain time τ and then return to the neutral state. Then, by analogy with Ref. 8, the density of the defects in the charged states can be estimated in the following manner:

$$N^+ = N^- = \frac{NP(T)\tau}{aP(T)\tau + 1}. \tag{2}$$

In the absence of an electric field the hopping probabilities in different directions are equal. In an electric field with an intensity **E** the hopping probabilities in the direction of **E** and in the opposite direction differ by the quantity $\exp(\pm eRE/kT)$.

Thus, uncompensated dipoles appear in the bulk of the crystal. We obtain their concentration by multiplying $P(T)$ in Eq. (2) by $\sinh(eRE/kT)$:

$$N_{\text{dip}} = \frac{NP(T)\tau \sinh\left(\dfrac{eRT}{kT}\right)}{2P(T)\tau \sinh\left(\dfrac{eRE}{kT}\right) + 1}. \tag{3}$$

 1063-7826/97/060610-05$10.00

Using the relations $P=N_{\text{dip}}\,p=N_{\text{dip}}\,eR$, $P=\varepsilon_0\chi E$, and (3), we determine the additional contribution to the dielectric susceptibility caused by hopping charge exchange among defects:

$$\chi_p=\frac{NP(T)\tau\,\sinh\left(\dfrac{eRE}{kT}\right)}{\left[2P(T)\tau\,\sinh\left(\dfrac{eRE}{kT}\right)+1\right]}\,\frac{eR}{\varepsilon_0 E}. \tag{4}$$

In the case of weak fields Eq. (4) is simplified:

$$\chi_p=\frac{NP(T)\tau e^2R^2}{\varepsilon_0 kT}. \tag{5}$$

When $P(T)\tau\ll 1$, according to (2), the product $NP(T)\tau$ is the total concentration of dipoles [in contrast to (3), in which the concentration of uncompensated dipoles is given]. We then have

$$\chi_p=\frac{N^+e^2R^2}{\varepsilon_0 kT} \tag{6}$$

and χ_p coincides to within a factor of 3 with the quantity specified by the Debye-Langevin formula[9]

$$\chi=\frac{Ne^2R^2}{3\varepsilon_0 kT}, \tag{7}$$

which describes the dielectric susceptibility of a crystal with N dipoles.

Thus, hopping charge exchange among multiply charged defects that create deep levels in the band gap should lead to an increase in the dielectric constant in the presence of an external electric field.

In deriving (4) and (5) we assumed that $\tau=\text{const}$. In this case the additional contribution to χ_p caused by hopping charge exchange can be observed only for the frequencies $f\leqslant 2/\tau$. However, the times τ for different defects can differ from one another. If they fall in the range $\tau_{\min}\leqslant\tau\leqslant\tau_{\max}$, χ_p should decrease above the frequency $f\simeq 2/\tau_{\max}$ and then vanish at $f>2/\tau_{\min}$.

2. EXPERIMENTAL RESULTS AND DISCUSSION

Capacitors, in which plates of the materials investigated with a thickness of 0.45 mm served as the insulator, were prepared for the measurements of the temperature dependence of the dielectric constant of the semi-insulating materials $Cd_{1-x}Mn_xTe$ ($0\leqslant x\leqslant 0.7$). The capacitor plates were obtained by applying a current-conducting silver paste to the surfaces of the plates. The capacitance and the resistance were measured by an E7-14 digital immittance meter at the frequencies 0.1, 1, and 10 kHz. The accuracy of the measurements was $\pm 0.1\%$. The temperature was varied from 80 to 450 K. The accuracy of the temperature measurements was ± 0.5 K.

Figures 1 and 2 present plots of the temperature dependence of capacitors with $Cd_{1-x}Mn_xTe$ insulators of various composition. It is seen from the figures that at low temperatures the dielectric constant is equal to about 9 and coincides with the value obtained from optical measurements in the infrared region of the spectrum.[10] Table I presents the values

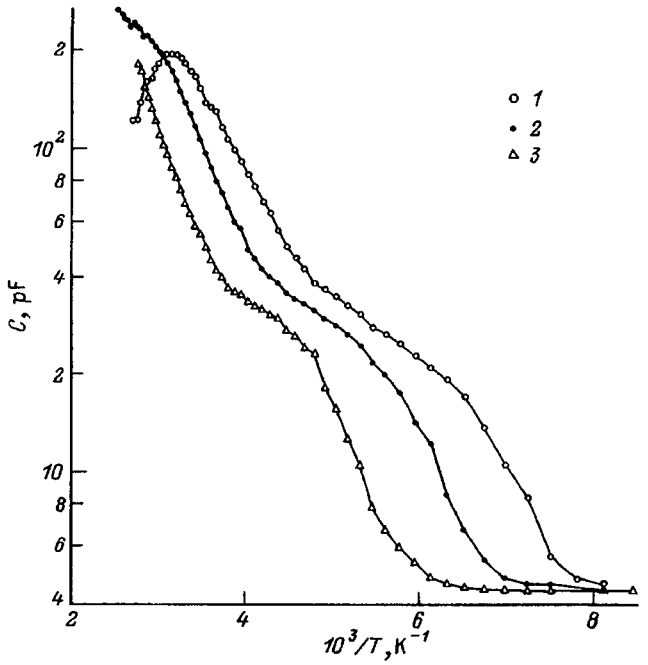

FIG. 1. Plots of the temperature dependence of the capacitance of $Cd_{0.85}Mn_{0.15}Te$ for various measurement frequencies f, kHz: *1* — 0.1, *2* — 1, *3* — 10.

of the activation energy for an increase in the dielectric constant ΔE^C relative to the edge of the conduction band, which were determined from the plots of $\log C=f(1/T)$ for semiconductors of various composition. As the measurement frequency is increased, a decrease in the capacitance is observed, as follows from Eqs. (4) and (5).

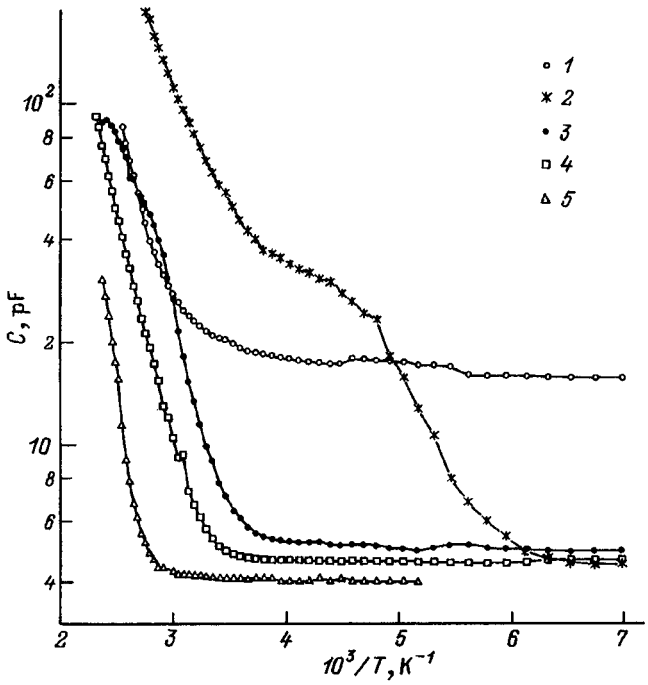

FIG. 2. Plots of the temperature dependence of the capacitance of the materials $Cd_{1-x}Mn_xTe$ ($0\leqslant x\leqslant 0.7$) for $f=10$ kHz and various values of x: *1* — 0, *2* — 0.15, *3* — 0.3, *4* — 0.5, *5* — 0.7.

TABLE I. Activation energies for the dielectric constant (ΔE_i^C) and the conductivity (ΔE_i^R) in the first ($i=1$) and second ($i=2$) stages of the increase in C and σ, as well as the band-gap width E_g for $Cd_{1-x}Mn_xTe$ semiconductors.

x	ΔE_1^C, eV	ΔE_1^R, eV	ΔE_2^C, eV	ΔE_2^R, eV	E_g, eV
0	<0.12	–	0.25 ± 0.05	0.28 ± 0.05	1.50
0.15	0.12 ± 0.03	0.12 ± 0.03	0.14 ± 0.03	0.13 ± 0.03	1.71
0.30	0.27 ± 0.05	0.29 ± 0.05	Not detected		1.90
0.50	0.25 ± 0.05	0.25 ± 0.05	in the temperature		2.19
0.70	0.60 ± 0.10	0.57 ± 0.10	range measured		2.40

Figure 3 presents plots of the temperature dependence of the resistance of a sample of $Cd_{0.85}Mn_{0.15}Te$. The resistance displays a significant dependence on the measurement frequency, attesting to the hopping mechanism of charge transfer in it.[6] According to Ref. 6, the dependence of the conductivity on the frequency in this case is described by the expression

$$\sigma=\sigma_0 f^s, \tag{8}$$

where $s\leqslant 0.8$. The expression (8) is valid only in the temperature ranges where the conductivity is determined by hopping charge exchange among defects of a single type. Accordingly, the temperatures at which a drop in resistance is observed for all three measurement frequencies were selected on the $R(1/T)$ curves (see Fig. 3). Figure 4 presents plots of the dependence of the conductivity on the measurement frequency for materials of different composition, as well as a plot of the dependence $\sigma=\sigma_0 f^{0.8}$. It is seen from Fig. 4 that the conductivity of all the materials investigated depends on the measurement frequency, and the exponent s in (8) is smaller than 0.8 in all cases. The agreement between the portions of the temperature dependences with increases

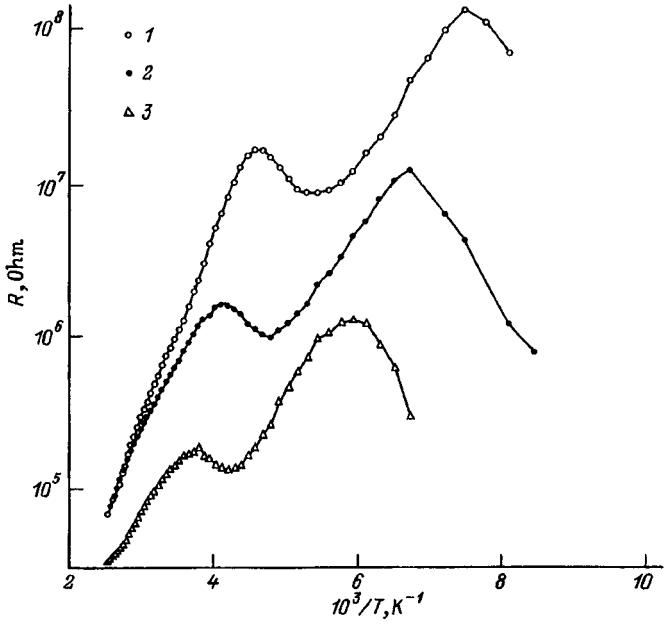

FIG. 3. Plots of the temperature dependence of the resistance of $Cd_{0.85}Mn_{0.15}Te$ for various measurement frequencies f, kHz: *1* — 0.1, *2* — 1, *3* — 10.

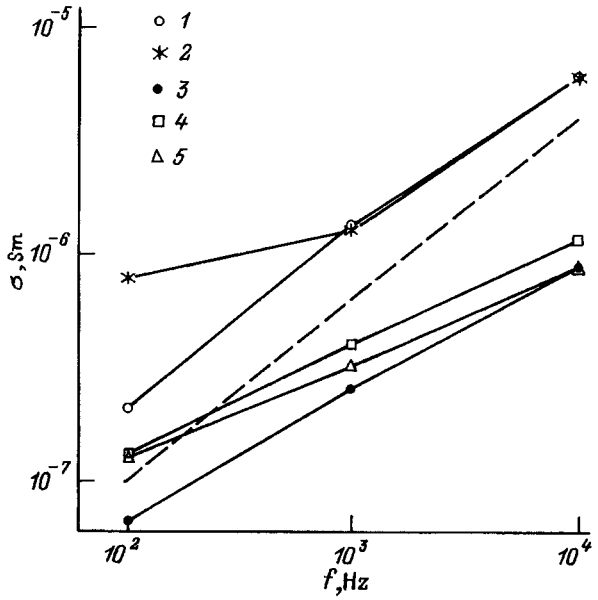

FIG. 4. Frequency dependence of the conductivity of the materials $Cd_{1-x}Mn_xTe$ ($0\leqslant x\leqslant 0.7$) for various compositions of the solid solution and measurement temperatures: *1* — $x=0$, $T=358$ K; *2* — $x=0.15$, $T=278$ K; *3* — $x=0.3$, $T=283$ K; *4* — $x=0.5$, $T=328$ K; *5* — $x=0.7$, $T=378$ K; dashed line — plot of $\sigma=\sigma_0 f^{0.8}$.

in the electric constant and the conductivity (Figs. 1 and 3) and between the values of the activation energies for increases in the capacitance (ΔE^C) and the conductivity (ΔE^R) (Table I) and the existence of frequency dependences of the capacitance and the conductivity can serve as evidence that all the processes enumerated above are determined by hopping charge among defects.

Defect densities of the order of $10^{19}-10^{20}$ cm^{-3} are needed for such a significant increase in the dielectric constant (to the values $\varepsilon\simeq 200$, i.e., more than a tenfold increase) to occur because of hopping charge exchange.[2] To determine the concentrations of the defects present in the materials $Cd_{1-x}Mn_xTe$, we measured the ESR spectra at $T=77$ K. The results of the measurements showed that the materials with $x\geqslant 0.15$ produce a broad isotropic line, whose parameters, viz., the g factor and the linewidth ΔH, as well as the concentrations of the defects responsible for its appearance, are presented in Table II. It follows from the ESR data that the $Cd_{1-x}Mn_xTe$ semiconductors contain paramagnetic centers, whose concentration can be sufficient for hopping charge exchange among them to cause an increase in the dielectric constant.

The dielectric constant of CdTe at 77 K is approximately three times greater than the value characteristic of materials with $x>0$ at that temperature. This means that in CdTe there

TABLE II. Results of ESR measurements (77 K) in $Cd_{1-x}Mn_xTe$ crystals.

x	g	ΔH, G	N, cm^{-3}
0.15	2.0035	390	2.22×10^{21}
0.30	2.0050	215	4.49×10^{21}
0.50	2.0128	240	7.58×10^{21}
0.70	2.0152	220	1.08×10^{22}

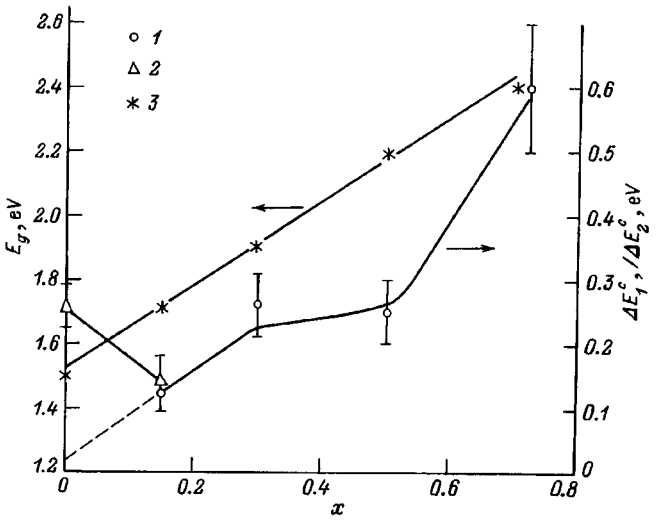

FIG. 5. Activation energies for hopping charge exchange ΔE_1^C and ΔE_2^C in the first (*1*) and second (*2*) stages of the increase in capacitance, as well as the band-gap width E_g (*3*) as a function of the concentration of Mn atoms.

is also a large concentration of defects which begin to participate in hopping charge exchange at temperatures lower than 77 K. It does not seem possible to say anything definite concerning the value of the activation energy for the dielectric constant. It can only be presumed that it does not exceed the value of ΔE_1^C for $x=0.15$, i.e., 0.12 eV.

It is seen from Table I and Fig. 2 that the defects responsible for the additional polarization of CdTe at low temperatures were not discovered in appreciable numbers after the introduction of Mn in a concentration $x=0.15$. Since Mn replaces Cd, it can be theorized that these defects are defects in the Te sublattice and that the introduction of Mn leads to variation of the position of their energy levels in the band gap and, consequently, in alteration of the $\varepsilon(1/T)$ curve.

Figure 5 presents the activation energies for hopping charge exchange and the band-gap width, which was obtained from reflectivity measurements, as functions of the Mn concentration. As is seen from Fig. 5, the plot of $E_g(x)$ is linear over the entire range of Mn concentrations investigated, while the $\Delta E_1^C(x)$ curve is not monotonic. The value of ΔE_1^C increases with increasing x up to $x=0.30$, then remains unchanged up to $x=0.50$, and finally increases abruptly.

A similar dependence on x is also observed for the linewidth of the ESR signal. The g factor is likewise a nonmonotonic function of x (Table II). An analysis of the results obtained, primarily of the nonmonotonic variation of the activation energies ΔE^C and ΔE^R, enabled us to develop a model for defects whose hopping charge exchange determines the dielectric constant and the ac conductivity of compensated $Cd_{1-x}Mn_xTe$ semiconductors. The properties of the defects are determined, first of all, by their microscopic structure, i.e., in our case by the number of Mn atoms appearing in them, which can take discrete values from 0 to 4, depending on the value of x. Therefore, it can be assumed that one Mn atom appears in the composition of a defect with an activation energy $\Delta E_1=0.12$ eV when $x=0.15$. When $x=0.3$ or 0.5, two Mn atoms can appear in a defect with

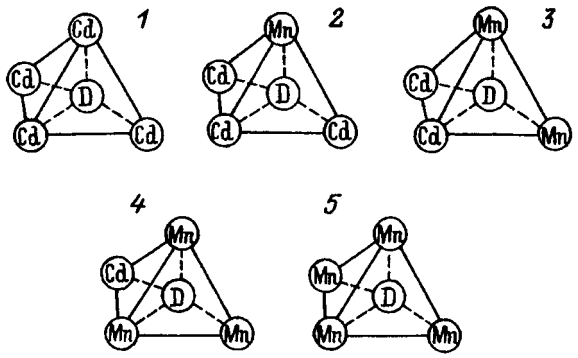

FIG. 6. Model of the structure of defects. *D* — a vacancy or impurity atom in a site in the Te sublattice.

$\Delta E_1 \simeq 0.27$ eV, and when $x=0.7$, three Mn atoms can appear in a defect with $\Delta E_1 \simeq 0.60$ eV. Defects of a second type, which appear in the first stage of the increase in the dielectric constant, can be impurity atoms or vacancies in the Te sublattice.

Figure 6 presents the model of the structure of the defects which can be responsible for the hopping charge-transport processes in the materials $Cd_{1-x}Mn_xTe$ ($0 \leqslant x \leqslant 0.7$). The proposed model of the structure of defects that differ with respect to the number of Mn atoms appearing in them can be used to account for the observed differences in the variations of the band-gap width E_g and the activation energy for hopping charge exchange ΔE_1^C with the Mn concentration (Fig. 5). The value of E_g is determined for the whole crystal and is a continuous function of the Mn concentration. At the same time, the properties of the defects are local and are determined by the small group of atoms appearing in their composition. Therefore, the properties of the defects should vary discretely together with the number of Mn atoms appearing in them. Consequently, the dependence of ΔE_1 on x should be a nonmonotonic function. At values of x close to 0 each defect is an impurity atom or a Te vacancy at a site in the Te sublattice, which is denoted by *D* in Fig. 6, and the activation energy for it $\Delta E_1 < 0.12$ eV. When $x \simeq 0.25$, a Mn atom appears in the defect, and $\Delta E_1 \simeq 0.12$ eV. At values of x in the vicinity of 0.5 the defect contains two Mn atoms. In this case $\Delta E_1=0.25$. At values of x in the vicinity of 0.75 the defect includes three Mn atoms, and its activation energy is 0.60 eV.

This model accounts for the nonlinear variation of the linewidth of the ESR signal and the g factor (Table 2) with the concentration of Mn. Each of the types of defects just described should be characterized by its own parameters for the ESR signal. The signal from $Cd_{1-x}Mn_xTe$ with different Mn concentrations is caused by a combination of defects of several types. This leads to nonlinear dependences of the g factor and the linewidth of the ESR signal on the concentration of Mn atoms.

CONCLUSIONS

Investigations of the dielectric properties of the ternary superconductor compounds $Cd_{1-x}Mn_xTe$ ($0 \leqslant x \leqslant 0.7$) have revealed a thermally activated increase in the dielectric con-

stant, which has a clearly expressed frequency dependence. A definite correlation has been established between the basic characteristics of this phenomenon and the Mn content in these materials. We have proposed some models of the structure of the defects, whose hopping charge exchange leads, in our opinion, to the increase in the dielectric constant of the semi-insulating compounds investigated.

[1] P. W. Zukowski, S. B. Kantorow, D. Maczka, and V. F. Stelmakh, Phys. Status Solidi A **112**, 695 (1989).
[2] P. W. Zukowski, S. B. Kantorow, K. Kiszczak, D. Maczka, A. Rodzik, V. F. Stelmakh, and E. Czarnecka-Such, Phys. Status Solidi A **128**, 117 (1991).
[3] P. V. Zhukovskiĭ, S. B. Kantorov, D. Monchka, A. Rodzik. K. Kishchak, and V. F. Stel'makh, Dokl. Akad. Nauk Beloruss. **37**, 41 (1993).
[4] S. A. Medvedev, S. N. Maksimovskiĭ, Yu. V. Klevkov, and P. V. Shapkin, *Cadmium Telluride* [in Russian], Nauka, Moscow (1968).
[5] *The Physics of $A^{II}B^{VI}$ Compounds* [in Russian], A. N. Georgobiani and M. K. Sheĭnkman (eds.), Nauka, Moscow (1986).
[6] N. F. Mott and E. A. Davis, *Electronic Processes in Non-Crystalline Materials*, 2nd ed., Clarendon Press, Oxford (1979) [Russ. transl., Mir, Moscow (1982)].
[7] S. S. Kirkpatrick, in *Proceedings of the 5th International Conference on Amorphous and Liquid Semiconductors*, Garmisch-Partenkirchen, 1973, p. 183.
[8] S. M. Ryvkin, *Photoelectric Effects in Semiconductors*, Consultants Bureau, New York (1964).
[9] C. Kittel, *Elementary Solid State Physics*, Wiley, New York (1962) [Russ. transl., Mir, Moscow (1965)].
[10] V. I. Gavrilenko, A. M. Grekhov, D. V. Korbutyak, and V. G. Litovchenko, *Optical Properties of Semiconductors. A Handbook* [in Russian], Naukova Dumka, Kiev (1987).

Translated by P. Shelnitz

Anomalous distribution of iron atoms following the simultaneous implantation of Co^+ and Fe^+ ions in silicon

G. G. Gumarov, V. Yu. Petukhov, V. A. Zhikharev, V. A. Shustov, and I. B. Khaĭbullin

E. K. Zavoiskiĭ Kazan' Physicotechnical Institute, Russian Academy of Sciences, 420029 Kazan', Russia
(Submitted March 13, 1996; accepted for publication October 25, 1996)
Fiz. Tekh. Poluprovodn. **31**, 719–721 (June 1997)

An anomalous two-peaked depth profile of Fe atoms has been observed following the simultaneous implantation of Fe^+ and Co^+ ions in Si at low ion current densities ($j \leqslant 10$ μA/cm^2) and a 1:3 ratio between iron and cobalt ions in the beam. Such a profile is formed on condition that the time of diffusion of the iron atoms to the sinks (the surfaces and the regions of linear defects in the bulk of the sample) is shorter than the effective time for silicide formation.
 [S1063-7826(97)01806-1]

The interest in compound silicides in microelectronics processing is attributable to their wide variety of physical properties, which expand the areas for their utilization. In particular, the double orthorhombic silicide β-$(Fe_{1-x}Co_x)Si_2$ is interesting as a semiconductor with a variable (as a function of x) band gap. The possibility of forming such a compound by the successive implantation of Fe^+ and Co^+ ions in Si with two-step thermal annealing after each implantation step was demonstrated in Ref. 1. We demonstrated elsewhere[2,3] the possibility of synthesizing a double silicide by simultaneously implanting ions of different $3d$ metals in silicon without any high-temperature treatment.

In the present work we studied the phase composition of ion-implanted films and the depth profiles of the implanted atoms that appear during the simultaneous implantation of Co^+ and Fe^+ ions in silicon (when the cobalt ions dominate in the beam, $x=0.75$) before and after heat treatment.

Plates of type ÉKDB-10 single-crystal (111) silicon served as the starting material. The implantation of $^{56}Fe^+$ and $^{59}Co^+$ was carried out simultaneously from a single source in an ILU-3 system at an energy of 40 keV and an integral dose of 2.5×10^{17} cm^{-2}. The ion current density was 10 μA/cm^2, and the ratio of the number of Fe^+ ions to the number of Co^+ ions in the beam was 1:3. The samples were securely held in a water-cooled duralumin holder. The sample temperature measured by a thermocouple did not exceed 100 °C.

The thermal annealing was carried out at $T=750$ °C for 32 h in a stream of dry nitrogen.

The phase composition of the films obtained was determined from reflection electron diffraction patterns recorded on an ÉMR-100 instrument at electron energies equal to 50 and 75 keV. Deeper layers were investigated by x-ray diffraction analysis in parallel glancing beams (the angle between them was $\alpha=2°$) using a DRON-3M diffractometer. Auger electron spectroscopy was employed to determine the elemental composition of the films synthesized and the depth profiles of the atoms.

Depth profiles of the elements in samples immediately after implantation (before the ensuing treatments), which were obtained by Auger electron spectroscopy, are shown in Fig. 1a. It is seen that the distribution profiles of the Co and Fe atoms differ strongly, which is surprising, since their atomic weights are close. Calculations of the distributions, according to a modified TRIM program for Fe^+ and Co^+ implanted in silicon with an energy of 40 keV, give nearly coinciding profiles with the following parameters: a mean

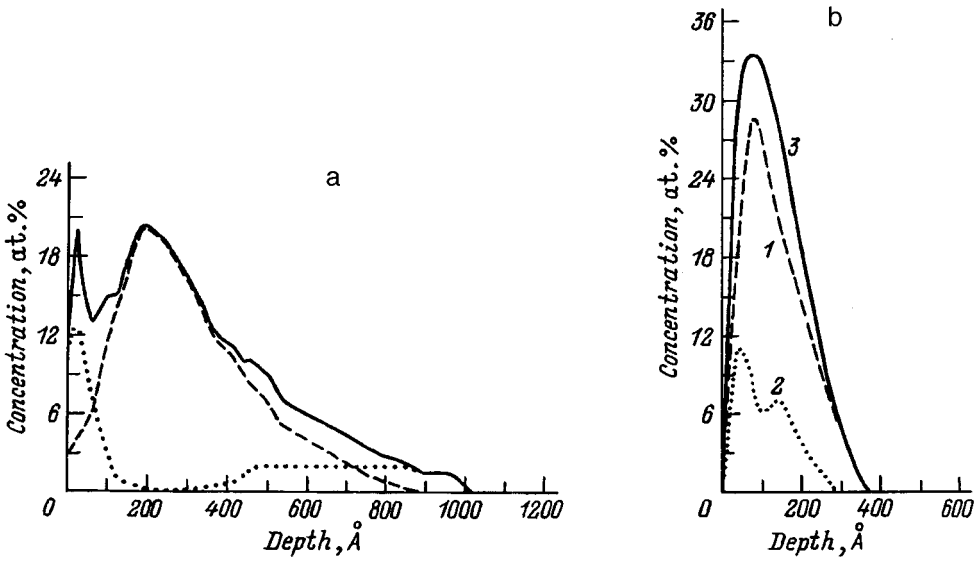

FIG. 1. Depth profiles of cobalt (*1*) and iron (*2*) atoms and their total content (*3*) obtained by Auger spectroscopy: a — immediately after implantation; b — after implantation and thermal annealing at 750 °C for 32 h.

 1063-7826/97/060615-03$10.00

projected range $\overline{R_p} \simeq 350$ Å and a mean projected deflection $\Delta\overline{R_p} \simeq 150$ Å. While the distribution of the cobalt atoms is close to the theoretically expected profile, the distribution of the iron atoms is anomalous and has two clearly expressed maxima of different intensity; the first peak is located in direct proximity to the surface and the second peak is located at the boundary of the cobalt distribution in the bulk of the sample. An analysis of the Auger spectra also demonstrates the presence of a thin carbon-containing film of thickness $10-20$ Å and a silicon oxide film with a thickness of several tens of Å in the near-surface region. Reflection electron diffraction analysis of a sample after implantation gives only reflections from polycrystalline cubic cobalt disilicide. The remaining phases, including the iron-containing phase, are amorphous according to the electron diffraction data. The x-ray diffraction patterns of a sample after implantation also demonstrated the formation of only a cubic phase of $CoSi_2$.

In contrast to the experiments with the simultaneous implantation of ions of two types, in the case of the bombardment of silicon in the same regimes by only Fe^+ (or Co^+) ions, no anomalous distribution or diffusion from the implantation region was observed.[4,5] This fact points to the decisive influence of the cobalt ions located in the implantation region on the anomalous distribution of the iron atoms (under the present implantation regimes).

Thermal annealing of the samples obtained at 750 °C for 32 h led to significant alteration of the distribution profiles of the implanted elements (Fig. 1b). Specifically, the profiles of the Fe and Co atoms contract and move toward the surface. At the same time, there are no appreciable changes in the thickness of the carbon-containing and oxide films. The electron diffraction patterns of the annealed sample contained lines corresponding to $CoSi_2$ and Fe_3O_4 phases. At the same time, an analysis of the x-ray diffraction spectra shows that the principal phases in the ion-implanted film after thermal annealing are $CoSi_2$ and β-$FeSi_2$.

A nonclassical implantation profile similar to the one in Fig. 1a for the iron atoms was also obtained in Ref. 6 following the implantation of only Ni^+ ions in Si. Wu *et al.*, attributed this effect exclusively to diffusion to sinks, which can be the substrate surface and the region of linear defects located beyond the normal distribution profile of the implanted atoms. In the case of the simultaneous implantation of ions of two types in silicon that we considered, we also took into account the phase formation processes. According to Ref. 7, the diffusion of Fe atoms to a surface (or to sinks of another kind) is possible, if the following condition holds for them during implantation:

$$\tau_d < \tau_c,$$

where $\tau_d \simeq a^2/D$ is the diffusion time from the implantation region to the sinks, a is the distance from the maximum on the distribution of the primary implanted atoms to the sinks, D is the diffusivity of the implanted atoms, and τ_c is the characteristic time for complexation, i.e., the formation of the Fe–Si complex in our case. As a result of the low solubility of $3d$ metals in silicon,[8] the formation of secondary phases (silicides) begins already after small implantation doses. Since the flux density of the Co^+ ions in beam is three times greater than the flux density of the Fe^+ ions, the cobalt-containing particles ($CoSi_2$) are dominant in the implantation region during implantation. During this process they probably prevent the formation of stable nuclei of iron silicides, i.e., they increase the effective time for silicide formation with the iron atoms. Because of their high diffusion rate in silicon,[8] the bulk of the iron atoms go into the sinks, i.e., the surface and the near-surface layer, as well as the region of linear defects in the bulk of the sample.[9]

When only iron ions are implanted in silicon or the implantation is carried out in a regime in which iron ions are dominant in the beam, the effective silicide formation time for the iron atoms is significantly smaller, and the two-peaked distribution does not form.

As has been reported,[10] the linear defects anneal out after thermal annealing at $T > 700$ °C. Therefore, during prolonged thermal annealing (750 °C) the Fe and Co atoms migrate to the region of the granular $CoSi_2$ film, which now serves as a sink, producing additional cobalt disilicide and forming iron silicide with the remaining silicon. Contraction of the profile of the implanted atoms upon the formation of silicides after thermal annealing has also been observed by some other researchers.[11,12] Judging from the total concentration of the metal, we can state that a continuous disilicide film consisting of $CoSi_2$ and β-$FeSi_2$ formed during such an anneal.

We have observed an anomalous, two-peaked depth profile of Fe atoms following the simultaneous implantation of Fe^+ and Co^+ ions in Si at low ion current densities ($j \leqslant 10$ $\mu A/cm^2$) and a 1:3 ratio between the numbers of iron and cobalt ions in the beam. Such a profile is formed on conditions that the diffusion time of the iron atoms to the sinks (the surfaces and regions of linear defects in the interior of the sample) is shorter than the effective time for silicide formation.

We wish to thank V. F. Makovskiĭ for obtaining the Auger electron spectra.

This work was carried out as part of the State Scientific-Technical Program ''Prospective Micro- and Nanoelectronics Technologies and Devices'' (Project No. 142/57/2).

[1] E. Wieser, D. Panknin, W. Skorupa, G. Querner, W. Henrion, and J. Albrecht, Nucl. Instrum. Methods Phys. Res., Sect. B **80/81**, 867 (1993).
[2] V. Yu. Petukhov, I. B. Khaıbullin, and G. G. Gumarov, in *Abstracts of Reports to the 1st Russian Conference on the Physics of Semiconductors, Nizhnıı Novgorod, 1993* [in Russian], Vol. 2, p. 353.
[3] G. G. Gumarov, V. Yu. Petukhov, V. A. Shustov, and I. B. Khaĭbullin, Vysokochist. Veshchestva (2), 95 (1995).
[4] V. Yu. Petukhov, I. B. Khaibullin, M. M. Zaripov, R. Groetzschel, H. Voelskow, and R. Klabes, Phys. Status Solidi A **96**, 463 (1986).
[5] K. Radermacher, S. Mantl, C. Dieker, H. Holzbrecher, W. Speier, and H. Luth, Proc. MRS **235**, 273 (1992).
[6] M. F. Wu, J. De Wachter, P. Hendrickx, A.-M. Van Bavel, H. Pattyn, G. Langouche, J. Vanhellemont, H. Bender, M. Maenhoudt, and Y. Bruyseraede, Appl. Phys. Lett. **63**, 542 (1993).
[7] V. L. Vinetskiĭ and G. A. Kholodar', *Radiation Physics of Semiconductors* [in Russian], Naukova Dumka, Kiev (1979).
[8] V. M. Glazov and V. S. Zemskov, *Physicochemical Principles of Semiconductor Doping*, Israel Program for Scientific Translations, Jerusalem (1968).
[9] V. Yu. Petukhov, I. B. Khaibullin, M. M. Zaripov, E. Wieser, R. Groet-

zschel, and H. Bartsch, Phys. Status Solidi A **117**, 477 (1990).
[10] K. Seshan and J. Washburn, Radiat. Eff. **37**, 147 (1978).
[11] C. W. T. Bulle-Lieuwma, A. H. van Ommen, and L. J. van IJzendoorn, Appl. Phys. Lett. **54**, 244 (1989).
[12] F. Namavar, N. M. Kalkhoran, J. M. Manke, L. Luo, and J. T. McGinn, Proc. MRS **235**, 285 (1992).

Translated by P. Shelnitz

Features of radiation-induced defect formation in *p*-type Si⟨B,Pt⟩

M. S. Yunusov, M. Karimov, M. Alikulov, A. Akhmadaliev, B. L. Oksengendler, and S. S. Sabirov

Institute of Nuclear Physics, Academy of Sciences of Uzbekistan, 702132 Ulugbek, Uzbekistan
(Submitted January 31, 1996; accepted October 25, 1996)
Fiz. Tekh. Poluprovodn. **31**, 722–723 (June 1997)

The results of an experimental study of radiation-induced defect formation in *p*-Si⟨B, Pt⟩ using deep-level transient spectroscopy (DLTS) are discussed. The significant influence of the initial presence of B and Pt impurities on the efficiency of the formation of radiation centers (especially with an energy $E_v+0.36$ eV) is demonstrated. This phenomenon is attributed to the presence of electrically neutral complexes consisting of an intrinsic interstitial atom and an impurity atom in *p*-type Si⟨B, Pt⟩, which effectively dissociate during γ irradiation and thereby influence the quasichemical radiation-induced defect formation reactions. © *1997 American Institute of Physics.* [S1063-7826(97)01906-6]

Several studies have focused on the electric and photoelectric properties of Si⟨Pt⟩.[1–3] Those studies have shown that platinum creates energy levels in the band gap at $E_c-0.26$ eV, $E_c-0.53$ eV, and $E_v+0.34$ eV. The effect of platinum on the radiation-induced defect-formation processes was found to be significant.[1,3] However, the mechanism of the radiation-induced processes in Si⟨Pt⟩ has not yet been thoroughly elucidated.

The present research was performed on *p*-type silicon grown by the Czochralski method with various concentrations of B ($N_B=10^{15}-10^{16}\text{cm}^{-3}$) and Pt ($N_{Pt}=6\times10^{13}-6\times10^{14}\text{cm}^{-3}$) impurity atoms. Platinum was introduced into *p*-type Si⟨B⟩ by thermal diffusion over the course of about 10 h. To take into account the influence of the heat treatment on the material, control samples of *p*-Si⟨B⟩ were annealed in parallel at the diffusion temperature. Schottky diodes were fabricated by sputtering Au and Sb onto the samples to perform the DLTS measurements.

Doped (*p*-Si⟨B,Pt⟩) and control (*p*-Si⟨B⟩) samples were irradiated by ^{60}Co γ rays with an intensity of 2500 R/s to integral doses of the order of 10^9 rad. Comparing the DLTS spectra of the irradiated samples with the literature data,[4,5] we concluded that the observed local energy level at $E_v+0.25$ eV should be assigned to a divacancy (V_2), the level at $E_v+0.36$ eV should be assigned to the complex $V_2+O_i+C_i$, where O_i and C_i are interstitial oxygen and carbon atoms, and the level at $E_v+0.44$ eV should be assigned to the familiar complex consisting of a vacancy and a boron atom, $V+B$. In addition, the efficiency of the introduction of these radiation centers is much higher in the Pt-doped samples than in the control samples.

Figure 1 presents plots of the dependence of the concentration of the radiation centers with an energy $E_v+0.36$ eV on the concentration of B (a) and on the concentration of Pt (b). An analysis of the results presented in the figure reveals that the concentration of radiation centers with an energy $E_v+0.36$ eV decreases as the concentration of platinum atoms N_{Pt} increases at a constant concentration of B atoms ($N_B=\text{const}$) (Fig. 1b). Nearly the same dependence of the concentration of these centers on the boron concentration N_B is observed in the case of a constant concentration of the dopant Pt in the sample ($N_{Pt}=\text{const}$) (Fig. 1a, curve *1*). However, the concentration of these centers is higher in the samples of *p*-Si⟨B,Pt⟩ than in a control sample of *p*-Si⟨B⟩ containing a similar concentration of B (Fig. 1a, curve *2*). In the latter case the dependence of N on N_B is significantly weaker. It follows from an analysis of these results that the efficiency of the introduction of radiation defects with an energy $E_v+0.36$ eV is influenced mainly by the presence of the dopant Pt.

Thus, the following experimental results have been obtained from investigating the effect of γ radiation on *p*-Si⟨B⟩ and *p*-Si⟨B,Pt⟩:

— the efficiency of the introduction of the observed radiation centers (especially with an energy $E_v+0.36$ eV) is higher in *p*-Si⟨B,Pt⟩ than in a sample of *p*-Si⟨B⟩ that does not contain platinum;

— the dependences of the efficiency of defect formation (especially for the defects with an energy $E_v+0.36$ eV) on the concentrations of B and Pt are similar; i.e., the efficiency decreases with increasing concentrations of B and Pt, but it is always higher in Si that contains platinum.

These nontrivial results could be explained by taking into account the amphoteric nature of the Pt impurity atoms in silicon and the participation of the intrinsic interstitials (I) and the decomposition product of $Pt+I$, along with the primarily generated vacancies (V) in quasichemical reactions. Let us examine the quasichemical radiation-induced defect-formation reactions in Si on the basis of these ideas.

The system of kinetic equations for such a process will have the form

$$d[V]/dt=\lambda-k_1[I][V]-k_2[V][B_i]-k_3[V][Pt]-[V]/\tau_V,$$

$$d[I]/dt=\lambda-k_1[I][V]-k_4[I][Pt]-[I]/\tau_I,$$

$$d[V_2+C_i+O_i]/dt=\lambda-k_2[V_2+C_i+O_i]-[V_2+C_i+O_i]/\tau_{VCO},$$

where k_j denotes the constants of the corresponding reactions, and the last terms in the equations of the form

 1063-7826/97/060618-02$10.00

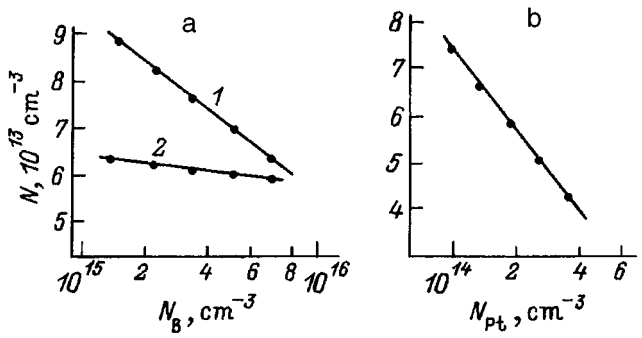

FIG. 1. Dependence of the concentration of radiation centers N with an energy $E_v+0.36$ eV: a — on the boron concentration N_B for p-Si⟨B,Pt⟩ (*1*) and p-Si⟨B⟩ (*2*), b — on the platinum concentration N_{Pt}.

$[A]/\tau_A$ specify the probability of the loss of defects of type A in sinks. The interaction of vacancies with interstitial boron B_i is taken into account here. For the case of silicon not doped by platinum ($[Pt]=0$), i.e., for p-Si⟨B⟩ and the steady-state condition with respect to I ($d[I]/dt=0$), we obtain

$$[I]=\lambda\tau_I, \quad [V](t)=\lambda T_V(1-e^{-t/T_V}),$$

where $1/T_V=k_1\lambda\tau_I+k_2[B_i]+1/\tau_V$. If it is assumed that the radiation-induced $V_2+C_i+O_i$ formed accumulates while undergoing virtually no dissociation (i.e., $\tau_{VCO}\to\infty$), we obtain

$$[V_2+C_i+O_i]=k_2[CO]\lambda T_V\{t+T_V(e^{-\tau/T_V}-1)\}.$$

We see, therefore, that the rate of accumulation of and the stationary value (as $t\to\infty$) of the concentration of $V_2+C_i+O_i$ decreases as the concentration of B_i increases. This finding corresponds to experiment. The explanation is that site boron (B_s) serves as a sink for the intrinsic interstitials I that displace B_s atoms from their sites in the crystal lattice,[6] which participate in the formation of $V+B_i$ radiation centers. The remaining interstitials I displace site oxygen (O_s) and carbon (C_s) atoms, which participate in the formation of $V_2+C_i+O_i$. The other component of the Frenkel pair, i.e., the vacancy, takes part mainly in the capture of interstitial boron to form $V+B_i$ and in the formation of $V_2+C_i+O_i$. These processes compete with one another, i.e., as the concentration of the originally present B decreases, the efficiency of the capture of B_i by a vacancy decreases, while the efficiency of the formation of $V_2+C_i+O_i$ increases.

Let us now examine the case of $[Pt]\neq 0$, i.e., the samples doped with platinum.

a. Let us assume that during the doping of silicon by Pt, its atoms interact predominantly with vacancies and form complexes with them (i.e., $k_3\gg k_4$). Upon irradiation, such complexes dissociate and thereby release additional vacancies, which participate in quasichemical defect-formation reactions. We can then show that

$$[V_2+C_i+O_i]=k_2[CO]\lambda\tilde{T}_V\{t+\tilde{T}_V(e^{-t/\tilde{T}_V}-1)\},$$

where $1/\tilde{T}_V=1/T_V+k_3[Pt]$. It is clear that

$$\frac{[V_2+C_i+O_i]_{[Pt]\neq 0}}{[V_2+C_i+O_i]_{[Pt]=0}}=\frac{k_1\lambda\tau_I+k_2[B_i]+1/\tau_V}{k_1\lambda\tau_I+k_2[B_i]+1/\tau_V+k_3[Pt]}<1.$$

In other words, regardless of the concentration of B, the formation of $V_2+C_i+O_i$ is always suppressed.

b. Similarly, it can be postulated that during the doping of p-type Si by Pt, its atoms predominantly form complexes with interstitials, and that these complexes dissociate upon irradiation, providing additional interstitial atomic states. The latter participate in the quasichemical radiation-induced defect-formation reactions and cause an increase in the efficiency of the formation of $V_2+C_i+O_i$, regardless of the concentration of B. For this case we have

$$\frac{[V_2+C_i+O_i]_{[Pt]\neq 0}}{[V_2+C_i+O_i]_{[Pt]=0}}=\frac{1+\tau_V(k_2[B_i]+k_1\lambda\tau_I)}{1+\tau_V\{k_2[B_i]+k_1\lambda\tau_I/(1+k_3[Pt]\tau_3)\}}>1.$$

We note that the results obtained can naturally be explained only when this fact is taken into account.

Thus, in analyzing the radiation-induced, defect-formation processes in silicon containing transition elements, particularly Pt, such important factors as the dominant formation of $Pt+I$ during the doping and the active role of the dissociation product of these complexes (I) in the quasichemical radiation-induced defect-formation reactions should be taken into account.

[1] A. A. Lebedev and N. A. Sultanov, Fiz. Tekh. Poluprovodn. **22**, 16 (1988) [Sov. Phys. Semicond. **22**, 9 (1988)].
[2] Y. K. Kwon, T. Ishikawa, and H. Kuwano, J. Appl. Phys. **61**, 1055 (1987).
[3] M.Yu. Yunusov, A. Akhmadaliev, and S. S. Sabirov, Fiz. Tekh. Poluprovodn. **29**, 665 (1995) [Semiconductors **29**, 346 (1995)].
[4] V. V. Emtsev and T. V. Mashovets, *Native Defects and Impurities in Semiconductors*, The Institute of Physics, Bristol (1993).
[5] in *Topics in the Radiation Semiconductor Technology* [in Russian], Nauka, Novosibirsk (1980).
[6] G. D. Watkins, *The Lattice Vacancy in Silicon: Deep Centers in Semiconductors*, Academic Press, New York (1986), Ch. 3, p. 147.

Translated by P. Shelnitz

Schottky barrier breakdown in Si stimulated by exciton drift in a nonuniform electric field at 4.2 K

A. M. Musaev

Kh. I. Amirkhanov Institute of Physics, Dagestan Scientific Center, Russian Academy of Sciences, 367003 Makhachkala, Russia

(Submitted February 6, 1996; accepted October 25, 1996)
Fiz. Tekh. Poluprovodn. **31**, 724–727 (June 1997)

The results of the experimental discovery and investigation of the mechanism for stimulating the breakdown of a Schottky barrier in silicon by photoexcitation in a strong electric field at $T=4.2$ K are presented. The influence of the photoexcitation intensity and the electric field strength, as well as the relative time delay between them, on the barrier breakdown mechanism is investigated. It is shown on the basis of an analysis of the results that Schottky barrier breakdown is associated with narrowing of the width of the space-charge region as a result of exciton drift in the nonuniform electric field and the recombination of electrons in ionized impurity levels of the barrier. © *1997 American Institute of Physics.* [S1063-7826(97)02006-1]

A reverse-biased Schottky barrier can lose its dielectric strength as a result of avalanche breakdown upon impact ionization of the semiconductor or as a result of the tunneling of electrons from the metal in a strong electric field.[1] The mechanisms and conditions for Schottky barrier breakdown depend not only on the composition of the semiconductor, its doping, and the methods used to fabricate the barrier, but also on external factors (temperature, pressure, magnetic fields, etc.). In a reverse-biased semiconductor with a low impurity concentration the charge carriers are created mainly by the generation of electron-hole pairs in the space-charge region. In this case the fraction of the generation current becomes decisive at low temperatures, since the thermionic component of the tunneling current decreases.[1]

In this paper we present the results of an experimental study of the mechanism for stimulating Schottky barrier breakdown and the appearance of a nonuniform distribution of the current in the electron-hole-plasma (EHP)/exciton system in silicon in strong electric fields at $T=4.2$ K. The investigations were performed on samples of n-Si⟨P⟩ with an impurity concentration $N_D-N_A\simeq 8\times 10^{12}$ cm^{-3}, which were prepared in the form of rectangular parallelepipeds measuring $4.6\times 1.1\times 0.8$ mm with the [111] crystallographic direction parallel to the long edge of the sample. The experimental setup and the configuration of the electric field and the photoexcitation source relative to the crystallographic axes of the sample are shown in Fig. 1. The sample and the photoexcitation source were placed directly in liquid helium to eliminate the incidence of phonon radiation from without.

To create contacts with the Schottky barriers, Au or Sn was deposited on opposite faces measuring 1.1×0.8 mm by vacuum sputtering. After the sputtering step, the contacts were subjected to high-temperature treatment in a vacuum for the purpose of improving their electrical properties and increasing their stability. The technological recommendations presented in Refs. 1 and 2 were observed in fabricating the contacts. Uniform photoexcitation of the carriers was performed on a 4.6×1.1 face using pulses from a source of monochromatic radiation based on GaAs infrared light-emitting diodes with a quantum energy $\hbar\omega\simeq 1.5\text{eV}>\varepsilon_G^{\text{Si}}$. The duration of the photoexcitation pulses, which was equal to 40 μs, ensured the establishment of a stationary state with respect to the concentrations of carriers and excitons. Since the cross section for the formation of excitons is very large, the bulk of the nonequilibrium electron-hole pairs are bound in excitons at $T=4.2$ K. The maximum photoexcitation intensity corresponded to the generation of electron-hole pairs in a concentration equal to $\sim 5\times 10^{14}$ cm^3. The distribution of the excitons in the sample was assumed to be uniform, since, because of the large diffusion coefficient, the electron-hole pairs generated in the thin near-surface layer filled the sample after a time $\sim 10^{-6}$ s. The photoexcitation pulses were accompanied by pulses of a constant electric field with a duration up to 150 μs, which were supplied to the sample with a delay of $0-1.0$ ms relative to the photoexcitation pulses. The pulse repetition rate was 3 Hz, which ensured the establishment of a temperature of 4.2 K in the sample before the beginning of each pulse.

Figure 2 presents oscillograms of the current through the sample for various delay times between the electric field pulse and the photoexcitation pulse for $E=\text{const}$ and $I_p=\text{const}$.

As can be seen from the oscillograms, a conduction current pulse appears with a certain delay after each electric field pulse is supplied. The delay time τ_B of the pulse decreases as the electric field strength is increased. When $\tau_E\neq 0$, a characteristic feature of the time dependence of the conductivity is the appearance of a single primary current peak followed by the appearance of one of the following types of fluctuations: single pulses, relaxational fluctuations, or random fluctuations. When the photoexcitation and electric field pulses are supplied simultaneously, there is no delay between the peak and the ensuing fluctuations.

Figure 3 shows the dependence of the breakdown delay time τ_B on the delay time before the supply of the electric field pulses τ_E relative to the photoexcitation pulses for $E=\text{const}$ and $I_p=\text{const}$.

Figure 4 shows a typical current-voltage characteristic

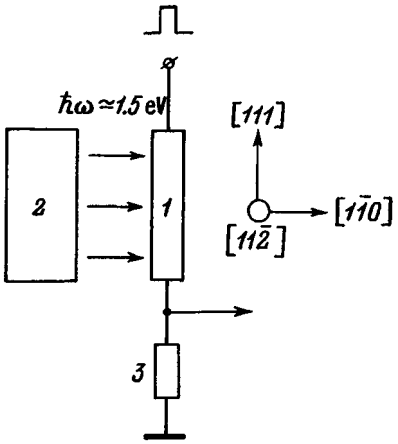

FIG. 1. Experimental setup and crystallographic orientation of the sample: *1* — sample; *2* — photoexcitation source (a GaAs light-emitting diode); *3* — load resistance.

(the current was averaged over the duration of the pulse), which was obtained for rectangular pulses with a duration equal to 10 μs and a delay time before the supply of the electric field pulse $\tau_E=10$ μs. The threshold breakdown field E_B depends on the photoexcitation intensity I_p and on the delay time τ_E of the electric field pulse relative to the photoexcitation pulse. The threshold breakdown field increases as the photoexcitation intensity is lowered and as the delay time τ_E is increased. Both *S*-shaped and *N*-shaped segments of negative differential resistance are observed on the dynamic current-voltage characteristic.

To account for the experimental results, the physical processes taking place in reverse-biased and forward-biased Schottky barriers must be considered. Figure 5 shows a schematic representation of the band diagram of a sample with Schottky barriers when an external electric field is applied (a), as well as the distribution of the electric field in a reverse-biased barrier at different times during the application of a field (b).

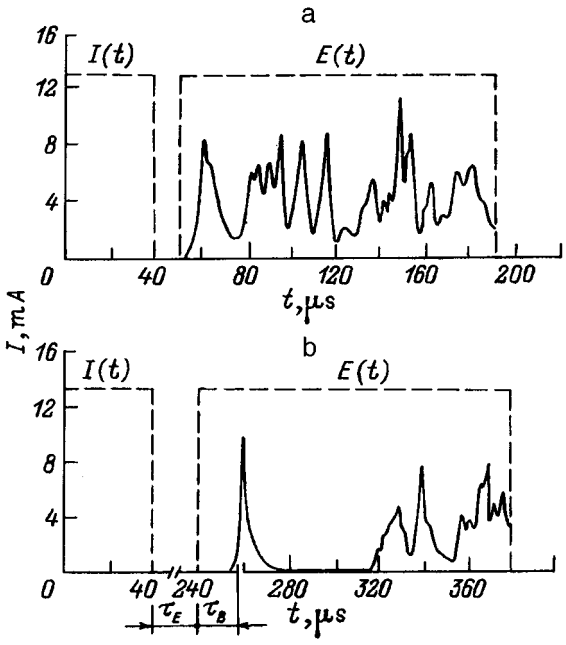

FIG. 2. Oscillograms of the current through the sample for $E=800$ V/cm, a photoexcitation intensity $I_p=0.8$ rel. units, delays of the electric field pulse relative to the photoexcitation pulse $\tau_E=10$ μs (a) and $\tau_E=200$ μs (b).

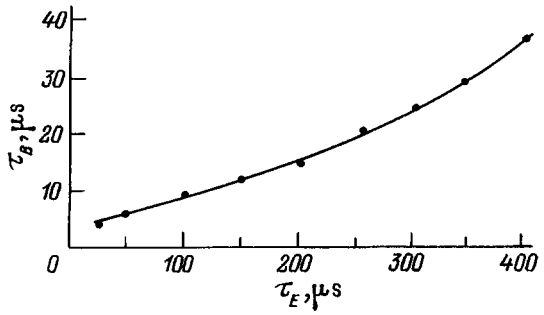

FIG. 3. Dependence of the breakdown delay time τ_B on the delay time τ_E before supply of the electric field pulse for a photoexcitation intensity $I_p=0.8$ arb. units and an electric field $E=800$ V/cm.

Pairs of carriers generated in the space-charge region separate under the action of the field formed in the barrier by the bending of the bands in the semiconductor. During this process, most of the electrons pass into the bulk of the semiconductor as a result of drift and diffusion, and the holes pass into the metal. In addition, some of the photoexcited electrons recombine in ionized impurities in the space-charge region.

In the bulk of the semiconductor, which is doped by shallow impurities in the concentration range $10^{12}-10^{16}$ cm^{-3}, most of the excitons are bound in isolated impurity atoms at low temperatures and low photoexcitation levels. A dynamic equilibrium is established between the excitons and free carriers in the first few microseconds after the exciting pulse: free carriers bind to form excitons, and excitons dissociate into free carriers. The formation of free carriers is governed not only by the dissociation of excitons, but also by their Auger recombination.[3] This equilibrium determines the standard concentrations of excitons (N_{ex}) and free carriers (n_e) at an assigned temperature. The values of N_{ex} and n_e decrease with time as a result of recombination, but the equilibrium between them is maintained for a long time. Accord-

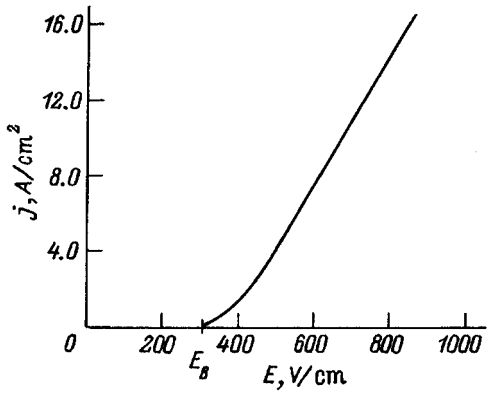

FIG. 4. Current-voltage characteristic of a sample at $T=4.2$ K. Here E_B is the threshold breakdown electric field.

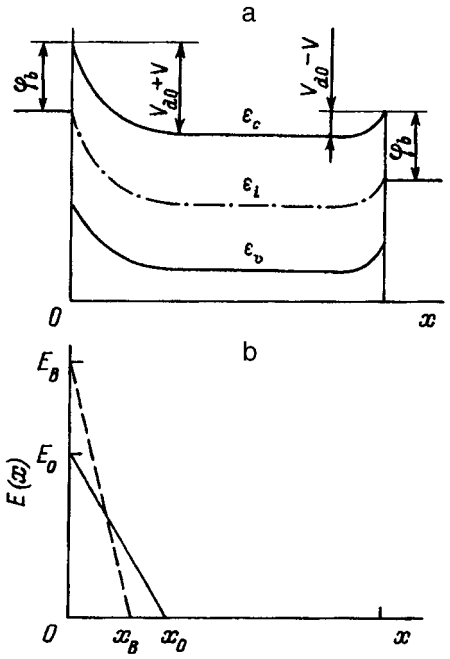

FIG. 5. Band diagram of a sample with Schottky barriers in an external electric field (a) and distribution of the electric field in a reverse-biased barrier (b): initial moment of application of the field (solid line), time when the space-charge region narrows to the critical value (dashed line).

ing to experimental data, the lifetime of free excitons in Si is $\sim 0.2-60$, and that of bound excitons is ~ 300 μs.[4,5]

At temperatures sufficient for the thermal generation of carriers with impurity levels, application of a reverse bias leads to changes in the width of the depleted region in the barrier, the charge within the space-charge region, and the charge outside that region due to displacement of the free electrons. At low temperatures an applied reverse bias does not expand the space-charge region and only alters the charge state of the barrier. Under the conditions of the photoexcitation of electron-hole pairs and the establishment of dynamic equilibrium between the excitons and free carriers in the base region of the sample, the applied electric field is located in the reverse-biased barrier. The distribution of the field appearing initially when the electric field E_0 is applied is shown schematically in Fig. 5b (solid line).

The most probable mechanism that accounts for the experimental results is based on narrowing of the width of the reverse-biased space-charge region to a value at which the electric field is critical for the appearance of interband impact ionization. Figure 5b shows the distribution of the electric field when its critical value E_B is achieved due to narrowing of the space-charge region (dashed line). The narrowing of the space-charge region is caused by the drift of free excitons in the nonuniform field of the barrier followed by recombination of the electrons in impurity centers in the space-charge region and transport of the free holes to the metal.

In a homogeneous semiconductor not subjected to external forces the spatial distribution of the excitons is determined directly by the excitation conditions, diffusion, and their recombination times. The effects of the external forces appearing, for example, as a result of pressure, magnetic fields, and exciton concentration gradients, as well as light pressure and phonon drag, lead to exciton drift. Being electrically neutral, excitons cannot drift in a uniform electric field; however, in a nonuniform electric field unequal forces act on the weakly bound electron and hole, and their resultant force is, therefore, not equal to zero. Excitons are then subjected to the following force, which tends to move them into a region with a higher field strength:

$$F = e \cdot l \cdot dE/dx,$$

where l is the Bohr radius of the exciton, and dE/dx is the electric field gradient.

In silicon excitons are weakly bound and have a large spatial expanse. The Bohr radius of an exciton is much greater than the interatomic distances and amounts to 49 Å.

Exciton drift in the space-charge region followed by recombination of the electrons in ionized donor impurities is also supported by the following experimental evidence:

– an increase in the exciton concentration in the base region of the sample leads to a decrease in the breakdown voltage and the breakdown delay time;

– probe measurements performed with weak photoexcitation of the carriers demonstrate the presence of a high-field domain on the cathode of the sample;

– measurements of the current with a separated cathode contact (in samples with a barrier of large area) demonstrate the nonuniformity of breakdown over the area of the barrier, which is characteristic of microplasma breakdown with localization of the current at isolated sites of small cross section;[6]

– an experiment with doubled pulses shows that the breakdown delay time τ_B decreases as the temperature of the crystal lattice increases.

The values of the breakdown delay time τ_B correspond to the barrier narrowing times and are governed by the drift of the excitons in the space-charge region and their diffusion in the base region. The $\tau_B(\tau_E)$ curve presented qualitatively confirms that a decrease in the exciton concentration in the base region leads to an increase in the barrier narrowing time. An increase in the carrier concentration in the space-charge region as a result of impact ionization leads to redistribution of the voltage between the space-charge region and the base of the sample, which, in turn, leads to the impact ionization of excitons. Confirmation of the ionization of excitons in the electric field is provided by the fact that the carrier concentration observed upon complete ionization significantly exceeds the concentration of the impurity centers in the sample. In addition, the concentration of ionized carriers depends on the photoexcitation intensity. The carrier concentration was determined using the known values of the mobilities of electrons and holes in a weak electric field $\mu_n \simeq \mu_p = 5\times 10^5$ cm^2/(V·s) at 4.2 K. The application of an electric field up to 1000 V/cm without photoexcitation did not result in the ionization of shallow impurity centers in the sample. This is attributed to the large value of the ionization energy of a phosphorus impurity in silicon, which amounts to ~ 39 meV at $T = 4.2$ K. The exciton binding energy determined from the absorption and emission spectra is located in

the range $\hbar\omega_{ex} \simeq 10-14$ meV. It is noteworthy that the threshold field and the sudden increase in concentration characteristic of impurity breakdown are not observed upon the impact ionization of excitons.

An investigation of the current instability mechanism shows that the mechanism of Schottky barrier breakdown which is detected is a source for the appearance of a highly nonequilibrium state in an EHP/exciton system in a strong electric field, which leads to fluctuations of the EHP density of the periodic or random type.

[1] E. H. Roderick, *Metal-Semiconductor Contacts*, Clarendon Press, Oxford (1980) [Russ. transl., Radio i Svyaz', Moscow (1982)].
[2] V. I. Strikha, E. V. Buzaneva, and I. A. Rédzievskiĭ, *Semiconductor Devices with a Schottky Barrier* [in Russian], Sov. Radio, Moscow (1974).
[3] B. M. Ashkinadze and F. K. Sultanov, Pis'ma Zh. Éksp. Teor. Fiz. **16**, 271 (1972) [JETP Lett. **16**, 190 (1972)].
[4] R. B. Hamond and R. N. Silver, Appl. Phys. Lett. **36**, 68 (1980).
[5] W. Schmid, Phys. Status Solidi B **84**, 529 (1977).
[6] Z. S. Gribnikov, Fiz. Tekh. Poluprovodn. **11**, 2111 (1977) [Sov. Phys. Semicond. **11**, 1239 (1977)].

Translated by P. Shelnitz

Influence of ytterbium on radiation-induced defect formation in silicon

F. M. Talipov

Tashkent State University, 700095 Tashkent, Uzbekistan
(Submitted May 20, 1996; accepted October 25, 1996)
Fiz. Tekh. Poluprovodn. **31**, 728–729 (June 1997)

The results of an investigation of the influence of γ irradiation on defect formation in ytterbium-diffusion-doped silicon are presented. It is shown that the charge-carrier elimination rates and the charge-carrier lifetime degradation constants in such samples are smaller than in samples not doped with the impurity. The results obtained are attributed to the formation of effective sinks for the radiation defects. © *1997 American Institute of Physics.* [S1063-7826(97)02106-6]

Radiation-induced defect formation in silicon can be influenced by doping it with rare-earth elements during growth.[1,2] However, doping can also be accomplished by high-temperature diffusion.[3–5] In contrast with doping during growth, diffusion doping makes it possible to obtain a more uniform distribution of the impurity and to regulate its concentration. At present, the literature contains practically no data on the influence of rare-earth elements introduced into silicon by high-temperature diffusion on radiation-induced defect formation in it. Such research would be not only of scientific interest, but also of definite practical interest due to the possibility of more precisely regulating and stabilizing the properties of silicon and silicon structures doped with these impurities. For this reason, in the present work we studied the influence of the rare-earth element ytterbium introduced by high-temperature diffusion on radiation-induced defect formation in silicon.

Samples of phosphorus-doped n-type silicon with a resistivity $\rho_0 = 65-75\ \Omega\cdot$cm and a lifetime of the minority charge carriers $\tau_0 = 60-65\ \mu$s were used in the investigations. The diffusion of ytterbium in silicon was carried out in the temperature range $T_d = 1100$–1200 °C in special quartz cells in an argon atmosphere from an ytterbium layer preliminarily sputtered in a high vacuum. As a result of diffusion, the resistivity of the samples decreased to $\rho_0 = 20-25\ \Omega\cdot$cm, and the lifetime of the minority charge carriers decreased to $\tau_0 = 45-55\ \mu$s. Then the samples were irradiated by γ rays at 70 °C in the range of integral fluxes $\Phi = 1\times10^{16}-5\times10^{18}$ cm^{-2}. The variation of the resistivity and the concentration of the majority charge carriers were monitored by measuring the Hall effect. The lifetime of the minority charge carriers was determined from the results of investigations of the transient processes occurring when a sinusoidal signal of large amplitude is passed through the semiconductor structures.[6] Radiation-induced defect formation was evaluated from the variation of the carrier elimination rate and the charge-carrier lifetime degradation constant. The carrier elimination rate during irradiation (K_n) was determined from the relation

$$K_n = \frac{\Delta n}{\Phi} = \frac{(n_0 - n)}{\Phi},$$

where n_0 is the initial carrier concentration, n is the carrier concentration following irradiation, and Φ is the irradiation dose. The charge-carrier lifetime degradation constant (K_τ) was determined from the relation[2]

$$K_\tau = \frac{1}{\Phi}\left(\frac{1}{\tau} - \frac{1}{\tau_0}\right),$$

where τ_0 and τ are the lifetimes of the minority charge carriers before and after irradiation.

TABLE I. Characteristics of the samples.

Samples	T_d, °C	ρ_0, Ω°cm	n_0, 10^{14} cm^{-3}	τ_0, μs	K_n, cm^{-1}	K_τ, cm$^2\cdot\mu$s^{-1}
Si⟨Yb⟩	1150	22.7	3.1	56	1.6×10^{-5}	1.4×10^{-13}
		23.0	3	57	1.1×10^{-5}	1.0×10^{-13}
Si⟨Yb⟩	1200	20.0	3	50	1.0×10^{-5}	7.6×10^{-14}
		18.4	3.2	55	1.0×10^{-5}	7.1×10^{-14}
Original Si		24.0	2	60	6.0×10^{-4}	3.0×10^{-13}

Note: All the samples had n-type conductivity.

Table I presents the experimental results obtained. It is seen that the values of the charge-carrier elimination rates and charge-carrier lifetime degradation constants are significantly smaller in the samples of Si⟨Yb⟩ than in the original (ytterbium-free) samples. It is noteworthy that the radiation-induced defect formation rate decreases as the ytterbium concentration increases, i.e., the presence of ytterbium significantly suppresses the rate of the formation and accumulation of radiation defects in silicon. A structural study of the present samples on an EVM-100 BR transmission electron microscope using the two-step carbon replica technique followed by tungsten oxide contrasting revealed the formation of ytterbium impurity clusters with dimensions no greater than 0.3 μm, which are two to three orders of magnitude smaller than the values observed in the case of doping during growth.[1] These clusters apparently serve as sinks for the components of the Frenkel pairs formed during γ irradiation, causing a decrease in the rate of radiation-induced defect formation.

We thank M. K. Bakhadyrkhanov for some useful discussions.

[1] Yu. A. Karpov, V. V. Petrov, and V. S. Prosolovich, Fiz. Tekh. Poluprovodn. **17**, 1530 (1983) [Sov. Phys. Semicond. **17**, 974 (1983)].
[2] V. A. Zaitov, Yu. M. Dobrovinskiĭ, and V. M. Tsmots', Fiz. Tekh. Polu-

 1063-7826/97/060624-02$10.00

provodn. **21**, 2082 (1987) [Sov. Phys. Semicond. **21**, 1262 (1987)].
[3] D. É. Nazyrov, V. P. Usacheva, G. S. Kulikov, and R. Sh. Malkovich, Pis'ma Zh. Tekh. Fiz. **14**, 1102 (1988) [JETP Lett. **14**, 1102 (1988)].
[4] M. K. Bakhadyrkhanov, F. M. Talipov, N. V. Sultanova, U. S. Dzhurabekov, Sh. Sh. Shasaidov, A. S. Lyutovich, and A. A. Kasymov, Izv. Akad. Nauk SSSR., Neorg. Mater. **26**, 458 (1990).
[5] D. É. Nazyrov, G. S. Kulikov, and R. Sh. Malkovich, Fiz. Tekh. Poluprovodn. **25**, 1653 (1991) [Sov. Phys. Semicond. **25**, 997 (1991)].
[6] S. M. Gorodetskiĭ and M. A. Litovskiĭ, Fiz. Tekh. Poluprovodn. **23**, 580 (1989).

Translated by P. Shelnitz

Photoluminescence of SiO_2 layers implanted with Si^+ ions and annealed in a pulsed regime

G. A. Kachurin, I. E. Tyschenko, K. S. Zhuravlev, N. A. Pazdnikov, V. A. Volodin, A. K. Gutakovskiĭ, and A. F. Leĭer

Institute of Semiconductor Physics, Russian Academy of Sciences, Siberian Branch, 630090 Novosibirsk, Russia

W. Skorupa and R. A. Yankov

Rossendorf Research Center, D-01314 Dresden, Germany
(Submitted May 25, 1996; accepted for publication October 25, 1996)
Fiz. Tekh. Poluprovodn. **31**, 730–734 (June 1997)

SiO_2 layers thermally grown on Si are implanted with Si^+ ions at energies of 100 and 200 keV in a dose equal to $\sim 10^{17}$ cm^{-2}. Two types of pulsed anneals are employed: at 900–1200 °C for 1 s and at 1050–1350 °C for 20 ms. Photoluminescence is observed in the visible and near-infrared regions of the spectrum after implantation. In the initial annealing stages the photoluminescence intensity drops, but after an anneal at 1200 °C for 1 s or at 1350 °C for 20 ms, it increases sharply by tens of times. According to the data from Raman spectroscopy and high-resolution electron microscopy, this corresponds to the formation of Si nanocrystals in SiO_2. The anneal times employed rule out the diffusion-controlled growth of Si nanocrystals, but they could form as a result of the solid-phase crystallization of amorphous inclusions. The correlation between the sharp enhancement of the luminescence and the formation of Si nanocrystals attests to a quantum-size mechanism for its appearance. © *1997 American Institute of Physics.* [S1063-7826(97)02206-0]

Silicon, the main material for microelectronics at present and in the foreseeable future, is sparingly used in optoelectronics. The reason for this is the low probability of radiative recombination due to the mismatch of the absolute extrema of the band structure in k space. The discovery of intense visible luminescence in porous Si, which has been attributed to quantum-size effects in silicon nanocrystals, opened up the way to the possible integration of electrical and optical silicon devices in instruments that process optical information. The practical and scientific interest in Si nanocrystals prompted a deluge of research aimed at the development of methods for producing them and at the study of their properties. Visible photoluminescence was observed in samples obtained by the oxidation of microcrystalline or amorphous Si,[1–3] the partial crystallization of amorphous Si,[4] the precipitation of excess silicon in oxides,[5–7] the sputtering of Si layers in various media,[8] and spark processing.[9] Special efforts were concentrated on obtaining Si nanocrystals using ion implantation, which is regarded as the cleanest and most controllable method.[10–15]

Despite such a great amount of research, the mechanism underlying the appearance of the visible luminescence is still incompletely clear even for porous silicon, which has been studied for a long time.[16] Along with the interpretation within the quantum-size formalism, explanations based on the possible formation of chemical compounds, structural imperfections, phase boundaries, etc. have been advanced.[16] The interpretative difficulties are due to the fact that different investigators observed the luminescence peaks in very different portions of the spectrum from the ultraviolet to the infrared (IR) region, depending on the experimental conditions. The peaks also differed from one another with respect to their intensity, relaxation times, and excitation conditions. All this suggests that the nature of the centers and the mechanism for visible luminescence in silicon nanostructures can vary. To determine them, the relationships between the atomic processes in the layers investigated and the luminescence parameters must be revealed. Pulsed anneals make it possible to monitor such processes with great precision; therefore, they were employed in the present work to achieve a better understanding of the reasons for the appearance of luminescence in silicon nanostructures.

EXPERIMENTAL METHOD

SiO_2 layers of thickness 500 nm were thermally grown on Si(100). The layers were implanted with Si^+ ions at two energies, viz., 200 keV in a 1×10^{17} cm^{-2} dose and then 100 keV in a 6×10^{16} cm^{-2} dose, with target temperatures from -60 to -20 °C. This provided a resultant concentration of excess Si of about 7×10^{21} cm^{-3} at depths from 100 to 300 nm. Control samples, in which the doses at the same energies were reduced by factors of 2.5 and 10, were also used. Two types of pulsed anneals were employed: with a duration of 1 s at 900−1200 °C in an argon atmosphere and with a duration of 20 ms at 1050–1350 °C (with a constant 600 °C component) in a N_2 atmosphere. After this treatment, the samples were held in a forming gas at 400 ° C for 30 min.

Photoluminescence was excited at 300 and 78 K by the output from an Ar laser with a wavelength $\lambda = 488$ nm and a power of about 20 mW and was recorded by a cooled photomultiplier in the photon-counting mode. The spectra presented in this paper were normalized to the sensitivity of the instrumentation. The Raman scattering at 300 K was studied

 1063-7826/97/060626-05$10.00

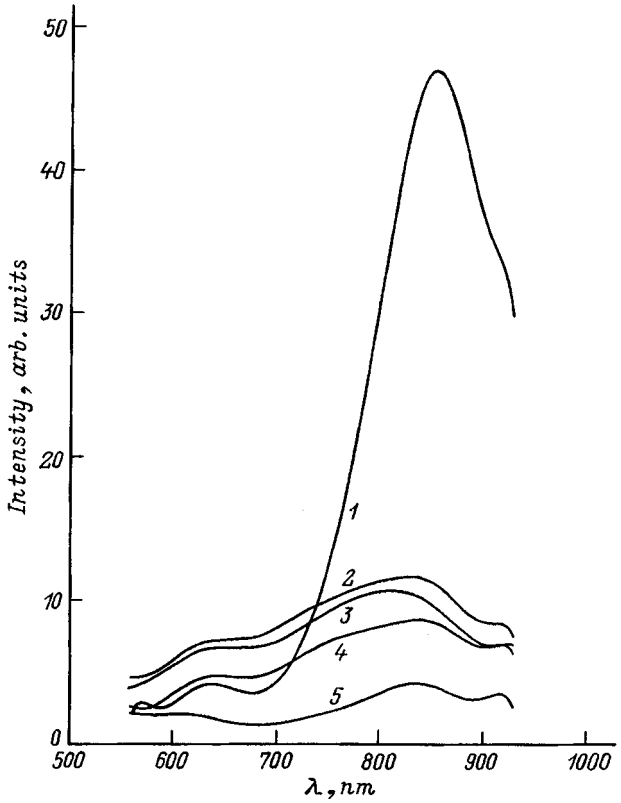

FIG. 1. Room-temperature photoluminescence of samples before (*2*, *5*) and after (*1*, *3*, *4*) pulsed anneals for an anneal time of 20 ms and various anneal temperatures, °C: *3* — 1050, *4* — 1200, *1* — 1350; *5* — the implantation dose of the Si^+ ions was reduced by an order of magnitude.

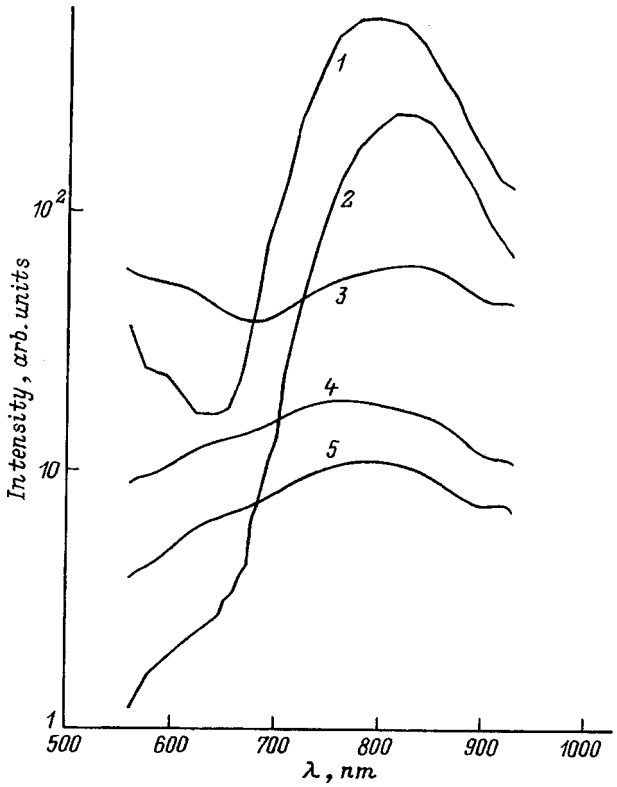

FIG. 2. Room- (*2*, *4*, *5*) and nitrogen-temperature (*1*, *3*) photoluminescence of samples after anneals with a duration of 1 s. Anneal temperature, °C: *3*, *4* — 900; *5* — 1050; *1*, *2* — 1200.

in a quasi-inverse recording geometry using the $\lambda = 488$ nm line of an Ar laser, a double-beam spectrometer, and a cooled multiplier in the photon-counting mode. Electron-microscopic investigations were performed using a JEM-4000 EX high-resolution microscope. To reach the depth interesting us, the top-most 100 nm of SiO_2 were removed in a 1:8 solution of $HF + H_2O$, and then the samples were used on the rear side for chemical jet etching.

EXPERIMENTAL RESULTS

The unirradiated SiO_2 films did not exhibit photoluminescence in the wavelength range $\lambda = 550-1000$ nm. After Si^+ ions were implanted, luminescence appeared at room temperature over the entire range investigated even before the pulsed anneals (Fig. 1). Weakly expressed maxima were observed near 650 and 850 nm. The pre-anneal luminescence vanished almost completely when the dose of Si^+ ions was lowered by an order of magnitude (Fig. 1). Pulsed anneals up to certain temperatures led to weakening of the photoluminescence at all wavelengths (Figs. 1 and 2). These threshold temperatures were 1200 and 1050 °C for anneal times equal to 20 ms and 1 s, respectively. Raising the temperature only 150 °C above these levels led to an extremely sharp increase in the luminescence intensity (Figs. 1 and 2). The maximum at 830−850 nm was dominant. The visible light with shorter wavelengths was maintained, but its intensity continued to decrease with increasing anneal temperature even after the threshold indicated above was surpassed. Figure 2 presents the spectra recorded at 78 K in addition to the luminescence spectra at room temperature. Cooling the samples enhances the luminescence by several fold over the entire spectral range investigated. The additional increase in the luminescence intensity seen in Fig. 2 at 600 nm is probably attributable to scattering of the exciting laser radiation in the cryostat.

The Raman scattering data are presented in Fig. 3. The strong peak at 520 cm^{-1} corresponds to scattering on long-wavelength longitudinal-optical phonons in single-crystal silicon and is produced by the substrate. Apart from the peak at 520 cm^{-1}, unimplanted SiO_2 layers displayed only a band at 430 cm^{-1}, which is caused by the Si–O bonds. After the implantation of Si^+ ions, clearly expressed scattering appeared near 480 cm^{-1}, which corresponds to the Si–Si bonds in amorphous silicon (Fig. 3, curve *3*). A control sample, for which the implantation dose was reduced by a factor of 2.5, did not exhibit such a pronounced peak, but additional scattering was noticeable at 450−490 cm^{-1} (Fig. 3, curve *2*). Pulsed anneals at 1200 °C for 1 s and 1350 °C for 20 ms led to weakening of the scattering at 480 cm^{-1} and to the simultaneous appearance of a band near 500−520 cm^{-1}, which could be caused by the formation of silicon nanocrystals.

Figure 4 presents the high-resolution electron-microscopic image of a portion of a sample after an anneal at 1350 °C over the course of 20 s and the microdiffraction pattern of the same portion. The diffraction pattern is char-

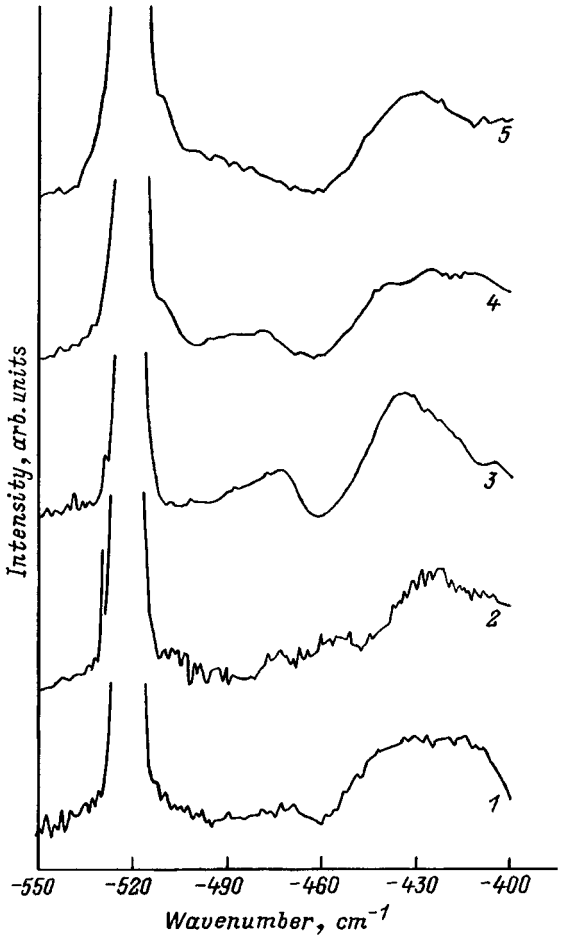

FIG. 3. Raman spectra from samples: *1* — unimplanted layer of SiO_2, *2* — implantation of 40% of the total dose of Si^+, *3* — implantation of the total dose of Si^+, *4* — after an anneal at 1200 °C for 1 s, *5* — after an anneal at 1350 °C for 20 ms.

acteristic of a polycrystal and attests to the presence of a large number of silicon crystallites that are misoriented relative to one another (the point reflections are from the substrate). It is seen from the electron-microscopic image that there are at least two phases, viz., an amorphous matrix containing crystalline inclusions measuring 2–6 nm. In most cases the interplanar distances in the crystals are close to 0.314 nm, i.e., the distance between the {111} planes in Si. The total area of the crystallites occupies about 30% of the observation field, although there are regions where there are fewer crystallites. Microscopy of a transverse cut surface provides approximately the same results; therefore, it can be concluded that the nanocrystallites have comparable dimensions in all directions. Even after pulsed annealing at the highest temperature used, structural defects are observed in the nanocrystals. If no crystallization had taken place, microscopy would have revealed only darker regions measuring $2-10$ nm and differing in contrast from the amorphous matrix. In this case the diffraction pattern would be typical of the amorphous substance.

DISCUSSION OF RESULTS

The most important experimental results can be formulated concisely in the following manner. When a certain dose for the implantation of Si^+ ions in SiO_2 is achieved, photoluminescence appears in the visible and infrared regions of the spectrum with two weakly expressed peaks already before the pulsed anneals. As the temperature of the subsequent pulsed anneals is increased, the luminescence intensity at first decreases slowly, but then it increases sharply in a narrow temperature range, and a pronounced maximum appears near $830-850$ nm.

We assume that the luminescence observed before the pulsed anneals is associated with the formation of regions with a Si excess up to the formation of inclusions of amorphous silicon. It follows from our results that high concentrations of excess Si, rather than SiO_2 defects, are needed for the appearance of the luminescence. Lowering the dose of Si^+ ions by an order of magnitude led to the almost complete disappearance of the luminescence (Fig. 1); however, even such diminished doses are sufficient for the repeated displacement of each atom in the layer investigated. In addition, the appearance of the luminescence correlates with the formation of a band at 480 cm^{-1} in the Raman spectra, which is characteristic of amorphous silicon (Fig. 3). This band practically disappears in response to a relatively small decrease in the dose (Fig. 3). Finally, pre-anneal luminescence was previously noted in SiO_2 subjected to implantation by large doses of Si^+ in Refs. 13 and 14. In particular, it was pointed out in Ref. 11 that the replacement of Si^+ ions by Ar^+, B^+, or Al^+ ions leads to the disappearance of the luminescence in SiO_2.

The abrupt increase in the photoluminescence intensity when a certain pulsed anneal temperature is reached is naturally attributed to the formation of Si nanocrystals. This is indicated by the disappearance of the band at 480 cm^{-1} in the Raman spectrum, which is characteristic of amorphous Si, and the appearance of additional scattering near the peak at 520 cm^{-1}, which is characteristic of single-crystal Si (Fig. 3). The observed red shift relative to 520 cm^{-1} is a consequence of a size effect and can be utilized to estimate the dimensions of the crystallites. Such estimates give a mean value of about 3 nm. This value agrees well with the high-resolution electron- microscopic data, which directly confirm the formation of silicon nanocrystals (Fig. 4).

Silicon nanocrystals can form either as a result of the diffusional transport of Si atoms to nuclei when a supersaturated solid solution dissociates or as a result of crystallization of the amorphous inclusions already present. The pulsed anneals with durations of 1 s and 20 ms that we employed restricted the possibilities of the diffusion-controlled growth of Si crystals. According to Ref. 17, in the temperature range interesting us from 1100 to 1300 °C the diffusivity of Si in SiO_2 equals $10^{-16}-10^{-15}$ cm^2/s. In the case of the 20-ms regime the diffusion length is less than 0.05 nm, which is totally insufficient for the formation of the experimentally observed Si crystals. On the other hand, in the same 20-ms regime the solid-phase crystallization of amorphous nanometer-scale inclusions requires rates equal to ~ 150 nm/s, which are achieved in pure silicon already at ~ 700 °C, and during 1 s a Si crystal grows by 3 ns at ~ 550 °C.[18] Thus, the rates of solid-phase growth are fully adequate for the formation of nanocrystals from amorphous inclusions, but

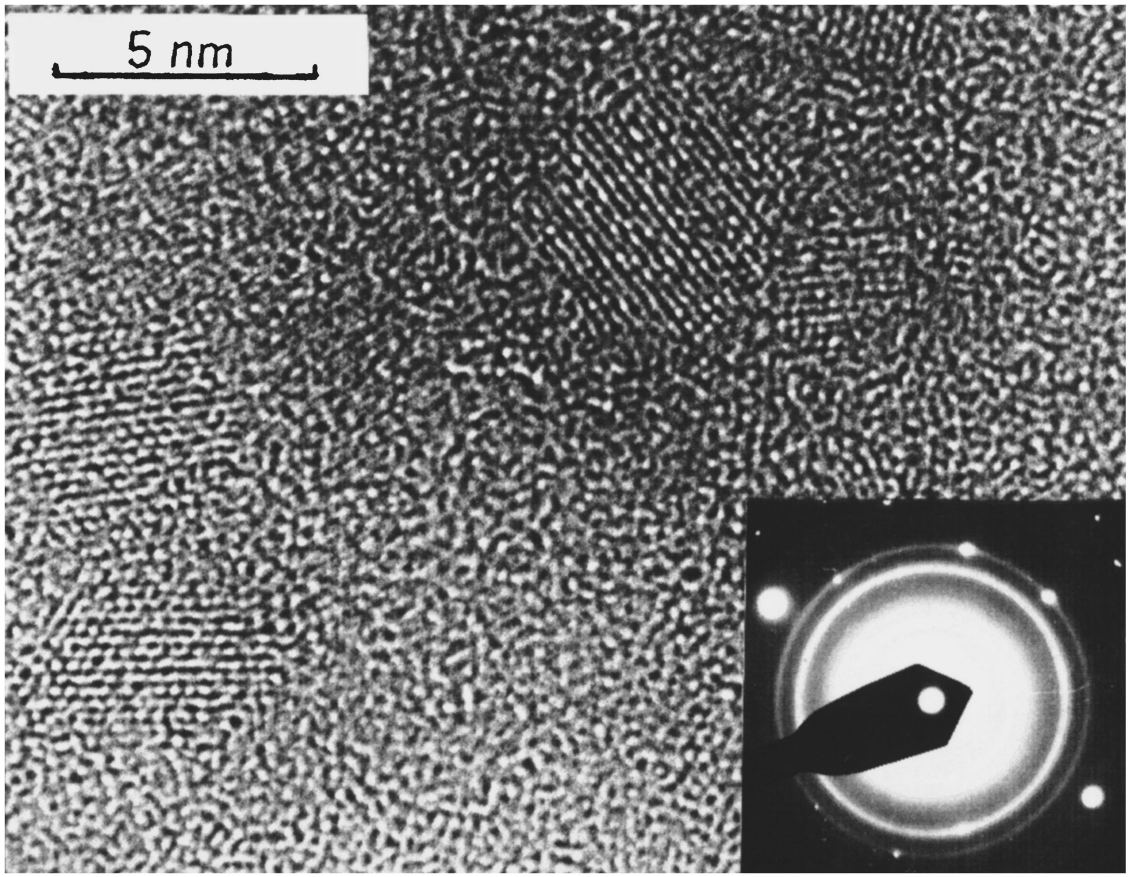

FIG. 4. High-resolution electron-microscopic image and microdiffraction pattern after the annealing of implanted SiO_2 layers at 1350 °C for 20 ms.

we should ask why crystallization was still observed at far higher temperatures. According to the data in Refs. 17 and 19, the crystallization of Si is slowed significantly in SiO_x films with a 10–20% silicon excess relative to the composition of SiO_2, although separation into the oxide and inclusions of amorphous silicon occurred even before annealing. For example, anneals at 700 °C for 72 h or at 800 °C for 18 h were found to be insufficient for crystallization.[17] After an anneal at 900 °C for 30 min, the Raman spectrum revealed the presence of amorphous (480 cm^{-1}) and crystalline Si (520 cm^{-1}).[19] Only anneals at 1100 °C for 15–30 min led to complete crystallization of the Si inclusions.[17,19] The reason apparently lies in the high oxygen content, which is known to slow the solid-phase crystallization of silicon.[20] Microscopy shows that the nanocrystals formed contain twin boundaries or other defects (Fig. 4), and the striking enhancement of the luminescence observed when the samples are cooled to 78 K, which is almost uniform over the entire spectrum, points to the presence of channels for nonradiative recombination even after high-temperature anneals.

The correlation between the formation of silicon nanocrystals and the sharp increase (tens of times) in the luminescence intensity is a weighty argument in favor of the quantum-size origin of the visible and IR radiation in the present case. This does not necessarily mean direct electron-hole recombination, and many researchers have pointed out the important role of centers near the $Si–SiO_2$ boundary.[2,11–13,16] As for the luminescence observed before the nanocrystals form, its proposed quantum-size origin must be verified. Its intensity is small and rapidly subsides upon moderate heating. Since the band width in SiO_x can vary from ~ 9 eV for $x=2$ to 1.1 eV for $x=0$, we can imagine the existence, in principle, of centers which provide for recombination with radiation in the visible and near-IR regions. Nevertheless, the luminescence is clearly associated with the depositions of excess silicon.

CONCLUSIONS

The implantation of Si ions with energies ranging from 100 to 200 keV in doses at the 10^{17} cm^{-2} level in SiO_2 leads to the appearance of visible and IR photoluminescence. The Raman spectra simultaneously display a band at 480 cm^{-1}, which is characteristic of Si–Si bonds in amorphous silicon. Subsequent pulsed anneals with durations equal to 1 s and 20 ms as the temperature is raised to 1050 and 1200 °C, respectively, lower the luminescence intensity. However, temperatures above these values result in sharp, manyfold enhancement of the luminescence. The data from electron microscopy and Raman scattering attest to the formation of Si nanocrystals. The brevity of the anneals ruled out the possibility of the growth of nanocrystals according to a mechanism involving the diffusive transport of Si atoms to nuclei, but fully permitted the solid-phase crystallization of nanometer-scale amorphous silicon inclusions formed as a result of implantation. The sharp manyfold enhancement of

the luminescence, which correlates with the formation of the Si nanocrystals, is evidence in support of the quantum-well mechanism of its appearance.

[1] T. Kawaguchi and S. Miyazima, Jpn. J. Appl. Phys. **32**, J215 (1993).
[2] M. Ruckschloss, B. Landkammer, and S. Veprek, Appl. Phys. Lett. **63**, 1474 (1993).
[3] H. Tamura, M. Ruckschloss, T. Wirschem, and S. Veprek, Appl. Phys. Lett. **65**, 1537 (1994).
[4] X. Zhao, O. Schoenfeld, S. Komuro, J. Aoyagi, and T. Sugano, Phys. Rev. B **50**, 18 654 (1994).
[5] Q. Zhang, S. C. Bayliss, and D. A. Hutt, Appl. Phys. Lett. **66**, 1977 (1995).
[6] Q. Zhang, S. C. Bayliss, A. Al-Ajili, D. A. Hutt, and P. Harris. Nucl. Instrum. Methods Phys. Res., Sect. B **97**, 329 (1995).
[7] B. H. Augustine, E. A. Irene, J. J. He, K. J. Price, Z. E. McNeil, K. N. Christensen, and D. M. Maher, J. Appl. Phys. **78**, 4020 (1995).
[8] P. Wickboldt, H. M. Cheong, D. Pang, J. H. Chen, and W. Paul, Mater. Res. Soc. Symp. Proc. **368**, 127 (1995).
[9] M. H. Ludwig, J. Menniger, and R. E. Hummel, J. Phys.: Condens. Matter. **7**, 9081 (1995).
[10] H. A. Awater, K. V. Shcheglov, S. S. Wong, K. J. Vahala, R. C. Flagan, M. I. Brongersma, and A. Polman, Mater. Res. Soc. Symp. Proc. **316**, 409 (1994).
[11] T. Shimizu-Iwayama, K. Fujita, S. Nakao, K. Saitoh, T. Fujita, and N. Itoh, J. Appl. Phys. **75**, 7779 (1994).
[12] T. Shimizu-Iwayama, S. Nakao, and K. Saitoh, Appl. Phys. Lett. **65**, 1814 (1994).
[13] T. Komoda, J. P. Kelly, A. Nejim, K. P. Homewood, P. L. F. Hemment, and B. J. Sealy, Mater. Res. Soc. Symp. Proc. **368**, 163 (1995).
[14] J. G. Zhu, C. W. White, J. D. Budai, S. P. Withrow, and Y. Chen, J. Appl. Phys. **78**, 4386 (1995).
[15] P. Mutti, G. Ghislotti, S. Bertori, Z. Bonolde, G. F. Cerafolini, L. Meda, E. Grilli, and M. Guzzi, Appl. Phys. Lett. **66**, 851 (1995).
[16] B. Hamilton, Semicond. Sci. Technol. **10**, 1187 (1995).
[17] L. A. Nesbit, Appl. Phys. Lett. **46**, 38 (1985).
[18] A. V. Dvurechenskiĭ, G. A. Kachurin, E. N. Nidaev, and L. S. Smirnov, *Pulsed Annealing of Semiconductor Materials* [in Russian], Nauka, Moscow (1982).
[19] A. Harstein, J. C. Tsang, D. J. Di Maria, and D. W. Dong, Appl. Phys. Lett. **36**, 836 (1980).
[20] G. A. Kachurin, Mikroelektronika **23**, 83 (1994).

Translated by P. Shelnitz

Quantum efficiency of Schottky photodiodes near the long-wavelength edge

V. G. Ivanov and V. I. Panasenkov

''Elektron'' Central Research Institute, 194223 St. Petersburg, Russia

G. V. Ivanov

A. F. Ioffe Physicotechnical Institute, Russian Academy of Sciences, 194021 St. Petersburg, Russia
(Submitted September 30, 1996; accepted for publication October 25, 1996)
Fiz. Tekh. Poluprovodn. **31**, 735–739 (June 1997)

The spectral dependence of the photoemission of hot electrons across a metal silicide-silicon Schottky barrier at photon energies comparable to the barrier height is investigated. An expression for the spectral dependence of the photoemission quantum efficiency is obtained in the diffusion approximation using the Green's function formalism for different values of the ratio between the layer thickness (d) and the elastic (L_p) and inelastic (L_e) mean free paths for hot electrons. A strong influence of the value of L_e/d on the increase in amplitude and the form of the spectral dependence of the quantum efficiency, which deviates significantly from the Fowler dependence at increased quantum efficiencies, has been observed. Satisfactory agreement between the theoretical and experimental spectral dependences of the quantum efficiency is demonstrated for the silicides of Pt, Co, and Ge, making it possible to experimentally evaluate L_e and to optimize the technology for fabricating Schottky barriers for infrared detectors in some cases. The reasons for the anomalously sharp increase in the photoemission of hot electrons with increasing energy of the exciting quantum at energies close to the potential energy of the Schottky barrier are discussed.
[S1063-7826(97)02306-5]

1. INTRODUCTION

A significant increase in the external quantum efficiency of metal silicide-silicon Schottky photodiodes in the infrared (IR) portion of the spectrum was observed in a number of studies[1–5] when the thickness of the silicide was reduced to tens of angstroms. This phenomenon, which is called ''hot-electron resonance,'' was not exhaustively explained from the standpoint of Fowler's theory[4] and was subsequently investigated in several theoretical and experimental studies.[5–7] It was established that the form of the spectral dependence of the internal quantum efficiency (Y_i) at quantum energies close to the Schottky barrier height differs appreciably from the Fowler dependence. The physical parameters determining Y_i, its possible limit, and the form of the spectral dependence are still a subject of investigation.

The models of the photoemission of hot electrons (holes) across a Schottky barrier[5–7] assume that the single-transmission probability of a Schottky barrier can be described on the basis of the ballistic motion of hot electrons in the metal silicide layer, and that electrons reflected from a Schottky barrier pass into the bulk of the silicide and do not participate in photoemission. These assumptions lead to an expression for the quantum efficiency in the form of Fowler's formula multiplied by a correction factor, which takes into account the enhancement of the photoemission,

$$Y_i = Y_F G(d, L_e, L_p, Y_F), \tag{1}$$

where d is the thickness of the metal silicide layer, L_e is the hot-electron inelastic mean free path, L_p is the hot-electron elastic mean free path,

$$Y_F = C_1 \frac{(h\nu - \varphi_0)^2}{h\nu}, \tag{2}$$

Y_F is the Fowler internal quantum efficiency, C_1 is the photoemission coefficient, $h\nu$ is the photon energy, and φ_0 is the Schottky barrier height.

It follows from Refs. 5–7 that in the most interesting case of large Y_i the limit $Y_i \to \infty$, rather than the physical limit

$$Y_T = \frac{h\nu - \varphi_0}{h\nu}, \tag{3}$$

is obtained upon the limiting transition $L_e \to \infty$ or $d \to 0$; therefore, such an approach is justified only for thick silicide layers, where hot-electron resonance is weakly expressed. Mooney and Silverman[8] calculated Y_i with allowance for a large number of collisions of the hot electrons in the silicide layer. According to their results, when $L_e \to \infty$, $Y_i \to Y_T$, which is the limit given by (3). However, when $d \to 0$, as previously, $Y_i \to \infty$. Here, as previously, it is assumed that the single-transmission probability of a Schottky barrier is given in the form (2). Actually, Y_F is the emission probability averaged over the electron energy, and Y_i exhibits a nonlinear dependence on the single-transmission probability of the Schottky barrier. This situation makes it incorrect to interchange the procedure for averaging over the energy with the procedure for calculating the transmission probability of an electron with a fixed energy across a Schottky barrier. This point was disregarded in Ref. 8. The correct approach is to first calculate the probability for the emission of a hot electron with a given energy E, with allowance for all the

 1063-7826/97/060631-04$10.00

possible collisions, under the assumption that the single-transmission probability $\rho(E)$ is given, as in Ref. 8, by the expression

$$\rho(E)=\frac{E-E_F-\varphi_0}{4E_F}, \tag{4}$$

where E_F is the Fermi energy in the metal silicide.

The averaging over the energy is performed in the final step in the range $E_F<E<E_F+h\nu$.

The possible collisions are taken into account on the basis of a description of the motion of the hot electrons in the diffusion approximation. Such an approach is possible because of the small value of Y_T and, consequently, the large number of electron collisions taking place at the boundaries of the silicide film (which is of order L_e/d) and within it (which is of order L_e/L_p). The general scheme for calculating Y_i on the basis of the arguments presented above and some individual consequences were briefly discussed in Ref. 9. In this paper we analyze the results of a calculation of the spectral dependence of the internal quantum efficiency of Schottky photodiodes on the basis of the diffusion model and we also compare these results with experiment.

2. MODEL AND CALCULATION RESULTS

We assume that $L_e \gg L_p$ and restrict the discussion to the case in which an increase in the quantum efficiency is observed, i.e, the case $L_e \gg d$. We also assume that the photoemission of hot electrons takes place (in the case of the photoemission of holes, only replacement of the corresponding signs is necessary). Let $n(r,t)$ be the number density of the hot electrons with a certain energy E at the time t in the vicinity of the point $\mathbf{r}(x,y,z)$. The surface of the silicide film lies in the x,y plane, and the thickness is measured from the surface $(z=0)$ to the Schottky barrier $(z=d)$. We write the continuity equation in the form

$$\frac{\partial n}{\partial t}=-\frac{n}{\tau_e}+D\Delta n+f(\mathbf{r},t), \tag{5}$$

where $D=L_p v_0/3$ is the diffusivity of the hot electrons, v_0 is the velocity of the electrons on the Fermi surface, and $\tau_e=L_e/\nu_0$ is the lifetime of the hot electrons before colliding with cold electrons.

Here $f(\mathbf{r},t)$ is construed as the number of hot electrons with the energy E generated at the time t in the vicinity of the point $\mathbf{r}$. We write the boundary conditions for (5) in the form

$$\begin{cases} \partial n/\partial z=0, & z=0, \quad (6)\\ D(\partial n/\partial z)=n\nu_0\rho(E)=0, & z=d. \quad (7)\end{cases}$$

The internal quantum efficiency for electrons with an energy E is

$$Y_i(E)=\frac{-D\int_S(\partial n/\partial z)_{z=d}dS}{\int_V f(\mathbf{r},t)d\nu}, \tag{8}$$

where S is the area of the Schottky barrier, and V is the volume of the metal silicide film

Averaging (8) over the energy gives the solution of the problem for the quantum efficiency:

$$Y_i=\langle Y_i(E)\rangle\equiv\frac{1}{h\nu}\int_{E_F}^{E_F+h\nu}Y_i(E)dE. \tag{9}$$

The system of equations (5)–(7) for the stationary case can be solved analytically using the Green's function formalism.[10] For the case of the uniform absorption of radiation in the silicide film, i.e., for $\alpha d \ll 1$ (α is the radiation absorption coefficient), the expression for $Y_i(E)$ has a simple form,

$$Y_i(E)=\frac{L^*}{d}\left[\coth\frac{d}{L^*}+\frac{D}{L^*\nu_0\rho(E)}\right]^{-1}, \tag{10}$$

where $L^*=\sqrt{L_pL_e/3}$.

Averaging of (10) over the energy according to (9), we finally obtain

$$Y_i=\frac{L^*}{d}\tanh\left(\frac{d}{L^*}\right)\left\{\frac{h\nu-h\nu_0}{h\nu}-\frac{4E_F}{h\nu}\sqrt{\frac{L_p}{3L_e}}\tanh\left(\frac{d}{L^*}\right)\times\ln\left[1+\frac{h\nu-h\nu_0}{4E_F}\sqrt{\frac{3L_e}{L_p}}\coth\left(\frac{d}{L^*}\right)\right]\right\}. \tag{11}$$

Before averaging over the energy, (10) coincides with the analogous expression presented in Ref. 6. This serves as additional confirmation of the applicability of the diffusion model in the problem under consideration.

A calculation of Y_i in a Schottky barrier with platinum silicide on the basis of the diffusion model was also performed in Ref. 11. Since a function describing the generation of hot holes (a source function) was not introduced into the continuity equation, only the disappearance of the light-generated hot holes by ''cooling'' or emission across the barrier was considered. The solution for $Y_i(E)$ was obtained only in the form of a series of products of several functions containing integrals over the thickness of the silicide. The complicated form of the expression obtained makes it difficult to compare it directly with (10) and the data from other studies. However, for the very simple case of a Schottky barrier with a low transmission probability or weak elastic scattering after averaging over the energy, the expression for Y_i gives the correct limiting transition $(Y_i \to Y_T)$ for both $L_e \to \infty$ and $d \to 0$, as well as correspondence to the experimental data for a PtSi/Si Schottky barrier and $L_e \simeq 4000$ Å.

Let us consider the limiting cases of Eq. (11).

a) When $L_e \to \infty$ or $d \to 0$, $Y_i \to Y_T$; i.e. the probability of photoemission approaches the theoretical limit.

b) When $L_p \to 0$ or $L_e \to 0$, $Y_i \to 0$; i.e., the probability for the photoemission in a layer with very strong scattering is small.

c) For moderately thin silicide layers with $(L_eL_p/3)^{1/2} < d \ll 1/\alpha$, $Y_i \to (L_e/d)Y_F$; i.e., the spectral dependence of Y_i maintains the Fowler form, and the absolute value of Y_i increases by a factor of L_e/d. In this approximation the result coincides with the data in Ref. 5.

Figures 1 and 2 present families of spectral curves of the internal quantum efficiency in $(Y_i h\nu)^{1/2}=f(h\nu)$ coordinates, which are usually used to describe Schottky photodetectors. The curves approach the linear Fowler dependence only at small values of L_e or large values of d. As Y_i increases and approaches Y_T, the curves deviate significantly from a linear

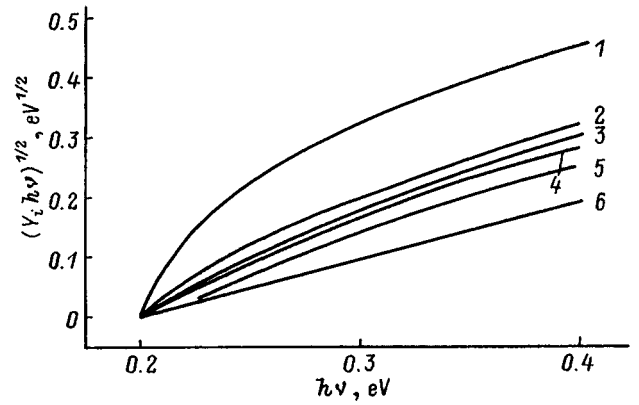

FIG. 1. Probability of the photoemission of hot electrons across Schottky barriers as a function of the energy of the absorbed photons for different values of the inelastic collision lengths L_e, Å: *2* — 2500, *3* — 2000, *4* — 1500, *5* — 1000, *6* — 500; *1* — the theoretical limit $L_e \to \infty$. $L_p = 70$ Å, $E_F = 5$ eV, $d = 10$ Å.

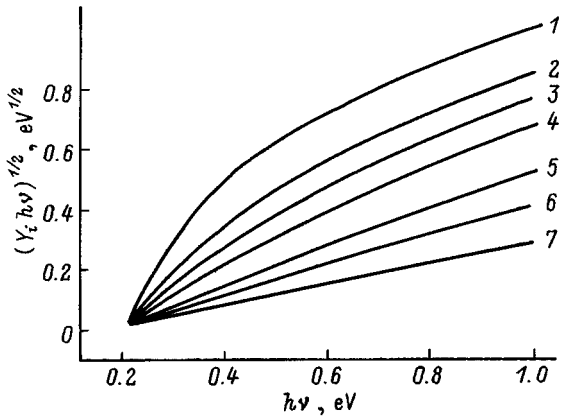

FIG. 2. Probability of the photoemission of hot electrons across Schottky barriers as a function of the energy of the absorbed photons for different values of the thickness of the metal silicide d, Å: *2* — 5, *3* — 10, *4* — 20, *5* — 50, *6* — 100, *7* — 200; *1* — the theoretical limit $d \to 0$. $L_p = 70$ Å, $E_F = 5$ eV, $L_e = 1000$ Å.

dependence, especially at small values of $h\nu - \varphi_0$. In addition, Figs. 1 and 2 illustrate the strong dependence of Y_i on L_e and d. There is also a dependence on E_F (a decrease in E_F from 5 to 1 eV increases Y_i by about four fold). The influence of L_p as it varies in the range 5–1000 Å is weakly displayed.

In developing devices with Schottky photodiodes there is interest not only in Y_i, but also in the external quantum efficiency (Y_{ex}), i.e., the ratio of the number of photoelectrons (or photoholes) emitted to the number of photons impinging on the photodiode. The usual goal is to maximize the average external quantum efficiency for an assigned spectrum

$$\overline{Y_{ex}} = \int_{\varphi_0}^{\infty} Y_i(h\nu) Y_{opt}(h\nu) R(h\nu, T) d(h\nu), \tag{12}$$

where Y_{opt} is the probability of photon absorption, which takes into account the absorption in the silicide and the action of the optical trap, and $R(h\nu, T)$ is the normalized Planck radiation function of the object being recorded at the temperature T (this function can be assigned for a selective emitter).

Without going into the procedure for optimizing (12) here, we note that it permits determination of the thickness of the metal silicide film, the value of L_e, and the parameters of the optical trap that provide for the maximum value of Y_{ex} for a concrete form of the function $R(h\nu, T)$. Knowledge of this quantity makes it possible to quickly estimate the number of electrons in the signal accumulated in the potential well of the Schottky barrier and to calculate the signal-to-noise ratio of the photodetector. The results of the calculation of Y_{opt} for several types of optical traps were presented in Ref. 9.

3. COMPARISON WITH EXPERIMENT AND DISCUSSION OF RESULTS

The curves in Figs. 1 and 2 constructed on the basis of Eq. (11) point out the absence of a linear dependence of $(Y_i h\nu)^{1/2}$ on $h\nu$ at small values of $h\nu - \varphi_0$.

Figure 3 presents experimental plots of the dependence of the internal quantum efficiency in $(Y_i h\nu)^{1/2} = f(h\nu - \varphi_0)$ coordinates on a log–log scale for various metal silicides[3,12,13] and germanium silicide.[14] For the theoretical limit we have a straight line with a slope equal to 1/2 in accordance with (3). All the other curves lie below the theoretical limit and have a variable slope. A slope equal to unity, which reflects the Fowler form of the spectral dependence of the quantum efficiency, is obtained in a certain approximation only in the range $0.06 \leqslant (h\nu - \varphi_0) \leqslant 0.2$ eV for metal silicides. The curve for germanium silicide is closest to the theoretical limit and has a slope close to unity at values of $h\nu - \varphi_0$ ranging from 0.02 to 0.06 eV. When $h\nu - \varphi_0 \geqslant 0.1$ eV, nearly all the curves tend to a slope equal to 1/2, which is characteristic of $Y_T(h\nu - \varphi_0)$. When photons with an energy not much greater than the barrier height ($10^{-2} \leqslant h\nu - \varphi_0 \leqslant 6 \times 10^{-2}$ eV) are absorbed in a Schottky barrier, the slope of the plots becomes significantly greater than unity, and the dependence for platinum silicide is nearly exponential. Such behavior of the internal quantum efficiency does not follow from (11) or from the results of other studies.[5–9,11] There are several possible reasons for the rapid increase in the internal quantum efficiency with increasing $h\nu$ at small values of $h\nu - \varphi_0$.

First, as the energy of the hot electrons increases, the probability of tunneling through the barrier increases, since the thickness of the barrier decreases with increasing energy. If the barrier has a triangular shape, its thickness decreases linearly as $h\nu$ increases. This leads to an exponential dependence of the barrier transmission probability on the energy of the hot electrons.

Second, when $T \neq 0$, there is nonzero population of the energy levels in the silicide with energies above the Fermi level. The energy range of this ''tail'' extends from $2kT$ to $3kT$, and the number of electrons with a given energy drops exponentially with increasing energy. If it is assumed that the cross section for the capture of photons by electrons does not depend on the electron energy, an increase in $h\nu$ will be accompanied by an exponential increase in the number of

electrons with energies exceeding the barrier height and, therefore, a rapid increase in Y_i. This increase will occur until the energies of the absorbed photons increase so much that hot electrons begin to be generated from the Fermi level.

The character of the plots shown in Fig. 3 for PtSi/Si and $Si_{0.7}Ge_{0.3}$/Si at small values of $h\nu-\varphi_0$ can be qualitatively explained on the basis of a second mechanism of injection across the Schottky barrier. However, the data on $CoSi_2$ cannot be explained on this basis.

As was noted above, in the case of a not excessively thin silicide layer, for which

$$(L_pL_e/3)^{1/2}<d\ll 1/\alpha, \tag{13}$$

the plot of $(Y_ih\nu)^{1/2}=f(h\nu-\varphi_0)$ has a region of linearity, where $Y_i\rightarrow L_eY_F/d$. In this region, knowing d, we can estimate L_e, i.e., the main parameter which provides for an increase in the quantum efficiency of Schottky barriers. When $d=30-40$ Å, the right-hand side of the inequality (13) holds only for small L_p and not very large L_e, $L_e<10^3$ Å. Assuming that these conditions are satisfied for our PtSi/Si Schottky barriers, we obtain

$$L_e\simeq 8C_2E_Fd, \tag{14}$$

where C_2 is the experimental value of the photoemission coefficient.

In the PtSi/Si Schottky barriers that we fabricated $d=40$ Å, and $C_2=0.3$ eV^{-1}. Assuming $E_F=8.5$ eV, we obtain $L_e=800$ Å. Such a value of L_e is five times lower than the value given in Ref. 13 for the PtSi/Si Schottky barriers investigated in Ref. 15. This finding is possibly due to the poorer degree of cleanness of the silicon surface before the creation of the Schottky barriers in our structures (and, thus, the somewhat smaller internal quantum efficiency).

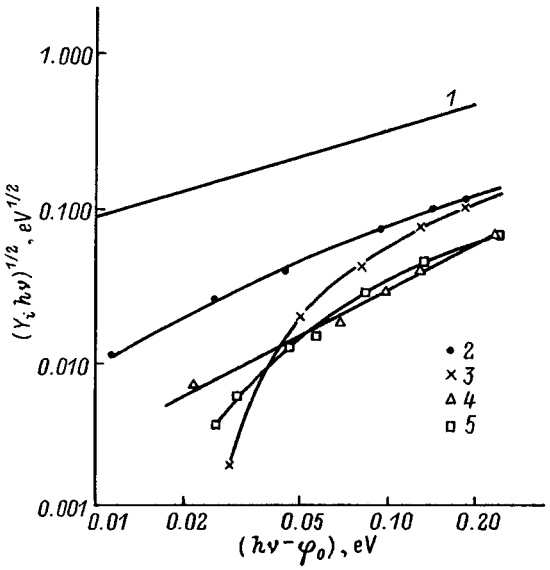

FIG. 3. Spectral dependences of the quantum efficiency of Schottky photodiodes formed by various silicides: *2* — $Si_{0.7}Ge_{0.3}$/Si; *3* — PtSi/Si;[15] *4* — $CoSi_2$; *5* — PtSi/Si;[9] *1* — theoretical limit.

4. CONCLUSIONS

The diffusion model of the emission of nonequilibrium hot electrons across Schottky barriers has been used to obtain the dependence of the internal quantum efficiency of Schottky barriers with metal silicides on the energy of the quanta of exciting radiation for different values of the ratio between the thickness of the silicide film and the inelastic and elastic mean free paths. The solution of the diffusion equation (and the expression for the quantum efficiency) has been obtained in an analytic form using the Green's function formalism. When the ''cooling'' distances of the hot electrons are sufficiently large (i.e., when $L_e/d\gg 1$), as the inelastic mean free path increases, the dependence of the quantum efficiency on the photon energy deviates appreciably from the Fowler dependence, increasing by severalfold in the region of the long-wavelength photosensitivity edge. Conversely, variation of the elastic mean free path over a broad range has only a weak influence on the quantum efficiency. Since the cooling distance is determined mainly by electron-electron collisions in the silicide layer, to increase the quantum efficiency at the long-wavelength edge, it is preferable to fabricate the Schottky barrier on the basis of the silicide of a degenerate semiconductor rather than on the basis of the metal silicide. Quantitative agreement between the plots of the dependence of the internal quantum efficiency on the difference between the photon energy and the Schottky barrier height $(h\nu-\varphi_0)$ obtained is observed for the experimental PtSi, $CoSi_2$, and GeSi Schottky barriers when $h\nu-\varphi_0>kT$. When $h\nu-\varphi_0\simeq kT$, the experimental results show a rapid (in some cases, nearly exponential) increase in the quantum efficiency with increasing $h\nu$, which does not follow directly from the model considered and is possibly due to the need to take into account the thermal spread of the electron concentration near the Fermi level in the silicide layer.

[1] J. Cohen, J. Vilms, and R. J. Archer, Hewlett-Packard Laboratories, Palo Alto, CA, Final Report AFCRL-69-0287, June 1969.
[2] R. J. Acher and J. Cohen, in *Device Research Conference*, Rochester, New York, 1969.
[3] H. Elabd and W. Kosonoky, RCA Rev. **43**, 569 (1982).
[4] R. H. Fowler, Phys. Rev. **38**, 45 (1931).
[5] E. O. Kane, Phys. Rev. **147**, 335 (1966).
[6] V. L. Dalal, J. Appl. Phys. **42**, 2227 (1971).
[7] V. E. Vichers, Appl. Opt. **10**, 2190 (1971).
[8] J. M. Mooney and J. Silverman, IEEE Trans. Electron. Dev. **ED-32**, 33 (1985).
[9] V. G. Ivanov, S. A. Kassirov, V. I. Panasenkov, and V. S. Troyanovskiĭ, in *Abstracts of Reports to the 4th Conference on Charge-Coupled Devices and Systems Based on Them ''CCD-92,''* Moscow, 1992 [in Russian], p. 24.
[10] V. I. Smirnov, *A Course in Higher Mathematics, Vol. 4: Boundary Value Problems, Integral Equations and Partial Differential Equations*, Addison-Wesley, Reading, Mass. (1964)
[11] D. E. Mercer and C. R. Helms, J. Appl. Phys. **65**, 5035 (1989).
[12] J. Kuriansky, Y. Vermairen, C. Claeys, W. Stessens, K. Maex, and R. De Keersmaecker, SPIE, Infrared Technol., **1157**, 145 (1989).
[13] T.-L. Lin, J.-S. Park, T. George, E. W. Jones, R. W. Fathauer, and J. Maserjian, Appl. Phys. Lett. **62**, 3318 (1993).
[14] T.-L. Lin, J.-S. Park, S. D. Ganapala, E. W. Jones, and H. M. Del Castillo, Opt. Eng. **33**, 716 (1994).
[15] J. M. Mooney, J. Silverman, and M. M. Weeks, SPIE, Infrared Sens. Sens. Fusion **782**, 99 (1987).

Translated by P. Shelnitz

The photoconductivity of $Cd_xHg_{1-x}Te$ ($x=0.2-0.3$) with an aluminum thin-film coating

É. Yu. Salaev, É. K. Guseĭnov, and N. D. Ismaĭlov

Institute of Photoelectronics, Azerbaidzhan Academy of Sciences, 370141 Baku, Azerbaidzhan

Atesh Tezer

TUBITAK, Marmara Research Center, 41470 Gebze, Turkey
(Submitted June 13, 1996; accepted for publication October 25, 1996)
Fiz. Tekh. Poluprovodn. **31**, 740–744 (June 1997)

The results of an experimental investigation of the photoconductivity of n- and p-$Cd_xHg_{1-x}Te$ $\times(x=0.2-0.3)$ deposited on the surface of aluminum thin films are presented. The results obtained are analyzed with allowance for the influence of the surface space-charge region and the recombination process in it. The values of the rate of surface recombination and the surface mobility of the charge carriers are determined from measurements of the photoconductivity and the barrier photocurrent. © *1997 American Institute of Physics.* [S1063-7826(97)02406-X]

1. INTRODUCTION

The unwavering interest in $Cd_xHg_{1-x}Te$ single crystals due to their widespread use in optoelectronics has stimulated comprehensive investigations of their physical properties, including their microscopic properties. The study of these properties and an ability to regulate the surface parameters are essential for creating photodetectors with superb photoelectric parameters. Surface-controlled photodetectors have an increased photosensitivity, a lower noise level, and a smaller recombination surface than do ordinary photodetectors, which influence the characteristics of the devices.[1] The surface doping of $Cd_xHg_{1-x}Te$ with Ag and Au from neutral solutions, which is one of the methods for regulating the surface state,[2] causes a drop in the photosensitivity in the short-wavelength region of the spectrum of $Cd_xHg_{1-x}Te$, which is associated with an increase in the rate of surface recombination. At the same time, an investigation of the photoconductivity of $Cd_xHg_{1-x}Te$ after various metals are deposited on $Cd_xHg_{1-x}Te$ single crystals by thermal vacuum evaporation showed that the drop in photosensitivity in the short-wavelength region of the spectrum is caused not only by an increase in surface recombination, but also, to a considerable degree, by a decrease in the surface mobility of the charge carriers. Aluminum stands out among the series of metals used, since a considerable increase in the photosensitivity in the short-wavelength region of the spectrum is observed when it is deposited on a $Cd_xHg_{1-x}Te$ surface.

In this paper we present the results of a comprehensive study of the photoconductivity of $Cd_xHg_{1-x}Te$ ($x=0.2-0.3$) single crystals when aluminum thin films are deposited on a chemically etched surface by thermal vacuum evaporation.

2. EXPERIMENTAL METHOD

Single crystals of n-type $Cd_xHg_{1-x}Te$ ($x=0.2-0.3$) with $N_d=1-0.13\times10^{15}$ cm^{-3} and $\mu_n=3-6\times10^4$ cm^2/(V·s) and p-type crystals of the same composition with $N_a=3-5\times10^{15}$ cm^{-3} and $\mu_p=4.5-5.5\times10^2$ cm^2/(V·s) were used in the experiments. The surface of the plates was subjected to chemical-mechanical polishing followed by etching in a 4% bromine-containing etchant. Ohmic contacts were created on each plate by the electrochemical deposition of indium. Aluminum films with thicknesses from 10 to 300 Å were deposited by thermal vacuum evaporation in a system with a turbomolecular pumping system. The thickness of the aluminum film was monitored using an MII-4 interference microscope by measuring the metallization on a glassy plate located closer to the evaporation source than the sample. When aluminum was sputtered, the ohmic contacts on the sample were covered by a special mask, which provided a gap with a width of about 100 μm between the ohmic contacts and the aluminum gate. To form a contact with the semitransparent gate, a silver strip measuring 50×300 μm^2 was sputtered at the transverse center of the sample, and a steel wire spring was pressed against it. The magnitude of the surface band bending was determined from measurements of the photoelectromotive force.[3] The current-voltage characteristics were measured at a frequency of 50 Hz, and the capacitance-voltage characteristics determined by the resonance method were measured at the frequencies in the range 0.1–3 MHz. The remaining details of the experimental procedure were described in Refs. 4 and 5. All the measurements were performed at 77 K.

3. RESULTS AND DISCUSSION

The experiments reveal that after deposition of the aluminum films on the surfaces of n- and p-$Cd_xHg_{1-x}Te$ there are significant changes in the spectral characteristics and relaxation kinetics of the photoconductivity. In comparison to the original data for a free $Cd_xHg_{1-x}Te$ surface (Fig. 1, curve *1*), slight increases in the surface lifetime τ_s and the photosensitivity in the short-wavelength region of the spectrum σ_s are observed as the thickness of the aluminum film increases (in the range of thicknesses 20–80 Å) (Fig. 1, curve *2*). The increases in τ_s and σ_s continue to saturation at film thicknesses at which the films exhibit appreciable conductivity (thicknesses greater than 100 Å) (Fig. 1, curve *3*). The largest increases in these parameters, up to 50 fold for $x=0.28-0.3$, are observed for uncompensated and weakly compensated samples, which have comparatively low values

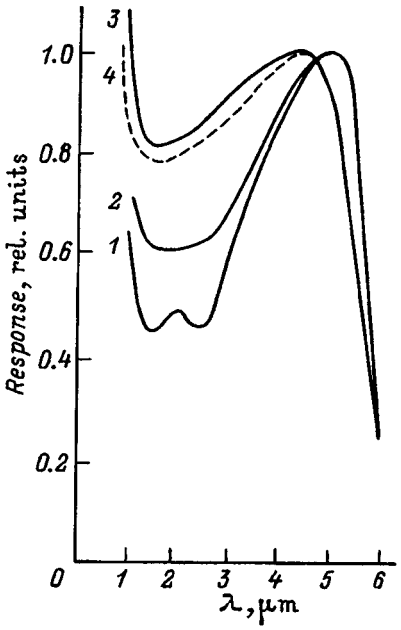

FIG. 1. Spectral dependence of the photoconductivity of $Cd_{0.28}Hg_{0.72}Te$ with $\tau_\nu = 1$ μs at 80 K: *1* — with a free surface; *2–4* — with a surface covered by an aluminum film of thickness: *2* — 50 Å ($\tau_s = 2$ μs); *3* — 150 Å ($\tau_s = 10$ μs); *4* — 150 Å ($\tau_s = 5$ μs) with illumination.

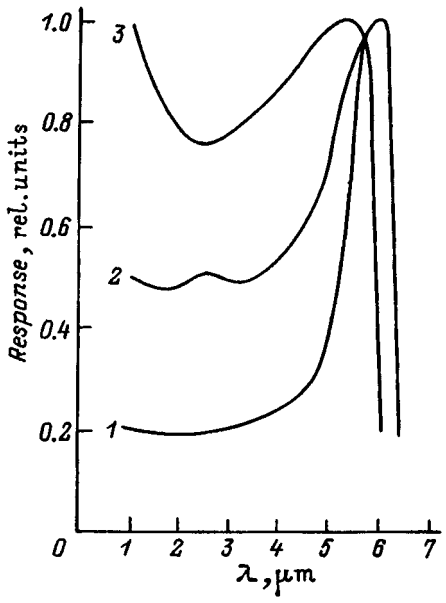

FIG. 2. Spectral dependence of the photoconductivity of n-$Cd_{0.27}Hg_{0.73}Te$ with $\tau_\nu = 12$ μs at 80 K: *1* — with a free surface ($\tau_s = 12$ μs); *2* — with a surface coated by an aluminum film of thickness 170 Å ($\tau_s = 12$ μs); *3* — spectrum of the barrier photoelectromotive force of an Al–$Cd_{0.27}Hg_{0.73}Te$ structure.

for the bulk carrier lifetime $\tau_\nu = 0.3 - 6 - 1.0 \times 10^{-6}$ s. This effect weakens considerably as the gap width of the $Cd_xHg_{1-x}Te$ single crystal decreases. The factor by which the photosensitivity increases in the short-wavelength region of the spectrum $K_\sigma = \sigma_s/\sigma_s^0$ is smaller than the factor by which the surface lifetime increases $K_\tau = \tau_s/\tau_s^0$ (where σ_s^0 and τ_s^0 are the original values of the photoconductivity and the surface lifetime of the charge carriers on the free surface of the samples, and σ_s and τ_s are the values for a surface with a sputtered aluminum layer). For the strongly compensated samples with $\tau_\nu > 10^{-5}$ s the surface lifetime τ_s remains nearly the same, while the photoconductivity σ_s decreases in most cases severalfold (sometimes 20 fold) (Fig. 2, curve *2*) in comparison to the original value of σ_s for the free surface. As E_g decreases, a decrease in τ_s in comparison with τ_ν is observed. For the samples with a coating the kinetics of the drop in the photocurrent at small levels of photoexcitation correspond to a simple exponential law (Fig. 3a, curve *1*); as the level of pulsed illumination is increased, a fast component of the decrease in the photoresponse with a time constant τ_s, which approaches τ_ν, appears. Additional constant illumination diminishes τ_s (Fig. 3a, curve *3*), but the distribution of the photosensitivity in the short-wavelength region of the spectrum is lowered to a considerably smaller degree (Fig. 1, curve *4*).

It follows from the current-voltage characteristics of the Al–$Cd_xHg_{1-x}Te$ structures that the dielectric gap between the metal and the semiconductor is tunneling-opaque to the charge carriers even when a bias voltage as large as 1 V is applied. This allows us to use the capacitance-voltage method, which is used to analyze metal-insulator-semiconductor (MIS) structures with a thick insulator, to determine the surface parameters. The estimated value of the density of surface states is $N_{ss} \approx 10^{12}$ cm^{-2}. An analysis of these characteristics for structures based on n- and p-type $Cd_xHg_{1-x}Te$ points out depleting band bending at $U = 0$. This is also indicated by the identical value of the saturation photoelectromotive force ($\varphi_s \leqslant 60$ mV for $x = 0.28$ at 77 K) in the presence of the thermal background acting on these structures. The background radiation generation current can lower the initial barrier height φ_s by 30–50 mV, and thus it can be assumed that $\varphi_s \simeq 0.1$ V. However, the use of these values of φ_s and N_{ss} for the formation of a barrier according to the Bardeen model does not provide a satisfactory explanation for the results obtained for n- and p-type $Cd_xHg_{1-x}Te$ of the same composition. In the case of metal–$Cd_xHg_{1-x}Te$ structures, the violation of the stoichiometry in the surface layer upon deposition of the metal due to the weakly bound mercury atoms, whose vacancies create acceptor levels in the band gap,[6] must be taken into account. Therefore, the factors determining the heights of the barriers on n- and p-Cd_xHg

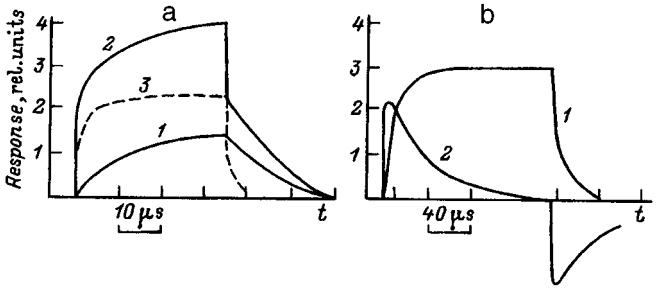

FIG. 3. Photoconductivity relaxation kinetics. a: *1*, *2* — for low and high levels of pulsed illumination, *3* — in the presence of constant illumination and a barrier photocurrent. b: *1* — for $R_0 = 1$ MΩ, *2* — for $R_0 = 0.3$ kΩ in an Al–$Cd_{0.28}Hg_{0.72}Te$ structure.

$_{1-x}$Te can differ. Apparently, the weak variation of the bending of the surface bands in the initial stage of deposition of the aluminum films is attributable to the formation of a transition layer and restructuring of the system of surface states. The problem of barrier formation calls for a special study; therefore, below we shall consider only the results obtained for aluminum layers of thickness 100–300 Å.

Let us analyze the observed features of the photoconductivity with allowance for the photoconductivity of the surface space-charge region and the recombination occurring in it. As was shown in Ref. 5, upon depletion the photoconductivity of $Cd_xHg_{1-x}Te$ ($x=0.2-0.3$) is localized in the surface space-charge region and is approximated by the expression

$$\sigma(\alpha)=eI\eta(1+b)\{\mu_{ps}\tau_s[1-\exp(-\alpha l)/(1+\alpha l)] + [\mu_{pv}\tau_v\exp(-\alpha l)/(1+\alpha L_d)]\}, \quad (1)$$

where I is the rate of the generation of electron-hole pairs, μ_v and μ_s are the bulk and surface mobilities of the charge carriers, $b=\mu_{nv}/\mu_{pv}\simeq\mu_{ns}/\mu_{ps}$, α is the absorption coefficient, l is the width of the space-charge region, L_d is the diffusion length for the minority charge carriers, and η is the quantum efficiency of the internal photoeffect. In the region of intense absorption, where we have

$$\sigma_s=eI\eta(1+b)\mu_s\tau_s, \quad (2)$$

$$\tau_s^{-1}=\tau_v^{-1}[(1+L_-^{\tau})/(1+L_-)]+S/L_d(1+L_-), \quad (3)$$

where

$$L_-=L_d^{-1}\int_0^l \exp[-\varphi(x)]dx,$$

$$L_-^{\tau}=L_d^{-1}\int_0^l \exp[-\varphi(x)]\tau_p\tau^{-1}(x)dx,$$

and upon depletion

$$L_-=L_eL_d^{-1}\int_0^l \exp(-\varphi_s)/\sqrt{-\varphi_s-1}. \quad (4)$$

If the surface band bending increases after deposition of the metal on the surface of the sample, then, as follows from (3), at small rates of surface recombination $[S<L_d(1+L_-)\tau_v^{-1}]$ and recombination in the space-charge region ($L_-^{\tau}<L_-$), the surface lifetime of the charge carriers τ_s increases. In this case, as is observed for weakly compensated $Cd_xHg_{1-x}Te$ samples, the photosensitivity increases in the short-wavelength region of the spectrum. For the samples with a high degree of compensation of the carrier concentration and comparatively large values of τ_v, it is difficult to achieve the condition $\tau_s>\tau_v$ due to the restriction of τ_s by the rates of surface recombination and recombination in the space-charge region. Consequently, as follows from (2), for these samples the decrease in the photosensitivity in the short-wavelength portion of the spectrum following film deposition can be caused by the smaller values of the surface mobility μ_s of the charge carriers compared with the bulk mobility μ_v. Under the condition of localization of the photoconductivity in the space-charge region with $\mu_s=\mu_v$ and $\tau_s=\tau_v$, the spectral dependence of $\sigma(\alpha)$ is identical to the spectral dependence of the capacitive photoelectromotive force $U_\sigma(\alpha)$.[7] Therefore, the lowering of $\sigma(\alpha)$ relative to the $U_\sigma(\alpha)$ curve in the short-wavelength portion of the spectrum is proportional to μ_v/μ_s. The surface mobility of the charge carriers $\mu_s=2\times10^4$ cm^2/(V·s) was determined from a comparison of the $U_\sigma(\alpha)$ and $\sigma(\alpha)$ curves (Fig. 2, curves *2* and *3*) using the value $\mu_v=6\times10^4$cm^2/(V·s) for *n*-$Cd_xHg_{1-x}Te$.

When the level of pulsed illumination is increased or constant illumination is provided, the surface bands straighten, causing the appearance of a fast component in the decrease in the photocurrent with τ_s approaching τ_v. The photosensitivity in the short-wavelength portion of the spectrum should decrease by the same factor. However, as the bands straighten, the condition of localization of the photoconductivity in the space-charge region is violated, and the contribution of the surface to the total photoconductivity decreases. During this process, μ_s approaches μ_v, and this accounts for the weak decrease in $\sigma(\alpha)$ upon continuous illumination. Thus, the observed decrease in σ_s following the deposition of an aluminum film on a sample is governed by the smaller values of μ_s compared with μ_v, rather than by the rate of surface recombination.

To determine S it is convenient to use the relaxation curves of the photocurrent in an Al–$Cd_xHg_{1-x}Te$ surface-barrier structure (Fig. 3a). In the open-circuit regime $R_0>R_\omega$ (where R_0 is the resistance of the load, and R_ω is the resistance of the space-charge region) the time constant $\tau_1=R_\omega\cdot C_\omega$ (where C_ω is the capacitance of the space-charge region). In the short-circuit regime ($R_0\ll R_\omega$) the photocurrent increases with the time constant $\tau_2=R_0\cdot R_\omega$ and, after achieving a certain value, decreases with the time constant τ_r, which is related to S by the relation[8]

$$\tau_r=L_e(-\varphi_s^L)[(S_{pe}+S^*)\sqrt{-\varphi_s^L}]^{-1}, \quad (5)$$

where S_{pe} is the rate of the emission of charge carriers through the dielectric gap. In our case $S_{pe}\ll S^*$. After determining the values $\varphi_s^L=7$, $\tau_r=4\times10^{-5}$ s, and $L_e=6\times10^{-5}$ cm, from (5) we find $S^*=500$ cm/s, so that, in fact, $S^*\ll L_d\tau_v^{-1}(1+L_-)=6\times10^4$ cm/s.

Taking into account (4) and (5), we can write Eq. (3) in the form $\tau_s^{-1}=\tau_v^{-1}[(1+L_-^{\tau})/(1+L_-)]+\tau_r^{-1}$, from which it follows that τ_s can increase only under the condition that the second term is much smaller than the first, and the recombination rate in the space-charge region decreases as the surface band bending increases $[(1+L_-^{\tau})\to1]$. This conclusion is valid, if the tunneling effects in the space-charge region are disregarded, as was done in Ref. 8.

However, for $Cd_xHg_{1-x}Te$ with narrow-gap compositions these effects can predominate at low temperatures. Figure 4 presents plots of the dependence of the short-circuit photocurrent on the bias voltage in the structure. It can be seen that in a reverse bias the photocurrent in a structure based on a strongly compensated sample with $N_d\simeq10^{13}$ cm^{-3} decreases. A similar drop in the photocurrent was observed in an MIS structure based on *p*-type $Cd_{0.2}Hg_{0.8}Te$ with $N_a=3\times10^{15}$ cm^{-3} in Ref. 9 and was attributed to the tunneling of charge carriers via impurity centers in the space-charge region. As an analysis shows, this mechanism is un-

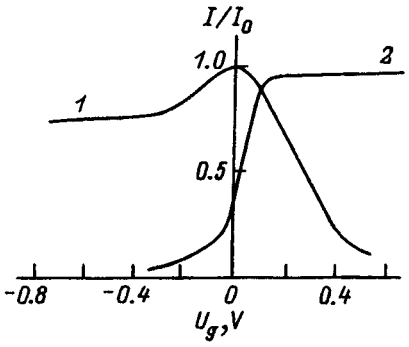

FIG. 4. Dependence of the short-circuit photocurrent on the applied gate voltage in different structures: *1* — Al–*n*-$Cd_{0.27}Hg_{0.73}Te$ with $N_d=10^{13}$ cm^{-3}, *2* — Al–*p*-$Cd_{0.3}Hg_{0.7}Te$ with $N_a=5\times10^{15}$ cm^{-3}.

acceptable for $N_d\simeq10^{13}$ cm^{-3}. In addition, no decrease in the photocurrent is observed for the *p*-type $Cd_xHg_{1-x}Te$ sample with $N_a=5\times10^{15}$ cm^{-3} within the range of bias voltages indicated in Fig. 4.

The features observed are explained well on a qualitative level by the fluctuation theory for barrier structures,[10] which states that in strongly compensated materials the tunneling of charge carriers in the space-charge region can be facilitated by the formation of pinholes, i.e., fluctuational accumulations of ionized donors and acceptors, which lead to local narrowing of the barrier. The tunnel currents restrict the increase in the barrier height and the surface lifetime. This factor becomes stronger as the gap width of the material decreases. For example, for $Cd_xHg_{1-x}Te$ with $x=0.2\times(E_g\simeq0.1$ eV) and $\tau_\nu=3\times10^{-6}$ s even a decrease in the surface lifetime to 5×10^{-7} s is observed after an aluminum layer is deposited. In our opinion, this accounts for the constancy or lowering of τ_s for strongly compensated samples of $Cd_xHg_{1-x}Te$ ($x=0.2-0.3$) after an aluminum layer is deposited on their surface.

4. CONCLUSIONS

The photoconductivity features observed for *n*- and *p*-type $Cd_xHg_{1-x}Te$ with a thin aluminum coating are interpreted well within a model which takes into account the photoconductivity in the surface space-charge region and the recombination occurring in it. For uncompensated and weakly compensated samples with $\tau_\nu=0.3\times10^{-6}-1.0\times10^{-6}$ s the bending of the surface bands increases after the deposition of an aluminum thin film. As a result of the small rate of surface recombination ($S\sim100$ cm/s), this results in an increase in τ_s and enhancement of the photosensitivity in the short-wavelength portion of the spectrum. No increase in τ_s is observed for the strongly compensated samples with $\tau_\nu>10^{-5}$ s. This is attributed to the significant tunneling and tunneling-recombination processes in the space-charge region. The values of the surface recombination rate and the surface mobility of the charge carriers have been determined from the results of combined measurements of the photoconductivity and the barrier photoelectromotive force for the two types of $Cd_xHg_{1-x}Te$ samples under the conditions of localization of the photoconductivity in the surface space-charge region. It is shown that the smaller values of the surface mobility compared with the bulk mobility can lead to a strong (up to 20-fold) decrease in the photosensitivity in the short-wavelength portion of the spectrum.

[1] N. R. Angin, V. V. Antonov, A. V. Voĭtsekhovskiĭ, and M. R. Pashkovskiĭ, Zarubezh. Elektron. Tekh. **5**, 49 (1984).
[2] E. P. Matsass, A. I. Vlasenko, E. A. Sal'kov, O. V. Snitko, and A. V. Lyubchenko, Ukr. Fiz. Zh. **26**, 670 (1981).
[3] A. Ya. Vul', K. V. Sanin, V. I. Fedorov, R.Yu. Khansevarov, and Yu. V. Shmartsev, Pis'ma Zh. Tekh. Fiz. **5**, 932 (1979) [Sov. Tech. Phys. Lett. **5**, 386 (1979)].
[4] É. K. Guseinov and N. D. Ismailov, Turkish J. Phys. **18**, 660 (1994).
[5] É. K. Guseĭnov and N. D. Ismaĭlov, Fiz. Tekh. Poluprovodn. **29**, 1790 (1995) [Semiconductors **29**, 934 (1995)].
[6] D. J. Peterman and D. J. Friedman, Appl. Phys. Lett. **42**, 886 (1980).
[7] V. A. Zuev, A. V. Sachenko, and K. V. Tolpygo, *Nonequilibrium Near-Surface Processes in Semiconductors and Semiconductor Devices* [in Russian], Radio i Svyaz', Moscow (1977).
[8] A. Ya. Vul', K. V. Sanin, A. T. Dideĭkin, Yu. S. Zinchenko, and A. V. Sachenko, Fiz. Tekh. Poluprovodn. **17**, 1471 (1983) [Sov. Phys. Semicond. **17**, 933 (1983)].
[9] V. V. Antonov, A. V. Voĭtsekhovskiĭ, A. V. Kriulin, D. A. Martsulov, M. S. Nikitin, A.Yu. Nikoforov, A. S. Petrov, and A. A. Umerenko, Mikroelektronika **16**, 407 (1987).
[10] M. E. Raĭkh and I. M. Ruzin, Fiz. Tekh. Poluprovodn. **21**, 456 (1987) [Sov. Phys. Semicond. **21**, 283 (1987)].

Translated by P. Shelnitz

Temperature dependence of the photoluminescence of porous silicon

P. K. Kashkarov, E. A. Konstantinova, S. A. Petrova, V. Yu. Timoshenko, and A. E. Yunovich

M. V. Lomonosov Moscow State University, 119899 Moscow, Russia
(Submitted June 26, 1996; accepted for publication October 25, 1996)
Fiz. Tekh. Poluprovodn. **31**, 745–748 (June 1997)

The photoluminescence of porous silicon in the temperature range from 300 to 400 K is investigated. It is shown that the experimental results are explained well on the basis of a model of the radiative recombination of excitons in silicon nanostructures. According to numerical estimates obtained by comparing the experimental and calculated curves, the exciton binding energy is ~0.2 eV. [S1063-7826(97)02506-4]

1. INTRODUCTION

The properties of luminescent porous silicon have been vigorously investigated in the last few years (see, for example, the reviews in Refs. 1–4). It has been found that one of the most important features of porous silicon is the existence of a nanostructure in the form of a net of silicon wires or partially isolated regions (fractals). The smallest dimensions of these fractals are of the order of 1–3 nm,[1] which is sufficient for the realization of an appreciable size-quantization effect.[2,3] The latter, as has been assumed in most studies, alters the optical properties of porous silicon, shifting the optical absorption edge toward larger quantum energies. However, there is no such clarity with respect to the luminescence, particularly the photoluminescence (PL) in porous silicon. Although many researchers believe that the radiative recombination of charge carriers takes place in a modified second quantization of the band structure of porous silicon,[1,2] there are many different opinions regarding the details of the recombination mechanism. The possibility of the direct recombination of free electrons and holes,[2] the binding of the latter in excitons that annihilate with the emission of optical quanta,[1,4] and radiative recombination on surface states of the nanostructure[1] have been considered. In addition, it has been theorized in several papers that the main contribution to the luminescence of porous silicon is made by optical excitation and excitation relaxation in a molecular coating of fractals.[1,3,4]

One of the important characteristics of the luminescence of porous silicon, knowledge of which would permit a choice between different models, is its temperature dependence. The so-called *S* band of PL in the visible region of the spectrum observed when the temperature of porous silicon is lowered below room temperature has been investigated in many studies.[1,4–9] However, the data obtained and their interpretation are very contradictory. The only general conclusion is, perhaps, that the PL intensity I_{PL} increases when the temperature T is lowered from 300 to 200–150 K. When porous silicon was cooled further, some investigators observed a drop in I_{PL},[5,6] which was attributed to a decrease in the population of the exciton singlet state and an increase in the population of the metastable triplet state.[6] In other studies, when T was lowered further, either no decrease in I_{PL} occurred,[8,9] or it was observed at $T<70$ K.[10] Some of the contradictions are possibly attributable to differences between the samples used. In fact, it was established in our work[11] that as the characteristic dimensions of the porous silicon nanostructure decrease and the original PL band shifts toward shorter wavelengths, the influence of the temperature on the PL intensity, as well as on the spectrum, decrease sharply. Another factor which influences the temperature variations of the PL can be the presence of defects which participate in nonradiative recombination.

The dependence of the *S* line of PL on the temperature as the latter is increased above room temperature was studied in Refs. 5, 9, and 12. However, it is difficult to correctly interpret these results, since the porous silicon was heated in air. Changes in the surface coating of the nanostructure which influence the PL are very likely in that case.[1] In fact, it has been reported that when freshly prepared porous silicon is heated above 500 K, the PL intensity drops irreversibly as a result of the loss of the hydrogen coating.[1,3] Similar effects probably occurred in the studies cited above in the form of a residual decrease in I_{PL} (Ref. 5) or its temperature hysteresis.[12]

Thus, there are presently no reliable data on the course of $I_{PL}(T)$ at temperatures above room temperature. At the same time, such information could be useful for identifying the PL mechanisms. For example, it was claimed in two theoretical studies[13,14] that excitons with binding energies E_{exc} can exist in nanometer-scale silicon wires. For wires of square cross section with a side d from 1.5 to 3.1 nm the value of E_{exc} varies from 140 to 70 meV, respectively.[14] Radiative transitions between exciton levels cause the PL of porous silicon. Appreciable values of E_{exc} permit excitons to exist at room temperature and can determine the thermal PL quenching.

The present work is devoted to an experimental investigation of the dependence of the PL of porous silicon when the temperature is raised from 300 to 420 K. The data obtained are analyzed on the basis of a model of the radiative recombination of excitons in quantum wires of a porous silicon nanostructure.

2. EXPERIMENTAL METHOD

Samples of porous silicon on a p-type Si substrate with a resistivity $\rho=10\ \Omega\cdot$cm and a surface having the (100) ori-

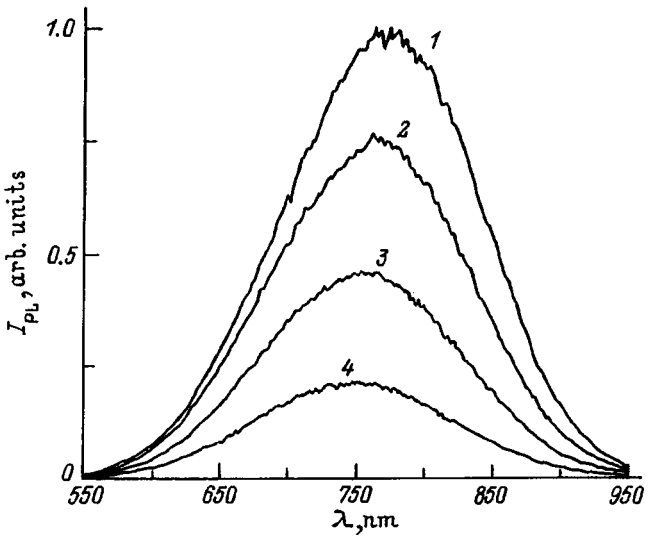

FIG. 1. Photoluminescence spectra of porous silicon. T, K: *1* — 300, *2* — 340, *3* — 370, 4 — 420.

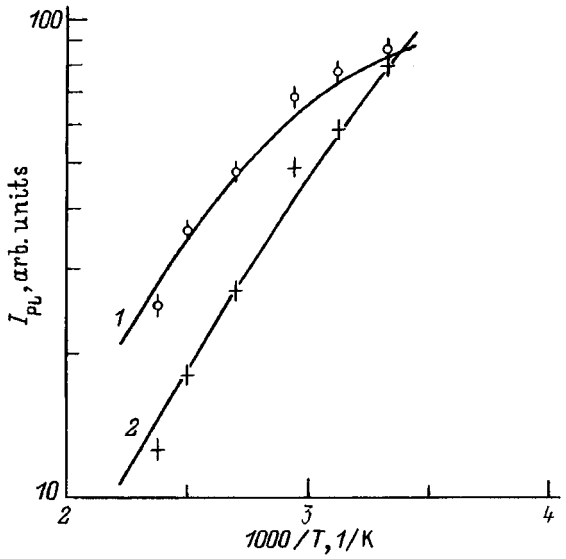

FIG. 2. Plots of the dependence of the photoluminescence of porous silicon on the reciprocal temperature for the wavelengths $\lambda_1=700$ nm (*1*) and $\lambda_2=850$ nm (*2*). Points — experimental data, curves — results of calculations according to (4) with the fitting parameters $\tau_{nr}=0.07$ μs, $E_{\text{exc1}}=0.2$ eV (*1*), and $E_{\text{exc2}}=0.18$ (*2*).

entation were investigated. Electrolytic anodization in a $HF-C_2H_5OH:H_2O$ mixture (1:2:1) at a current density $j=30$ mA/cm^2 over the course of $t=10$ min was used. Before the experiments were begun, the samples were stored in air for several months.

Immediately before the PL measurements, the porous silicon samples were subjected to prolonged vacuum treatment (at a residual pressure $P=10^{-3}-10^{-4}$ Pa) and heating at $T=450$ K. Such preliminary treatment made it possible to stabilize the adsorbed coating on porous silicon, whose variation can have a significant influence on the PL.[1] During the treatment employed, the weakly bound water molecules, in particular, are removed.[15] The latter can influence the recombination process in porous silicon under optical excitation.[11,16]

In the PL measurements excitation was effected by the output from an argon laser with a wavelength $\lambda=488$ nm and an intensity $I_0=0.1$ W/cm^2. As was previously established in Ref. 17, significant heating of the porous layer does not occur at such an excitation intensity. The experiments were carried out in a vacuum at $T=300-420$ K.

3. EXPERIMENTAL RESULTS AND DISCUSSION

The measured PL spectra of porous silicon at several fixed temperatures are presented in Fig. 1. It is seen that the PL spectrum of porous silicon at $T=300$ K is characterized by a broad band with a maximum at $\lambda_m\simeq 760$ nm (curve *1*). As the temperature is raised, the PL intensity decreases, and slight displacement (by ~ 10 nm) of the band toward shorter wavelengths is observed. The changes of porous silicon observed in the PL were completely reversible and reproducible in subsequent heat-treatment cycles.

According to the model proposed in Ref. 11, the PL band of porous silicon is the result of the superposition of the emission from nanostructures of different sizes. For simplicity we assume that the porous layer investigated is a set of wires with transverse dimensions of the order of several nanometers. This corresponds to the type of substrate that we used and the regime for obtaining porous silicon, in which the porous layer has a highly porous coralloidal structure.[18] Then, to within the error determined by the specific shape and orientation of the silicon wires,[19] each energy (wavelength) in the PL spectrum corresponds to a definite wire diameter d. If the binding energy of the excitons in the silicon wires is taken into account, then, in accordance with Ref. 14, the wavelengths $\lambda_1=700$ nm and $\lambda_2=850$ nm correspond to luminescence from wires with $d_1=2$ nm and $d_2=3$ nm, respectively.

Figure 2 presents plots of the dependence of the PL intensity on the reciprocal temperature in semilogarithmic coordinates for λ_1 and λ_2. A sharper temperature dependence is observed for λ_2, i.e., for nanostructures with the larger diameter d_2. Qualitatively, this corresponds well to smaller values of E_{exc} and can be explained within a model of exciton recombination. However, the $I_{\text{PL}}(1/T)$ curves cannot be approximated by exponential laws with the activation energies E_{exc} calculated in Ref. 14. In semilogarithmic coordinates the slopes of the corresponding straight lines are not consistent with experiment. It is also difficult to attribute the differences between the experimental plots of I_{PL} for λ_1 and λ_2 to the recombination of free charge carriers or radiative recombination in defects.

To quantitatively analyze the experimental data obtained, let us consider a system of intersecting silicon wires under the conditions of weak continuous excitation. We assume that there are two subsystems of noninteracting charge carriers, viz., free electrons and holes with a pair concentration n and excitons with a concentration N. We can then write the kinetic equations

$$dN/dt=Cn-AN-N/\tau_r,$$
$$dn/dt=g-Cn+AN-n/\tau_{nr}, \qquad (1)$$

where C and A are the probabilities for the binding of the carriers in excitons and thermal decay of the latter, respectively, g is the rate of the generation of electron-hole pairs, and τ_r and τ_{nr} are the times for radiative exciton annihilation and the nonradiative recombination of electron-hole pairs, respectively.

In (1) the contribution of the excitonic processes to the excitation of charge carriers upon the absorption of light is ignored in accordance with Ref. 14.

Under steady-state conditions ($d/dt=0$) we obtain

$$g=n/\tau_{nr}+N/\tau_r. \tag{2}$$

We presume Boltzmann statistics,

$$n/N=\exp(-E_{\text{exc}}/kT). \tag{3}$$

From (2) and (3) we obtain

$$N=g\tau_r/[1+(\tau_r/\tau_{nr})\exp(-E_{\text{exc}}/kT)]. \tag{4}$$

Let us use (4) to analyze the experimental dependence of the PL on the temperature. We assume that $I_{\text{PL}}\sim N\sim g$. The latter is in good agreement with our data[17] and the literature data,[1,4] indicating a linear dependence of the PL intensity on the excitation level up to 1 W/cm^2, at which photoinduced heating is already significant. Then, according to Ref. 14, the radiative recombination times for d_1 and d_2 are equal to $\tau_{r1}=70$ μs and $\tau_{r2}=170$ μs, respectively, and depend weakly on the temperature. We note that the literature does not offer any unequivocal and reliable data for τ_{nr}; therefore, it is a fitting parameter in our description.

Figure 2 presents curves calculated from Eq. (4). The best fit between the calculated curves and the experimental points was achieved for $\tau_{nr}=0.07$ μs, $E_{\text{exc1}}=0.2$ eV (for λ_1), and $E_{\text{exc2}}=0.18$ eV (for λ_2). The values for the latter exceed the values of the exciton binding energies obtained in Ref. 14: $E_{\text{exc1}}\simeq 0.1$ eV and $E_{\text{exc2}}\simeq 0.07$ eV. In our opinion, there are two possible reasons for such a disparity. First, as is seen from (4), the presence of an activation barrier to nonradiative recombination with an energy E_a of the form $\tau_{nr}\sim\exp(E_a/kT)$ makes a contribution to the thermal PL quenching. Second, the exciton binding energy in the silicon wires will be greater, if the difference between the dielectric constants of the wire material and the surrounding empty space is taken into account.[20] According to our estimates based on the calculations in Refs. 14 and 20, the latter factor causes an increase in the binding energy by a factor of 1.5–2, which is consistent with the results of the calculation in the model described. Further investigations are needed to make a final choice between the two possibilities presented above. Nevertheless, we note that the good agreement between the experimental points and the curves calculated within the exciton model supports the latter possibility.

Thus, the dependence of the PL of porous silicon in the temperature range from 300 to 420 K has been investigated experimentally in this work. The results obtained attest to behavior of the thermal PL quenching that is more complicated than a simple thermal-activation law and can be explained within an exciton model of the luminescence of porous silicon.

This work was supported as part of the Physics of Solid-State Nanostructures Program (Project No. 1-064).

[1] K. Jung, S. Shih, and D. Kwong, J. Electrochem. Soc. **140**, 346 (1993).
[2] M. S. Bresler and I. N. Yassievich, Fiz. Tekh. Poluprovodn. **27**, 873 (1993) [Semiconductors **27**, 475 (1993)].
[3] Ṣ. V. Svechnikov, A. V. Sachenko, G. A. Sukach, A. M. Evstigneev, and É. B. Kaganovich, Optoelektron. Poluprovodn. Tekh. **27**, 3 (1994).
[4] J. B. Xia and K. W. Cheah. Appl. Phys. A **59**, 227 (1994).
[5] C. Perry, F. Lu, F. Namavar *et al.*, Appl. Phys. Lett. **60**, 3117 (1992).
[6] G. Mauckner, K. Thonke, T. Baier, T. Walter, and R. Sauer, J. Appl. Phys. **75**, 4167 (1994).
[7] J. Oswald, J. Pastrnak, A. Hospodkova, and J. Pangrac, Solid State Commun. **89**, 297 (1994).
[8] G. W. 't Hooft, Y. A. R. R. Kessener, G. L. J. A. Rikken, and A. H. J. Venhuizen, Appl. Phys. Lett. **61**, 2344 (1992).
[9] A. A. Lebedev, A. D. Remenyuk, and Yu. V. Rud', Fiz. Tekh. Poluprovodn. **27**, 1846 (1993) [Semiconductors **27**, 1017 (1993)].
[10] T. Suemoto, K. Tanaka, and A. Nakajima, Phys. Rev. B **49**, 11 005 (1994).
[11] P. K. Kashkarov, V. Yu. Timoshenko, E. A. Konstantinova, and S. A. Petrova, Fiz. Tekh. Poluprovodn. **28**, 100 (1994) [Semiconductors **28**, 60 (1994)].
[12] V. G. Gaĭvoron, Yu. F. Ogrin, T. P. Kolmykova, and V. I. Sidorov, Pis'ma Zh. Tekh. Fiz. **20** (8), 70 (1994) [Tech. Phys. Lett. **20**, 336 (1994)].
[13] P. D. J. Calcott, K. J. Nash, L. T. Canham, M. J. Kane, and D. Brumhead, J. Phys.: Condens. Matter. **5**, L91 (1993).
[14] G. D. Sanders and Y.-C. Chang, Phys. Rev. B **45**, 9202 (1992).
[15] V. F. Kiselev and O. V. Krylov, *Electronic Phenomena in Adsorption and Catalysis on Semiconductors and Dielectrics*, Springer-Verlag, Berlin–New York (1987).
[16] T. Dittrich and V. Yu. Timoshenko, J. Appl. Phys. **75**, 5436 (1994).
[17] T. Dittrich, P. K. Kashkarov, E. A. Konstantinova, and V. Yu. Timoshenko, Thin Solid Films **255**, 74 (1995).
[18] R. L. Smith and S. D. Collins, J. Appl. Phys. **70**, R1 (1992).
[19] C. Delerue, G. Allan, and M. Lanoo, Phys. Rev. B **48**, 11 024 (1993).
[20] V. S. Babichenko, L. V. Keldysh, and A. P. Silin, Fiz. Tverd. Tela **22**, 1238 (1980) [Sov. Phys. Solid State **22**, 723 (1980)].

Translated by P. Shelnitz

Use of a low-temperature emitter in investigating the spectral characteristics of infrared photodetectors

V. V. Vasil'ev, Yu. P. Mashukov, and V. N. Ovsyuk

Institute of Semiconductor Physics, Russian Academy of Sciences, Siberian Branch, 630090 Novosibirsk, Russia

(Submitted July 8, 1996; accepted for publication October 25, 1996)
Fiz. Tekh. Poluprovodn. **31** 749–752 (June 1997)

A method for determining the cutoff wavelength λ_c of the photosensitivity spectrum of an infrared photodetector by measuring two photosignals obtained from two blackbody sources of radiation at different temperatures is examined. It is shown that it is expedient to use blackbody sources at low temperatures for $\lambda \simeq 10-14$ μm. The photosignal of an element of a p-type $Cd_xHg_{1-x}Te$ photodiode array with $x=0.225$ is measured for a blackbody, whose temperature is varied in the range 150–450 K. The values of λ_c for several temperature ranges are calculated from a comparison of the experimental and theoretical curves. The corrections to λ_c associated with the deviation of the real photosensitivity spectrum from the ideal spectrum are calculated. Arguments regarding the selection of the optimum temperature ranges for the emitters are advanced.
[S1063-7826(97)02606-9]

Multielement photodetection devices intended for operation in the mid-IR region (5–14 μm) have become widespread.[1] When the photosensitivity of such devices is measured, it is necessary to deal with the following factors: a) the small value of the area of an individual element; b) the appreciable disparity between the doped region and the photocarrier collection area; c) the possible mutual influence of the elements on one another.

Exact measurements of the photoelectric characteristics of such structures using a monochromator is often difficult because of the complexity of the equipment and because of the small value of the radiated power falling on an individual element. Consequently, it has also become common to employ a blackbody directly, without a monochromator, for irradiation. In particular, a simple method was proposed in Ref. 2 for determining the wavelength of the photosensitivity edge using two emitters at different temperatures. A special feature of the work just cited is that the photosensitivity was investigated using a blackbody, whose temperature was varied over a broad range, including values below room temperature. The use of a low-temperature emitter to investigate long-wavelength photodetectors with a photosensitivity edge at $\lambda_c \sim 10$ μm and longer wavelengths has definite advantages. At a sufficiently low temperature, at which the emissivity maximum is located at a wavelength longer than λ_c, a sharper dependence of the photosignal on λ_c is observed.

To determine λ_c it is convenient to take the ratio between the photosignals at two emitter temperatures. Several parameters can then be eliminated: the area of the photodetector, the reflection losses, and the quantum efficiency. The ratio of the two photosignals at two emitter temperatures as a function of λ_c is plotted in Fig. 1. It was assumed in the calculations that the photoresponse is proportional to the number of photons having a wavelength shorter than λ_c, and this number was determined by integrating Planck's formula:[3,4]

$$Q(\lambda_c)=\int_0^{\lambda_c}\frac{c_1' d\lambda}{\lambda^4(e^{c_2/\lambda T}-1)}, \tag{1}$$

where $c_1'=1.88365\times10^{23}$ $\mu m^3/s\cdot cm^2$ and $c_2=1.43879\times10^4$ $\mu m\cdot K$.

We see that the plots in Fig. 1 are sufficiently sharp to determine λ_c very accurately, especially at reduced temperatures. However, the actual accuracy depends on how closely the particular spectral dependence of the power-current sensitivity corresponds to the ideal dependence and on how accurately the measurements can be performed. To perform the corresponding analysis, we consider Figs. 2 and 3, which present the data from measurements of one of the elements of a 2×64 photodiode array fabricated on a p-type $Cd_xHg_{1-x}Te$ substrate with $x=0.225$, in which $n-p$ junctions were formed by ion-implanting boron.

EXPERIMENTAL METHOD

Figure 2 shows the true spectral power-current sensitivity characteristic, which differs significantly from the ideal curve. The measurements were performed at a sample temperature equal to 78 K. Figure 3 presents the experimental dependence of the photocurrent on the emitter temperature, as well as several theoretical plots, which were constructed under the same assumptions as the curves in Fig. 1. In addition, it was assumed that the reflection losses amount to 30%, that the carrier collection area is equal to the area of the $p-n$ junction (50×70 μm^2), that the emissivity of the blackbody is $\alpha=0.95$, and that the effective angle of sight is $2\theta_{\text{eff}}=15°$. The measurements were performed in a nitrogen cryostat, whose working volume accommodated a sample, a model of a blackbody, and a device for displacing the probe. The blackbody was made from brass and had a radiating surface with a diameter of 8 mm, which was blackened by the adhesive BF-2 mixed with porous graphite. The heater used was a copper-wire winding, which was glued to the blackbody by the same adhesive to achieve better thermal

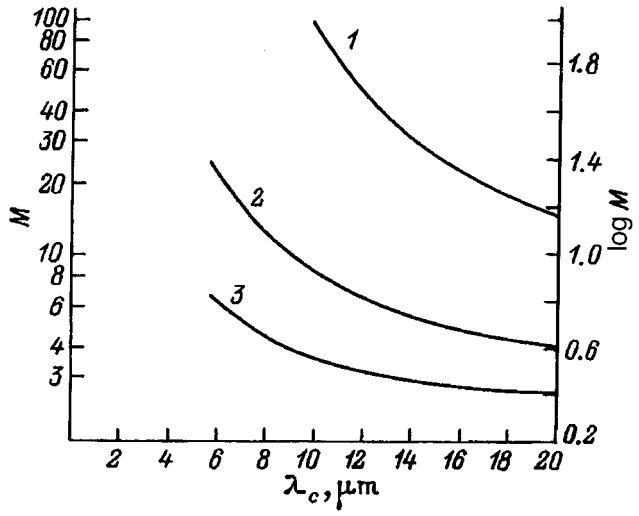

FIG. 1. Theoretical plots of the ratio between the photosignals of an ideal photon photodetector for a perfect blackbody at two temperatures as a function of the cutoff wavelength of the photodetector: *1* — 250 and 150 K; *2* — 350 and 250 K; *3* — 450 and 350 K.

contact. Since the surface of the sample was at an angle φ relative to the axis of the emitter, the irradiance should be determined using the expression

$$\sin^2\theta_{\text{eff}} = \sin^2\theta \cdot \cos\,\varphi, \tag{2}$$

where θ and φ are the angles shown in the inset in Fig. 3. Two positions of the blackbody relative to the sample were used: a far position ($2\theta_{\text{eff}} = 15°$) and a near position ($2\theta_{\text{eff}} = 49°$). In Fig. 3 either the experimental values of the photocurrent for the far position or appropriately recalculated values for the near position are plotted. The near position of the source was employed for more exact measurements at low temperatures.

A movable cooled shield was positioned between the emitter and the array element for use in the measurements of the photocurrent. The lower limit of the measurable photocurrent values was $\sim 1\times10^{-10}$ A. The temperature of the blackbody was measured using a copper-constantan thermocouple soldered to it, whose other end was placed in liquid nitrogen.

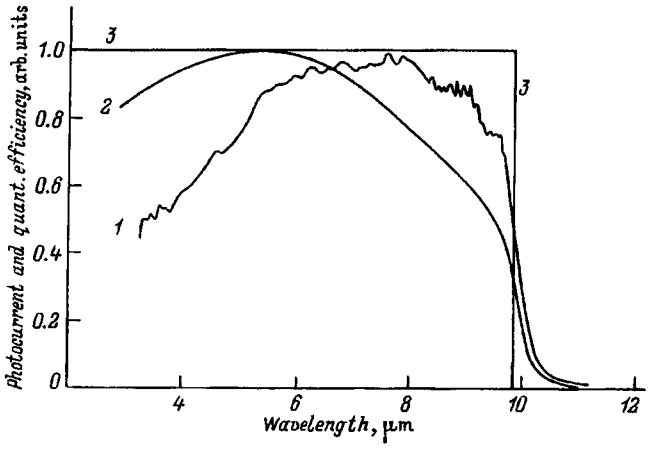

FIG. 2. Spectral dependence of the power–current sensitivity (*1*) for one of the elements of a 2×64 array on p-type $Cd_xHg_{1-x}Te$ with $x=0.225$, spectral dependence of the quantum efficiency taken for the calculations (*2*), and ideal spectral dependence of the quantum yield.

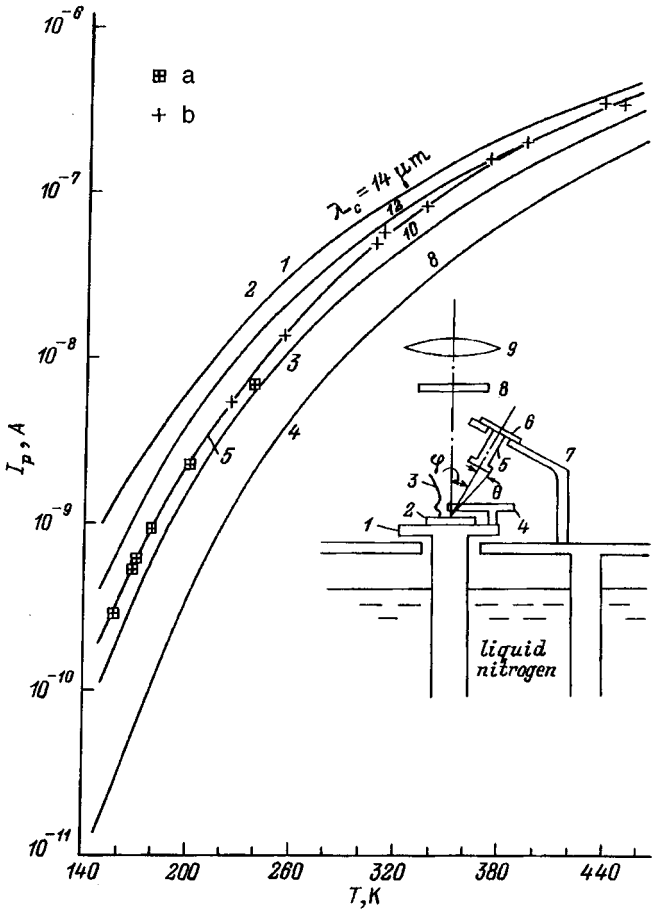

FIG. 3. Dependence of the photocurrent of one of the elements of a photodiode array on the emitter temperature: *1–4* — calculated plots, *5* — experimental plot; a — near position of the emitter; b — far position. The measurement setup is shown in the inset: *1* — sample stage, *2* — sample, *3* — regulated probe, *4* — movable shield, *5* — emitter, *6* — PTFE thermal insulator, *7* — cold screen, *8* — one of three glass windows in the cryostat, *9* — objective lens of a binocular microscope.

DISCUSSION OF RESULTS

Let us compare the theoretical curves shown in Fig. 3 with the experimental curve. Since we know from Fig. 2 that $\lambda_c = 10\ \mu$m, we make the comparison for just that curve. The fact that the experimental curve is above the theoretical curve over its entire course can be attributed to a photocarrier collection area that is larger than presumed. If the difference

TABLE I.

T, K	N_p/N_i
150	0.705
200	0.720
250	0.741
300	0.767
350	0.792
400	0.811
450	0.828

for moderate temperatures is taken, we find that the carrier collection area is 45% greater than the area of the doped region. This value is too small for there to be overlap between two neighboring elements. However, additional measurements show that there is, in fact, some optical coupling between the array elements: the sum of the photocurrents for two elements located next to one another was somewhat smaller when they were switched on simultaneously than when they were switched on separately. At the same time, there is no inverse conducting channel coupling these two elements.

The determination of λ_c from curves *1–3* in Fig. 1 gives the values $\lambda_c = 11.0$, 9.7, and 10.2 μm, respectively. The spread amounts to 1.3 μm or 13% of the measured value. In our opinion, this result is sufficiently satisfactory, if it is taken into account that there is a whole series of factors that promote the appearance of errors: the large dynamic range of the measured quantity, the possible dependence of the emissivity of the source on the wavelength and the temperature, and the possible instability of the properties of the photodiode.

Let us evaluate the error in λ_c associated with the difference between the real and ideal spectral dependences. On the basis of Fig. 2, we introduce the quantum efficiency $\eta(\lambda)$. Since the photocurrent is proportional to the number of photons and the quantum efficiency, and the number of photons is, in turn, proportional to λ (for the same radiated power), we can write

$$\eta(\lambda) = k \frac{I_p(\lambda)}{\lambda}, \tag{3}$$

where k is a certain coefficient, which is determined from the normalization condition. We normalize $\eta(\lambda)$ to unity at the maximum (Fig. 2). Multiplying $\eta(\lambda)$ by Planck's function and calculating the corresponding integral, we obtain the number of photoelectrons. We next calculate the number of photoelectrons in the ideal case, i.e., under the assumption that $\eta(\lambda) = 1$ for $\lambda < \lambda_c$ and 0 for $\lambda > \lambda_c$ ($\lambda_c = 9.8$ μm), and then we take the ratio of the number of photoelectrons obtained in the former case N_p to the number of photoelectrons obtained in the latter case N_i (see Table I). It is seen that as the emitter temperature is lowered, the disparity between the results for the ideal and real spectral dependences increases. Consequently, if we would construct the curves in Fig. 1 for the real spectrum, they would be above the curves drawn, and the values of λ_c determined from the experimental data in Fig. 3 would consequently be higher. To calculate the correction $\Delta\lambda_c$ we proceed in the following manner: 1) we determine the slope of the curve selected in the vicinity of $\lambda_c = 10$ μm from Fig. 1, $f' = (\Delta \log M/\Delta\lambda_c)$; 2) we determine the logarithm of the ratio between the values for the respective pair of temperatures, $\delta \log M$; 3) we determine $\Delta\lambda_c = (\Delta \log M/f')$. The calculations give the following values for λ_c with allowance for the correction instead of the former values: 11.2, 10.0, and 10.8 μm for curves *1–3* in Fig. 1, respectively.

Let us consider the choice of the optimum temperature range in the method for determining λ_c under consideration. The condition for the maximum of the derivative of the number of photons with respect to λ_c, i.e., $dQ(\lambda_c)/d\lambda_c$, could serve as the optimality criterion. This derivative is equal to the integrand in Eq. (1), for which the maximum is determined by Wien's law:[3]

$$\lambda_{\max} \cdot T = a', \tag{4}$$

where $a' = 3669.73 \mu\text{m} \cdot \text{K}$.

Thus, in our case the corresponding temperature is equal to about 370 K. However, as the calculations show, the relative variation of the number of photons, i.e., the quantity $(1/Q(\lambda_c))(dQ(\lambda_c)/d\lambda_c)$, increases continuously as the temperature decreases from the value just indicated, so that the dependence on λ_c is displayed increasingly more clearly. Therefore, it is apparently reasonable to lower the temperature below the value indicated until new restrictive factors, such as the small amplitude of the effective signal, the appearance of false signals from other parts of the cryostat, the influence of the form of the true spectral dependence, and the presence of appreciable photosensitivity beyond the edge, begin to operate (we recall that at an emitter temperature of 150 K only 0.3% of all the photons correspond to the range $\lambda < 10$ μm). It is perfectly possible that the best value of λ_c that we obtained for curve *2* in Fig. 1, which covers the temperature range 250–350 K, confirms the foregoing statement.

CONCLUSIONS

It can be concluded from the analysis performed and the experimental data that the determination of λ_c by the method used in this work does not give us any guarantee that we will obtain a high absolute accuracy, which can be estimated as ± 0.5 μm in the vicinity of ~ 10 μm. In fact, the very concept of λ_c for a real spectrum is not fully defined. However, utilization of the simple design of a model of a perfectly blackbody located within the cryostat and the simplicity of the measurement method are remarkable. The method can certainly be very effective in measuring a large collection of elements (an array, a matrix), and the relative accuracy will already be far higher ($\sim \pm 0.1$ μm). As in Ref. 2, there should, of course, be two emitters with different temperatures and a device for mechanically displacing them.

We thank A. Suslyakov for measuring the photosensitivity spectrum, as well as for some useful discussions.

[1] A. Rogalski and I. Piotrowski, Prog. Quantum Electron. **12**, 87 (1988).
[2] R. M. Liberati, N. Sparvieri, and M. Marini. Ingr. Phys. **31**, 361 (1991).
[3] R. D. Hudson Jr., *Infrared System Engineering*, Wiley, New York (1969) [Russ. transl., Mir, Moscow (1972)].
[4] *Tables of Physical Constants. A Handbook* [in Russian], I. K. Kikoin (Ed.), Atomizdat, Moscow (1976).

Translated by P. Shelnitz

Laser-stimulated displacement of the $p-n$ junction boundary in direct-gap GaAsP structures

G. A. Sukach

Institute of Semiconductors Physics, Ukrainian National Academy of Sciences, 252028 Kiev, Ukraine
(Submitted July 31, 1996; accepted for publication October 25, 1996)
Fiz. Tekh. Poluprovodn. **31**, 753–756 (June 1997)

Displacement of the $p-n$ junction boundary in direct-gap GaAsP structures exposed to intense, strongly absorbed laser radiation was observed experimentally. It is shown that this phenomenon is caused primarily by the diffusion fluxes of zinc ions from the p-type region into the n-type region, which are manifested as fields of thermoelastic stresses created by significant temperature gradients. The dependences of characteristics of $p-n$ junction displacement on the laser irradiation parameters are established. © *1997 American Institute of Physics.* [S1063-7826(97)02706-3]

Regulation of the parameters of semiconductor devices after their fabrication is of great current interest because of the requirements imposed by modern micro- and optoelectronics, particularly, on the quality of their rectifying boundaries ($p-n$ junctions) and nonrectifying (low-resistivity ohmic) contacts. The processes and mechanisms involved in the displacement of $p-n$ junctions, which are generally fabricated by isothermal diffusion, in external thermal, electric, optical, and radiation fields has been the subject of many studies (see, for example, Refs. 1–4). One common feature of all these studies is that the $p-n$ junctions were displaced in stationary (gradient-free) temperature,[1] photon,[2] and radiation[3] fields. The driving force for displacement of the $p-n$ junction was generally the original dopant concentration gradient.[1–5] In addition, the displacement of a $p-n$ junction caused by external stationary fields took place along the dopant gradient.

In our opinion, the investigation of the processes and mechanisms involved in the displacement of $p-n$ junctions in external gradient fields created, in particular, by exposing the semiconductor structure to strongly absorbed laser radiation would be more interesting. In this case a qualitatively new situation can arise due to the large number of possibilities for regulating the parameters of a semiconductor structure.

Our goal was to experimentally study the processes and mechanisms involved in the displacement of $p-n$ junctions in external fields created by a temperature gradient and the thermoelastic stresses associated with it.

SAMPLES, METHODS, AND EXPERIMENTAL RESULTS

We investigated experimental samples of GaAsP $p-n$ junctions grown by a hybrid chloride technology[6] on n-type GaAs substrates with an n-type GaAsP intermediate layer of variable composition and an n-type layer of $GaAs_{1-x}P_x$ ($x \simeq 0.35-0.38$) of constant composition and with a total thickness $d \simeq 10$ μm. The tellurium concentration in them (N_d) corresponded to the electron density $n_0 = 2-4\times10^{17}$ cm^{-3}. A $p-n$ junction was created at a depth of $w_0 \simeq 2.5$ μm by the isothermal diffusion of the acceptor impurity zinc (with a concentration N_a) from the gas phase into the preliminarily annealed n-type $GaAs_{1-x}P_x$. In order that the space-charge region would be located predominantly in the p-region, the structure was doped in such a manner that the surface concentration of zinc in the contact region would not exceed 4×10^{18} cm^{-3} and the hole concentration would be $p_0 \simeq 1-2\times10^{18}$ cm^{-3} in the bulk and would decrease to $p_0 = n_0$ at the $p-n$ junction boundary. The surface area of the sample was 0.35×0.35 mm^2.

The source of the temperature gradient was the second harmonic of a Q-switched neodymium laser (the output wavelength was $\lambda = 0.53$ μm, the pulse duration was $t_p = 40$ ns, and the absorption coefficient was $\alpha \geqslant 10^5$ cm^{-1}). The entire sample surface was irradiated in the direction perpendicular to the plane of the $p-n$ junction by a photon flux that does not cause destruction of the surface of the material (the energy in a single pulse was $E \lesssim 10^{-2}$ J/cm^2). To eliminate the influence of the electric field of the potential barrier on the dopant diffusion processes, the $p-n$ junctions were subjected to laser irradiation under short-circuit conditions.

The profile of the dominant impurity in the p-region, which contains information on the depth of the $p-n$ junction, was investigated by analyzing differential capacitance-voltage characteristics (dC/dV characteristics) and by the two-frequency method for measuring the capacitance of a reverse-biased diode at the difference frequency.[7,8] Control experiments were performed to determine the position of the $p-n$ junction using the oblique section technique and scanning electron microscopy.

Figure 1 presents the concentration profile of the dominant impurity in the high-resistivity p-region ($N_a^* = N_a - N_d \simeq p_0$) before and after laser irradiation ($E = 2\times10^{-2}$ J/cm^2) of a GaAsP $p-n$ structure. For clarity the distances were measured from the upper surface of the epitaxial p-layer. The figure contains a schematic representation of the characteristic zinc-doping front, which consists of a high-speed high-concentration part and two ''plateaus.''[5] The position of the $p-n$ junction was determined from the point of passage from the space-charge region to the completely compensated region, i.e, the rapid descent on the impurity profile, which changes into a straight

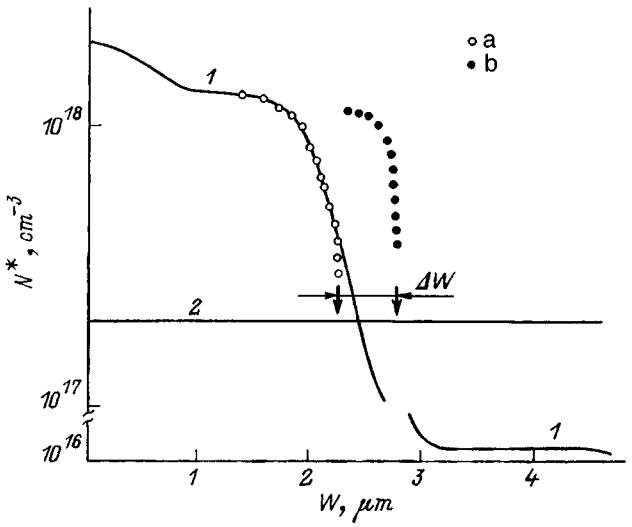

FIG. 1. Distribution profiles of zinc before (a) and after (b) the irradiation of a $p-n$ junction by a laser pulse. Irradiation regime: $\lambda=0.53$ μm, $E=2\times10^{-2}$ J/cm^2, $t_p=4\times10^{-8}$ s, $K=100$. Solid lines – typical distribution of zinc (*1*) and tellurium (*2*) in the original samples.

drop (in Fig. 1 it is marked by vertical arrows). It is seen that after irradiation by $K=100$ pulses, the $p-n$ junction is displaced into the n-region over a distance $\Delta w=0.550\pm0.002$ μm (from a depth of $w_0=2.25$ μm). In addition, after laser irradiation, an increase was observed in the steepness of the $N_a^*(w)$ curve (variation of the energy had little effect on the shape of the profile), and N_a^* decreased only slightly on the portion of the curve corresponding to saturation. Figure 2 presents plots of the dependence of the magnitude of the displacement Δw on the energy and number of irradiation pulses. A linear relationship between Δw and E, as well as a linear dependence of Δw on K, which becomes sublinear (at $K>100$), are observed. We note that a tendency for motion of the $p-n$ junction in the same direction (into the n-$GaAs_{1-x}P_x$ layer) was observed in all cases.

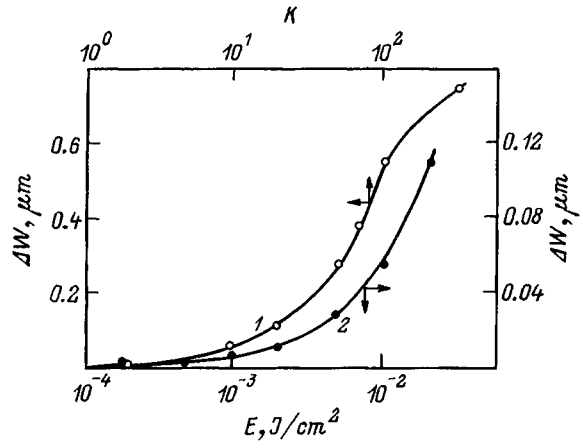

FIG. 2. Dependence of the magnitude of the displacement of the $p-n$ junction into the n-region on the number of laser irradiation pulses for $E=2\times10^{-2}$ J/cm^2 (*1*) and on the pulse energy for $K=20$ (*2*).

DISCUSSION OF THE EXPERIMENTAL RESULTS

The constancy of the sign and the linear character of the $\Delta w(E)$ curve are evidence that the mechanism for displacement of the $p-n$ junction upon laser irradiation remains the same over the entire range of variation of the energies (up to disintegration of the materials). It is known that in the range of energies that do not lead to disintegration of a semiconductor material, laser irradiation is accompanied by the coherent generation of active hypersonic waves, a plasma, defects of the vacancy and interstitial types, lowering of the potential barriers, charge exchange involving impurity atoms, and heating. However, in our case either one particular mechanism is predominant, or a set of mechanisms act in one direction.

Since the $p-n$ junctions were irradiated in the short-circuited state, the main external factors determining their displacement are gradient, fields, mechanical fields (due to the thermoelastic stresses), or temperature fields (the factors of an electrical nature are reduced to a minimum).

The irradiation of a semiconductor structure by an intense photon flux from the region of characteristic absorption leads to the creation of a nonuniform density of point defects of the vacancy and interstitial types in the bulk of the material, which always leads to distortion of the crystal structure and the appearance of internal mechanical stresses in a continuous solid with limited possibilities for expansion. Such a situation promotes anomalous sharp acceleration of the impurity diffusion processes.[9] The generation of hypersonic waves also acts in this direction. The impurity atoms diffuse under the action of the mechanical force F_G of plastic deformation,[10,11]

$$F_G=\frac{4}{3}\frac{1-\nu^2}{(1-2\nu)^2}\,G(\Omega_i-\Omega_0)\nabla(\beta T), \tag{1}$$

where ν is Poisson's ratio, G is the shear modulus, Ω_0 and Ω_i are the elementary volumes of the host and the impurity, respectively, ∇ is Poisson's operator, β is the coefficient of linear thermal expansion of the semiconductor material, and T is the temperature.

On the other hand, under nonuniform heating caused by enormous temperature gradients, forces which transport impurity atoms from hot to cold sites appear in a solid. The appearance of thermal diffusion of an acceptor aluminum impurity deposited on an n-Si surface in a temperature-gradient field was observed in Ref. 12. The expression for the thermal force (F_T) acting on an impurity atom has the form[11]

$$F_T=-\frac{1}{3}\Omega_0 C\langle\sigma_0/\sigma_i\rangle\nabla T, \tag{2}$$

where C is the specific heat of the material, and $\langle\sigma_0/\sigma_i\rangle$ is the averaged ratio between the photon scattering cross sections on the host and the impurity, respectively.

Here it should be noted that the physical formalisms by which thermodynamic and strain-induced factors act on an impurity atom are identical.

The rate of motion of impurity atoms in fields created by thermoelastic stresses or a temperature gradient[5,11]

$$V=\frac{D}{kT}(F_G+F_T) \tag{3}$$

depends on the ratio between F_G and F_T. In (3) D is the diffusivity.

Estimates of F_G and F_T using (1) and (2) showed that for the parameters of the laser pulses presented above the absolute value of the elastic deformation force always exceeds the thermal force. Therefore, the direction of flow of the dopant depends on the sign of the difference $\Omega_i-\Omega_0$.

Let us analyze the data on the variation of the Zn distribution profile after laser irradiation (Fig. 1). Since, on the one hand, the diffusion flux J is related to the dopant concentration N by the direct proportionality[5]

$$J=VN \tag{4}$$

and, on the other hand, it is seen from (1)–(3) that $V\sim$ grad T, i.e., in the region where the largest values of N and grad T are attained, the rate of motion of the acceptors (zinc ions in gallium sites, i.e., Zn_{Ga}^-) is maximal. Therefore, as the integral flux of laser radiation increases, an increase in the steepness of the $N^*(\Delta w)$ profile will be observed (see Fig. 1).

Let us consider the mechanisms for the displacement of a $p-n$ junction observed when a nonuniformly doped GaAsP structure is laser-irradiated by strongly absorbed light in comparison to the results of a numerical analysis of the processes occurring in a uniformly doped semiconductor upon pulsed heating.[11]

In our case the ionic radius of the Zn_{Ga}^- acceptors is somewhat greater than the covalent radius of the Ga atoms,[13] i.e., $\Omega_i>\Omega_0$. Therefore, the Zn_{Ga}^- ions will move in the direction of the temperature gradient. Numerical evaluations showed that the temperature gradient, which reaches values of 10^5 K/cm (Refs. 11 and 12), is located at a distance $l_0=(4\lambda\rho^{-1}C^{-1}t_p)^{1/2}\leqslant 0.1$ μm from the p-GaAsP surface. This inequality is enhanced when the sharp temperature dependence $\lambda\sim T^{-m}$, where $m=1-2$ (Ref. 14), is taken into account. Consequently, the Zn_{Ga}^- ions move from the l_0 plane under the action of the summed force F_G+F_T, first, toward the surface of the semiconductor structure, where they form a heavily doped surface p^+-layer[1)] and, second, into the semiconductor structure, where they promote diffusion of the zinc profile and, therefore, displacement of the $p-n$ junction from the surface into the n-region of the GaAsP structure.

Since the concentration of zinc interstitials (Zn_i^+) in the p-region of a GaAsP structure is two or more orders of magnitude smaller than the concentration of Zn_{Ga}^- ions,[5] their contribution to the total flux can be neglected. However, we note that since the ionic radius of Zn_i^+ is smaller than the covalent radius of Ga,[13] the Zn_i^+ front moves against the direction of the temperature gradient, and this impurity diffuses toward the l_0 plane. This point is especially important for the second plateau on the zinc profile, which is caused by a dissociative diffusion mechanism.[5] In this case the zinc interstitials which penetrated far into the n-region of the GaAsP structure in the fabrication stage diffuse toward the $p-n$ junction in a considerably weaker temperature gradient. As they move toward the surface, they encounter gallium vacancies appearing as a result of the laser irradiation and thereby promote movement of the $p-n$ junction into the n-region, although to a considerably lesser degree than do the Zn_{Ga}^- ions.

As for the movement of the other dopant, viz., tellurium (Te_{As}^+ or Te_P^+ ions), whose concentration is constant across the entire thickness of the GaAsP structure in the original samples and remains unchanged ($N_d\simeq 2\times 10^{17}$ cm^{-3}), its ionic radius is greater than the covalent radii of As (1.21 nm) and P (1.10 nm).[13] Therefore, tellurium diffuses in the direction of the temperature gradient. The motion of the tellurium ions toward the p-surface scarcely makes any contribution (because $N_{Zn}\gg N_{Te}$) to the specific junction resistance. The motion of tellurium away from the l_0 plane and toward the n-GaAsP region is manifested most profoundly near the boundary between the n- and p-regions. Such a situation leads to only slight displacement of the $p-n$ junction toward the p-surface of the semiconductor structure (because of the small magnitude of the T gradient in the vicinity of the $p-n$ junction). It also promotes a slight increase in the minimum concentration of the dominant impurity detected on the boundary between the space-charge region and the compensated region after laser irradiation (which is marked by vertical arrows in Fig. 1). Since $N_{Zn}\gg N_{Te}$ in the p-region and since there is a difference between the temperature gradients in the regions where the diffusion processes associated with these impurities are most strongly displayed, the flux of zinc ions is considerably stronger than the flux of tellurium ions. As a result, the $p-n$ junction boundary should move into the n-GaAsP region, as is observed experimentally (see Figs. 1 and 2). In this case an increase in the temperature and the thermoelastic stresses causes the diffusivities of the impurities to significantly surpass those not only for the stationary case, but also for the case of the diffusion of these impurities in a liquid (by three to four orders of magnitude[9]).

An estimate of the rate of motion of zinc ions in a field of elastic stresses gave $V\simeq 14$ cm/s. We note that in the theoretical study[11] the maximum value of the rate of migration of impurity copper atoms was $V\simeq 180$ cm/s. However, according to the results of the numerical calculations in Ref. 11, the velocity dropped with increasing distance from the region of the maximum temperature gradient. Thus, the experimental values of V that we obtained closely fit the model of the thermoelastic interaction of the impurity atoms with the semiconductor lattice.

Movement of the $p-n$ junction boundary into the bulk of the n-$GaAs_{1-x}P_x$ region was observed in Ref. 3 following the irradiation of direct-gap structures by a stream of fast neutrons, which penetrated the semiconductor material with practically no attenuation. However, the physical mechanisms of the motion of the $p-n$ junctions in these two cases are different. In the case of neutron irradiation the main reason for the movement of the $p-n$ junction is the uniform generation of gallium vacancies throughout the entire volume of the semiconductor structure. Such a situation promotes the migration of Zn_{Ga}^- ions under the effect of the concentration gradient and the ion fluxes associated with the intrinsic electric field. In the case of laser irradiation by strongly absorbed light, there is an exponential decrease in

the intensity of the radiation penetrating the sample and, therefore, in the concentration of the vacancies created by it, particularly of gallium. Therefore, the contribution of the mechanism associated with the generation of gallium vacancies weakens (about 10^{10}-fold at a depth of $w_0 = 2.25$ μm) as the geometric boundary between the p- and n-regions is approached.

Thus, it can be concluded on the basis of this research that the main mechanism underlying the motion of a $p-n$ junction during irradiation by strongly absorbed light is associated with the thermoelastic stresses, which provide for anomalously accelerated diffusion of the zinc ions during plastic deformation. The phenomena discovered have demonstrated the possibility of obtaining $p-n$ junctions with a series of assigned properties.

[1)]This is evidenced by the decrease in the surface cracking resistance after laser irradiation of a GaAsP $p-n$ junction measured on test structures.

[1] É. L. Savin and B. I. Boltaks, Fiz. Tekh. Poluprovodn. **5**, 1331 (1971) [Sov. Phys. Semicond. **5**, 1173 (1972)].

[2] B. I. Boltaks, S. M. Gorodetskiĭ, T. D. Dzhafarov, G. S. Kulikov, and R. Sh. Malkovich, Fiz. Tverd. Tela **13**, 3420 (1971) [Sov. Phys. Solid State **13**, 2877 (1972)].

[3] G. A. Sukach, Fiz. Tekh. Poluprovodn. **27**, 697 (1993) [Semiconductors **27**, 461 (1993)].

[4] A. V. Dvurechenskiĭ, G. A. Kachurin, E. V. Nidaev, and L. S. Smirnov, *Pulsed Annealing of Semiconductor Materials* [in Russian], Nauka, Moscow (1982).

[5] B. I. Boltaks, *Diffusion and Point Defects in Semiconductors* [in Russian], Nauka, Moscow (1972).

[6] M. M. Artamonov, E. N. Vigdorovich, and V. A. Fedorov, Elektron. Tekh. Mater. (8), 63 (1977).

[7] L. S. Berman, *Capacitance Methods for Investigating Semiconductors* [in Russian], Nauka, Leningrad (1972).

[8] I. B. Puzin, Prib. Tekh. Éksp. (4), 155 (1983).

[9] L. N. Larikov, V. M. Fal'chenko, V. F. Mazanko, S. M. Gurevich, G. K. Kharchenko, and A. I. Ignatenko, Dokl. Akad. Nauk SSSR, **221**, 1073 (1975) [Sov. Phys. Dokl. **20**, 287 (1975)].

[10] J. D. Eshelby, ''The continuum theory of lattice defects,'' in *Solid State Physics, Vol. 3*, F. Seitz and D. Turnbull (eds.), Academic Press, New York (1956), pp. 79–144 [Russ. transl., IL, Moscow (1963)].

[11] V. P. Voronkov and G. A. Gurchenok, Fiz. Tekh. Poluprovodn. **24**, 1831 (1990) [Sov. Phys. Semicond. **24**, 1141 (1990)].

[12] V. I. Fistul' and A. M. Pavlov, Fiz. Tekh. Poluprovodn. **17**, 854 (1983) [Sov. Phys. Semicond. **17**, 535 (1983)].

[13] S. S. Strel'chenko and V. V. Lebedev, $A^{III}B^{V}$ *Compounds. A Handbook* [in Russian], Metallurgiya, Moscow (1984).

[14] A. L. Zakharov and E. I. Asvadurova, *Calculation of the Thermal Parameters of Semiconductor Devices* [in Russian], Radio i Svyaz' (1983).

Translated by P. Shelnitz

Capacitive Methods of Semiconductor Purity Control

L. S. Berman
Fiz. Tekh. Poluprovodn. **31** (June 1997)

[S1063-7826(97)02906-2]

The increasingly more stringent quality requirements for semiconductor materials and devices are stimulating improvements in both fabrication and purity control methods. Together with the standard methods (neutral-activation and spectral analysis), in recent years the capacitive method of semiconductor purity control on the basis of deep-level centers has been rapidly advancing. Neutron-activation and spectral analysis make it possible to identify impurities irrespective of whether or not they are electrically active. These methods are destructive. The capacitive method makes it possible to identify deep-level centers, i.e., lattice imperfections which directly influence the parameters of a semiconductor. The capacitive method is highly sensitive, and for devices with p-n junctions or Schottky barriers it is nondestructive.

Successful application of the capacitive method of semiconductor purity control requires a knowledge not only of the possibilities but also the physical foundations of the method and procedures for performing the measurements themselves as well as analyzing the results of the measurements. These questions are the content of this monograph. Chapter 1 examines the physical foundations of the method: trapping and thermal emission of electrons and holes in the space-charge region and capacitance and current relaxation accompanying charge exchange on a deep level. The principle of identification of deep-level centers on the basis of the temperature-dependence of the thermal emission time is substantiated. Chapter 2 is devoted to measurements. The experimental methods of relaxation spectroscopy of deep-level centers are examined in detail: isothermal capacitance relaxation and DLTS, the constant capacitance method, double isothermal capacitance relaxation and double DLTS, the isothermal current relaxation method, and current DLTS. The applicability of the DLTS methods is analyzed. The principal measurement setups are described: a setup with an analog bridge and a setup with a digital bridge. Chapter 3 gives a series of nonstandard examples of the application of the method. It is shown that the range of applicability of the method can be expanded by thermal and radiation activation of the impurities. Chapter 4 examines the characteristic features of the identification of deep-level centers in low-resistivity semiconductors, taking account of the effect of a strong electric field, and in high-resistivity semiconductors, taking account of the effect of the impedance of the diode base. The regions of applicability of the capacitance and current methods are compared for a diode with a high-resistivity base. A contact-free method of identifying deep-level centers in semiconductor materials is examined in an Appendix.

The proposed monograph is the first such work in worldwide literature concerning this question. It is intended for a wide range of specialists concerned with the development and investigation of semiconductor materials and devices.

The English language edition of this book has been published in St. Petersburg.

A Russian language edition will be published in 1997.

Translated by M. E. Alferieff

 1063-7826/97/060649-01$10.00

Dear Readers,

An international scientific seminar on the subject ''Fundamental aspects of ultrathin insulators for silicon-based semiconductor devices'' will be held in St. Petersburg on August 4–8, 1997.

The purpose of the seminar is to discuss the latest progress in the physics and chemistry of ultrathin insulators (oxides, nitrides, and oxynitrides) based on silicon, silicon carbide, and Se–Ge compounds.

The seminar is sponsored by the NATO Science Committee.

Contacts:

Eric Garfunkel
Rutgers University
Piscataway, NJ 08855-0849
USA
Tel: 1-908-445-2747
Fax: 1-908-445-5312
E-mail: garf@rutchem.rutgers.edu

Aleksandr Yakovlevich Vul'
A. F. Ioffe Physicotechnical Institute
194021 St. Petersburg, Politekhnicheskaya 26
Tel: 7-812-247-91-07
Fax: 7-812-247-58-94
E-mail: vul@vul.ioffe.rssi.ru

 1063-7826/97/060650-01$10.00